

**CHARACTERIZATION OF THE STRUCTURE, FUNCTION, AND PROTEIN-
PROTEIN INTERACTIONS INVOLVED IN THE ASSEMBLY OF THE TYPE III
SECRETION SYSTEM TIP COMPLEX AND THE TRANSLOCON OF SALMONELLA
AND SHIGELLA**

By

©2013

Srirupa Chatterjee

M.Sc., University of Calcutta, 2007

Submitted to the graduate degree program in Molecular Biosciences and the
Graduate Faculty of the University of Kansas
in partial fulfillment of the requirements for the degree of
Doctor of Philosophy

Committee members:

Chairperson Roberto N. De Guzman

Mark Richter

Krzysztof Kuczera

Audrey Lamb

P. Scott Hefty

Christopher J Fischer

Date Defended: 17 April, 2013

The Dissertation Committee for Srirupa Chatterjee certifies that this is the approved version of the following dissertation

**CHARACTERIZATION OF THE STRUCTURE, FUNCTION, AND PROTEIN-
PROTEIN INTERACTIONS INVOLVED IN THE ASSEMBLY OF THE TYPE III
SECRETION SYSTEM TIP COMPLEX AND THE TRANSLOCON OF SALMONELLA
AND SHIGELLA**

Committee members:

Chairperson Roberto N. De Guzman

Mark Richter

Krzysztof Kuczera

Audrey Lamb

P. Scott Hefty

Christopher J Fischer

Date approved: 10 June, 2013

This dissertation is dedicated to my parents Sudhansu and Anita Chattopadhyay and to my grandmother Juthika Chakraborty

Abstract

The type III secretion system (T3SS) is a macromolecular structure assembled by many Gram-negative bacteria in order to invade target host cells. A functional T3SS contains a syringe-like structural component known as the needle apparatus, which works in concert with an export apparatus that recognizes the cargo and an ATPase complex that energizes the transport of bacterial effector proteins. Effectors transported directly into the host cell cytoplasm modulate host cellular functions such as cytoskeletal dynamics and cellular signaling in order to enable the pathogens to invade, survive, and multiply within the host environment.

Gram-negative bacteria harboring the T3SS include *Salmonella*, *Shigella*, enteropathogenic *E. coli*, *Yersinia*, *Burkholderia*, *Pseudomonas*, as well as *Chlamydia*. These organisms are responsible for infectious diseases in humans and pose a threat to human health worldwide. Inactivation of the T3SS, by knocking out structural or functional proteins, renders pathogens incapable of causing infection. *Salmonella* and *Shigella* are responsible for millions of cases of food-borne diarrhea annually throughout the world. In addition, large-scale food recalls due to frequent outbreaks of food poisoning has a negative impact on the food industry in the United States. No preventive vaccines are available against *Salmonella* and *Shigella*. Study of the T3SS thus has a scope for the development of strategies to combat these pathogens.

The T3SS among different bacterial species share common features but also show unique structural and functional characteristics. Therefore, the T3SS provides a suitable target for the development of specific anti-infectives. The needle apparatus of the T3SS consists of a base followed by an extracellular needle. The needle is attached to a tip complex and a translocon. The tip complex serves as a platform for the assembly of the translocon that punctures a

translocation pore within the host cell membrane. The tip complex is assembled from several copies of a hydrophilic tip protein and the translocon is assembled from two hydrophobic translocon proteins. This dissertation describes structural and functional studies, as well as characterization of the protein-protein interactions that are important in the assembly of the tip complex and the translocon of *Salmonella* and *Shigella*.

In *Salmonella*, the tip complex is formed by the tip protein SipD. A translocon made up of the translocon proteins SipB and SipC is attached on the tip complex. A combination of X-ray crystallography, Nuclear magnetic resonance (NMR) spectroscopy, site-directed mutagenesis, as well as functional assays were applied to determine the structure of the *Salmonella* tip protein SipD and show that the C-terminus is crucial for the function and an antiparallel β -sheet is important for the tertiary structure of SipD. The function of the T3SS can be regulated by small molecules such as bile salts. The T3SS of *Salmonella* is down regulated by bile salts. The tip protein SipD directly binds to the bile salt deoxycholate using an unknown mechanism. The crystal structures of SipD bound to bile salts reported herein show that the interaction between bile salts and SipD is predominantly hydrophobic. Further, deoxycholate induced the degradation of the *Salmonella* translocon protein SipB. These observations have led to the hypothesis that deoxycholate might interfere with the interaction between SipD and SipB leading to a down regulation of the T3SS in *Salmonella*. The structure of the translocon and how it is attached to the tip complex is not clear. Preliminary structural characterization of a folded, hydrophilic domain at the N-terminus of SipB was undertaken to locate two fragments of SipB within residues 82-240 and 82-226, which produced well-dispersed 2D-NMR spectra. Paramagnetic relaxation enhancement (PRE) was employed to define the interaction between SipD and the N-terminal hydrophilic domain of SipB. A region within residues Asp207-Asn283

of SipB bound to a mixed α/β region of SipD. PRE was also used to study how the *Shigella* tip protein IpaD binds to its needle protein MxiH in order to assemble the tip complex in *Shigella*. MxiH was shown to bind to the lower portion of a coiled coil region in IpaD.

Secretion through the T3SS is enabled by extensive cross-talk within its components. The assembly of the needle apparatus requires polymerization of multiple copies of several different proteins. Regulation of secretion is most probably an outcome of conformational changes relayed in sequence through the needle apparatus. Work described in this dissertation shows that weak protein-protein interactions are a common theme in the assembly of the needle apparatus. Further, T3SS proteins contain discreet functional domains. For example, the coiled coil of the tip protein allows the assembly of the tip complex while the mixed α/β region attaches to the translocon. The structure of the T3SS proteins varies depending upon the role it plays. For example, the extracellular needle is assembled from a small polar protein but the translocon proteins contain both hydrophilic and hydrophobic domains. Nevertheless, further studies are required to fully appreciate certain aspects of the T3SS such as how large proteins are transported through the needle, how the T3SS switches between active and inactive states of secretion, how substrate specificity is controlled, and how effector secretion is energized. Complete understanding of the T3SS requires the determination of high resolution structures of the needle apparatus, direct binding studies analyzing how isolated components of the needle apparatus interact with each other and behave *in vitro*, computational modeling of larger substructures, and functional assays to test the physiological implications of these *in vitro* studies.

Acknowledgements

I would like to thank those who have supported me in various ways throughout the years of graduate school.

Above all, I would like to thank my mentor Dr. Roberto N. De Guzman for his leadership, guidance, support, and critiques which were essential not only for scientific research but also for life in general. I thank him for introducing me to the dynamic fields of structural biology, protein biochemistry, and NMR spectroscopy. He has also taught me how to convey scientific observations in an articulate and simplistic manner to any audience.

All the current and former members of the De Guzman Lab have helped me in research as well as day-to-day life. I would specifically like to thank Dr. David Fernando Estrada and Dr. Dalian Zhong for their continuous guidance that has enabled me to complete the research work described in this dissertation. I thank all the members of my dissertation committee for investing their valuable time and for their intellectual contributions towards the improvement of my research work. I thank Dr. Audrey Lamb for her guidance that helped me immensely during my comprehensive oral examination. I would also like to thank Dr. Scott Lovell and Dr. Asokan Anbanandam for technical assistance during the crystallization of SipD and acquisition of NMR data.

My friends have been a massive source of strength and support during all the trials and tribulations of graduate school. I thank Sukanya Chaudhury, Srayanta Mukherjee, Jennifer Hackett, and Laticia Abu-sharar. Lastly, I would like to express my deepest gratitude to my father Sudhansu Chattopadhyay, my mother Anita Chattopadhyay, and my sister Sreemoyee Vardhan for firmly believing in me at all times.

Table of Contents

	Page
Abstract	iv
Acknowledgements	vii
Table of Contents	viii
List of Figures	xii
List of Tables	xvi
List of Abbreviations	xvii
Chapter 1. Introduction	
1.1. Introduction to the type III secretion system	1
1.2. Structural components of the T3SS	4
1.2.1. The basal body	4
1.2.2. The needle	6
1.2.3. The tip complex	8
1.2.4. The translocon	9
1.3. The functional components of the T3SS	9
1.3.1. The export apparatus	9
1.3.2. The ATPase complex	11
1.3.3. T3SS chaperones	13
1.3.4. T3SS effectors	14
1.4. The T3SS of <i>Salmonella</i> and <i>Shigella</i>	15
1.4.1. Pathogenesis of <i>Salmonella</i> and <i>Shigella</i>	15
1.4.2. Genetic organization of the T3SSs in <i>Salmonella</i> and <i>Shigella</i>	17
1.4.3. The needle apparatus of <i>Salmonella</i> and <i>Shigella</i>	20
1.5. Studies on the tip complex of <i>Salmonella</i> and <i>Shigella</i>	24
1.5.1. Crystal structure of the <i>Salmonella</i> tip protein SipD	24
1.5.2. The interaction between SipD and bile salts	25
1.5.3. The interaction between the <i>Shigella</i> tip protein and the needle protein	26
1.6. Studies on the <i>Salmonella</i> translocon protein SipB	28
1.7. References	30
Chapter 2. Materials and Methods	
2.1. Protein expression and purification	44
2.1.1. Amino acid specific labeling of SipD ³⁹⁻³⁴³	46
2.1.2. ¹³ C-ILV labeling of SipD ³⁹⁻³⁴³	47
2.2. Protein crystallization & Data collection	47
2.2.1. Free SipD ³⁹⁻³⁴³ and SipD ³⁹⁻³⁴³ bound to bile salts	47
2.2.2. SipD ¹³¹⁻³⁴³	48
2.3. Crystal structure determination	49
2.3.1. Free SipD ³⁹⁻³⁴³ and SipD ³⁹⁻³⁴³ bound to bile salts	49
2.3.2. SipD ¹³¹⁻³⁴³	50

2.4. CD spectroscopy and thermal denaturation	51
2.5. NMR spectroscopy	51
2.5.1. Two-dimensional NMR spectra of SipD	51
2.5.2. NMR titrations of ^{15}N -SipD ³⁹⁻³⁴³ with unlabeled SipB ⁸²⁻³¹²	52
2.5.3. Dilution experiments and NMR titrations of ^{15}N -MxiH ^{V68AV70A} with unlabeled IpaD	52
2.6. Paramagnetic relaxation enhancement	53
2.6.1. Spin labeling of SipB ⁸²⁻³¹² , IpaD ³⁸⁻³³² , and IpaD ¹³¹⁻³³²	53
2.6.2. Single time point PRE using ^{15}N -specifically labeled SipD ³⁹⁻³⁴³ and SipB ⁸²⁻³¹²	53
2.6.3. Single time point PRE using ^{15}N -MxiH ^{CΔ5} and IpaD ³⁸⁻³³² or IpaD ¹³¹⁻³³²	54
2.7. HADDOCK modeling of the SipD ³⁹⁻³⁴³ -SipB ⁸²⁻²²⁶ complex	54
2.8. <i>Salmonella</i> invasion assay	55
2.8.1. Construction of knockout strains of <i>S. typhimurium</i>	55
2.8.2. <i>Salmonella</i> invasion assay	56
2.9. Immunoblotting	57
2.9.1. Affinity purification of antibodies	57
2.9.2. Extraction of T3SS proteins secreted into the growth medium	57
2.9.3. Extraction of T3SS proteins from bacterial cytoplasm	58
2.9.4. Transfer of proteins to a nitrocellulose membrane	59
2.9.5. Membrane blocking and protein detection	59
2.10. References	60
Chapter 3. The crystal structure of the <i>Salmonella</i> tip protein SipD	
3.1. Introduction	63
3.2. Results	66
3.2.1. Protein expression and purification	66
3.2.2. Crystal structure of SipD ³⁹⁻³⁴³	68
3.2.3. Crystal structure of SipD ¹³¹⁻³⁴³	72
3.2.4. Functional characterization of truncated forms of SipD	72
3.2.5. Structural characterization of truncated forms of SipD	74
3.3. Discussion	77
3.3.1. Comparison with the structures of other tip proteins	77
3.3.2. Significance of the N-terminal α -helical hairpin	83
3.3.3. Deletion mutants of SipD	84
3.4. References	85
Chapter 4. Characterization of the interaction between the <i>Salmonella</i> tip protein SipD and bile salts	
4.1. Introduction	88
4.2. Results	89
4.2.1. Crystal structure of SipD ³⁹⁻³⁴³ -deoxycholate and SipD ³⁹⁻³⁴³ -chenodeoxycholate complexes	89

4.2.2. Effect of deoxycholate on the invasiveness of <i>Salmonella</i>	93
4.2.3. Effect of mutagenesis around the bile salt binding site	95
4.2.4. Effect of deoxycholate on the secretion of SipD and SipB	95
4.3. Discussion	102
4.3.1. Heterogeneity of the bile salt binding sites	102
4.4. References	106
Chapter 5. Expression of the <i>Salmonella</i> translocon protein SipB for NMR studies	
5.1. Introduction	108
5.2. Results	109
5.2.1. Expression and purification of SipB	109
5.2.2. CD spectroscopy	113
5.2.3. ¹ H- ¹⁵ N-TROSY spectra of SipB constructs	116
5.2.4. 3D-HNCA experiments with SipB ⁸²⁻²²⁶	116
5.2.5. Size exclusion chromatography of SipB	118
5.3. Discussion	118
5.4. References	124
Chapter 6. The interaction between the <i>Salmonella</i> tip protein SipD and the N-terminal hydrophilic domain of the translocon protein SipB	
6.1. Introduction	127
6.2. Results	128
6.2.1. NMR titrations of SipD ³⁹⁻³⁴³ with the N-terminal hydrophilic region of SipB	128
6.2.2. Paramagnetic Relaxation Enhancement (PRE)	132
6.2.3. HADDOCK modeling of the SipD ³⁹⁻³⁴³ -SipB ⁸²⁻²²⁶ complex	137
6.2.4. <i>Salmonella</i> invasion assay and Immunoblotting	141
6.3. Discussion	141
6.4. References	150
Chapter 7. The interaction between the <i>Shigella</i> needle protein MxiH and the tip protein IpaD	
7.1. Introduction	155
7.2. Results	156
7.2.1. Backbone NMR assignments of a full length, functional double mutant of MxiH	156
7.2.2. NMR titration of ¹⁵ N-MxiH ^{V68AV70A} with unlabeled IpaD ³⁸⁻³³² and IpaD ¹³⁰⁻³³²	156
7.2.3. PRE experiments with ¹⁵ N-MxiH ^{V68AV70A} and IpaD	159
7.2.4. PRE experiments with ¹⁵ N-MxiH ^{CA5} and IpaD ³⁸⁻³³²	159
7.3. Discussion	164

7.4. References	172
Chapter 8. Summary and future directions	
8.1. The structure of SipD	174
8.1.1. Comparison of SipD and IpaD	174
8.1.2. Implications of the crystal structure of SipD ¹³¹⁻³⁴³	176
8.1.3. Potential applications of the crystal structures of SipD	176
8.1.4. Mutagenesis of SipD	180
8.2. Implications of the interaction between SipD and bile salts	186
8.3. The needle-tip interaction in <i>Shigella</i>	187
8.4. Interaction between SipD and SipB: implications for the assembly of the translocon	190
8.5. Conclusions	194
8.6. References	194

List of Figures

Figure	Page
1-1. Electron micrograph image of the T3SS needle complex	5
1-2. Cartoon of the T3SS needle apparatus	7
1-3. Structure of the translocation pore from EPEC	10
1-4. Pathogenesis of <i>Salmonella</i> and <i>Shigella</i>	16
1-5. Genetic organization of the T3SSs in <i>Salmonella</i> and <i>Shigella</i>	18
1-6. Models of the T3SS needles from <i>Shigella</i> and <i>Salmonella</i>	23
3-1. Cartoon model of the T3SS showing components of the needle apparatus	64
3-2. SDS-PAGE showing the purification of SipD ³⁹⁻³⁴³	67
3-3. Crystals of SipD ³⁹⁻³⁴³ WT, SipD ³⁹⁻³⁴³ C244S, and SipD ¹³¹⁻³⁴³	69
3-4. Crystal structure of SipD ³⁹⁻³⁴³	71
3-5. Crystal structure of SipD ¹³¹⁻³⁴³	73
3-6. Results of <i>Salmonella</i> invasion assay using deletion mutants of SipD	75
3-7. Structure of SipD ³⁹⁻³⁴³ showing the location of tryptophan residues and the deletions	76
3-8. CD and thermal denaturation of WT and deletion mutants of SipD	78
3-9. ¹ H- ¹⁵ N-TROSY spectra of SipD ³⁹⁻³⁴³ WT and deletion mutants of SipD	79
3-10. Comparison of the structure of T3SS tip proteins	80
3-11. Differences in the packing of the helices of SipD and IpaD	81
4-1. Overlay of the structures of SipD ³⁹⁻³⁴³ -deoxycholate and SipD ³⁹⁻³⁴³ -chenodeoxycholate complexes	90

4-2. The bile salt binding pocket formed by three molecules of SipD	91
4-3. Expanded view of the bile salt binding pocket of SipD ³⁹⁻³⁴³	92
4-4. Effect of deoxycholate on the invasiveness of <i>Salmonella</i>	96
4-5. Structure of SipD ³⁹⁻³⁴³ showing the interactions between the two molecules in the asymmetric unit	98
4-6. <i>Salmonella</i> invasion assay with SipD containing point mutations around the bile salt binding site	99
4-7. An immunoblot showing the effect of deoxycholate on the secretion of SipD and SipB in <i>Salmonella</i>	100
4-8. Crystal structure of IpaD ¹²¹⁻³¹⁹ bound to deoxycholate	103
4-9. Crystal structure of the SipD ¹²⁷⁻³⁴³ -PrgI fusion molecule bound to deoxycholate	104
5-1. Secondary structure prediction of SipB	110
5-2. Location of the predicted transmembrane helices of SipB	111
5-3. Schematic representation of the different regions of SipB	112
5-4. SDS-PAGE showing the purification of SipB ⁸²⁻³¹² and SipB ⁴³⁶⁻⁵¹⁸	114
5-5. CD and thermal denaturation of SipB ⁸²⁻³¹² , SipB ⁸²⁻²⁶⁷ , SipB ⁸²⁻²⁴⁰ , and SipB ⁸²⁻²²⁶	115
5-6. ¹ H- ¹⁵ N-TROSY spectra of SipB ⁸²⁻³¹² , SipB ⁸²⁻²⁶⁷ , SipB ⁸²⁻²⁴⁰ , and SipB ⁸²⁻²²⁶	117
5-7. Signals from 3D-HNCA experiments on ¹⁵ N- ¹³ C-SipB ⁸²⁻²²⁶	119
5-8. Size exclusion chromatograms of SipB ⁸²⁻³¹² , SipB ⁸²⁻²⁴⁰ , and SipB ⁸²⁻²²⁶	120
6-1. NMR titration of ¹⁵ N-SipD ³⁹⁻³⁴³ with unlabeled SipB ⁸²⁻³¹²	129
6-2. Residues of SipD ³⁹⁻³⁴³ affected on interaction with SipB ⁸²⁻³¹²	130
6-3. NMR titration of ¹³ C-ILV-SipB ⁸²⁻²²⁶ with unlabeled SipD ³⁹⁻³⁴³	131

6-4. Model of SipB ⁸²⁻³¹² showing the position of each spin label	133
6-5. CD spectra of SipB ⁸²⁻³¹² WT, SipB ⁸²⁻³¹² with cysteine mutants, and spin-labeled SipB ⁸²⁻³¹²	134
6-6. ¹ H- ¹⁵ N-HSQC spectra of ¹⁵ N-AIKM-SipD ³⁹⁻³⁴³ titrated with diamagnetic and paramagnetic SipB ⁸²⁻³¹²	135
6-7. ¹ H- ¹⁵ N-TROSY spectra of ¹⁵ N-Leu-SipD ³⁹⁻³⁴³ titrated with diamagnetic and paramagnetic SipB ⁸²⁻³¹²	136
6-8. Results of PRE experiments with AIKM-SipD ³⁹⁻³⁴³ and SipB ⁸²⁻³¹²	138
6-9. Results of PRE experiments with Leu-SipD ³⁹⁻³⁴³ and SipB ⁸²⁻³¹²	139
6-10. Summary of the results of PRE experiments with SipD ³⁹⁻³⁴³ and SipB ⁸²⁻³¹²	140
6-11. HADDOCK predicted model of the SipD ³⁹⁻³⁴³ -SipB ⁸²⁻²²⁶ complex	144
6-12. <i>Salmonella</i> invasion assay with point mutants of SipB	146
6-13. An immunoblot showing the expression of SipB in sipB ⁺ and sipB K211A strains of <i>Salmonella</i>	147
6-14. A functional model of the interaction between SipD and SipB	149
7-1. Overlay of the ¹ H- ¹⁵ N-HSQC spectra of MxiH ^{CΔ5} and MxiH ^{V68AV70A}	157
7-2. Assignment of the backbone NMR resonances of ¹⁵ N-MxiH ^{V68AV70A}	158
7-3. A portion of the 3D-HNCA strips used for backbone assignment of ¹³ C- ¹⁵ N-MxiH ^{V68AV70A}	160
7-4. NMR titration of ¹⁵ N-MxiH ^{V68AV70A} with unlabeled IpaD ³⁸⁻³³²	161
7-5. NMR titration of ¹⁵ N-MxiH ^{V68AV70A} with IpaD ¹³⁰⁻³³²	162
7-6. Results of PRE experiments with ¹⁵ N-MxiH ^{V68AV70A} and IpaD ³⁸⁻³³²	163
7-7. Structure of IpaD ³⁸⁻³³² showing the positions of the spin-labels	165

7-8. Results of the PRE experiments with ^{15}N -MxiH ^{CΔ5} and IpaD ³⁸⁻³³²	166
7-9. Structure of MxiH showing the residues most affected by a spin label at R132 of IpaD ³⁸⁻³³²	167
7-10. ^1H - ^{15}N -HSQC spectra of ^{15}N -MxiH ^{V68AV70A} showing concentration- dependent chemical shift changes	168
8-1. Proposed states of SipD before and during transport through the needle	177
8-2. A proposed model of SipD assembled into the tip complex	178
8-3. Proposed functional roles of the C-terminus of SipD	181
8-4. Proposed functional role of loop α 3- α 4 of SipD	183
8-5. Structures of the tip complexes of <i>Shigella</i> and <i>Yersinia</i>	184
8-6. A homology model of the <i>Shigella</i> needle	189
8-7. Proposed model of the assembled translocon of <i>Salmonella</i>	193

List of Tables

Table	Page
1. Classification of the T3SS	3
2. Protein components of the T3SSs of <i>Salmonella</i> and <i>Shigella</i>	12
3. Sequence of the oligonucleotide primers used in construction of expression plasmids	45
4. Crystallographic statistics for WT and C244S SipD ³⁹⁻³⁴³ and SipD ¹³¹⁻³⁴³	70
5. Crystallographic statistics for SipD ³⁹⁻³⁴³ -deoxycholate and SipD ³⁹⁻³⁴³ -chenodeoxycholate	94
6. Rationale behind the design of SipD mutants around the bile salt binding site	97
7. Active residues of SipD ³⁹⁻³⁴³ and SipB ⁸²⁻²²⁶ used for HADDOCK modeling	143

List of Abbreviations

CD	Circular dichroism
DOC	Deoxycholate
DMEM	Dulbecco's Modified Eagle Medium
EPEC	Enteropathogenic <i>E. coli</i>
EHEC	Enterohaemorrhagic <i>E. coli</i>
HSQC	Heteronuclear Single Quantum Coherence
IPTG	Isopropyl- β -D-thiogalactopyranoside
MTSL	(1-Oxyl-2,2,5,5-tetramethyl- Δ 3-pyrroline-3-mehtyl) methanethiosulfonate
NMR	Nuclear Magnetic Resonance
PRE	Paramagnetic Relaxation Enhancement
RMSD	Root-Mean-Square Deviation
SPI-1	<i>Salmonella</i> Pathogenicity Island 1
SPI-2	Salmonella Pathogenicity Island 2
TROSY	Transverse Relaxation Optimized Spectroscopy
T3SS	Type III Secretion System

CHAPTER 1: Introduction

1.1. Introduction to the type III secretion system

Secretion of proteins across the cell membrane is a fundamental characteristic of all bacteria (1). The secreted proteins perform a multitude of functions including extraction of nutrients from the surroundings, motility, intercellular communication, and formation of the cell membrane (1). Secretion of proteins in Gram-positive bacteria occurs through the general secretory pathway (1, 2). However, additional specialized secretory mechanisms are required to transport proteins across the outer membrane of Gram-negative bacteria (1, 2). Secretion machineries in Gram-negative bacteria are classified into seven groups (types I through VII) based on their structure, regulation, and substrate specificities (3, 4). The type III secretion system (T3SS) was initially discovered as a set of gene clusters required for virulence of several pathogenic Gram-negative bacteria (2).

The T3SS can be differentiated from other secretion systems by the following characteristics: the substrates are secreted through both the inner and outer bacterial membranes, several accessory proteins are required for the secretion process, the T3SS substrates lack a cleavable sec-dependent signal sequence, and several extracellular signals are required for the full activation of the T3SS(2). A functional T3SS includes a needle apparatus, which works in concert with an export apparatus and an ATPase complex that are associated with the needle apparatus at the bacterial inner membrane (5). The needle apparatus spans the bacterial cell membranes, the extracellular space, and the host cell membrane (6). The needle apparatus is essentially a hollow channel through which substrates or bacterial effectors are transported from the bacterial cytoplasm to the cytoplasm of the target host cell (6). The export apparatus controls

substrate specificity and the order of secretion through the needle apparatus and the ATPase complex energizes the unidirectional transport of effectors through the needle apparatus (5, 6). Prior to secretion through the needle apparatus, effectors remain bound to chaperones, which maintain them in a secretion-competent state within the bacterial cytoplasm (7). Upon delivery into the host cytoplasm the effectors modulate several host cellular processes such as cytoskeletal dynamics, progression of cell cycle, apoptosis, endocytic trafficking, and gene expression (8). The membrane bound components of the needle apparatus, export apparatus, and the ATPase complex are well conserved among several Gram-negative bacteria pathogenic to both animals (*Salmonella*, *Shigella*, *Yersinia*) and plants (*Xanthomonas*, *P. syringae*, *Erwinia*, etc.) (4). Additionally, genes coding for a T3SS were also found in several symbiotic and non-pathogenic bacteria (4). These core components also bear structural and functional resemblance to the flagellar export apparatus (4). The conserved nature of the T3SS is thought to be due to horizontal gene transfer because the G+C content of T3SS genes is distinct from the rest of the bacterial genome (2).

T3SS are classified into seven families based on sequence conservation (9) [Table 1]. Out of the seven, three families of T3SS most commonly occur among bacteria that are pathogenic to human beings (9). These are the Ysc family, the Inv-Mxi-Spa family, and the Esc family. These names also denote the T3SS gene clusters in *Yersinia*, *Shigella*, and *E. coli* respectively (9). The Ysc family includes the T3SS of *Yersinia*, *Pseudomonas*, and *Aeromonas* (9). *Salmonella* contains two sets of T3SS genes located within *Salmonella* pathogenicity islands 1 and 2 (SPI-1 & SPI-2). The SPI-1 T3SS belongs to the Inv-Mxi-Spa family along with that of *Shigella* and *Burkholderia* (9). The SPI-2 T3SS from *Salmonella* belongs to the

Table 1: Classification of the T3SS.

T3SS family	Bacterial species	Diseases caused
Inv-Mxi-Spa	<i>Salmonella typhimurium</i> (SPI-1)	Salmonellosis
	<i>Shigella flexneri</i>	Shigellosis
	<i>Burkholderia pseudomallei</i>	Melioidosis
Esc	<i>Salmonella typhimurium</i> (SPI-2)	Salmonellosis
	<i>Enteropathogenic E. coli</i> (EPEC)	Diarrhea
	<i>Enterohaemorrhagic E. coli</i> (EHEC)	Hemolytic-uremic syndrome
Ysc	<i>Yersinia pestis</i>	Bubonic plague
	<i>Pseudomonas aeruginosa</i>	Infection in immunocompromised
	<i>Aeromonas salmonicida</i>	Furunculosis in fish
Chlamydiales	<i>Chlamydia trachomatis</i>	Trachoma, genital infections
	<i>Chlamydia pneumoniae</i>	Acute respiratory disease
Rhizobium	<i>Rhizobium</i> sp.	Plant symbiont
Hrp1	<i>Pseudomonas syringae</i>	Infections in plants
Hrp2	<i>Xanthomonas campestris</i>	Infections in plant

Esc family along with those from enteropathogenic *E. coli* (EPEC) and enterohaemorrhagic *E. coli* (EHEC) (9). These T3SS-harboring bacterial species are the causative agents of a variety of diseases ranging from Bubonic plague (caused by *Yersinia pestis*), food-poisoning (caused by *Salmonella*, *Shigella*, and *E. coli*), hospital-acquired secondary infections (caused by *Pseudomonas aeruginosa*), and sexually transmitted diseases (caused by *Chlamydia*) (6). The T3SS is a key player in the development of these illnesses, which together pose a major threat to human health.

1.2. The structural components of the T3SS

1.2.1. The basal body - The needle apparatus forms the structural component of the T3SS and has been visualized in detail using three-dimensional electron microscopy [**Figure 1-1**] (10). The needle apparatus of several bacteria including *Salmonella* (11), *Shigella* (12), *Yersinia* (13), *Escherichia* (14), and *Pseudomonas* (15) show a common syringe-like appearance and is thus called an injectisome. Over 20 different proteins assemble the needle apparatus, which is divided into a basal body, a needle, a tip complex, and a translocon (9). The structure of a prototypical needle apparatus is depicted in **Figure 1-2**. The basal body contains two radially symmetrical multimeric rings that span the bacterial inner membrane (IM ring), and the outer membrane (OM ring) (9) [**Figure 1-2**]. A tubular structure called the inner rod connects the IM ring to the OM ring through the periplasmic space (10). The basal body measures approximately $250 \text{ \AA} \times 300 \text{ \AA}$ and encloses an inner channel about 20-30 \AA in diameter (10). The basal body forms the core secretory unit and secretes structural proteins into the extracellular space, which then assemble the rest of the needle apparatus.

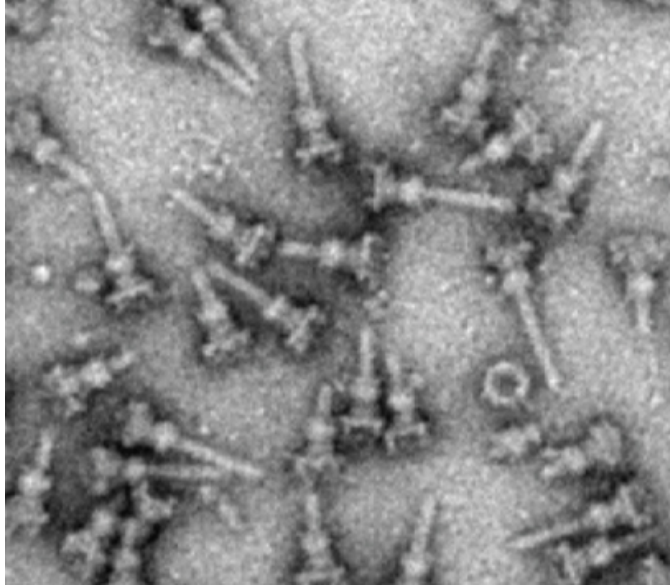


Figure 1-1: An electron micrograph image of purified *Salmonella* T3SS needle complexes that consist of the basal body and the needle (16). This research was originally published in Journal of Biological Chemistry. Zhong,D., Lefebvre, M., Kaur, K., McDowell, M. A., Gdowski, C., Jo, S., Wang, Y., Benedict, S. H., Lea, S. M., Galan, J. E., De Guzman, R. N. The *Salmonella* Type III Secretion System Inner Rod Protein PrgJ Is Partially Folded, *J. Biol.Chem.*, 2012; 287: 25303-11. © The American Society for Biochemistry and Molecular Biology. It is the policy of the American Society for Biochemistry and Molecular Biology to allow reuse of any material published in its journals (the Journal of Biological Chemistry, Molecular & Cellular Proteomics and the Journal of Lipid Research) in a thesis or dissertation at no cost and with no explicit permission needed.

1.2.2. The needle - A characteristic feature of the needle apparatus is a hollow cylindrical needle that connects the basal body within the bacterial membrane to the translocon within the host cell membrane [Figures 1-1 & 1-2]. The needle is approximately 400-800 Å in length with an outer diameter of 70-80 Å and an inner lumen of 20-30 Å (17). The diameter of the inner lumen is only sufficient to hold two well-folded α -helices. This implies that larger protein components of the T3SS have to be transported through the lumen in an unfolded or partially folded state. However, the process of transport of proteins through the needle is poorly understood. The needle is assembled by the helical polymerization of the needle protein (9). Needle proteins are around 6-9 kD in size and contain two α -helices connected by a P-X-X-P motif, where X is any amino acid (18, 19). The N-terminus and the C-terminus of the needle proteins is highly flexible and can adopt several conformations (19). The C-terminus of the needle proteins is important for the assembly of the needle as removal of only five residues from the C-terminus is sufficient to abrogate polymerization of the needle (20). Although, the three-dimensional structure of the needle has been studied extensively (18, 21-23), much less is known about the mechanism and regulation of transport of effectors through the needle. The transport of effector proteins through the needle lumen is activated only after the translocon attaches to the host cell membrane (24). This means that activation signals are relayed from the host cell membrane and across the needle to the export apparatus at the bacterial cell membrane. How the needle relays information to the export apparatus is poorly understood. Certain point mutations within the needle proteins can give rise to needles which constitutively secrete effectors in the absence of an activation signal (20). This has led to the hypothesis that contact with the host cell membrane might trigger conformational changes throughout the length of the needle and

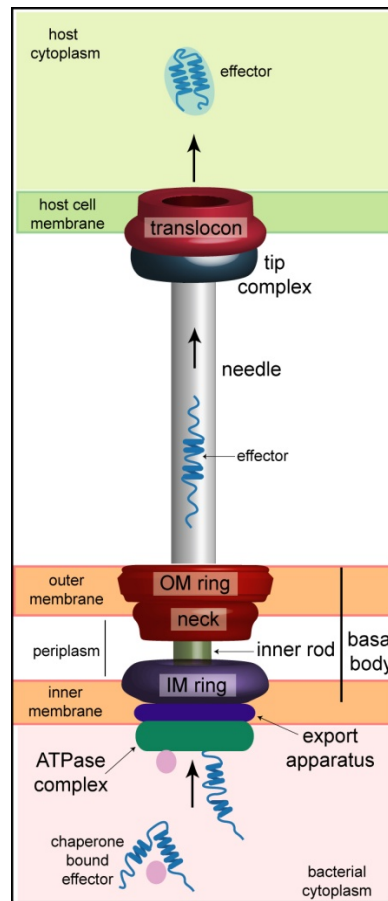


Figure 1-2: Cartoon of the T3SS showing the needle apparatus. The needle apparatus is divided into a basal body, a needle, a tip complex, and a translocon. The basal body contains an OM ring that spans the bacterial inner membrane and an IM ring that spans the bacterial outer membrane. An extension of the OM ring called the neck reaches into the periplasmic space. The IM and OM rings are connected by an inner rod. An export apparatus and ATPase complex are associated with the basal body. The needle bridges the extracellular space and is capped by a tip complex and a translocon. The translocon forms a translocation pore within the host cell membrane. The needle apparatus transports bacterial effectors directly into the host cytoplasm. Effectors remain bound to chaperones in the bacterial cytoplasm prior to transport through the needle.

the mutant needle proteins might assemble a needle that mimics the activated conformation of the WT needle. The flexible termini of the needle protein are thought to allow the WT needle to adopt different conformations. The active and inactive needle conformations however, are not known.

1.2.3. The tip complex - An oligomeric tip complex plugs the opening of the needle until contact with host cell is established (25) [Figure 1-2]. Following contact with the host cell membrane the tip complex is thought to undergo a conformational change, which triggers the assembly of the translocon. The translocon sits on the tip complex and integrates into the host cell membrane to form the translocation pore that allows the delivery of effectors into the host cell cytoplasm. Thus, the tip complex regulates the secretion of effectors and also acts as a platform for the formation of the translocon. The tip complex is composed of multiple copies of the tip protein (26, 27). The atomic structures of tip proteins from several bacterial species have been determined by X-ray crystallography (28-30). Tip proteins are highly α -helical and roughly 30-40 kD in size with an overall elliptical shape. The sequence identity among the tip proteins ranges from 30-40 % with a higher degree of sequence conservation at the C-terminus. A long central coiled coil is conserved among all tip proteins (28). On either side of the coiled coil there is an N-terminal domain and a C-terminal domain that vary to a higher degree (28). Tip protein *Yersinia* LcrV and *Pseudomonas* PcrV are known to have cognate chaperones LcrG and PcrG respectively (31). However, no tip chaperones have been identified for the tip proteins of *Salmonella* and *Shigella*. The assembled tip complexes of *Yersinia* (26) and *Shigella* (27) have been visualized using electron microscopy. These pathogens assemble a pentameric tip complex formed by five tip proteins that are polymerized along their coiled coil domains. Nevertheless, the low resolution of these structures prevented detailed analysis of the molecular interactions

between the tip proteins and between the tip proteins and the needle proteins necessary for the assembly of the tip complex. In addition, how the tip complex senses the host cell membrane and triggers the assembly of the translocon is also poorly understood.

1.2.4. The translocon - The translocon is a membrane-embedded structure that sits on top of the tip complex and forms a pore in the host cell membrane [**Figure 1-2**]. The translocon proteins, which are responsible for assembling the translocon, were identified within the T3SS loci as genes encoding two membrane proteins and were adjacent to the genes for the tip protein (32). The translocon proteins colocalize with the tip protein on the bacterial surface (33). Studies using osmoprotectants of different sizes showed that translocons form 30-50 Å wide pores within the eukaryotic cell membrane (12, 34). Intact translocons formed by EPEC were visualized by electron microscopy and were found to contain 6-8 lobe-like structures (35) [**Figure 1-3**]. This strongly suggests that the translocon is polymerized from multiple protein units. The crystal structures of small fragments from the translocon proteins *Salmonella* SipB and *Shigella* IpaB showed that these proteins contain trimeric coiled coils (36). However, the structure, stoichiometry, and the mechanism of assembly of the translocon are currently unknown.

1.3. The functional components of the T3SS

1.3.1. The export apparatus - The assembly of the needle apparatus begins with the formation of the IM and OM rings of the basal body (5). The inner rod and the needle are assembled soon after. The tip protein and the translocon proteins are secreted following the assembly of the needle and the effectors are secreted last (24). Based on their order of secretion, the T3SS components are sometimes classified as early (inner rod and needle protein), middle

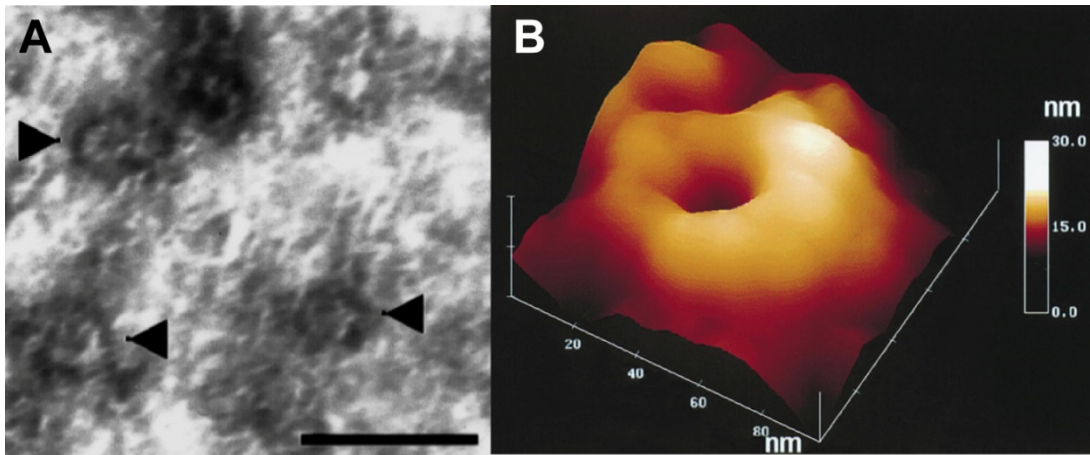


Figure 1-3: Structure of the translocation pore from EPEC (A) Electron micrograph image of translocation pores formed by EPEC within the cell membrane of a red blood cell. Translocation pores show a segmented appearance (35). (B) A three-dimensional image of a translocation pore from EPEC determined by atomic force microscopy (35). The translocation pore had a doughnut-like shape and contained 6-8 lobes. This figure was reproduced with permission from John Wiley and Sons. © 2001 Blackwell Science Ltd, *Cellular Microbiology*, **3**, 669-679

(tip protein), and late (translocon and effector proteins) effectors (24). The export apparatus is responsible for switching the substrate specificity from early to middle to late effectors and controlling the hierarchy of secretion through the basal body (37-39). Five highly conserved integral membrane proteins assemble the export apparatus, which is associated with the basal body within the bacterial inner membrane (5, 40). Although the structures of the cytosolic portions of some of the export apparatus proteins have been determined (37, 39, 41, 42), little is known about the molecular interactions between these proteins or the specific roles they play in the function of the export apparatus. One export apparatus protein belonging to the *Yersinia* YscU family (SpaS in *Salmonella* and Spa40 in *Shigella*, **Table 2**) contains a conserved NPTH motif that can undergo autocatalytic cleavage, which results in a conformational change (37-39). This phenomenon is thought to be important for switching of substrate specificity. The largest member of the export apparatus, which belongs to the *Yersinia* YscV family (InvA in *Salmonella* and MxiA in *Shigella*, **Table 2**), forms a multimeric ring below the base (42). Although the exact function of this ring is unknown, mutation of the residues lining the inner surface of this ring had a negative impact on effector secretion (42).

1.3.2. The ATPase complex - The ATPase complex couples hydrolysis of ATP with the secretion of effectors through the needle apparatus (7). The major component of the ATPase complex is a cytoplasmic ATPase belonging to the *Yersinia* YscN family (InvC in *Salmonella* and Spa47 in *Shigella*, **Table 2**) (43). The T3SS ATPase shares a high degree of sequence similarity with the β -subunit of the F_o - F_1 -ATPases and forms a double-hexameric ring below the export apparatus (43). Prior to secretion through the needle apparatus effectors are bound to their cognate chaperones (7). The ATPase recognizes and binds to the chaperone-effector

Table 2: Protein components of the T3SSs of *Salmonella* and *Shigella*

Role	<i>Salmonella</i>	<i>Shigella</i>
Translocon	SipB, SipC	IpaB, IpaC
Tip complex	SipD	IpaD
Needle	PrgI	MxiH
Base	InvG, PrgJ PrgK, PrgH	MxiD, MxiI, MxiJ, MxiG
Export apparatus	SpaP, SpaQ, SpaS, SpaR, InvA	Spa9, Spa24, Spa29, Spa40, MxiA
ATPase	InvC	Spa47

complex and catalyzes the release of the chaperones (7). The release of the chaperone from its cognate effector requires the hydrolysis of ATP (7). Studies with the flagellar apparatus suggest that the ATPase forms a complex with other proteins, which might regulate the hydrolysis of ATP and secretion of effectors (44). The *Shigella* ATPase Spa47 was also found to form complexes with cytoplasmic proteins MxiN, MxiK, and Spa33 (45, 46). The identities and functional roles of these proteins are poorly understood.

1.3.3. T3SS chaperones - T3SS chaperones are cytoplasmic proteins that bind to T3SS substrates and play several roles (9). T3SS chaperones are segregated into three classes based on the specific substrates they bind to (9). Class I chaperones bind to T3SS effectors and maintain them in a secretion-competent state within the bacterial cytoplasm. Class II chaperones bind to the two hydrophobic translocon proteins and partition them within the bacterial cytoplasm thereby preventing their premature degradation. Moreover, translocon proteins are toxic to the bacterial cell and the class II chaperones neutralize their toxicity. All class II chaperones contain 34-amino acid α -helical repeats called tetratricopeptide repeats (TPRs) (9). TPR motifs are also found in eukaryotic chaperones and promote protein-protein interactions. Class III chaperones bind to needle proteins and prevent their premature polymerization. The extracellular helical components of the *flagellum* and the needle proteins from *Yersinia*, *Pseudomonas*, and EPEC are recognized by specific class III chaperones (9). In contrast, no chaperones were identified for the needle proteins from *Salmonella*, *Shigella*, and *Burkholderia* (28).

T3SS chaperones bind to the chaperone-binding domain (CBD) present at the disordered N-terminus of their binding partners and allow them to be recognized by the export apparatus and the ATPase complex (7, 47). This might lead to an increase in the local concentration of the substrates at the basal body, which will promote their secretion through the needle apparatus (4).

T3SS chaperones are also thought to impose a secretion hierarchy by interacting with the export apparatus or ATPase complex with varying affinities. In the absence of their binding partners, the free chaperone might even inhibit transport through the T3SS. Some T3SS chaperones can stimulate or inhibit the membrane localization of their binding partners (4). There is also evidence suggesting that T3SS chaperones might act as transcriptional regulators (4).

1.3.4. T3SS effectors - Gram-negative animal pathogens use the T3SS to deliver six to twenty different effector proteins into the target cell (9). T3SS effectors perform two overall goals: host cytoskeletal rearrangements and modulation of the host immune response (48). Rearrangements in the host actin cytoskeleton can be caused by direct interaction of effectors with the cytoskeletal components leading to actin polymerization, bundling, and initiation of focal adhesion points (48). Effectors can also have enzymatic activity that promotes GDP/GTP nucleotide exchange in small GTPases like Rac1 and Cdc42 (48). In many cases, manipulation of the host cytoskeleton enables the pathogen to gain entry into nonphagocytotic host cells. Effectors can further influence cellular motility by targeting tubulin, kinesin, and vinculin (48). Depending upon the pathogen, host inflammatory responses can be stimulated or inhibited by T3SS effectors (48). For example, some T3SS effectors from *Salmonella* and *Shigella* (like SipB and IpaB respectively) are Interleukin-1 β -converting enzyme (ICE) cysteine proteases, which activate interleukins (49). These pathogens also activate NF- κ B, which releases proinflammatory cytokines like IL-8 (50, 51). In contrast, effectors delivered by *Yersinia* down regulate the host inflammatory response. For example, YopP blocks the release of tumor necrosis factor- α (TNF- α) by macrophages (52). T3SS effectors can also lead to a disturbance in the host immune system by triggering apoptosis of macrophages and through regulation of transcription (48). The list of effectors delivered by the T3SS is long and still incomplete (53).

1.4. The T3SSs of *Salmonella* & *Shigella*

1.4.1. Pathogenesis of *Salmonella* and *Shigella* - *Salmonella* and *Shigella* are rod-shaped Gram-negative bacteria belonging to the enterobacteriaceae family. All four species of *Shigella*, which include *S. flexneri*, *S. dysenteriae*, *S. boydii*, and *S. sonnei*, are responsible for Shigellosis (54). *Salmonella* has a more complicated classification and nomenclature. *Salmonella enterica* includes six subspecies, out of which *Salmonella enterica* subspecies *enterica* is further divided into serotypes Enteritidis, Typhimurium, Typhi, and Choleraesuis (54). *Salmonella enterica* subspecies *enterica* serotype Typhimurium is referred to as *Salmonella typhimurium* or simply *Salmonella* throughout this dissertation. *Salmonella typhimurium* is the causative agent of Salmonellosis.

Salmonella and *Shigella* are transmitted through the oral-fecal route. They enter the human body by means of contaminated food or water. Acid tolerance response (ATR) mechanisms allow the pathogens to survive the low pH inside the stomach and travel through the gastrointestinal tract (55, 56). *Salmonella* invades the small intestine (55), while *Shigella* invades the large intestine (56). The T3SS allows the uptake of bacteria by M cells of the host intestinal epithelium and also ensures the survival of bacteria within intracellular vacuoles. M cells are modified epithelial cells that sample the microenvironment of the host intestinal lumen. The M cells transcytose the bacteria to the basolateral side of the intestinal epithelium where they are taken up by macrophages (56). The two pathogens have slightly different fates upon phagocytosis. *Salmonella* takes up residence in *Salmonella*-containing vacuoles or SCVs within circulating macrophages and colonizes other organs such as the spleen and the liver (55). *Shigella*, on the other hand rapidly induces apoptosis in macrophages to ensure their survival

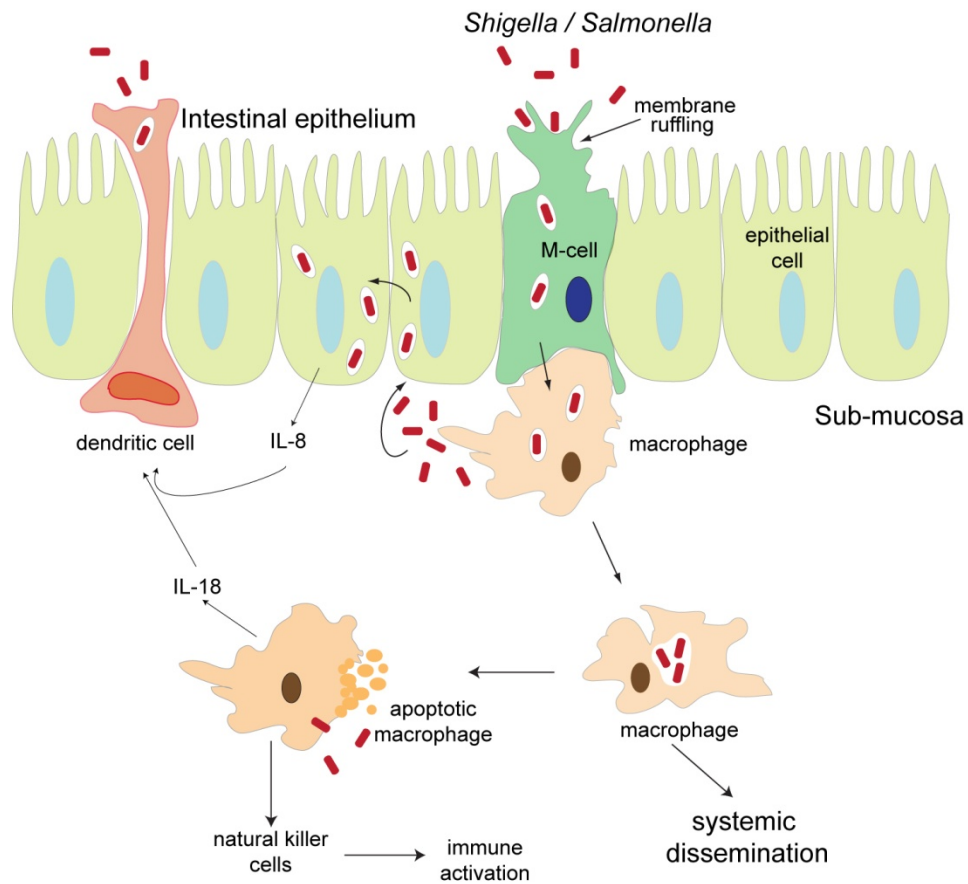


Figure 1-4: Pathogenesis of *Salmonella* (55) and *Shigella* (56). *Salmonella* and *Shigella* invade intestinal epithelial cells with the help of effectors that are injected into the host cell by a T3SS. The bacterium travels to the macrophage cells and induces apoptosis. *Salmonella* can travel to other organs like the spleen and kidneys through circulating macrophages. Bacteria within macrophages can induce apoptosis of macrophage which ultimately activates the host immune system.

(56). In both cases, induction of an acute and massive inflammatory response leads to the destruction of the intestinal epithelial tissue and causes symptoms characteristic of food-poisoning. The pathogenesis of *Salmonella* and *Shigella* is described in **Figure 1-4**. Symptoms for Salmonellosis and Shigellosis include severe diarrhea, fever, nausea, vomiting, abdominal cramps, and headaches. Shigellosis is further accompanied by rectal bleeding.

Salmonella are zoonotic parasites and infect humans and other non human animals. In contrast, *Shigella* infects primates and is more prevalent in developing countries. Together, *Salmonella* and *Shigella* are responsible for ~ 70,000 cases of food poisoning annually in the United States (57) and pose a major public health problem. In a healthy individual, the symptoms are usually resolved without medication in about 3-4 days. Severe cases can occur in children below 5 years of age, elderly, and immunocompromised individuals and are managed by oral rehydration and non specific antibiotics. No protective vaccines are available against *Salmonella typhimurium* and *Shigella* sp. and species resistant to the commonly used antibiotics are frequently encountered.

1.4.2. *Genetic organization of the T3SSs in Salmonella and Shigella* - Virulence-associated genes (like the T3SS) in bacteria are often placed in highly mobile clusters, which are subject to rapid horizontal transfer. These clusters are also known as pathogenicity islands and are characterized by unique nucleotide composition and codon usage as well as a high deletion frequency and the presence of insertion sequences (56).

Salmonella is known to contain up to five *Salmonella* pathogenicity islands (SPIs) containing genes for several different virulence determinants including T3SSs, flagella, adhesins, and genes for biofilm formation (55). SPI-1 and SPI-2 contain genes for two T3SSs named

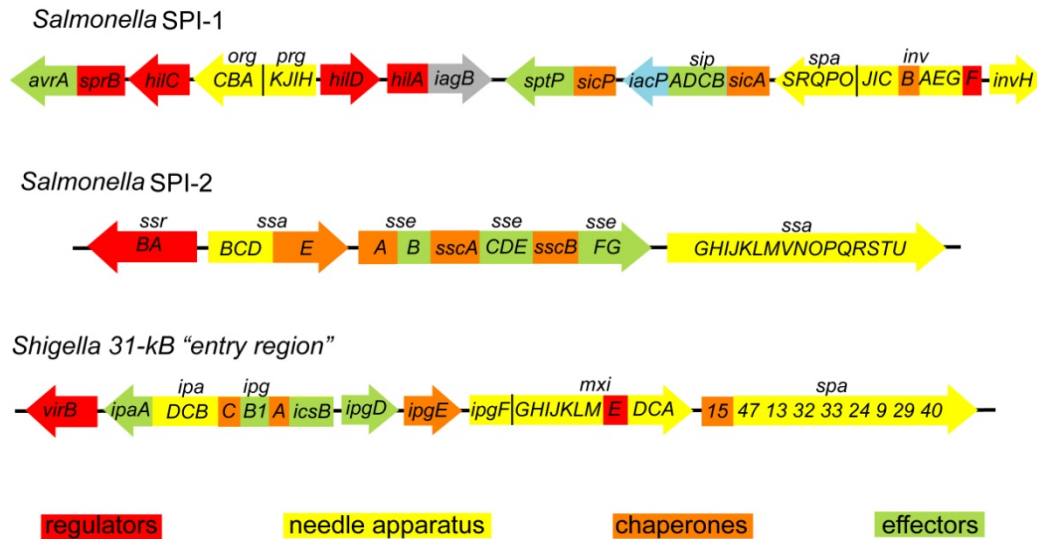


Figure 1-5: Genetic organization of the T3SSs in *Salmonella* (55) and *Shigella* (56). The T3SS is organized as clusters of genes according to the functional role played by their protein products.

T3SS-1 and T3SS-2 respectively. SPI-1 is positioned at centisome 63 in the chromosome of *Salmonella* where contiguous open reading frames code for proteins that form the structural and functional components of the T3SS (prg/org and inv/spa operons), T3SS effectors and translocon proteins (sic/sip operon) and also chaperones and other regulatory proteins. T3SS-1 secretes up to 13 different effector proteins which mediate actin cytoskeletal rearrangements in the host cell leading to the uptake of bacterial cells by intestinal M cells (55, 58). T3SS-1 effectors also signal the production of proinflammatory cytokines like IL-8 and TNF- α , which aids in propagation of infection by triggering the transmigration of neutrophils (55). Genes for the T3SS-2 are located at centisome 30 of the *Salmonella* chromosome and are arranged within four operons that code for regulatory proteins, structural proteins, effectors, and chaperones (59). T3SS-2 is activated by the low pH of the vacuolar environment inside the M cells (60). The primary goal of the effectors secreted through the T3SS-2 is to ensure the intracellular survival of the bacteria. In order to achieve this goal T3SS-2 effectors manipulate the host cytoskeleton and vesicular transport and prevent the action of antimicrobial host factors and enable the pathogen to acquire nourishment for growth and multiplication within the SCVs (60). The genetic loci coding for the T3SSs in *Salmonella* are depicted in **figure 1-5**. The coordination of T3SS-1 and T3SS-2 is complicated and has been reviewed elsewhere (61).

Genes for the T3SS in *Shigella* are located within a large virulence plasmid that is about 200 kb in size (56). The essential genes are located within a conserved 31-kb region called “entry region” whose products are required for entry into host cells and for macrophage cell death (56). T3SS genes in *Shigella* are also divided into four groups based on their function [**Figure 1-5**]. The first group codes for the ipa antigens, which are T3SS effectors and some components of the needle apparatus (tip complex and translocon). The second group contains genes for membrane

expression of ipa (mxi) and surface presentation of ipa (spa) antigens. These gene products assemble the T3SS (56). The plasmid also codes T3SS chaperones and transcriptional activators (regulators) for T3SS genes.

1.4.3. The needle apparatus of Salmonella and Shigella - The needle apparatus of *Salmonella* and *Shigella* retain the substructures that are conserved across all T3SS families. The basal body is composed of an IM ring, an OM ring, and an inner rod. In *Salmonella*, the proteins PrgH and PrgK form the IM ring, InvG forms the OM ring, and PrgJ forms the inner rod (10). The *Shigella* counterparts of these proteins are MxiJ and MxiG (IM ring), MxiD (OM ring), and MxiI (inner rod) (62). The proteins forming the needle apparatus of *Salmonella* and *Shigella* are listed in **Table 2**. The OM ring is estimated to have 12-15 fold symmetry and is assembled by InvG in *Salmonella* and MxiD in *Shigella* (10, 63). These proteins belong to the secretin family of membrane proteins, which are highly conserved not only across T3SSs but also in flagella, T2SS, and type IV pili (63). These proteins have a conserved protease-resistant C-terminal domain with a β -barrel structure known as the secretin fold (64). This domain forms the membrane-embedded portion of the OM ring while, the N-terminal periplasmic domain forms the neck region of the OM ring (10, 63). The neck region reaches deep into the periplasm and might help attach the OM ring to the IM ring (10) [**Figure 1-2**]. Secretins require a small lipidated protein called a pilotin which assists in the assembly of the OM ring (64). The IM ring has a 24-fold symmetry and consists of two concentric rings called the outer-IM ring and the inner-IM ring (10, 62). PrgK and MxiJ are periplasmic lipoproteins that form the inner-IM rings in *Salmonella* and *Shigella* respectively (6). The structure of EscJ from EPEC, which is a homolog of PrgK and MxiJ, shows that these proteins contain two mixed α/β domains connected by a flexible linker (65). *Salmonella* PrgH and *Shigella* MxiG form the outer IM ring and

contain an N-terminal cytoplasmic domain and a C-terminal periplasmic domain (63). The C-terminal periplasmic domain of PrgH is boot-shaped with three α/β domains connected by flexible linkers (63). The structure of the N-terminal cytoplasmic domain of MxiG is also known and was shown to bear resemblance to the forkhead-associated (FHA) domains, which are known to bind phosphothreonine and function in cell signaling pathways (66). However, the FHA-like domain of MxiG lacks conserved residues and does not bind phosphothreonine (66). All the proteins forming the basal body rings contain α/β domains connected by flexible linkers (63). These α/β domain contain two α -helices folded against a β -sheet and are a conserved structural motif in the proteins forming the basal body. It is possible that symmetrical ring structures are assembled using the α/β domain as a common ring-forming unit while, the variation in sequence allows for rings with varying sizes, stoichiometry, and unique surface features adapted to the specific physiology of the bacterial species (63). In contrast to the well folded globular domains present in the ring forming proteins, *Salmonella* PrgJ, which forms the inner rod in *Salmonella*, adopts a partially folded α -helical conformation (16).

The needles from *Salmonella* and *Shigella* have been subjected to extensive structural analysis (17, 18, 21, 22, 67). The *Salmonella* needle is polymerized from the *Salmonella* needle protein PrgI and the *Shigella* needle is polymerized from the *Shigella* needle protein MxiH. PrgI and MxiH are small α -helical hairpins with flexible termini (18, 19, 68). The tendency of the full length recombinant needle proteins to polymerize *in vitro* initially prevented their structure determination. However, it was found that deletion of five residues from the extreme C-terminus rendered these proteins unable to polymerize into needles both *in vitro* and inside the bacterial cell (20). The structures of PrgI^{C Δ 5} (19) and MxiH^{C Δ 5} (18) were then determined using NMR spectroscopy and X-ray crystallography respectively. Several different methods have been used

to generate needle models with both common and divergent features. Initially, three-dimensional reconstructions of the *Shigella* (69) and *Salmonella* (21) needles were reported using a combination of X-ray fiber diffraction and electron microscopy for *Shigella* and cryo-electron microscopy (cryo-EM) for *Salmonella*. The crystal structures of MxiH^{CA5} and PrgI^{CA5} were fitted into the *Shigella* (18) and *Salmonella* needle models respectively. The *Shigella* needle had an outer diameter of 70 Å and had an inner channel that was ~ 20 Å wide (17). The *Salmonella* needle was slightly wider with an outer diameter of 85 Å and an inner channel of 25 Å (21). However, the major difference between the two needles was that while, the *Shigella* needle had 5.6 subunits/turn the *Salmonella* needle was reported to have 6.3 subunits/turn (21). Higher resolution atomic models of the *Shigella* needle using cryo-EM (22) and the *Salmonella* needle using solid state NMR (ssNMR) (23) have been reported recently [Figure 1-6]. These models have major differences. The *Shigella* needle was polymerized from overexpression of recombinant full length MxiH, which formed an N-terminal α -helix facing the needle lumen, a loop facing the outer surface, and two short C-terminal α -helices with a β -hairpin in between lining the outer surface of the needle (22). The β -hairpin was formed by residues 51-64 and was suggested to act as a linchpin to stabilize the needle protein monomers within the polymerized needle (22). The *Salmonella* needle was also polymerized from full length recombinant needle protein PrgI, but in complete contrast to MxiH, the N-terminal helix of PrgI formed the outer surface of the needle with the extreme N-terminus adopting an extended conformation, while the C-terminal helix lined the needle lumen (23). It is uncertain why the needles of *Salmonella* and *Shigella*, which have homologous T3SSs, would assemble needles with completely contradictory features. Nonetheless, these observations imply that the other components of the *Shigella* and *Salmonella* needle apparatus, particularly the tip complex and the translocon, might also

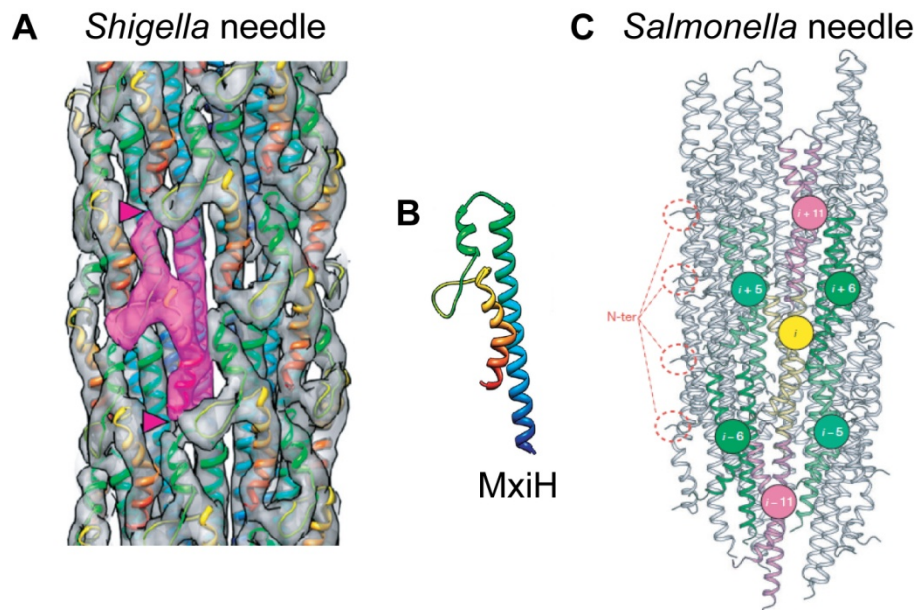


Figure 1-6: Models of the *Shigella* and *Salmonella* needles. (A) Three-dimensional reconstruction of the *Shigella* needle solved by cryo-EM (22). One monomer of MxiH is highlighted in pink. (B) The conformation of MxiH within the assembled needle. The N-terminus of MxiH faces the needle lumen and the C-terminus forms a β -turn. (A) and (B) From Fujii T., Cheung M., Blanco A., Kato T., Blocker A., Namba K., Structure of a type III secretion needle at 7 Å resolution provides insights into its assembly and signaling mechanisms, *Proc Natl Acad Sci.*, 2012 Mar 20; 109:4461-6. PNAS permits the use of original figures or tables published in PNAS for noncommercial and educational use. (C) A model of the *Salmonella* needle determined using solid state NMR, electron microscopy, and computational modeling (23). The N-terminus of PrgI faces the exterior of the needle. Reprinted by permission from Macmillan Publishers Ltd: [Nature May 20; 486: 276-9](#), © copyright 2012 Nature.

assemble with different structural features and using different mechanisms. The tip complex and the translocon are the major foci of this dissertation and are discussed in the following sections.

1.5. Studies on the tip complex of Salmonella and Shigella

1.5.1. Crystal structure of the Salmonella tip protein SipD - The tip complex is formed by the tip protein SipD (23) in *Salmonella* and IpaD in *Shigella* (28). The *ipaD* gene was discovered within the *ipa* locus along with the genes for the translocon proteins *ipaB* and *ipaC*, their chaperone *ipgC*, and the effector protein *ipaA* (70, 71). These proteins were termed *ipa* for invasion plasmid antigens because their gene products elicited a strong immune response during Shigellosis (72). Nonpolar deletion of *ipaD* rendered *Shigella* entry-deficient but secretion-competent (71). This meant that IpaD was required for entry into intestinal epithelial cells but not for the secretion of effectors. Further, deletion of *ipaD* led to an increase in the secretion of effectors suggesting that IpaD is involved in blocking the secretion of effectors (71). The *sipD* gene was discovered in *Salmonella* soon after and was found to bear high sequence identity with *ipaD* (73). Deletion of *sipD* showed a similar phenotype where *Salmonella* was entry-deficient but showed increased secretion of effectors (73). Transmission electron microscopy of immunogold labeled IpaD showed that it docks at the tip of the *Shigella* needles (25). Extensive mutagenesis revealed that IpaD has at least two roles (74). Loss of function mutations of IpaD lead to constitutive secretion of effectors in the absence of an inducer and *Shigella* was unable to form translocation pores and was thus non-invasive (74). However, these two roles were found to be independent of each other suggesting that IpaD has distinct functional domains (74). Biophysical characterization revealed that IpaD was highly soluble and predominantly α -helical with a biphasic thermal denaturation profile further confirming the presence of discrete domains that folded independently (75). The crystal structure of IpaD showed that the tip protein had an

N-terminal α -helical hairpin domain, a central coiled coil and a C-terminal domain containing both α -helices and β -sheets (28). A comparison with the structures of the homologous tip protein BipD (29) from *Burkholderia* and the *Yersinia* tip protein LcrV (30) showed that the coiled coil is conserved in other tip proteins while the N-terminal α -helical hairpin was unique to IpaD and BipD (28). The tip proteins assemble the tip complex on the needle and are thus exposed on the bacterial surface. Preliminary evidence shows that tip proteins have the potential to be adapted into T3SS-based protective vaccines (76-79). Therefore, structural and functional studies on the tip proteins provide a scope for the development of protective vaccines to combat pathogens that harbor a T3SS. *Salmonella* SipD is ~35% identical and ~50% similar to IpaD. Despite having close sequence similarity, SipD is unable to substitute for IpaD in the T3SS of *Shigella* (74). Therefore, the atomic structure of SipD was required in order to investigate the functional roles of SipD and analyze its molecular interactions with other components of the needle apparatus of *Salmonella* and thereby gain insight into the function of the tip complex. The determination of the atomic structure of SipD is described herein. Further, the functional significance of the different domains within SipD was probed by making short deletions and testing their effect on the ability of *Salmonella* to invade human intestinal epithelial cells. Structural and functional studies on SipD are described in chapter 3.

1.5.2. The interaction between SipD and bile salts - One of the roles of the tip complex is that of a negative regulator of effector secretion. This logically implies that the tip is also involved in receiving and translating the activation signal in order to trigger effector secretion. As the tip complex is exposed to the bacterial surface it is well suited to act as an environmental sensor. One way in which the tip complex could sample the microenvironment within the host is by sensing or responding to small molecules. In fact, small molecules are known to affect the

T3SS. For example, the presence of calcium in *Yersinia* blocks secretion through the needle (80). In another example, the presence of the small dye Congo red in *Shigella* mimics contact with host cells and induces the secretion of effectors through the T3SS needle (81). However, the mechanism by which the T3SS in these bacteria are regulated in response to small molecules is poorly understood. Several studies have demonstrated how small molecule could be utilized to inhibit the secretion of effectors through the T3SS of *Salmonella* (82), *Shigella* (83), *Yersinia* (84, 85), and *Chlamydia* (86). Hence, investigation of the interaction between small molecules and components of the T3SS could produce valuable information about T3SS function that can then be exploited for the development of therapeutics.

Bile salts are known to influence the physiology of non-pathogenic and pathogenic intestinal bacteria (87). Bile salts suppress the invasiveness of *Salmonella* but stimulate that of *Shigella* (88, 89). Further, the tip proteins SipD and IpaD can directly bind to the bile salt deoxycholate (90). However, the mechanism of interaction between bile salts and the tip proteins was unknown. SipD was thus crystallized in complex with the bile salts deoxycholate and chenodeoxycholate. The crystal structures of SipD bound to deoxycholate and chenodeoxycholate were the first to describe the interaction between any T3SS tip protein and a small molecule such as bile salt. Further, the effect of deoxycholate on the invasiveness of *Salmonella* and the secretion of the translocon protein SipB were analyzed. The interaction between SipD and deoxycholate is discussed in chapter 4.

1.5.3. The interaction between the Shigella tip protein and the needle protein - A 20 Å resolution three-dimensional reconstruction of the Shigella tip complex shows five IpaD molecules assembled at the tip of the Shigella needle (27). Similar structures of the Yersinia tip complex were also reported (26). The tip complex of Yersinia showed a distinct division into

head, neck, and base substructures (26). This characteristic helped in the orientation of the tip proteins within the *Yersinia* tip complex where the N-terminal domain of *Yersinia* LcrV formed the base while the C-terminal domain formed the head substructure (91). However, such a distinct division was absent in the tip complex of *Shigella* possibly because the N- and C-terminal domains in *Shigella* IpaD adopt are elongated as opposed to the globular domains in LcrV (28). Therefore, the exact orientation of IpaD within the tip complex is unclear. Deletion of residues at the extreme C-terminus of IpaD prevents the formation of the tip complex in *Shigella* (74). However, it is not known if the C-terminus is required for tip-tip interaction or needle-tip interaction. Further, how the IpaD tip complex blocks the secretion of effectors prior to contact with the host cell and the mechanism by which this negative regulation is relieved are unknown. It was suggested that contact with the host cell membrane triggers a conformational change within the tip complex (28). This conformational change is then relayed down the needle apparatus and leads to secretion of effectors. Detailed knowledge about the binding interfaces between the tip and needle proteins is required to understand the mechanism that regulates the secretion of effectors. However, attachment and entry of *Shigella* into host cells is rapid process and the tip complex and translocon are thus transient structural features. Therefore, it is challenging to obtain atomic resolution models of the tip complex using electron microscopy. We have therefore employed NMR spectroscopy to study the direct interaction between the tip protein IpaD and the needle protein MxiH. NMR spectroscopy was previously used to identify the binding site of the *Salmonella* needle protein PrgI on the tip protein SipD (92). However, *Salmonella* PrgI and *Shigella* MxiH were reported to form needles with drastic structural contrasts (22, 23). MxiH assembled needles with its N-terminal helix lining the needle lumen while, PrgI needles were assembled with the C-terminal helix towards the needle lumen [Figure

1-6]. Further, unlike PrgI the C-terminus of MxiH within the polymerized needle folded into three structural features: a short α -helix followed by a β -hairpin and a bent α -helix (22). These differences suggest that the tip proteins *Salmonella* SipD and *Shigella* IpaD might bind differently to their respective needle proteins. The PRE technique was used in order to locate the binding site of MxiH on IpaD. The studies on the interaction between IpaD and MxiH are described in chapter 7.

1.6. Studies on the *Salmonella* translocon protein SipB

The translocon is one of the least understood components of the T3SS. Translocon proteins SipB and SipC assemble the translocon of *Salmonella* and translocon proteins IpaB and IpaC assemble the translocon in *Shigella* (32). *Salmonella* SipB and *Shigella* IpaB are ~ 62 kD in size and contain two transmembrane helices. These are known as the major translocon proteins (94). The minor translocon proteins *Salmonella* SipC and *Shigella* IpaC are ~ 40 kD in size and contain one transmembrane helix (95). Nonpolar knockouts of the translocon proteins in *Salmonella* prevent bacterial entry and the translocation of effectors into the host cell (32). Deletion of the *Shigella* translocon proteins also produces a similar phenotype (71). In addition, deletion of *Shigella* IpaB also causes increased secretion of effectors (71). This suggests that *Shigella* IpaB plays the additional role of blocking premature effector secretion along with the tip protein IpaD. Not only are the translocon proteins crucial for the formation of the translocation pore [Figure 1-4] within the host cell membrane, but they are themselves translocated into the host cell cytoplasm where they act as effectors and interact with the actin cytoskeleton (96-99). Their role as effectors is key for bacterial entry into the host cells because latex beads coated with IpaB and IpaC can be internalized by *Shigella* (100). Further, IpaB and IpaC along with IpaD are required for the contact-dependent hemolytic activity of *Shigella* (12). Deletion of

SipB and SipC also affected contact-mediated lysis of RBC by *Salmonella* (34). In both cases RBC lysis occurred due to the formation of ~25-35 Å wide pores within the cell membrane. Thus, the translocon punctures holes in the host cell membrane. These translocation pores then act as a gateway for the entry of the translocon proteins and other effectors that induce cytoskeletal rearrangements and lead to internalization of *Shigella* and *Salmonella*.

The translocon is critical for initiation of infection by *Salmonella*, *Shigella*, and other T3SS – harboring pathogens. Therefore lack of structural and functional information regarding the translocon hinders the full understanding of how the T3SS functions. Immunofluorescence microscopy of *Salmonella* showed that SipB and SipC colocalize with the tip protein SipD on the bacterial surface after contact with the host cell (33). Moreover, in both *Shigella* and *Salmonella* the tip protein is necessary for the formation of the translocation pore (12, 34, 73). In *Shigella*, IpaB was shown to dock at the needle tip along with IpaD (90). Therefore, the tip complex might act as a platform for the assembly of the translocon and its correct insertion into the host cell membrane (101). However, because of the transient nature of the translocon and the rapid internalization of *Salmonella* into the host cells structural information on the translocon has been scarce (33, 71). NMR and CD spectroscopy were used to perform preliminary structural analysis of a hydrophilic, folded domain at the N-terminus of the *Salmonella* translocon protein SipB. In order to assemble on the tip complex platform, the translocon needs to attach itself on the tip complex. However, it is not known how the translocon attaches to the tip complex. The tip complex is hydrophilic in nature while, the translocon contains hydrophobic helices. Therefore, a hydrophilic domain at one end of SipB would be a suitable target to bind to the tip complex. In order to test this hypothesis, NMR spectroscopy and PRE were used to analyze the binding between the *Salmonella* tip protein SipD and the translocon protein SipB. This dissertation

includes the first description of how a tip protein binds to a translocon protein. Structural studies on SipB are described in chapter 5, while the interaction between SipD and SipB is described in chapter 6.

1.7. References

1. Gerlach, R. G., and Hensel, M. (2007) Protein secretion systems and adhesins: the molecular armory of Gram-negative pathogens, *International journal of medical microbiology : IJMM* 297, 401-415.
2. Galan, J. E., and Bliska, J. B. (1996) Cross-talk between bacterial pathogens and their host cells, *Annu Rev Cell Dev Biol* 12, 221-255.
3. Hayes, C. S., Aoki, S. K., and Low, D. A. (2010) Bacterial contact-dependent delivery systems, *Annu Rev Genet* 44, 71-90.
4. Buttner, D. (2012) Protein export according to schedule: architecture, assembly, and regulation of type III secretion systems from plant- and animal-pathogenic bacteria, *Microbiology and molecular biology reviews : MMBR* 76, 262-310.
5. Wagner, S., Konigsmair, L., Lara-Tejero, M., Lefebvre, M., Marlovits, T. C., and Galan, J. E. (2010) Organization and coordinated assembly of the type III secretion export apparatus, *Proc. Natl. Acad. Sci. U.S.A.* 107, 17745-17750.
6. Chatterjee, S., Chaudhury, S., McShan, A. C., Kaur, K., and De Guzman, R. N. (2013) Structure and Biophysics of Type III Secretion in Bacteria, *Biochemistry* 52, 2508-2517.
7. Akeda, Y., and Galan, J. E. (2005) Chaperone release and unfolding of substrates in type III secretion, *Nature* 437, 911-915.
8. Marlovits, T. C., and Stebbins, C. E. (2010) Type III secretion systems shape up as they ship out, *Curr Opin Microbiol* 13, 47-52.

9. Cornelis, G. R. (2006) The type III secretion injectisome, *Nat. Rev. Microbiol.* 4, 811-825.
10. Schraidt, O., and Marlovits, T. C. (2011) Three-dimensional model of Salmonella's needle complex at subnanometer resolution, *Science* 331, 1192-1195.
11. Kubori, T., Matsushima, Y., Nakamura, D., Uralil, J., Lara-Tejero, M., Sukhan, A., Galan, J. E., and Aizawa, S. I. (1998) Supramolecular structure of the *Salmonella typhimurium* type III protein secretion system, *Science* 280, 602-605.
12. Blocker, A., Gounon, P., Larquet, E., Niebuhr, K., Cabiliax, V., Parsot, C., and Sansonetti, P. (1999) The tripartite type III secretion system of *Shigella flexneri* inserts IpaB and IpaC into host membranes, *J. Cell Biol.* 147, 683-693.
13. Cornelis, G. R. (2002) *Yersinia* type III secretion: send in the effectors, *J. Cell Biol.* 158, 401-408.
14. Sekiya, K., Ohishi, M., Ogino, T., Tamano, K., Sasakawa, C., and Abe, A. (2001) Supermolecular structure of the enteropathogenic *Escherichia coli* type III secretion system and its direct interaction with the EspA-sheath-like structure, *Proc Natl Acad Sci USA* 98, 11638-11643.
15. Pastor, A., Chabert, J., Louwagie, M., Garin, J., and Attree, I. (2005) PscF is a major component of the *Pseudomonas aeruginosa* type III secretion needle, *FEMS Microbiol. Lett.* 253, 95-101.
16. Zhong, D., Lefebvre, M., Kaur, K., McDowell, M. A., Gdowski, C., Jo, S., Wang, Y., Benedict, S. H., Lea, S. M., Galan, J. E., and De Guzman, R. N. (2012) The *Salmonella* Type III Secretion System Inner Rod Protein PrgJ Is Partially Folded, *J. Biol. Chem.* 287, 25303-25311.

17. Cordes, F. S., Komoriya, K., Larquet, E., Yang, S., Egelman, E. H., Blocker, A., and Lea, S. M. (2003) Helical structure of the needle of the type III secretion system of *Shigella flexneri*, *J. Biol. Chem.* 278, 17103-17107.
18. Deane, J. E., Roversi, P., Cordes, F. S., Johnson, S., Kenjale, R., Daniell, S., Booy, F., Picking, W. D., Picking, W. L., Blocker, A. J., and Lea, S. M. (2006) Molecular model of a type III secretion system needle: Implications for host-cell sensing, *Proc. Natl. Acad. Sci. U.S.A.* 103, 12529-12533.
19. Wang, Y., Ouellette, A. N., Egan, C. E., Rathinavelan, T., Im, W., and De Guzman, R. N. (2007) Differences in the electrostatic surfaces of the type III secretion needle proteins PrgI, BsaL, and MxiH, *J. Mol. Biol.* 371, 1304-1314.
20. Kenjale, R., Wilson, J., Zenk, S. F., Saurya, S., Picking, W. L., Picking, W. D., and Blocker, A. (2005) The needle component of the type III secretion system of *Shigella* regulates the activity of the secretion apparatus, *J. Biol. Chem.* 280, 42929-42937.
21. Galkin, V. E., Schmied, W. H., Schraidt, O., Marlovits, T. C., and Egelman, E. H. (2010) The structure of the *Salmonella typhimurium* type III secretion system needle shows divergence from the flagellar system, *J. Mol. Biol.* 396, 1392-1397.
22. Fujii, T., Cheung, M., Blanco, A., Kato, T., Blocker, A. J., and Namba, K. (2012) Structure of a type III secretion needle at 7-A resolution provides insights into its assembly and signaling mechanisms, *Proc. Natl. Acad. Sci. U.S.A.* 109, 4461-4466.
23. Loquet, A., Sgourakis, N. G., Gupta, R., Giller, K., Riedel, D., Goosmann, C., Griesinger, C., Kolbe, M., Baker, D., Becker, S., and Lange, A. (2012) Atomic model of the type III secretion system needle, *Nature* 486, 276-279.

24. Deane, J. E., Abrusci, P., Johnson, S., and Lea, S. M. (2010) Timing is everything: the regulation of type III secretion, *Cell Mol Life Sci* 67, 1065-1075.
25. Espina, M., Olive, A. J., Kenjale, R., Moore, D. S., Ausar, S. F., Kaminski, R. W., Oaks, E. V., Middaugh, C. R., Picking, W. D., and Picking, W. L. (2006) IpaD localizes to the tip of the type III secretion system needle of *Shigella flexneri*, *Infect. Immun.* 74, 4391-4400.
26. Mueller, C. A., Broz, P., Muller, S. A., Ringler, P., Erne-Brand, F., Sorg, I., Kuhn, M., Engel, A., and Cornelis, G. R. (2005) The V-antigen of *Yersinia* forms a distinct structure at the tip of injectisome needles, *Science* 310, 674-676.
27. Epler, C. R., Dickenson, N. E., Bullitt, E., and Picking, W. L. (2012) Ultrastructural Analysis of IpaD at the Tip of the Nascent MxiH Type III Secretion Apparatus of *Shigella flexneri*, *J. Mol. Biol.* 420, 29-39.
28. Johnson, S., Roversi, P., Espina, M., Olive, A., Deane, J. E., Birket, S., Field, T., Picking, W. D., Blocker, A. J., Galyov, E. E., Picking, W. L., and Lea, S. M. (2007) Self-chaperoning of the type III secretion system needle tip proteins IpaD and BipD, *J. Biol. Chem.* 282, 4035-4044.
29. Erskine, P. T., Knight, M. J., Ruaux, A., Mikolajek, H., Wong Fat Sang, N., Withers, J., Gill, R., Wood, S. P., Wood, M., Fox, G. C., and Cooper, J. B. (2006) High Resolution Structure of BipD: An Invasion Protein Associated with the Type III Secretion System of *Burkholderia pseudomallei*, *J. Mol. Biol.* 363, 125-136.
30. Derewenda, U., Mateja, A., Devedjiev, Y., Routzahn, K. M., Evdokimov, A. G., Derewenda, Z. S., and Waugh, D. S. (2004) The structure of *Yersinia pestis* V-antigen, an

- essential virulence factor and mediator of immunity against plague, *Structure* 12, 301-306.
31. Blocker, A. J., Deane, J. E., Veenendaal, A. K., Roversi, P., Hodgkinson, J. L., Johnson, S., and Lea, S. M. (2008) What's the point of the type III secretion system needle?, *Proc. Natl. Acad. Sci. U.S.A.* 105, 6507-6513.
 32. Kaniga, K., Tucker, S., Trollinger, D., and Galan, J. E. (1995) Homologs of the Shigella IpaB and IpaC invasins are required for *Salmonella typhimurium* entry into cultured epithelial cells, *J.Bacteriol.* 177, 3965-3971.
 33. Lara-Tejero, M., and Galan, J. E. (2009) *Salmonella enterica* serovar typhimurium pathogenicity island 1-encoded type III secretion system translocases mediate intimate attachment to nonphagocytic cells, *Infect. Immun.* 77, 2635-2642.
 34. Miki, T., Okada, N., Shimada, Y., and Danbara, H. (2004) Characterization of *Salmonella* pathogenicity island 1 type III secretion-dependent hemolytic activity in *Salmonella enterica* serovar Typhimurium, *Microb. Pathog.* 37, 65-72.
 35. Ide, T., Laarmann, S., Greune, L., Schillers, H., Oberleithner, H., and Schmidt, M. A. (2001) Characterization of translocation pores inserted into plasma membranes by type III-secreted Esp proteins of enteropathogenic *Escherichia coli*, *Cell. Microbiol.* 3, 669-679.
 36. Barta, M. L., Dickenson, N. E., Patil, M., Keightley, A., Wyckoff, G. J., Picking, W. D., Picking, W. L., and Geisbrecht, B. V. (2012) The structures of coiled coil domains from type III secretion system translocators reveal homology to pore-forming toxins, *J Mol Biol* 417, 395-405.

37. Wiesand, U., Sorg, I., Amstutz, M., Wagner, S., van den Heuvel, J., Luhrs, T., Cornelis, G. R., and Heinz, D. W. (2009) Structure of the type III secretion recognition protein YscU from *Yersinia enterocolitica*, *J Mol Biol* 385, 854-866.
38. Deane, J. E., Graham, S. C., Mitchell, E. P., Flot, D., Johnson, S., and Lea, S. M. (2008) Crystal structure of Spa40, the specificity switch for the *Shigella flexneri* type III secretion system, *Mol Microbiol* 69, 267-276.
39. Zarivach, R., Deng, W., Vuckovic, M., Felise, H. B., Nguyen, H. V., Miller, S. I., Finlay, B. B., and Strynadka, N. C. (2008) Structural analysis of the essential self-cleaving type III secretion proteins EscU and SpaS, *Nature* 453, 124-127.
40. Diepold, A., Amstutz, M., Abel, S., Sorg, I., Jenal, U., and Cornelis, G. R. (2010) Deciphering the assembly of the *Yersinia* type III secretion injectisome, *EMBO J* 29, 1928-1940.
41. Worrall, L. J., Vuckovic, M., and Strynadka, N. C. (2010) Crystal structure of the C-terminal domain of the *Salmonella* type III secretion system export apparatus protein InvA, *Protein. Sci.* 19, 1091-1096.
42. Abrusci, P., Vergara-Irigaray, M., Johnson, S., Beeby, M. D., Hendrixson, D. R., Roversi, P., Friede, M. E., Deane, J. E., Jensen, G. J., Tang, C. M., and Lea, S. M. (2013) Architecture of the major component of the type III secretion system export apparatus, *Nat Struct Mol Biol* 20, 99-104.
43. Zarivach, R., Vuckovic, M., Deng, W., Finlay, B. B., and Strynadka, N. C. (2007) Structural analysis of a prototypical ATPase from the type III secretion system, *Nat Struct Mol Biol* 14, 131-137.

44. Minamino, T., and MacNab, R. M. (2000) FliH, a soluble component of the type III flagellar export apparatus of Salmonella, forms a complex with FliI and inhibits its ATPase activity, *Mol Microbiol* 37, 1494-1503.
45. Jouihri, N., Sory, M. P., Page, A. L., Gounon, P., Parsot, C., and Allaoui, A. (2003) MxiK and MxiN interact with the Spa47 ATPase and are required for transit of the needle components MxiH and MxiI, but not of Ipa proteins, through the type III secretion apparatus of Shigella flexneri, *Mol Microbiol* 49, 755-767.
46. Johnson, S., and Blocker, A. (2008) Characterization of soluble complexes of the Shigella flexneri type III secretion system ATPase, *FEMS Microbiol Lett* 286, 274-278.
47. Lunelli, M., Lokareddy, R. K., Zychlinsky, A., and Kolbe, M. (2009) IpaB-IpgC interaction defines binding motif for type III secretion translocator, *Proc. Natl. Acad. Sci. U.S.A.* 106, 9661-9666.
48. Cornelis, G. R., and Van Gijsegem, F. (2000) Assembly and function of type III secretory systems, *Annu. Rev. Microbiol.* 54, 735-774.
49. Hersh, D., Monack, D. M., Smith, M. R., Ghori, N., Falkow, S., and Zychlinsky, A. (1999) The Salmonella invasin SipB induces macrophage apoptosis by binding to caspase-1, *Proc Natl Acad Sci U S A* 96, 2396-2401.
50. Hobbie, S., Chen, L. M., Davis, R. J., and Galan, J. E. (1997) Involvement of mitogen-activated protein kinase pathways in the nuclear responses and cytokine production induced by Salmonella typhimurium in cultured intestinal epithelial cells, *J Immunol* 159, 5550-5559.
51. Nhieu, G. T., and Sansonetti, P. J. (1999) Mechanism of Shigella entry into epithelial cells, *Curr Opin Microbiol* 2, 51-55.

52. Boland, A., and Cornelis, G. R. (1998) Role of YopP in suppression of tumor necrosis factor alpha release by macrophages during Yersinia infection, *Infect Immun* 66, 1878-1884.
53. Galan, J. E. (2007) SnapShot: effector proteins of type III secretion systems, *Cell* 130, 192.
54. Brenner, F. W., Villar, R. G., Angulo, F. J., Tauxe, R., and Swaminathan, B. (2000) Salmonella nomenclature, *J Clin Microbiol* 38, 2465-2467.
55. Fabrega, A., and Vila, J. (2013) Salmonella enterica serovar Typhimurium skills to succeed in the host: virulence and regulation, *Clin Microbiol Rev* 26, 308-341.
56. Schroeder, G. N., and Hilbi, H. (2008) Molecular pathogenesis of Shigella spp.: controlling host cell signaling, invasion, and death by type III secretion, *Clin. Microbiol. Rev.* 21, 134-156.
57. CDC. (2012) Summary of Notifiable Diseases - United States, 2010, *Morbidity and Mortality Weekly Report* 59.
58. Zhou, D., and Galan, J. (2001) *Salmonella* entry into host cells: the work in concert of type III secreted effector proteins, *Microbes. Infect.* 3, 1293-1298.
59. Waterman, S. R., and Holden, D. W. (2003) Functions and effectors of the Salmonella pathogenicity island 2 type III secretion system, *Cell Microbiol* 5, 501-511.
60. Sherry, A. E., Inglis, N. F., Stevenson, A., Fraser-Pitt, D., Everest, P., Smith, D. G., and Roberts, M. (2011) Characterisation of proteins extracted from the surface of Salmonella Typhimurium grown under SPI-2-inducing conditions by LC-ESI/MS/MS sequencing, *Proteomics* 11, 361-370.

61. Moest, T. P., and Meresse, S. (2013) Salmonella T3SSs: successful mission of the secret(ion) agents, *Curr Opin Microbiol* 16, 38-44.
62. Hodgkinson, J. L., Horsley, A., Stabat, D., Simon, M., Johnson, S., da Fonseca, P. C., Morris, E. P., Wall, J. S., Lea, S. M., and Blocker, A. J. (2009) Three-dimensional reconstruction of the Shigella T3SS transmembrane regions reveals 12-fold symmetry and novel features throughout, *Nat Struct Mol Biol* 16, 477-485.
63. Spreter, T., Yip, C. K., Sanowar, S., Andre, I., Kimbrough, T. G., Vuckovic, M., Pfuetzner, R. A., Deng, W., Yu, A. C., Finlay, B. B., Baker, D., Miller, S. I., and Strynadka, N. C. (2009) A conserved structural motif mediates formation of the periplasmic rings in the type III secretion system, *Nat Struct Mol Biol* 16, 468-476.
64. Okon, M., Moraes, T. F., Lario, P. I., Creagh, A. L., Haynes, C. A., Strynadka, N. C., and McIntosh, L. P. (2008) Structural characterization of the type-III pilot-secretin complex from Shigella flexneri, *Structure* 16, 1544-1554.
65. Crepin, V. F., Prasannan, S., Shaw, R. K., Wilson, R. K., Creasey, E., Abe, C. M., Knutton, S., Frankel, G., and Matthews, S. (2005) Structural and functional studies of the enteropathogenic Escherichia coli type III needle complex protein EscJ, *Mol. Microbiol.* 55, 1658-1670.
66. McDowell, M. A., Johnson, S., Deane, J. E., Cheung, M., Roehrich, A. D., Blocker, A. J., McDonnell, J. M., and Lea, S. M. (2011) Structural and functional studies on the N-terminal domain of the Shigella type III secretion protein MxiG, *J. Biol. Chem.* 286, 30606-30614.

67. Loquet, A., Lv, G., Giller, K., Becker, S., and Lange, A. (2011) ^{13}C spin dilution for simplified and complete solid-state NMR resonance assignment of insoluble biological assemblies, *J Am Chem Soc* 133, 4722-4725.
68. Poyraz, O., Schmidt, H., Seidel, K., Delissen, F., Ader, C., Tenenboim, H., Goosmann, C., Laube, B., Thunemann, A. F., Zychlinsky, A., Baldus, M., Lange, A., Griesinger, C., and Kolbe, M. (2010) Protein refolding is required for assembly of the type three secretion needle, *Nat. Struct. Mol. Biol.* 17, 788-792.
69. Cordes, F. S., Daniell, S., Kenjale, R., Saurya, S., Picking, W. L., Picking, W. D., Booy, F., Lea, S. M., and Blocker, A. (2005) Helical packing of needles from functionally altered *Shigella* type III secretion systems, *J. Mol. Biol.* 354, 206-211.
70. Buysse, J. M., Stover, C. K., Oaks, E. V., Venkatesan, M., and Kopecko, D. J. (1987) Molecular cloning of invasion plasmid antigen (ipa) genes from *Shigella flexneri*: analysis of ipa gene products and genetic mapping, *J Bacteriol* 169, 2561-2569.
71. Menard, R., Sansonetti, P. J., and Parsot, C. (1993) Nonpolar mutagenesis of the ipa genes defines IpaB, IpaC, and IpaD as effectors of *Shigella flexneri* entry into epithelial cells, *J. Bacteriol.* 175, 5899-5906.
72. Oaks, E. V., Hale, T. L., and Formal, S. B. (1986) Serum immune response to *Shigella* protein antigens in rhesus monkeys and humans infected with *Shigella* spp, *Infect Immun* 53, 57-63.
73. Kaniga, D. T. a. J. G. (1995) Identification of two targets of the type III protein secretion system encoded by the *inv* and *spa* loci of *Salmonella typhimurium* that have homology to the *Shigella* IpaD and IpaA proteins, *J. Bacteriol.* 177, 7078-7085.

74. Picking, W. L., Nishioka, H., Hearn, P. D., Baxter, M. A., Harrington, A. T., Blocker, A., and Picking, W. D. (2005) IpaD of *Shigella flexneri* is independently required for regulation of Ipa protein secretion and efficient insertion of IpaB and IpaC into host membranes, *Infect. Immun.* 73, 1432-1440.
75. Espina, M., Ausar, S. F., Middaugh, C. R., Picking, W. D., and Picking, W. L. (2006) Spectroscopic and calorimetric analyses of invasion plasmid antigen D (IpaD) from *Shigella flexneri* reveal the presence of two structural domains, *Biochemistry* 45, 9219-9227.
76. Turbyfill, K. R., Hartman, A. B., and Oaks, E. V. (2000) Isolation and characterization of a *Shigella flexneri* invasin complex subunit vaccine, *Inf_Imm* 68, 6624-6632.
77. Heine, S. J., Diaz-McNair, J., Martinez-Becerra, F. J., Choudhari, S. P., Clements, J. D., Picking, W. L., and Pasetti, M. F. (2013) Evaluation of immunogenicity and protective efficacy of orally delivered *Shigella* type III secretion system proteins IpaB and IpaD, *Vaccine*.
78. Markham, A. P., Barrett, B. S., Esfandiary, R., Picking, W. L., Picking, W. D., Joshi, S. B., and Middaugh, C. R. (2010) Formulation and immunogenicity of a potential multivalent type III secretion system-based protein vaccine, *J Pharm Sci* 99, 4497-4509.
79. Overheim, K. A., Depaolo, R. W., Debord, K. L., Morrin, E. M., Anderson, D. M., Green, N. M., Brubaker, R. R., Jabri, B., and Schneewind, O. (2005) LcrV plague vaccine with altered immunomodulatory properties, *Infect Immun* 73, 5152-5159.
80. Mehigh, R. J., Sample, A. K., and Brubaker, R. R. (1989) Expression of the low calcium response in *Yersinia pestis*, *Microb Pathog* 6, 203-217.

81. Parsot, C., Menard, R., Gounon, P., and Sansonetti, P. J. (1995) Enhanced secretion through the *Shigella flexneri* Mxi-Spa translocon leads to assembly of extracellular proteins into macromolecular structures, *Mol Microbiol* *16*, 291-300.
82. Hudson, D. L., Layton, A. N., Field, T. R., Bowen, A. J., Wolf-Watz, H., Elofsson, M., Stevens, M. P., and Galyov, E. E. (2007) Inhibition of type III secretion in *Salmonella enterica* serovar Typhimurium by small-molecule inhibitors, *Antimicrobial agents and chemotherapy* *51*, 2631-2635.
83. Veenendaal, A. K., Sundin, C., and Blocker, A. J. (2009) Small-molecule type III secretion system inhibitors block assembly of the *Shigella* type III secretion, *J Bacteriol* *191*, 563-570.
84. Nordfelth, R., Kauppi, A. M., Norberg, H. A., Wolf-Watz, H., and Elofsson, M. (2005) Small-molecule inhibitors specifically targeting type III secretion, *Infect Immun* *73*, 3104-3114.
85. Swietnicki, W., Carmany, D., Retford, M., Guelta, M., Dorsey, R., Bozue, J., Lee, M. S., and Olson, M. A. (2011) Identification of small-molecule inhibitors of *Yersinia pestis* Type III secretion system YscN ATPase, *PLoS One* *6*, e19716.
86. Muschiol, S., Bailey, L., Gylfe, A., Sundin, C., Hultenby, K., Bergstrom, S., Elofsson, M., Wolf-Watz, H., Normark, S., and Henriques-Normark, B. (2006) A small-molecule inhibitor of type III secretion inhibits different stages of the infectious cycle of *Chlamydia trachomatis*, *Proc Natl Acad Sci U S A* *103*, 14566-14571.
87. Gunn, J. S. (2000) Mechanisms of bacterial resistance and response to bile, *Microbes Infect.* *2*, 907-913.

88. Pope, L. M., Reed, K. E., and Payne, S. M. (1995) Increased protein secretion and adherence to HeLa cells by *Shigella* spp. following growth in the presence of bile salts, *Infect. Immun.* 63, 3642-3648.
89. Prouty, A. M., and Gunn, J. S. (2000) *Salmonella enterica* serovar typhimurium invasion is repressed in the presence of bile, *Infect. Immun.* 68, 6763-6769.
90. Stensrud, K. F., Adam, P. R., La Mar, C. D., Olive, A. J., Lushington, G. H., Sudharsan, R., Shelton, N. L., Givens, R. S., Picking, W. L., and Picking, W. D. (2008) Deoxycholate interacts with IpaD of *Shigella flexneri* in inducing the recruitment of IpaB to the type III secretion apparatus needle tip, *J. Biol. Chem.* 283, 18646-18654.
91. Broz, P., Mueller, C. A., Muller, S. A., Philippsen, A., Sorg, I., Engel, A., and Cornelis, G. R. (2007) Function and molecular architecture of the *Yersinia* injectisome tip complex, *Mol. Microbiol.* 65, 1311-1320.
92. Rathinavelan, T., Tang, C., and De Guzman, R. N. (2011) Characterization of the Interaction between the *Salmonella* Type III Secretion System Tip Protein SipD and the Needle Protein PrgI by Paramagnetic Relaxation Enhancement, *J. Biol. Chem.* 286, 4922-4930.
93. Zhang, L., Wang, Y., Olive, A. J., Smith, N. D., Picking, W. D., De Guzman, R. N., and Picking, W. L. (2007) Identification of the MxiH needle protein residues responsible for anchoring invasion plasmid antigen D to the type III secretion needle tip, *J. Biol. Chem.* 282, 32144-32151.
94. Hume, P. J., McGhie, E. J., Hayward, R. D., and Koronakis, V. (2003) The purified *Shigella* IpaB and *Salmonella* SipB translocators share biochemical properties and membrane topology, *Mol. Microbiol.* 49, 425-439.

95. Picking, W. L., Coye, L., Osiecki, J. C., Barnoski, S. A., Schaper, E., and Picking, W. D. (2001) Identification of functional regions within invasion plasmid antigen C (IpaC) of *Shigella flexneri*, *Mol. Microbiol.* 39, 100-111.
96. Collazo, C. M., and Galan, J. E. (1997) The invasion-associated type III system of *Salmonella typhimurium* directs the translocation of Sip proteins into the host cell, *Mol Microbiol* 24, 747-756.
97. Myeni, S. K., and Zhou, D. (2010) The C terminus of SipC binds and bundles F-actin to promote *Salmonella* invasion, *J Biol Chem* 285, 13357-13363.
98. Tran Van Nhieu, G., Caron, E., Hall, A., and Sansonetti, P. J. (1999) IpaC induces actin polymerization and filopodia formation during *Shigella* entry into epithelial cells, *EMBO J* 18, 3249-3262.
99. Thirumalai, K., Kim, K. S., and Zychlinsky, A. (1997) IpaB, a *Shigella flexneri* invasin, colocalizes with interleukin-1 beta-converting enzyme in the cytoplasm of macrophages, *Infect Immun* 65, 787-793.
100. Menard, R., Prevost, M. C., Gounon, P., Sansonetti, P., and Dehio, C. (1996) The secreted Ipa complex of *Shigella flexneri* promotes entry into mammalian cells, *Proc Natl Acad Sci U S A* 93, 1254-1258.
101. Mueller, C. A., Broz, P., and Cornelis, G. R. (2008) The type III secretion system tip complex and translocon, *Mol. Microbiol.* 68, 1085-1095.

CHAPTER 2: Materials and methods

2.1. Protein expression and purification

The construction of the SipD³⁹⁻³⁴³ expression plasmid was described (1). The SipD³⁹⁻³⁴³ expression plasmid was used as the PCR template for subcloning of the SipD³⁹⁻³³⁸, SipD^{Δ116-124}, SipD^{Δ186-189}, SipD^{Δ187-188}, and SipD¹³¹⁻³⁴³ constructs. Expression plasmids for IpaD³⁸⁻³³² and IpaD¹³⁰⁻³³² were constructed by Dalian Zhong. To generate the IpaD³⁸⁻³³² and IpaD¹³⁰⁻³³² constructs, DNA segments coding for the respective polypeptides were PCR amplified from *S. flexneri* using suitable oligonucleotide primers and subcloned into pET-21A expression vector using restriction sites Nde1 and Sal1. The pET-21A expression vector was modified previously to append a His₆-GB1 tag followed by a Tobacco etch virus (TEV) protease cleavage site at the N-terminus of the polypeptide. The B1 immunoglobulin domain of streptococcal protein G (GB1) (2) was used as the GB1 tag to enhance the solubility of the recombinant protein (GB1 expression plasmid was obtained from Peter E. Wright, Scripps Research Institute, La Jolla, California). The TEV protease cleavage site was used for proteolytic removal of the His₆-GB1 tag after recombinant protein expression and purification. DNA segments coding for SipB residues 82 to 312 (SipB⁸²⁻³¹²), 340 to 404 (SipB³⁴⁰⁻⁴⁰⁴), 436 to 518 (SipB⁴³⁶⁻⁵¹⁸), and 521 to 593 (SipB⁵²¹⁻⁵⁹³) were PCR amplified from *S. typhimurium* strain SL1344 (ATCC) and subcloned into pET-22B expression vector using restriction sites Nde1 and Xho1, with the addition of amino acids LEH₆ at the C-terminus. SipB⁸²⁻²⁶⁷, SipB⁸²⁻²⁴⁰, and SipB⁸²⁻²²⁶ were generated using the SipB⁸²⁻³¹² construct as the template. A list of the oligonucleotide primers used in construction of expression plasmids is provided in **Table 3**.

Table 3: Sequence of the oligonucleotide primers used to generate various expression constructs.

Plasmid name	Primer sequence
SipD ¹³¹⁻³⁴³	F: GACGAGAGACATATGGAGATTTGGGATATG R: ACGCGTCGACTTATCCTTGCAGGAAGCTTTTGGC
SipD ³⁹⁻³³⁸	F: GACGAGAGACATATGATGCTTAATATTCAA R: ACGCGTCGACTTATTTGGCGGTTTCCAG
SipD ^{Δ116-124}	F: CCGACGTCGGCCCCGAGAACAACC R: GGTGTCTCGGGGCCGACGTCGG
SipD ^{Δ186-189}	F: GGTAAGGACGGTAATGATGTTACCTCACTC R: GAGTGAGGTAACATCATTACCGTCCTTACC
SipD ^{Δ187-188}	F: GACGGTAATACCCTAGATGTTACC R: GGTAACATCTAGGGTATTACCGTC
SipB ⁸²⁻³¹²	F: GACCAGGTCCATATGGAAGGGCAATTGACATTACTGCTTGGCAAGTTAATG R: GGTGGTGGTGGTGGTGCTCGAGCGGTTTCGTTTCCTCGGCTTTG
SipB ⁸²⁻²⁶⁷	F: GACCAGGTCCATATGGAAGGGCAATTGACATTACTGCTTGGCAAGTTAATG R: GGTGGTGGTGGTGGTGCTCGAGCACAATCTCAATAAACATGGCCAT
SipB ⁸²⁻²⁴⁰	F: GACCAGGTCCATATGGAAGGGCAATTGACATTACTGCTTGGCAAGTTAATG R: TCAGTGGTGGTGGTGGTGCTCGAGATTCTGAGAGGC
SipB ⁸²⁻²²⁶	F: GACCAGGTCCATATGGAAGGGCAATTGACATTACTGCTTGGCAAGTTAATG R: TCAGTGGTGGTGGTGGTGCTCGAGAATGTTATCCGCTTT
SipB ³⁴⁰⁻⁴⁰⁴	F: GAGAGAGAGCATATGAGTCTGGCGCTGGCTGCGGTGGGA R: CCGCTCGAGCTCTGCCGTTTTCTTATCG
SipB ⁴³⁶⁻⁵¹⁸	F: GAGAGAGAGCATATGAAACTGGGTAACGCGCTGAGCAAA R: CGCGGGATCCTTATGACTGGGCTGCGGTATTTCGTG
SipB ⁵²¹⁻⁵⁹³	F: GAGAGAGAGCATATGGGTGTTGCCGAGGGCGTATTTA R: CGCGGGATCCTTATGCGCGACTCTGGC
IpaD ³⁸⁻³³²	F: GAGAGAGAG CAT TCTCATCCTGTAAGT R: CGCGGGATCCGAAATGGAGAAAAAGTTTATCTG
IpaD ¹³⁰⁻³³²	F: GAGAGAGAGCATATGTCTCATAGAGAACTGTGGGC R: CGCGGGATCCGAAATGGAGAAAAAGTTTATCTG

All sequences are from 5' to 3' direction.

F stands for the forward primer and R stands for reverse primer.

Site-directed mutants, including truncations of SipD (SipD^{Δ116-124}, SipD^{CΔ5}, SipD^{Δ186-189}, and SipD^{Δ187-188}), were generated using the Stratagene QuickChange kit and confirmed by DNA sequencing.

For protein expression, plasmids were transformed in *E. coli* BL21 (DE3) DNAY cells and grown at 37 °C until mid-log phase in 1 L LB broth (to obtain unlabeled proteins) or M9 minimal media (to obtain ¹⁵N or ¹⁵N, ¹³C-labeled proteins). Recombinant protein expression was induced with 1 mM isopropyl-β-D-thiogalactopyranoside (IPTG) and bacterial growth was continued overnight at 15 °C in incubator with aeration at 200 rpm. The bacterial cells were harvested by centrifugation for 15 minutes at 4000 rpm (2704 xg) and 4 °C and resuspended in ~ 30 ml binding buffer (20 mM Tris-HCl pH 8.0, 500 mM NaCl, and 5 mM imidazole) and lysed by sonication in a Branson Digital Sonifier for 5 minutes of 2 seconds long pulses at 30% power and 6 seconds of gap. Cellular debris was removed by centrifugation at 13000 rpm (18254.3 xg) at 4 °C for 15 minutes and recombinant protein was purified from the supernatant using Ni⁺²-affinity chromatography as described (1). Proteins containing the His₆-GB1 tag were digested with TEV protease and subjected to a second Ni⁺²-column purification as described (1). The purified recombinant proteins were dialyzed in buffer and concentrated in centrifugal filters units (Millipore) for further use. The buffer conditions and protein concentration for each experimental approach are denoted under the appropriate sections.

*2.1.1. Amino acid specific labeling of SipD³⁹⁻³⁴³ – SipD³⁹⁻³⁴³ was separately labeled with [¹⁵N]Ala, Ile, Lys, and Met and [¹⁵N]Leu to generate ¹⁵N-AIKM-SipD and ¹⁵N-Leu-SipD respectively. *E. coli* BL21 (DE3) DNAY cells expressing SipD³⁹⁻³⁴³ were grown overnight in 1 L LB-broth at 37 °C. Cells from the overnight culture were harvested and resuspended in two flasks containing 500 ml M9 minimal media supplemented with 125 mg/L of ¹⁵N-labeled amino*

acids, 300-450 mg/L of unlabeled amino acids until an OD₆₀₀ of ~ 0.6 - 0.8 was reached. Cells were grown at 37 °C for 10 minutes and a final concentration of 1 mM IPTG was added to induce recombinant protein expression. Cell growth was continued at 37 °C until the OD₆₀₀ was ~ 2.5 – 3.0 (~ 4hrs.). Cells were harvested and the recombinant protein was purified as described (1).

2.1.2. ¹³C-ILV labeling of SipD³⁹⁻³⁴³ - The methyl groups of isoleucine, leucine, and valine residues of SipD³⁹⁻³⁴³ were ¹³C-specifically labeled as described (3). Briefly, *E. coli* BL21 (DE3) DNAY cells expressing SipD³⁹⁻³⁴³ were grown in 1 L M9 minimal media at 37 °C with aeration. At OD₆₀₀ ~ 0.4, the growth medium was supplemented with 100 mg of 2-ketobutyric acid-4-¹³C sodium salt hydrate (δ methyl group of Ile) and 100 mg of 2-keto-2-(methyl-¹³C)-butyric acid-4-¹³C sodium salt (γ1 and γ2 methyl group of Leu and Val) (Sigma Aldrich) dissolved in sterile water. Recombinant protein expression was induced with 1 mM IPTG at OD₆₀₀ ~ 0.6-0.8 and cell growth was continued overnight at 15 °C.

2.2. Protein crystallization & Data collection

2.2.1. Free SipD³⁹⁻³⁴³ and SipD³⁹⁻³⁴³ bound to bile salts - About 20 mg/ml of WT and C244S SipD³⁹⁻³⁴³ in buffer (20 mM Tris-HCl pH 8.0, 196 mM NaCl) were screened for crystallization using Compact Jr (Emerald Biosystems) sitting drop plates with 0.75 µl of protein and 0.75 µl crystallization solution, equilibrated in 100 µl of crystallization solution (Hampton Research). WT SipD³⁹⁻³⁴³ yielded crystals in Hampton Research index screen condition 69 (25% (w/v) PEG 3350, 100 mM Tris-HCl pH 8.5, 200 mM (NH₄)₂SO₄) and C244S SipD³⁹⁻³⁴³ yielded crystals in Index screen condition 45 (25% (w/v) PEG 3350, 100 mM Tris-HCl pH 8.5). Crystallization was observed in ~ 24 hours at 20 °C. Single crystals were added to cryoprotectant solution (25%

(w/v) PEG 3350, 100 mM Tris-HCl pH 8.5 and 10% glycerol) and flash cooled in presence of 15-20% glycerol.

C244S SipD³⁹⁻³⁴³ was co-crystallized with bile salt deoxycholate by mixing 1 µl of 400 mM sodium deoxycholate (Amresco) dissolved in buffer (20 mM Tris-HCl pH 8.0, 196 mM NaCl) with 100 µl of 0.3 mM C244S SipD³⁹⁻³⁴³ and incubating on ice for ~ 30 minutes. The C244S SipD³⁹⁻³⁴³-deoxycholate mixture was screened for crystallization in hanging drops containing 1.5 µl C244S SipD³⁹⁻³⁴³-deoxycholate and 1.5 µl of crystallization solution in presence of 600 µl of reservoir volume at 25 °C. Initial crystals grew in 12 days in 0.2 M magnesium formate dihydrate and 20% (w/v) PEG 3350. Diffraction quality crystals were obtained in 8 days in an optimized crystallization solution containing 0.2 M magnesium formate dihydrate and 15% PEG 3350. Crystals of WT SipD³⁹⁻³⁴³ bound to bile salt chenodeoxycholate were obtained by soaking crystals of WT SipD³⁹⁻³⁴³ in 4 mM chenodeoxycholate (Sigma) dissolved in crystallization solution. Crystals were soaked in 80% crystallization solution and 20% glycerol and flash cooled in liquid nitrogen before x-ray diffraction.

2.2.2. *SipD*¹³¹⁻³⁴³ - SipD¹³¹⁻³⁴³ was purified and crystallized by Anindita Basu (Graduate student) as part of her rotation project. SipD¹³¹⁻³⁴³ concentrated to 40 mg/ml in buffer (196 mM NaCl, 20 mM Tris-HCl pH 8.0) was screened for crystallization at 20 °C in Compact Clover (Emerald BioSystems) sitting drop vapor diffusion plates using 0.75 µl of protein and 0.75 µl of crystallization solution equilibrated against 75 µl of the latter. Prismatic crystals were obtained in approximately 4 days from the Salt Rx screen condition B3 (Hampton Research, 1.0 M ammonium citrate, 100 mM sodium acetate pH 4.6). Single crystals were transferred to a fresh drop of cryoprotectant solution containing 80% crystallization solution and 20% glycerol.

2.3. Crystal structure determination

2.3.1. *Free SipD³⁹⁻³⁴³ and SipD³⁹⁻³⁴³ bound to bile salts* - X-ray diffraction data were collected by Kevin Battaile (Argonne National Laboratory) and the crystal structure was solved by Scott Lovell (Director, Protein structure Laboratory at the University of Kansas). Diffraction data were collected at the Advanced Photon Source (APS) beamline 17BM (IMCA-CAT) to 1.9 Å using an ADSC Q210 CCD detector. Diffraction data were integrated and scaled with the HKL2000 package (4). A C-centered orthorhombic or a C-centered monoclinic lattice with a β -angle $\sim 90^\circ$, was obtained for the SipD³⁹⁻³⁴³-deoxycholate crystals. The correct space group (C2) was determined by checking the Laue class using POINTLESS (5). The asymmetric unit contained two molecules of SipD³⁹⁻³⁴³ having a solvent content of 46.2% and V_m of 2.3 Å³/Da. The self-rotation function was calculated with POLARRFN (6) using data from 15 Å – 3.5 Å resolution and an integration radius of 20 Å resulting in a peak on the $\kappa = 180^\circ$ section at $\omega = 49.1^\circ$, and $\phi = 180^\circ$ corresponding to a 2-fold non-crystallographic axis. Structure solution was achieved by molecular replacement using the program Phaser (7). The pathogenicity island 1 effector protein from *Chromobacterium violaceum* (PDB id: 2P7N), sharing 50% sequence identity with SipD, was used as the search model and the program Chainsaw (6) was used to generate the homology model. Rotation and translation searches were performed to obtain a clear solution for two molecules in the asymmetric unit. Initial refinement converged at $R = 42\%$ and $R_{\text{free}} = 46\%$. Automated model building using ARP/wARP (8) and successive rounds manual model building followed by refinement with Coot (9) and REFMAC (10) were performed to further improve the structure. A cloning artifact of residues Gly-36, His-37, and Met-38 was fitted into the residual electron density. Further, a Ni⁺² ion, possibly acquired during protein purification, was coordinated in a square planar arrangement to residues Gly-36 and His-

37 of molecule A, and His-40 of another molecule A related by crystallographic 2-fold symmetry. The structures of WT SipD³⁹⁻³⁴³, C244S SipD³⁹⁻³⁴³, and SipD³⁹⁻³⁴³ bound to chenodeoxycholate were solved by molecular replacement using MOLREP (11) and the protein portion of the refined structure of SipD-deoxycholate as the homology model. MolProbity (12) and PyMOL (13) were used to validate and analyze the structures.

2.3.2. *SipD*¹³¹⁻³⁴³ - Data collection and structure solution was performed by Scott Lovell. X-ray diffraction data were collected at 93K using a Rigaku RU-H3R rotating anode generator (Cu-K_α) equipped with Osmic Blue focusing mirrors and a Rigaku R-axis IV++ image plate detector. Diffraction data were integrated and scaled with XDS (14) and Scala (5) respectively. The Laue class was checked with POINTLESS (5), which indicated that 6/mmm was most probable and the possible space groups were P6₁22 or P6₅22. Based on the calculated molecular weight of 23,434 Da, the Matthew's coefficient (15) was 2.86 with a solvent content of 57% and one molecule in the asymmetric unit. Structure solution was carried out by molecular replacement with Phaser (7) using the free WT SipD³⁹⁻³⁴³ structure as the search model (PDB: 3NZZ) (16) with N-terminal residues up to Glu-133 removed. All possible chiral space groups in the Laue class 6/mmm were tested and the highest score was obtained for P6₁22. Automated model building was conducted with ARP/wARP (8) followed by manual model building and refinement with Coot (9) and PHENIX (17) respectively. Disordered side chain residues were truncated to the point to which electron density could be observed. Structure validation was conducted with MolProbity (12).

2.4. CD spectroscopy and thermal Denaturation

CD spectra were acquired using a JASCO J-815 Spectropolarimeter. Typical CD samples were prepared with 1 – 2 μ M of protein in either distilled water or buffer (5 mM sodium phosphate pH 7.0, 5 mM NaCl). Initially, the CD of a blank sample containing only buffer or distilled water was measured and subtracted from the protein spectrum. Subtraction of the blank did not have any effect on the CD spectrum of the protein and therefore, this step was omitted in later experiments. CD spectra were acquired in triplicate at 20 °C with a scan rate of 50 nm/minute. Thermal denaturation scans were performed by measuring the ellipticity at 222 nm over a temperature range of 20 °C to 80 °C and a temperature ramp rate of 2 °C/minute. CD values in ellipticity (mdeg) were converted to molar ellipticity (θ = degcm²/dmole) by using the formula $\theta = \{\text{mdeg} \times \text{molecular weight (daltons)}\} / \{\text{concentration (mg/ml)} \times 10\}$. The melting temperature (T_m) was calculated using the JASCO CD software.

2.5. NMR Spectroscopy

2.5.1. *Two dimensional NMR spectra of SipD* - Two-dimensional ¹H-¹⁵N-TROSY (18) spectra of SipD³⁹⁻³⁴³, SipD³⁹⁻³³⁸, SipD^{Δ186-189}, and SipD^{Δ187-188} were acquired using 0.8 mM of protein dissolved in buffer (10 mM sodium phosphate pH 7.0, 10 mM NaCl, 5% D₂O). All NMR data were collected at 25 °C in a Bruker Avance 800 MHz spectrometer equipped with a cryogenic triple resonance probe (unless otherwise mentioned). Typical acquisition parameters were 40 scans, 30 ppm ¹⁵N sweep width centered at 118 ppm, 2048 ¹H complex points, and 160 ¹⁵N complex points. NMR data were processed using NMRpipe (19) and analyzed using NMRview (20).

2.5.2. *NMR titrations of ^{15}N -SipD³⁹⁻³⁴³ with unlabeled SipB⁸²⁻³¹²* - ^{15}N -SipD³⁹⁻³⁴³ was titrated with unlabeled SipB⁸²⁻³¹² using 0.2 mM ^{15}N -SipD³⁹⁻³⁴³ dissolved in buffer (10 mM sodium phosphate pH 7.0, 100 mM NaCl, 10% D₂O). Five molar ratios of SipD to SipB of 1:0, 1:0.5, 1:1, 1:2, and 1:3 were used to acquire ^1H - ^{15}N -TROSY (18) spectra at 30 °C with 48 scans, 30 ppm ^{15}N sweep width centered at 118 ppm, 2048 ^1H complex points, and 260 ^{15}N complex points. Previously reported backbone assignments (1) were used to calculate the intensity ratios for 182 non-overlapping peaks of SipD³⁹⁻³⁴³.

2.5.3. *Dilution experiments and NMR titrations of ^{15}N -MxiH^{V68A-V70A} with unlabeled IpaD* - MxiH^{V68A-V70A} was titrated with IpaD³⁸⁻³³² and IpaD¹³⁰⁻³³² using 0.4 mM ^{15}N -MxiH^{V68A-V70A} dissolved in NMR buffer (10 mM sodium phosphate pH 7.0, 10 mM NaCl, 10% D₂O). Molar ratios of ^{15}N -MxiH^{V68A-V70A} to IpaD of 1:0, 1:0.25, 1:0.5, 1:1, and 1:2 were used to acquire five ^1H - ^{15}N -HSQC (21) spectra. The dilution experiments were acquired with progressively decreasing concentrations (1.8 mM, 0.9 mM, 0.6 mM, 0.3 mM, and 0.125 mM) of ^{15}N -MxiH^{V68A-V70A} dissolved in NMR buffer. ^1H - ^{15}N -HSQC (21) spectra were acquired at 25 °C with 12 scans, 20 ppm ^{15}N sweep width centered at 118 ppm, 2048 ^1H complex points, and 128 ^{15}N complex points. The backbone resonances of MxiH-V68A-V70A were assigned in order to analyze the results of NMR titrations and dilution experiments. The backbone resonances of MxiH^{V68A-V70A} were completed using 3D-HNCA (22), and 3D-CBCA(CO)NH (22) datasets acquired on 1.5 mM ^{15}N , ^{13}C -MxiH^{V68A-V70A} dissolved in NMR buffer.

2.6. Paramagnetic relaxation enhancement

2.6.1. *Spin labeling of SipB⁸²⁻³¹², IpaD³⁸⁻³³², and IpaD¹³⁰⁻³³²* – Specific residues on SipB⁸²⁻³¹², IpaD³⁸⁻³³², and IpaD¹³⁰⁻³³² were mutated to cysteine in order to attach a (1-Oxyl-2,2,5,5-tetramethyl- Δ 3-pyrroline-3-methyl) methanethiosulfonate (MTSL) as the spin label. Proteins to be spin labeled were dialyzed in PRE buffer (20 mM sodium phosphate pH 7.0, 20 mM NaCl) along with 5 mM DTT to inhibit the formation of intermolecular disulfide bonds. Prior to addition of MTSL, the DTT was removed by passing 500 μ l of the protein solution through a NAP5 column (GE Healthcare) equilibrated with PRE buffer and eluted with 1000 μ l PRE buffer. The MTSL (10 mg) was dissolved in 250 μ l acetone to make a 150 mM stock solution. 50 μ l of the MTSL stock solution was added to 1 ml of \sim 0.6 mM protein (\sim 10 \times molar excess of MTSL). The protein-MTSL solution was incubated overnight in the dark at room temperature. Excess MTSL was removed by passing the protein-MTSL solution through another NAP5 column. The resultant spin-labeled protein was concentrated when needed and Electrospray ionization mass spectroscopy (ESI-MS) was used to confirm the successful attachment of the spin-label to the protein.

2.6.2. *Single time point PRE using ¹⁵N-specifically labeled SipD³⁹⁻³⁴³ and SipB⁸²⁻³¹²* - PRE was determined by using the single time point method (23). Identical 2D-NMR spectra were collected for a diamagnetic (protein without the spin-label) and a paramagnetic (protein labeled with MTSL) sample and PRE was determined from the intensity ratio $I_{\text{para}}/I_{\text{dia}}$ for each non-overlapping peak. 2D-¹H-¹⁵N-HSQC (21) (AIKM SipD³⁹⁻³⁴³) or 2D-¹H-¹⁵N-TROSY (18) (Leu-SipD³⁹⁻³⁴³) datasets were acquired with 0.8 mM ¹⁵N-specifically labeled SipD³⁹⁻³⁴³ and 0.4 mM unlabeled (Diamagnetic) or spin-labeled (paramagnetic) SipB⁸²⁻³¹². Protein concentration, buffer conditions, and acquisition parameters were identical for the diamagnetic and paramagnetic

datasets. The backbone resonances of AIKM-SipD³⁹⁻³⁴³ and Leu-SipD³⁹⁻³⁴³ were derived from the published backbone resonances of ¹⁵N-SipD³⁹⁻³⁴³ (1). The ¹H-¹⁵N-HSQC (21) spectra were acquired at 25 °C with 24 scans, 18 ppm ¹⁵N sweep width centered at 124 ppm, 2048 ¹H complex points, and 160 ¹⁵N complex points. ¹H-¹⁵N-TROSY (18) spectra were acquired at 30 °C with 32 scans, 17 ppm ¹⁵N sweep width centered at 121.5 ppm, 2048 ¹H complex points, and 120 ¹⁵N complex points.

2.6.3. Single time point PRE using ¹⁵N-MxiH^{CA5} and IpaD³⁸⁻³³² or IpaD¹³¹⁻³³² - NMR spectra was acquired at 25 °C with a Bruker Avance 600 MHz spectrometer equipped with an inverse triple resonance probe. Initially, PRE experiments were conducted with 0.4 mM of ¹⁵N-MxiH^{V68A-V70A} and 0.4 mM of IpaD. However, full-length MxiH, equimolar protein ratios, and high protein concentrations produced a non-specific PRE effect due to protein oligomerization on MxiH residues irrespective of the position of the spin label on IpaD. Therefore, for later experiments, 0.1 mM ¹⁵N-MxiH¹⁻⁷⁸ and 0.05 mM IpaD³⁹⁻³³² or IpaD¹³⁰⁻³³² were used.

2.7. HADDOCK modeling of the SipD³⁹⁻³⁴³ – SipB⁸²⁻²²⁶ complex

Results from NMR titrations of ¹⁵N-SipD³⁹⁻³⁴³ with SipB⁸²⁻³¹² and paramagnetic relaxation enhancement were used to generate a structural model of the SipD³⁹⁻³⁴³ and SipB⁸²⁻²²⁶ complex using the HADDOCK webserver (24). The HADDOCK webserver required a list of active and passive residues for both SipD³⁹⁻³⁴³ and SipB⁸²⁻²²⁶. Active residues are directly involved in binding and passive residues are adjacent to the active residues and are indirectly involved in binding. The surface exposed residues showing the largest decrease in peak intensity upon titration with SipB⁸²⁻³¹² were defined as the active residues for SipD³⁹⁻³⁴³. Spin labels on helices α 3 and α 4 of SipB⁸²⁻³¹² produced the strongest PRE effect on SipD³⁹⁻³⁴³. However, because helix

$\alpha 4$ was absent in the crystal structure of SipB⁸²⁻²²⁶, surface exposed residues on helix $\alpha 3$ were defined as active residues for SipB⁸²⁻²²⁶. Active residues for SipD³⁹⁻³⁴³ and SipB⁸²⁻²²⁶ are listed in Table 4. The docking was performed according to default parameters and 200 models of the SipD³⁹⁻³⁴³-SipB⁸²⁻²²⁶ complex were generated.

2.8. *Salmonella* invasion assay

2.8.1. Construction of knockout strains of S. typhimurium - The lambda Red recombinase method (25) was used to generate *sipD* (*sipD*⁻) and *sipB* (*sipB*⁻) nonpolar knockout strains of *S. typhimurium*. Knockout strains of *S. typhimurium* were made by Dalian Zhong. A linear DNA segment containing a chloramphenicol resistance gene sandwiched between the regions flanking *sipD/sipB* was added to *S. typhimurium* in the presence of lambda Red recombinase.

Homologous recombination between the *sipD/sipB* flanking sequences in the linear segment and the bacterial genome causes the replacement of *sipD/sipB* with the chloramphenicol resistance gene creating a *sipD*⁻/*sipB*⁻ *S. typhimurium* strain, which is resistant to chloramphenicol. Plasmids pKD3 (containing chloramphenicol resistance gene) and pKD46 (containing genes for lambda Red-mediated recombination) were sourced from the *E. coli* Genetic Stock Center (Yale University) and the WT *S. typhimurium* SL1344 strain was a kind gift from Dr. Bradley Jones (University of Iowa). The linear DNA segment was PCR amplified from pKD3 using primers containing sequences complementary to the chloramphenicol resistance gene and the *sipD/sipB* flanking regions. Meanwhile, the temperature-sensitive plasmid pKD46 was electroporated into WT *S. typhimurium* SL1344 strain and grown at 30 °C. The linear DNA segment was then electroporated into the SL1344/pKD46 strain and grown at 37 °C to expel the pKD46 plasmid. Successfully transformed colonies with the null mutation were selected against chloramphenicol resistance and confirmed by PCR and DNA sequencing. WT or point mutants of *sipD/sipB* were

subcloned into the rescue plasmid pRK2 using Nde1 and Sal1 restriction sites and electroporated into *sipD*⁻/*sipB*⁻ strains of *S. typhimurium*. Bacterial strains (*sipD*⁻ and *sipB*⁻) stably expressing WT or mutant *sipD*/*sipB* were stored at -80 °C in 10% glycerol.

2.8.2. *Salmonella* invasion assay - The *Salmonella* invasion assay was used to test whether mutations in *sipD*/*sipB* affected the ability of *S. typhimurium* to invade intestinal epithelial cells. Single colonies of the bacterial strains were grown overnight in 10 ml LB-broth containing 25 mg/L Trimethoprim, 50 mg/L Ampicillin, and 25 mg/L Chloramphenicol, and grown overnight without aeration at 37 °C. The overnight culture was diluted 1:10 in LB containing 1 mM IPTG and grown until OD₆₀₀ was ~ 0.4. For the *Salmonella* invasion assays with bile salts, increasing concentrations of deoxycholate or chenodeoxycholate were added to the growth medium at this stage. Henle-407 cells (American Type Culture Collection CCL-6) were grown in 24 well plates in Dulbecco's modified Eagle's medium (DMEM) with 10% fetal bovine serum at 37 °C and 5% CO₂. A 1:4 dilution (15 ml to 60 ml) of a confluent 75 cm² flask was used to seed the 24 well plates. Prior to addition of bacterial cultures, each well was washed with 500 µl of DMEM. Bacterial cultures (10 µl/well) were added to Henle-407 cells in 300 µl DMEM and incubated at 37 °C for 1 hour. After 1 hour, wells were washed three times with 500 µl DMEM containing 5% fetal bovine serum and 100 mg/L Gentamicin and incubated for 1.5 hours in the same medium to kill any extracellular bacteria. Intracellular bacteria were protected from the antibiotic, as it could not be permeabilized. Following antibiotic treatment, wells were rinsed with 500 µl fresh DMEM and cells were lysed in 200 µl 1% Triton X-100 dissolved in 1X PBS. The cell lysate was serially diluted (1:10) and 100 µl of the third dilution was spread on an LB-agar plate and incubated overnight at 37 °C. Percent invasiveness was calculated by counting the

number of colonies on each plate. The *sipD*⁻/*sipB*⁻ strain with WT *sipD/sipB* (in pRK2) was considered the positive control and denoted 100% invasiveness.

2.9. Immunoblotting

2.9.1. *Affinity purification of antibodies* - The expression of SipD and SipB (carrying point mutations) was tested by immunoblotting of proteins secreted by various strains of *S. typhimurium* with anti-SipD and anti-SipB antibodies. Antisera against purified recombinant SipD³⁹⁻³⁴³ (rat) and SipB⁸²⁻³¹² (rabbit) were obtained from the Proteintech Group Inc. (Chicago, USA). The AminoLink kit (Thermo scientific) was used to purify polyclonal anti-rat SipD³⁹⁻³⁴³ and anti-rabbit SipB⁸²⁻³¹² antibodies from the antisera. Purified antibodies were dialyzed in 1X PBS with 0.05% sodium azide and 50% glycerol (v/v) was added after dialysis. Aliquots containing 50 µl of purified antibodies were stored at -20 °C and concentration was estimated by measuring absorbance at 280 nm (MW ~ 150 kD and molar extinction coefficient ~ 210,000 M⁻¹ cm⁻¹).

2.9.2. *Extraction of T3SS proteins secreted into the growth medium* - LB-agar plates with appropriate antibiotics (chloramphenicol for *sipD*⁻/*sipB*⁻, trimethoprim for strains containing pRK2) were streaked with *S. typhimurium* strains from a glycerol stock and incubated overnight at 37 °C. A single colony was used to inoculate 10 ml LB containing 0.3 M NaCl (1 LB: 10 gm tryptone, 5 gm yeast extract, 17.53 gm NaCl, pH 7.0) and grown overnight at 37 °C with shaking at <150 rpm. Overnight cultures were diluted 1:10 in fresh LB (0.3 M NaCl) containing a final concentration of 1 mM IPTG and bacteria were grown until OD₆₀₀ ~ 1.0 was reached. Cell pellets were collected by centrifugation at 4000 rpm (3220 xg) at 4 °C for 40 minutes. Proteins extracted from the growth medium and the intact cell pellets were subjected to SDS-PAGE and immunoblotting. Cell pellets were resuspended in 1 ml of 1X PBS and transferred to a 1.7 ml

ependorf tube and centrifuged at 13,000 rpm (16060 xg) at 20 °C for 15 minutes. The supernatant was discarded and pellets were resuspended in ~ 20 µl 1X PBS.

The growth medium was passed through a 0.45 µ filter and treated with 1 ml of 10% Trichloroacetic acid (TCA) and incubated on ice for 1 hour. Precipitated proteins were pelleted by centrifugation at 4000 rpm (3220 xg) at 4 °C for 40 minutes. The supernatant was discarded and pellets were resuspended in 200 µl of 2% SDS solution and the volume was made up to 10 ml with acetone. The acetone solution was incubated overnight at -20 °C. The following day the acetone solution was centrifuged for 40 minutes at 4000 rpm (3220 xg) at 4 °C. The supernatant was discarded and the pellets were air-dried. Samples for SDS-PAGE were prepared by adding 8M Urea (100 µl) and 2X SDS sample buffer (100 µl) to the pellets. The remaining 5 µl of untreated cell pellets in 1X PBS was mixed with 50 µl 2X SDS sample buffer and all the samples were subjected to SDS-PAGE.

2.9.3. Extraction of T3SS proteins from bacterial cytoplasm - Cytoplasmic proteins were extracted by treating the bacterial cells with lysis buffer (20 mM Tris-HCl pH 8.0, 100 mM NaCl, 1 mM EDTA, 0.5 mg/ml Lysozyme, 1 mM PMSF, and 0.1% TritonX). A portion (15 µl) of the cell pellets in 1X PBS was resuspended in 1ml Lysis buffer and incubated on ice for 30 minutes followed by centrifugation at 13,000 rpm (16060 xg) at 20 °C for 10 minutes. The supernatant was treated with 100 µl of 10% TCA and incubated on ice for 1 hour followed by centrifugation at 13,000 rpm (16060 xg) for 15 minutes at 20 °C. The pelleted cytoplasmic proteins were resuspended in 15 µl of 2% SDS and the volume was made up to 1 ml with acetone. The acetone solution was centrifuged for 15 minutes at 13,000 rpm (16060 xg) at 20 °C and treated similar to that obtained from the growth medium.

2.9.4. Transfer of proteins to a nitrocellulose membrane - A semi-dry blotter (Amersham) was used to transfer proteins from the polyacrylamide gel to a nitrocellulose membrane. The gels were removed from the cast, trimmed and stored in transfer buffer (25 mM Tris-HCl pH 8.0, 192 mM glycine, 7.5 % methanol, 0.1% SDS). Nitrocellulose membranes were trimmed according to size of the gels and soaked in methanol for 15 seconds, followed by a rinse in distilled water and then soaked in transfer buffer. A sandwich of blotting papers-gel-nitrocellulose membrane-blotting paper was prepared and placed on the blotter. A small quantity of transfer buffer was placed on the sandwich and blotting was conducted at 70 mA for 1.15 hours.

2.9.5. Membrane blocking and protein detection - Once the transfer was complete, the nitrocellulose membranes were incubated in 5% non-fat dry milk dissolved in water for 1 hour. Blots were incubated overnight in the primary antibodies (50 μ l polyclonal anti-rat SipD³⁹⁻³⁴³ and 17 μ l anti-rabbit SipB⁸²⁻³¹²) dissolved in 50 ml buffer (1% non-fat dry milk, 0.1% Tween-20, 1X TBS) at 4 °C. The following day, the blots were subjected to three consecutive 30 minutes washes in wash buffer (0.1% Tween-20, 1X TBS). The blots were incubated in 5 μ l anti-rat IgG (1: 10,000 dilution of IrDye 680LT) and 2.5 μ l anti-rabbit IgG (1:20,000 dilution of IRDye 800CW) dissolved in 50 ml wash buffer for 1 hour at room temperature. After incubation in the secondary antibodies, blots were rinsed in wash buffer again for three consecutive 30-minute periods. Finally, the blots were placed in 1X PBS and visualized with Licor Odyssey imaging system.

2.10. References

1. Wang, Y., Nordhues, B. A., Zhong, D., and De Guzman, R. N. (2010) NMR Characterization of the Interaction of the *Salmonella* Type III Secretion System Protein SipD and Bile Salts, *Biochemistry* 49, 4220-4226.
2. Huth, J. R., Bewley, C. A., Jackson, B. M., Hinnebusch, A. G., Clore, G. M., and Gronenborn, A. M. (1997) Design of an expression system for detecting folded protein domains and mapping macromolecular interactions by NMR, *Protein Sci.* 6, 2359-2364.
3. Tugarinov, V., Kanelis, V., and Kay, L. E. (2006) Isotope labeling strategies for the study of high-molecular-weight proteins by solution NMR spectroscopy, *Nat Protoc* 1, 749-754.
4. Otwinowski, Z., and Minor, W. (1997) Processing of X-ray Diffraction Data Collected in Oscillation Mode, *Methods in Enzymology* 276, 307-326.
5. Evans, P. R. (2006) Scaling and assessment of data quality, *Acta Cryst. D62*, 72-82.
6. Collaborative Computational Project, N. (1994) The CCP4 suite: programs for protein crystallography, *Acta Cryst. D50*, 760-763.
7. McCoy, A. J., Grosse-Kunstleve, R. W., Adams, P. D., Winn, M. D., Storoni, L. C., and Read, R. J. (2007) Phaser crystallographic software, *J. Appl. Cryst.* 40, 658-674.
8. Cohen, S. X., Jelloul, M. B., Long, F., Vagin, A., Knipscheer, P., Lebbink, J., Sixma, T. K., Lamzin, V. S., Murshudov, G. N., and Perrakis, A. (2008) ARP/wARP and molecular replacement: the next generation, *Acta Cryst. D64*, 49-60.
9. Emsley, P., and Cowtan, K. (2004) Coot: model-building tools for molecular graphics, *Acta Crystallogr D Biol Crystallogr* 60, 2126-2132.

10. Murshudov, G. N., Vagin, A. A., and Dodson, E. J. (1997) Refinement of macromolecular structures by the maximum-likelihood method, *Acta Cryst. D53*, 240-255.
11. Vagin, A. A., and Teplyakov, A. (1997) *MOLREP*: an automated program for molecular replacement, *J. Appl. Cryst.* 30, 1022-1025.
12. Lovell, S. C., Davis, I. W., Arendall, W. B., 3rd, de Bakker, P. I., Word, J. M., Prisant, M. G., Richardson, J. S., and Richardson, D. C. (2003) Structure validation by Ca geometry: phi,psi and Cb deviation, *Proteins* 50, 437-450.
13. DeLano, W. L. (2002) *The PyMOL Molecular Graphics System* DeLano Scientific, San Carlos, California, U.S.A.
14. Kabsch, W. (1988) Automatic indexing of rotation diffraction patterns, *J. Appl. Cryst.* 21, 67-72.
15. Matthews, B. W. (1968) Solvent content of protein crystals, *J Mol Biol* 33, 491-497.
16. Chatterjee, S., Zhong, D., Nordhues, B. A., Battaile, K. P., Lovell, S. W., and De Guzman, R. N. (2011) The Crystal Structure of the Salmonella Type III Secretion System Tip Protein SipD in Complex with Deoxycholate and Chenodeoxycholate, *Protein Sci.* 20, 75-86.
17. Adams, P. D., Afonine, P. V., Bunkoczi, G., Chen, V. B., Davis, I. W., Echols, N., Headd, J. J., Hung, L. W., Kapral, G. J., Grosse-Kunstleve, R. W., McCoy, A. J., Moriarty, N. W., Oeffner, R., Read, R. J., Richardson, D. C., Richardson, J. S., Terwilliger, T. C., and Zwart, P. H. (2010) PHENIX: a comprehensive Python-based system for macromolecular structure solution, *Acta Crystallogr D Biol Crystallogr* 66, 213-221.

18. Czisch, M., and Boelens, R. (1998) Sensitivity enhancement in the TROSY experiment, *J. Magn. Reson.* 134, 158-160.
19. Delaglio, F., Grzesiek, S., Vuister, G. W., Zhu, G., Pfeifer, J., and Bax, A. (1995) NMRPipe: a multidimensional spectral processing system based on UNIX pipes, *J. Biomol. NMR* 6, 277-293.
20. Johnson, B. A. (2004) Using NMRView to visualize and analyze the NMR spectra of macromolecules, *Methods Mol. Biol.* 278, 313-352.
21. Bodenhausen, G., David J. Ruben. (1980) Natural abundance nitrogen-15 NMR by enhanced heteronuclear spectroscopy, *Chemical Physics Letters* 69, 185-189.
22. Grzesiek, S., Dobei, H., Gentz, R., Garotta, G., Labhardt, A. M., and Bax, A. (1992) ^1H , ^{13}C , and ^{15}N NMR backbone assignments and secondary structure of human interferon-gamma, *Biochemistry* 31, 8180-8190.
23. Gillespie, J. R., and Shortle, D. (1997) Characterization of long-range structure in the denatured state of staphylococcal nuclease. I. Paramagnetic relaxation enhancement by nitroxide spin labels, *J. Mol. Biol.* 268, 158-169.
24. de Vries, S. J., van Dijk, M., and Bonvin, A. M. (2010) The HADDOCK web server for data-driven biomolecular docking, *Nat Protoc* 5, 883-897.
25. Datsenko, K. A., and Wanner, B. L. (2000) One-step inactivation of chromosomal genes in *Escherichia coli* K-12 using PCR products, *Proc. Natl. Acad. Sci. U.S.A.* 97, 6640-6645.

CHAPTER 3: The crystal structure of the *Salmonella* tip protein SipD

3.1. Introduction

Salmonella typhimurium causes Salmonellosis, one of the most common food-borne illnesses in humans worldwide. The pathogenesis of *Salmonella* is dependent on the T3SSs encoded within the SPI-1 & SPI-2, which manipulate the host cellular machinery by delivering bacterial effectors directly into the host cell cytoplasm (1). The SPI-1 T3SS is required for bacterial entry into non-phagocytotic cells of the human intestinal epithelium (2), while the SPI-2 T3SS is required for intracellular survival and replication of *Salmonella* (3). Bacterial effectors delivered by the SPI-1 T3SS induce host actin cytoskeletal rearrangement, which in turn leads to membrane ruffling and bacterial uptake (2). The T3SS is critical for the infectivity of *Salmonella* because non-functional mutations in the genes coding for T3SS proteins abolish the ability of *Salmonella* to invade eukaryotic cells (4).

The structural component of the T3SS known as the needle apparatus consists of a basal complex that spans the inner and outer bacterial membranes, a needle, a tip complex, and a translocon [Figure 3-1]. The base, the needle, and the tip complex are assembled sequentially (5). However, secretion of the translocon and effectors is blocked by the tip complex until specific environmental signals are received (5). Specific cues including contact with the host cell (6) trigger the secretion of the translocon proteins, which assemble on the tip complex to form a functional translocon (6). The translocon forms a pore in the host cell membrane through which the effectors are translocated into the host cell cytoplasm (7). The tip complex is therefore multifunctional; it receives environmental stimuli and regulates the secretion of

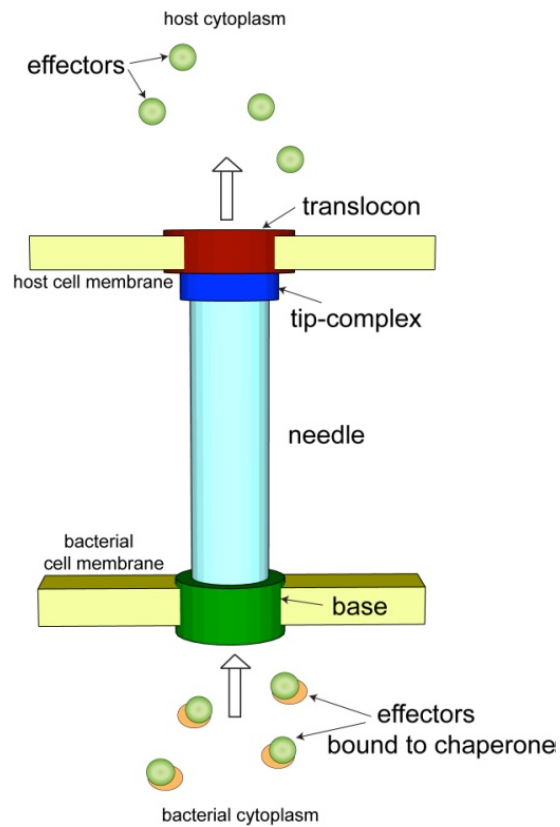


Figure 3-1: A cartoon model showing the structural and functional components of the type III secretion system (T3SS). The structural component is the needle apparatus, which consists of the base, needle, tip complex, and the translocon. The functional components include the effectors and their cognate chaperones

translocon proteins and effectors. The tip complex also acts as a structural platform for the assembly of the translocon. The tip complex is composed of several copies of the tip protein SipD (6) in *Salmonella typhimurium*, IpaD (8) in *Shigella flexneri*, BipD (9) in *Burkholderia pseudomallei*, LcrV (10) in *Yersinia pestis*, and PcrV (11) in *Pseudomonas aeruginosa*.

The tip proteins are highly α -helical and range from 32-37 kD in size. IpaD and BipD have elliptical shapes and they contain a central coiled coil, a C-terminal domain of mixed α -helices and β -sheets, and an N-terminal α -helical hairpin [**Figures 3-10B and C**]. LcrV also contains the central coiled coil but lacks the N-terminal α -helical hairpin and adopts a dumbbell-like shape due to the globular domains on either side of the coiled coil [Figure 3-10A]. Moreover, LcrV and PcrV are chaperoned by the small cytoplasmic proteins LcrG and PcrG respectively (12). The presence of the N-terminal α -helical hairpin domain and the absence of cognate chaperones has led to the hypothesis that IpaD and BipD are self-chaperoned by the N-terminal α -helical hairpin (13).

The T3SSs of *Salmonella*, *Shigella*, and *Burkholderia* belong to the SPI-1 family of injectisomes (1) and the amino acid sequence of SipD is 36% identical and 50% similar to IpaD, and 22% identical and 36% similar to BipD. Therefore, SipD is expected to share a closer resemblance to IpaD and BipD rather than LcrV and PcrV, which belong to the Ysc family of injectisome (1).

The structure of SipD however was unknown. Here the crystal structures of SipD in the presence and absence of the N-terminal α -helical hairpin domain are reported. The atomic structures of SipD are useful in understanding the molecular mechanisms underlying the assembly of the tip complex and the translocon as well as the regulation of the T3SS of

Salmonella. This knowledge will ultimately advance the development of novel therapeutics to target the T3SS.

3.2. Results

3.2.1. Protein expression and purification - The N-terminal 30-38 residues were disordered in the crystal structures of IpaD and BipD. Therefore, the first 38 residues of SipD were truncated to generate SipD³⁹⁻³⁴³. IpaD and BipD also shared the N-terminal α -helical hairpin, which is hypothesized to be a self-chaperone for the tip proteins (13). In order to test the effect of deletion of the self-chaperoning domain on the three-dimensional structure of SipD, residues 1-130 were truncated to yield SipD¹³¹⁻³⁴³. The single cysteine residue in SipD was mutated to serine (C244S) to reduce the formation of intermolecular disulfide bonds. Wild-type and C244S SipD³⁹⁻³⁴³ and SipD¹³¹⁻³⁴³ were expressed in *E. coli* BL21 (DE3) DNAY cells with a GB1 tag fused to the N-terminus to enhance the expression levels and solubility of the recombinant protein. The GB1 tag also contained His₆ residues at the N-terminus to aid in protein purification by Ni⁺²-affinity chromatography [Figure 3-2]. A tobacco etch virus (TEV) protease site was placed after the His₆-GB1 tag to obtain purified SipD after digestion with TEV protease.

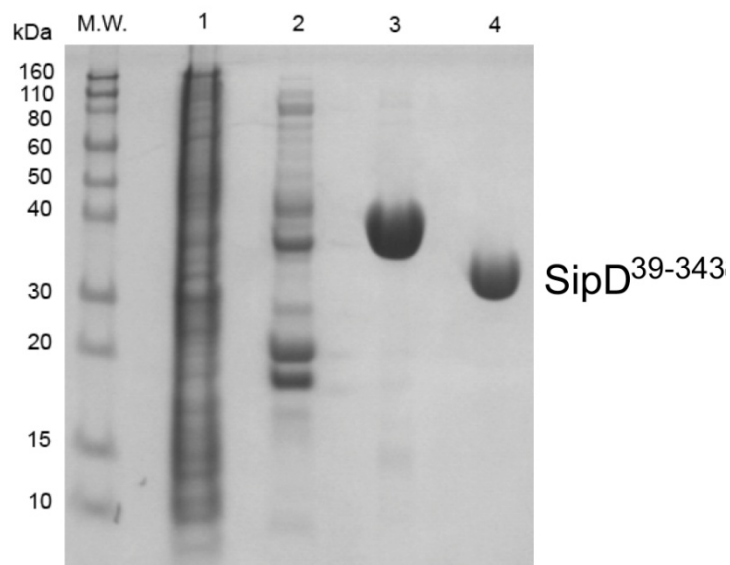


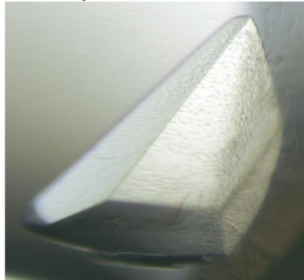
Figure 3-2. SDS-PAGE showing the purification of SipD³⁹⁻³⁴³ by Ni⁺²-affinity chromatography. Lane 1 shows the *E. coli* cell pellet. Lane 2 shows *E. coli* supernatant before purification. Lane 3 shows purified SipD³⁹⁻³⁴³ fused to His₆-GB1 tag. Lane 4 shows purified SipD³⁹⁻³⁴³ after TEV digestion and without the His₆-GB1 tag.

3.2.2. *Crystal structure of SipD³⁹⁻³⁴³* - Crystals of WT and C244S SipD³⁹⁻³⁴³, belonging to C2 space group, grew within a day in sitting drop vapor diffusion plates [**Figure 3-3**]. Diffraction data was processed and refined to 1.7 Å for WT SipD³⁹⁻³⁴³ and 1.9 Å for C244S SipD³⁹⁻³⁴³ [**Table 4**]. The asymmetric unit contained two molecules (A and B) in both WT and C244S SipD³⁹⁻³⁴³. Molecule A contained residues 36 to 342 and molecule B contained residues 47 to 336 (WT) or 47 to 334 (C244S). Residues Gly-36, His-37, and Met-39 were part of the cloning artifact. A Ni⁺² ion was coordinated within residues Gly-36 and His-37 of molecule A and His-40 from a symmetry mate of molecule A. This interaction might be important in crystal packing. The three-dimensional structure of SipD³⁹⁻³⁴³ was highly α -helical with 62% of residues within eight α -helices (α 1- α 8) while, 6% of the residues formed five β -strands (β 1- β 5) and the remaining residues made up the random coils or disordered regions. The overall structure of SipD³⁹⁻³⁴³ could be divided into an N-terminal α -helical hairpin (α 1 & α 2), followed by a short α -helix (α 3), a long coiled coil (α 4 & α 8), and a C-terminal region containing three α -helices (α 5, α 6, and α 7) and two β -strands (β 3 & β 4) [**Figure 3-4**]. A three-stranded antiparallel β -sheet (β 1, β 2, & β 5) was present at the arbitrary “top” of SipD³⁹⁻³⁴³ as depicted in **Figure 3-4**. A loop region (residues 110 to 132) connecting the short helix α 3 to helix α 4 was disordered in both the molecules of WT and C244S SipD³⁹⁻³⁴³ [**Figure 3-4**]. Additionally, C244S SipD³⁹⁻³⁴³ was missing electron density for residues 219 to 221 (molecule B), which were part of the mixed α/β region. The coiled coil divided SipD into a concave face and a convex face. The concave face of the coiled coil was in contact with the N-terminal α -helical hairpin, at the arbitrary “bottom” of SipD³⁹⁻³⁴³ (α 1 & α 2). The convex face of the coiled coil was in contact with helix α 3 and the disordered loop region (residues 110-132) [**Figure 3-4**].

A SipD³⁹⁻³⁴³ WT



B SipD³⁹⁻³⁴³ C244S



C SipD¹³¹⁻³⁴³



Figure 3-3: Crystals of WT SipD³⁹⁻³⁴³ (A), C244S SipD³⁹⁻³⁴³ (B), and SipD¹³¹⁻³⁴³ (C) grew in sitting drop plates in Hampton research index screen condition 69, index screen condition 45, and Salt Rx screen condition B3 respectively.

Table 4. Crystallographic statistics for WT and C244S SipD³⁹⁻³⁴³ and SipD¹³¹⁻³⁴³

	WT SipD ³⁹⁻³⁴³	C244S SipD ³⁹⁻³⁴³	SipD ¹³¹⁻³⁴³
PDB ID	3NZZ	3O00	-
Data collection			
Unit-cell parameters (Å, °)	a = 203.06 b = 52.25 c = 57.52 β = 90.05	a = 203.35 b = 52.15 c = 57.56 β = 90.45	a = 76.54 c = 158.57
Space group	C2 (No. 5)	C2 (No. 5)	P6 ₁ 22
Resolution range ^a	50.0-1.65 (1.71-1.65)	50.0-1.85 (1.92-1.85)	28.61-2.10 (2.21-2.10)
Wavelength (Å)	1.0000	1.0000	1.5418
Temperature (K)	100	100	93
Observed reflections	256,708	195,676	229,573
Unique reflections	69,282	50,006	16,824
Mean <I/σ(I)> ^a	39.2 (1.9)	36.1 (3.5)	22.5 (4.5)
Completeness	95.5 (76.1)	97.0 (81.6)	100.0 (100.0)
Redundancy ^a	3.7 (3.0)	3.9 (3.3)	13.6 (13.7)
R _{merge} (%) ^{a,b}	4.4 (49.6)	5.3 (32.4)	12.0 (67.6)
Refinement			
Resolution (Å)	25.35 – 1.65	32.07 – 1.85	28.61-2.10
Reflections (working/test)	62,042/3,296	46,099/2,477	15,906 / 850
R _{factor} /R _{free} (%) ^c	19.7/23.7	19.5/24.6	19.7 / 23.2
No. of atoms (protein A:B)/Ni ²⁺ /ligand/water)	2,190:2,018/1/348	2,186:2,019/1/297	1,156 / 12 / 92
Model quality			
R.m.s deviations			
Bond lengths (Å)	0.014	0.015	0.013
Bond angles (°)	1.478	1.461	1.286
Average B factor (Å ²)			
All atoms	29.6	29.7	28.0
Protein (chain A/B)	29.0 / 29.2	28.6 / 30.3	29.4
Ni ²⁺	22.0	21.3	-
Glycerol	-	-	45.3
Water	35.4	34.0	32.6
Coordinate error based on maximum likelihood (Å)	0.25	0.26	0.17
Ramachandran plot			
Most favored (%)	99.1	98.9	99.0
Additionally allowed (%)	0.9	1.1	1.0

^a Values in parentheses are for highest resolution shell

^b $R_{\text{merge}} = \sum_{hkl} \sum_i |I_i(hkl) - \langle I(hkl) \rangle| / \sum_{hkl} \sum_i I_i(hkl)$, where $I_i(hkl)$ is the intensity measured for the i th reflection and $\langle I_i(hkl) \rangle$ is the average intensity of all reflections with indices hkl .

^c $R_{\text{factor}} = \sum_{hkl} ||F_{\text{obs}}(hkl)| - |F_{\text{calc}}(hkl)|| / \sum_{hkl} |F_{\text{obs}}(hkl)|$; R_{free} is calculated in an identical manner using 5% of randomly selected reflections that were not included in the refinement

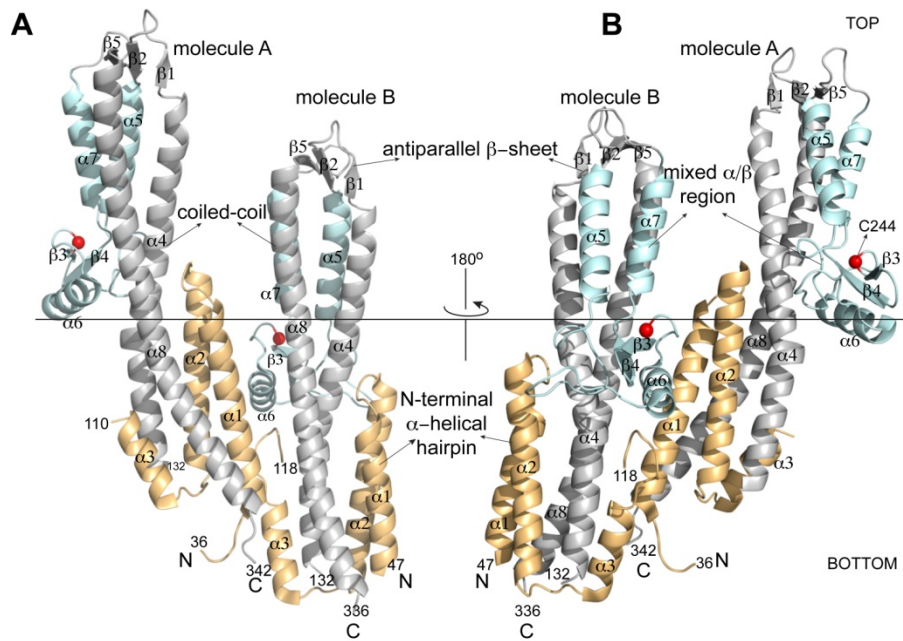


Figure 3-4: Structure of SipD³⁹⁻³⁴³ showing the two molecules in the asymmetric unit. The N-terminal α -helical hairpin is colored yellow, the coiled coil is colored gray, and the mixed α/β region is colored cyan. The location of the C244S point mutation is shown as a red sphere.

The two molecules of SipD³⁹⁻³⁴³ were held together by intermolecular interactions between helix $\alpha 1$ of molecule A, which packs on top of helix $\alpha 3$ of molecule B. Hydrogen bonding between residues in the N-terminal α -helical hairpin of molecule A and the mixed α/β region of molecule B may also be important for the dimerization of SipD³⁹⁻³⁴³.

3.2.3. *Crystal structure of SipD¹³¹⁻³⁴³* - The structure of WT SipD³⁹⁻³⁴³ (residues 133 to 343) was used as a search model to solve the structure of SipD¹³¹⁻³⁴³ by molecular replacement. The 2.1 Å resolution crystal structure of SipD¹³¹⁻³⁴³ contained one molecule in the asymmetric unit [Table 4]. The predominantly α -helical secondary structure and overall architecture of SipD³⁹⁻³⁴³ was maintained even after the removal of the N-terminal α -helical hairpin [Figure 3-5]. The molecule contained five α -helices ($\alpha 4$ - $\alpha 8$) and five β -strands ($\beta 1$ - $\beta 5$) divided into the central coiled coil, the three-stranded antiparallel β -sheet on the “top”, and the C-terminal mixed α/β region [Figure 3-5]. The electron densities for several regions were missing in the crystal structure of SipD¹³¹⁻³⁴³. Notably, the C-terminal region following Ser-328 could not be visualized except for a three-residue (333-336) loop [Figure 3-5]. In addition, N₈₂ of Asn-141 and the backbone NH group of Ser-247 coordinated two molecules of glycerol possibly obtained from the cryoprotectant solution.

3.2.4. *Functional characterization of truncated forms of SipD* - In order to determine which regions of the tip protein are important for T3SS function, the effect of four truncated forms of SipD on the ability of *Salmonella* to invade cultured human epithelial cells was tested. Deletions were made in loop $\alpha 3$ - $\alpha 4$, which is the loop region connecting helices $\alpha 3$ and $\alpha 4$ (SipD ^{$\Delta 116-124$}),

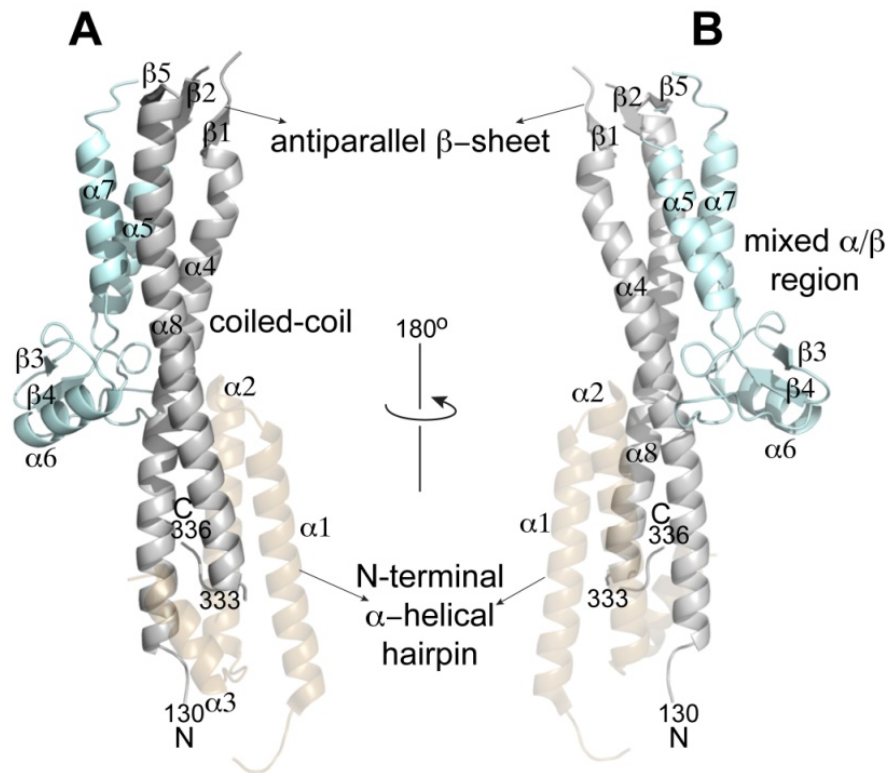


Figure 3-5: Structure of SipD¹³¹⁻³⁴³ showing the coiled coil (gray) and mixed α/β region in cyan. The N-terminal α -helical hairpin domain, which is lacking in the SipD¹³¹⁻³⁴³ construct, is shown as a transparent contour to show its relative position in SipD¹³¹⁻³⁴³.

the β -strand $\beta 2$ (SipD $^{\Delta 186-189}$ and SipD $^{\Delta 187-188}$), and five residues from the C-terminus (SipD $^{C\Delta 5}$) of SipD [Figure 3-7]. The 25-residue loop $\alpha 3$ - $\alpha 4$ was disordered in the crystal structure of SipD $^{39-343}$ but not in the homologous protein *Shigella* IpaD. A flexible loop might be important in protein-protein interactions or in regulating the opening of the needle channel. Thus, a nine-residue deletion $\Delta 116-124$ was generated in order to test the importance of loop $\alpha 3$ - $\alpha 4$ in the function of the T3SS. The β -strand $\beta 2$ is part of an antiparallel β -sheet that is conserved in tip proteins *Shigella* IpaD, *Burkholderia* BipD, and *Yersinia* LcrV. Conserved structural motifs might play important functional roles [Figure 3-10]. Thus the β -strand $\beta 2$ was selected for mutagenesis. The extreme C-termini of the needle proteins *Salmonella* PrgI (14) and *Shigella* MxiH (15) are critical for the polymerization of the needle. To test if the same principle applies to the tip proteins, five residues were deleted from the C-terminus of SipD. In order to test the effect of these deletions on the invasiveness of *Salmonella*, an invasion assay was performed with a strain of *Salmonella* lacking SipD (*sipD* $^-$), which was complemented with the rescue plasmid (pRK2) expressing either full length (*sipD* $^+$) or truncated SipD. The invasiveness of *Salmonella* expressing SipD $^{\Delta 116-124}$ was comparable to that expressing full length SipD or the WT strain SL1344 [Figure 3-6]. In contrast, SipD $^{\Delta 186-189}$, SipD $^{\Delta 187-188}$, and SipD $^{C\Delta 5}$ resulted in a drastic reduction in the invasiveness of *Salmonella* suggesting that these regions are important for the function of SipD [Figure 3-6].

3.2.5. *Structural characterization of truncated forms of SipD* - CD spectroscopy was used to assess the folding of the truncated forms of SipD. WT and truncated SipD yielded CD spectra characteristic of proteins with highly α -helical secondary structures with minima at 208 nm and 222 nm and a ratio of molar ellipticity at 222 nm and 208 nm ($\theta_{222}/\theta_{208}$) of ~ 1.0 [Figure 3-8A]. However, thermal denaturation of SipD $^{\Delta 186-189}$ and SipD $^{\Delta 187-188}$ monitored by CD spectroscopy at

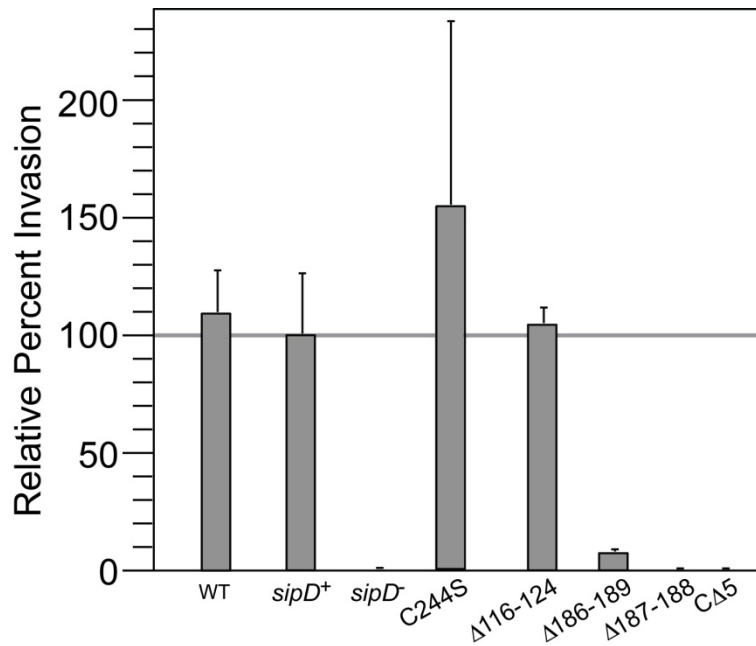


Figure 3-6: Results of *Salmonella* invasion assay performed with a WT *Salmonella* strain or that containing a non-polar knockout *sipD*⁻ or *sipD*⁻ harboring a rescue plasmid pRK2 coding for WT (*sipD*⁺) or mutant SipD. C244S SipD and SipD^{Δ116-124} did not affect the invasiveness of *Salmonella*. However, SipD^{CΔ5}, SipD^{Δ186-189}, and SipD^{Δ187-188} produced non-invasive phenotypes.

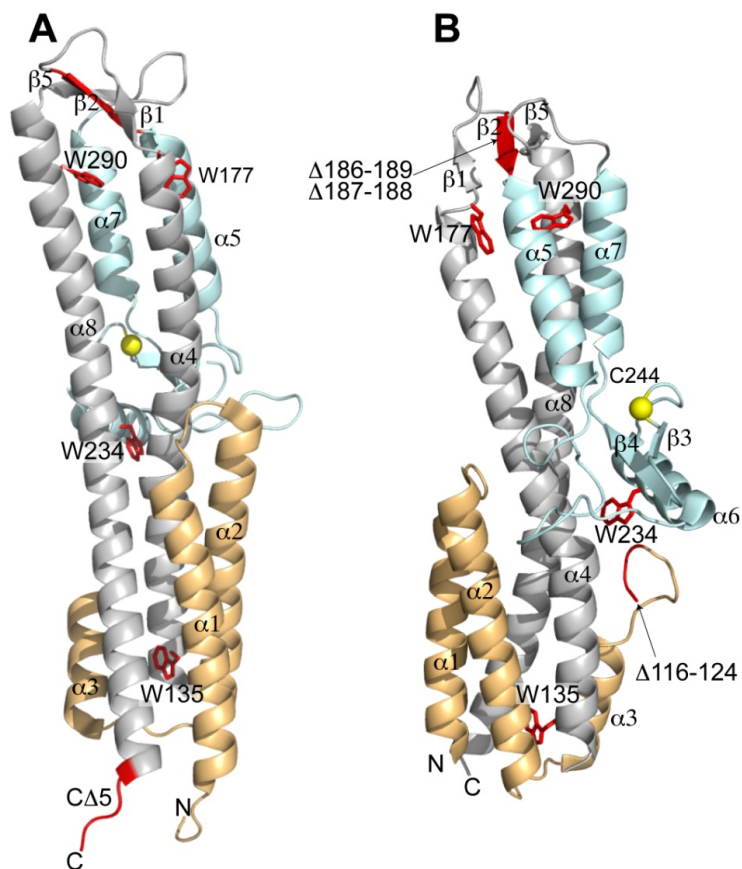


Figure 3-7: (A) Molecule A from the crystal structure of SipD³⁹⁻³⁴³ shows the deletion CΔ5. (B) Molecule B from the crystal structure of SipD³⁹⁻³⁴³ shows the deletions Δ116-124, Δ186-189, and Δ187-188. The four tryptophan residues W135, W177, W234, and W290 shown in (A) and (B) were used for structural characterization of the non-invasive SipD deletion mutants.

222 nm showed a single transition temperature of 63.4° as opposed to the two transition temperatures (47° and 70°) observed for WT SipD. The different melting behavior of SipD^{Δ186-189} and SipD^{Δ187-188} suggested conformational changes in the folding of these mutants [**Figure 3-8B**].

The folding of the non-invasive mutants SipD^{Δ186-189}, SipD^{Δ187-188}, and SipD^{CA5} was further characterized using NMR spectroscopy. All three forms of SipD showed ¹H-¹⁵N-TROSY spectra characteristic of a folded protein and were comparable to that of WT SipD [**Figure 3-9**]. Additionally, the side chain NMR resonances of the four tryptophan residues were used to assess the conformational changes in truncated SipD [**Figure 3-9**]. SipD contained four tryptophan residues located at different regions of the protein as depicted in **Figure 3-7**. W135 was buried in a pocket at the bottom of the coiled coil formed by α -helices α 1-3, α 4, and α 8. W177 was located in between the C-terminal end of helix α 4 and the N-terminal end of helix α 5 and directly below the β -strand β 2. W234 was located at the middle of helix α 6 and W290 was located at the N-terminal end of helix α 8 and facing the mixed α/β region. SipD^{Δ186-189} showed the most drastic deviation in the side chain resonance of W177 and W290 but the NMR resonances of the other two tryptophan side chains were unaffected suggesting local conformational changes in the chemical environment of around β 2 [**Figure 3-9B**].

3.3. Discussion

3.3.1. Comparison with the structures of other tip proteins - The tip proteins assemble on the T3SS needle to form a tip complex, which functions to sense environmental stimuli and regulate the assembly of the translocon. The structure of SipD was unknown prior to this work. The crystal structure of the *Salmonella* tip protein SipD was determined at 1.9 Å resolution.

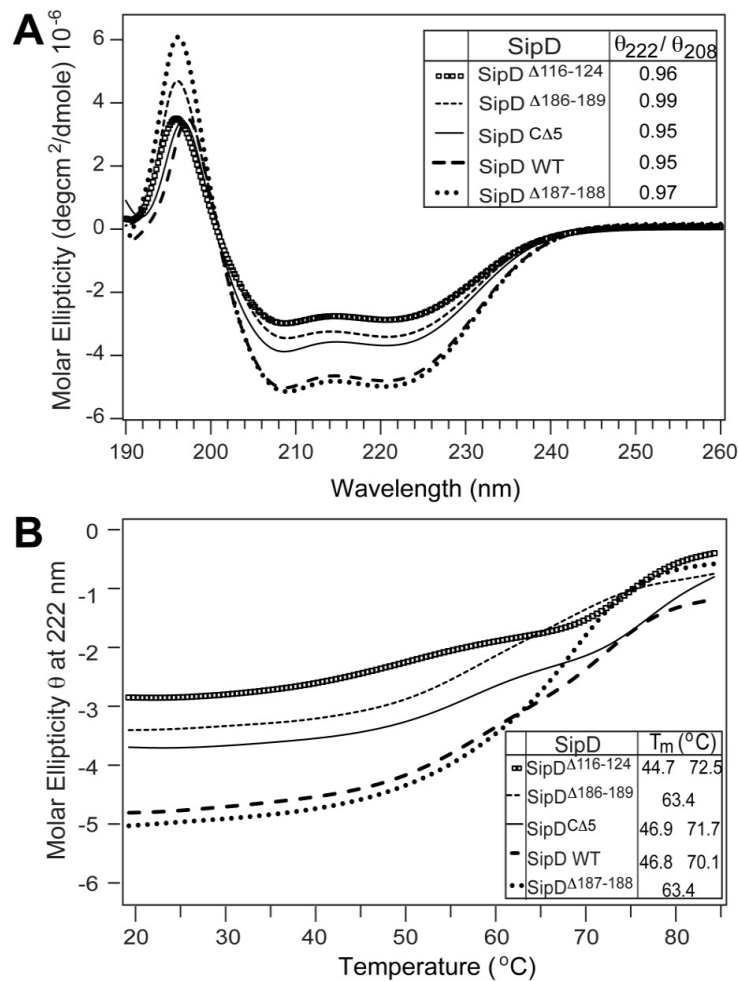


Figure 3-8: (A) CD spectra of WT and deletion mutants of SipD. The inset shows $\theta_{222}/\theta_{208}$ ratios, which are close to 1.0 indicating extensive inter-helical contacts. (B) Thermal denaturation curves of WT or deletion mutants of SipD over a temperature range of 20 °C to 90 °C, monitored by measuring CD at 222 nm. Inset shows the estimated transition temperatures

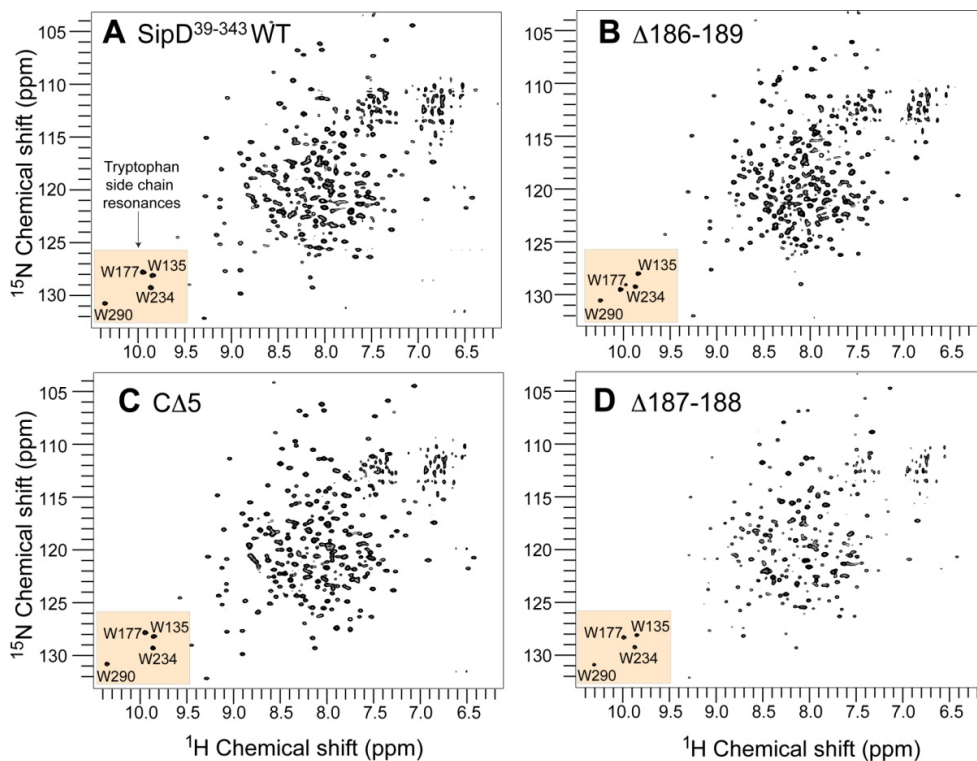


Figure 3-9: ^1H - ^{15}N -TROSY spectra of SipD³⁹⁻³⁴³ (A), SipD ^{Δ 186-189} (B), SipD ^{Δ 5} (C), and SipD ^{Δ 187-188} (D). The boxed regions show the tryptophan side chain resonances, which were reported previously (16). SipD ^{Δ 186-189} showed a change in the side chain NMR resonance of W177.

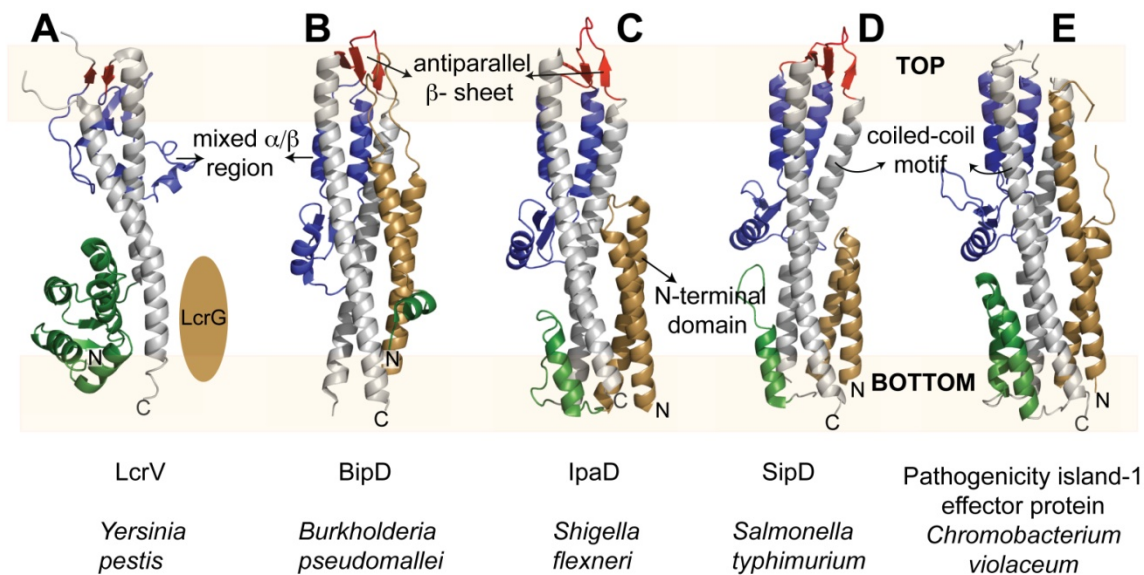


Figure 3-10: Comparison of the structures of the T3SS tip proteins: *Yersinia* LcrV (10) (A), *Burkholderia* BipD (17) (B), *Shigella* IpaD (13) (C), *Salmonella* SipD (D), and the SipD homolog from *Chromobacterium violaceum*. The N-terminal region was composed of the α -helical hairpin (yellow) and short α -helices (green) in B-E but formed a globular domain (green) in A. The coiled coil (gray) and the mixed α/β region (blue) were common to all the tip proteins. The antiparallel β -sheet at the top is colored red. This region was disordered in E. This figure was generated using PDB codes 1R6F (LcrV), 2IXR (BipD), 2J0O (IpaD), 3NZZ (SipD), and 2P7N (Pathogenicity island-1 effector protein).

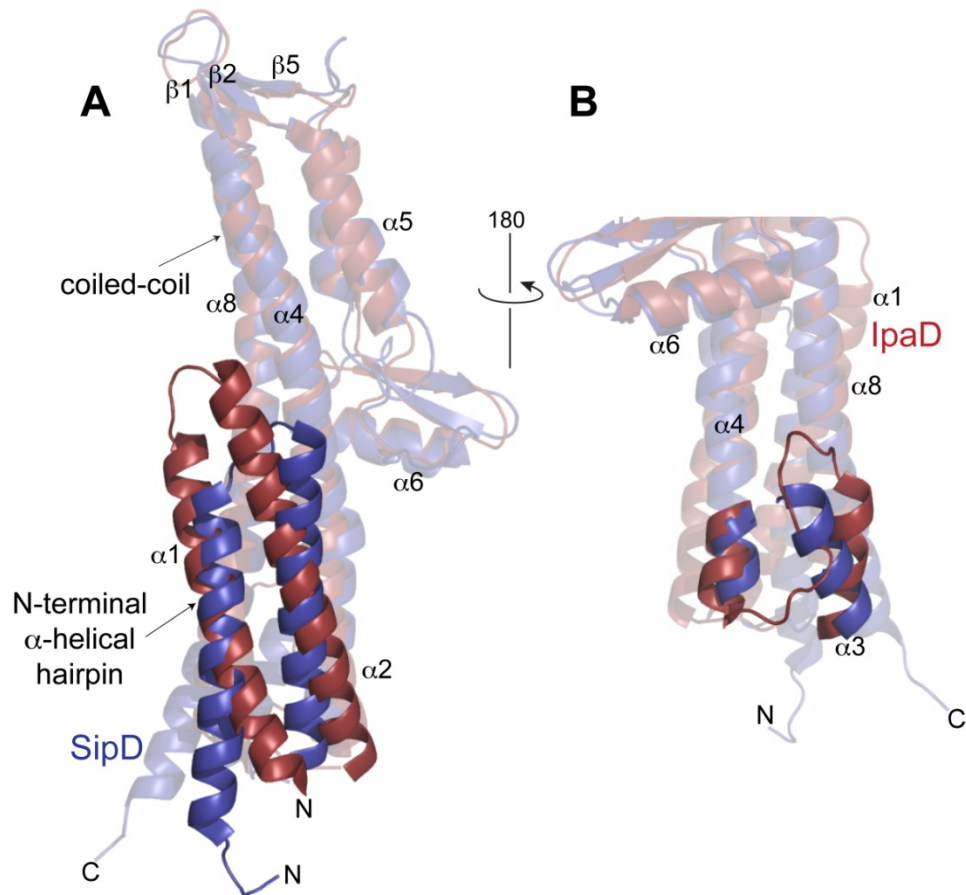


Figure 3-11: Differences in the packing of the helices $\alpha 1$ -3 in SipD and IpaD. In IpaD (red) the longitudinal axis of helices $\alpha 1$ and $\alpha 2$ was rotated 18° counter-clockwise (**A**) and that of helix $\alpha 3$ was rotated 26° clockwise (**B**) in comparison to SipD (blue).

SipD was oblong in shape and retained the coiled coil motif of all tip proteins and closely resembled *Shigella* IpaD, *Burkholderia* BipD, and the SipD homolog from Gram-negative soil bacterium *Chromobacterium violaceum* [Figure 3-10]. The closest structural similarity of SipD was with the *Shigella* IpaD and the two tip proteins shared a backbone C_α rmsd of 1.4 Å (for 186 C_α atoms). There were however, subtle differences in how the helices of the N-terminal hairpin domain of the two tip proteins packed against their respective coiled coils [Figure 3-11]. For example, the longitudinal axis made by helices α1 and α2 was rotated 18° counter clockwise [Figure 3-11A] and the helix α3 was rotated 26° clockwise [Figure 3-11B] in IpaD as compared to SipD. These differences might be significant in the overall structure of the assembled tip complex of *Shigella* and *Salmonella*.

Lunelli *et al.* (18) recently reported the crystal structure of full length SipD containing four molecules (A to D) in the asymmetric unit. Similar to the SipD structure reported herein, about 30 to 40 residues from the N-terminus were disordered in their SipD structure, and molecules A and B in both structures aligned with a backbone C_α rmsd ~ 1 Å. However, unlike the SipD structures reported herein, Thr-128 to Asp-147 of molecules C and D in their SipD structure packed against each other as bent α-helices and were oriented almost perpendicular to the longitudinal axis of helix α4 (18). Furthermore, the electron densities for the N-terminal hairpin of molecules C and D were absent, and this was probably because this domain moved away to avoid steric clash with the bent helices at the bottom of helix α4 (18). A similar feature was noted in the structure of SipD¹³¹⁻³⁴³ reported herein, where the disordered C-terminus (residues 333-336) was bent compared to the longitudinal axis of helix α8 [Figure 3-5]. Although their functional significance is yet to be established, these observations highlight the conformational flexibility of the coiled coil of SipD.

3.3.2. *Significance of the N-terminal α -helical hairpin* - A common feature in *Salmonella* SipD and *Shigella* IpaD but absent in *Yersinia* LcrV is the N-terminal α -helical hairpin made up of helices $\alpha 1$ and $\alpha 2$ on the concave side of the coiled coil and a short helix $\alpha 3$ on the convex side of the coiled coil [Figure 3-10A, C, D, and E]. The *Burkholderia* BipD also contains the hairpin domain but helix $\alpha 1$ is very short and helices $\alpha 2$ and $\alpha 3$ are much longer with the turn region reaching up to the three-stranded β -sheet at the top of the molecule [Figure 3-10B]. A thermal melting scan of IpaD shows two transition temperatures at 40 °C and 70 °C but deletion of the N-terminal hairpin (residues 1 – 131) resulted in the loss of the 40 °C transition temperature suggesting that the hairpin folds independently of the rest of the tip protein (19). Removal of the hairpin also induces self-oligomerization of IpaD (13) suggesting that this domain might be responsible for preventing self-oligomerization of the tip protein. Further, a *Shigella* strain lacking the hairpin domain of IpaD is still able to invade intestinal epithelial cells suggesting that this region is dispensable for T3SS function (20). Lastly, ITC could detect a direct binding between SipD¹³²⁻³⁴³ that lacked the hairpin domain and the *Salmonella* needle protein PrgI but not between full length SipD and PrgI suggesting that the hairpin might also hinder needle-tip interactions (18). All these observations support the hypothesis that the N-terminal α -helical hairpin acts as a self-chaperone for the tip proteins IpaD and SipD and prevents premature tip-tip or needle tip-interactions.

How the assembly of SipD on the PrgI needle is regulated by self-chaperoning is poorly understood. In order to gain more insight into the structure of SipD in the absence of the hairpin domain, we solved the crystal structure of SipD¹³¹⁻³⁴³ that lacks helices $\alpha 1$ - $\alpha 3$. Removal of the hairpin domain induced conformational flexibility in the tip protein resulting in several disordered regions in the crystal structure of SipD¹³¹⁻³⁴³ [Figure 3-5]. Nevertheless, the coiled

coil and the mixed α/β region in SipD¹³¹⁻³⁴³ maintain the overall conformation observed in SipD³⁹⁻³⁴³ and the two molecules share a C α rmsd of 1.3 Å. The folding of SipD¹³¹⁻³⁴³ was also corroborated by the recently reported structures of SipD¹³²⁻³⁴³ (18) and IpaD¹²²⁻³¹⁹ (21). Our structure of SipD¹³¹⁻³⁴³ will be useful in further studies such as constrained modeling of the tip complex.

3.3.3. *Deletion mutants of SipD* - Deletion of residues 186 to 189 (SipD ^{Δ 186-189}), 187 to 188 (SipD ^{Δ 187-188}), and the terminal five residues 339 to 343 (SipD^{C Δ 5}) of SipD negatively affected the ability of *Salmonella* to invade human intestinal epithelial cells [Figure 3-6]. The non-invasiveness of *Salmonella* strains with sipD^{A186-189} and sipD^{A187-188} could be attributed to local conformation changes around the β -strand β 2 of SipD ^{Δ 186-189} and SipD ^{Δ 187-188}. This highlights the significance of the antiparallel β -sheet motif in the folding of SipD [Figures 3-8B, 3-9B, and 3-9D]. SipD^{C Δ 5} also showed a non-invasive phenotype even though it was folded similarly to WT SipD. Interestingly, deletion of the terminal five residues of IpaD disrupts the invasiveness of *Shigella* as well as the presentation of IpaD on the bacterial surface (20). A plausible explanation of these observations is that the C-terminus of the tip proteins is involved in the assembly of the tip complex either by facilitating interactions with needle proteins or other tip proteins. In contrast, deletion of SipD residues 116-124 did not affect the invasiveness [Figure 3-6] of *Salmonella* suggesting that either this region is not important for T3SS function or the deletion of nine residues does not have an appreciable effect on the structure or function of the assembled tip complex.

3.4. References

1. Cornelis, G. R. (2006) The type III secretion injectisome, *Nat. Rev. Microbiol.* 4, 811-825.
2. Zhou, D., and Galan, J. (2001) *Salmonella* entry into host cells: the work in concert of type III secreted effector proteins, *Microbes. Infect.* 3, 1293-1298.
3. Figueira, R., and Holden, D. W. (2012) Functions of the *Salmonella* pathogenicity island 2 (SPI-2) type III secretion system effectors, *Microbiology* 158, 1147-1161.
4. Hueck, C. J. (1998) Type III protein secretion systems in bacterial pathogens of animals and plants, *Microbiol. Mol. Biol. Rev.* 62, 379-433.
5. Deane, J. E., Abrusci, P., Johnson, S., and Lea, S. M. (2010) Timing is everything: the regulation of type III secretion, *Cell Mol Life Sci* 67, 1065-1075.
6. Lara-Tejero, M., and Galan, J. E. (2009) *Salmonella enterica* serovar typhimurium pathogenicity island 1-encoded type III secretion system translocases mediate intimate attachment to nonphagocytic cells, *Infect. Immun.* 77, 2635-2642.
7. Mueller, C. A., Broz, P., and Cornelis, G. R. (2008) The type III secretion system tip complex and translocon, *Mol. Microbiol.* 68, 1085-1095.
8. Espina, M., Olive, A. J., Kenjale, R., Moore, D. S., Ausar, S. F., Kaminski, R. W., Oaks, E. V., Middaugh, C. R., Picking, W. D., and Picking, W. L. (2006) IpaD localizes to the tip of the type III secretion system needle of *Shigella flexneri*, *Infect. Immun.* 74, 4391-4400.
9. Stevens, M. P., Haque, A., Atkins, T., Hill, J., Wood, M. W., Easton, A., Nelson, M., Underwood-Fowler, C., Titball, R. W., Bancroft, G. J., and Galyov, E. E. (2004)

- Attenuated virulence and protective efficacy of a *Burkholderia pseudomallei* bsa type III secretion mutant in murine models of melioidosis, *Microbiology* 150, 2669-2676.
10. Derewenda, U., Mateja, A., Devedjiev, Y., Routzahn, K. M., Evdokimov, A. G., Derewenda, Z. S., and Waugh, D. S. (2004) The structure of *Yersinia pestis* V-antigen, an essential virulence factor and mediator of immunity against plague, *Structure* 12, 301-306.
 11. Sato, H., and Frank, D. W. (2011) Multi-Functional Characteristics of the *Pseudomonas aeruginosa* Type III Needle-Tip Protein, PcrV; Comparison to Orthologs in other Gram-negative Bacteria, *Front. Microbiol.* 2, 142.
 12. Blocker, A. J., Deane, J. E., Veenendaal, A. K., Roversi, P., Hodgkinson, J. L., Johnson, S., and Lea, S. M. (2008) What's the point of the type III secretion system needle?, *Proc. Natl. Acad. Sci. U.S.A.* 105, 6507-6513.
 13. Johnson, S., Roversi, P., Espina, M., Olive, A., Deane, J. E., Birket, S., Field, T., Picking, W. D., Blocker, A. J., Galyov, E. E., Picking, W. L., and Lea, S. M. (2007) Self-chaperoning of the type III secretion system needle tip proteins IpaD and BipD, *J. Biol. Chem.* 282, 4035-4044.
 14. Wang, Y., Ouellette, A. N., Egan, C. E., Rathinavelan, T., Im, W., and De Guzman, R. N. (2007) Differences in the electrostatic surfaces of the type III secretion needle proteins PrgI, BsaL, and MxiH, *J. Mol. Biol.* 371, 1304-1314.
 15. Kenjale, R., Wilson, J., Zenk, S. F., Saurya, S., Picking, W. L., Picking, W. D., and Blocker, A. (2005) The needle component of the type III secretion apparatus of *Shigella* regulates the activity of the secretion apparatus, *J. Biol. Chem.* 280, 42929-42937.

16. Wang, Y., Nordhues, B. A., Zhong, D., and De Guzman, R. N. (2010) NMR Characterization of the Interaction of the *Salmonella* Type III Secretion System Protein SipD and Bile Salts, *Biochemistry* 49, 4220-4226.
17. Erskine, P. T., Knight, M. J., Ruaux, A., Mikolajek, H., Wong Fat Sang, N., Withers, J., Gill, R., Wood, S. P., Wood, M., Fox, G. C., and Cooper, J. B. (2006) High Resolution Structure of BipD: An Invasion Protein Associated with the Type III Secretion System of *Burkholderia pseudomallei*, *J. Mol. Biol.* 363, 125-136.
18. Lunelli, M., Hurwitz, R., Lambers, J., and Kolbe, M. (2011) Crystal structure of PrgI-SipD: insight into a secretion competent state of the type three secretion system needle tip and its interaction with host ligands, *PLoS Pathog.* 7, e1002163.
19. Espina, M., Ausar, S. F., Middaugh, C. R., Picking, W. D., and Picking, W. L. (2006) Spectroscopic and calorimetric analyses of invasion plasmid antigen D (IpaD) from *Shigella flexneri* reveal the presence of two structural domains, *Biochemistry* 45, 9219-9227.
20. Picking, W. L., Nishioka, H., Hearn, P. D., Baxter, M. A., Harrington, A. T., Blocker, A., and Picking, W. D. (2005) IpaD of *Shigella flexneri* is independently required for regulation of Ipa protein secretion and efficient insertion of IpaB and IpaC into host membranes, *Infect. Immun.* 73, 1432-1440.
21. Barta, M. L., Guragain, M., Adam, P., Dickenson, N. E., Patil, M., Geisbrecht, B. V., Picking, W. L., and Picking, W. D. (2012) Identification of the bile salt binding site on IpaD from *Shigella flexneri* and the influence of ligand binding on IpaD structure, *Proteins* 80, 935-945.

CHAPTER 4: Characterization of the interaction between the *Salmonella* tip protein SipD and bile salts

4.1. Introduction

The liver secretes bile to aid in the digestion of lipids. Bile contains bile acids, which are amphipathic molecules derived from cholesterol. Bile acids can react with sodium to form bile salts (1). The concentration of bile acids ranges from ~8% in the gall bladder to ~2% in the small intestine (1). Bile acids produced in the liver are known as primary bile acids. Resident bacteria in the gut can convert the primary bile acids into secondary bile acids (2). Cholic acid and chenodeoxycholic acid are the most abundant primary bile acids and deoxycholic acid and taurodeoxycholic acid are the most abundant secondary bile acids (2).

Bile acids have antimicrobial properties, therefore enteric pathogens like *Salmonella* and *Shigella* alter the expression of a variety of genes to escape the harmful effects of bile acids (1). These pathogens modulate the expression of genes governing the lipopolysaccharide, toll proteins, efflux pumps, as well as virulence factors like the (T3SS) in response to bile acids (1). In the presence of bile, *Salmonella* represses the transcription of genes that regulate the T3SS and the ability of *Salmonella* to invade epithelial cells is reduced by a factor of 96% (3). In contrast, the bile salt deoxycholate increased the invasiveness of *Shigella* and enhanced the secretion of Ipa proteins (4). In addition, growth in deoxycholate induced the surface presentation of the *Shigella* translocon protein IpaB (5). Electron microscopy of T3SS needles from *Shigella* showed that the surface exposed IpaB was bound at the tip of the needles, in the presence of deoxycholate (5). Further, deoxycholate could directly bind to the *Shigella* tip protein IpaD (6). Computational docking predicted that deoxycholate bound to a pocket between

the coiled coil and the N-terminal α -helical hairpin domain of IpaD (6). Deoxycholate also bound to the *Salmonella* tip protein SipD (6). In order to determine how bile salts interact with SipD, the tip protein was crystallized with bile salts deoxycholate and chenodeoxycholate. The crystal structures of SipD³⁹⁻³⁴³ bound to bile salts provide insights in understanding why *Salmonella* and *Shigella* show contrasting responses to bile.

4.2. Results

4.2.1. *Crystal structure of the SipD³⁹⁻³⁴³-deoxycholate and SipD³⁹⁻³⁴³-chenodeoxycholate complexes* - Crystals of the SipD³⁹⁻³⁴³-deoxycholate complex were obtained by co-crystallization of SipD³⁹⁻³⁴³ C244S with sodium deoxycholate. Crystals of the SipD³⁹⁻³⁴³-chenodeoxycholate complex were obtained by soaking the crystals of WT SipD³⁹⁻³⁴³ in a solution of sodium chenodeoxycholate. Crystals of WT SipD³⁹⁻³⁴³ were also soaked in taurodeoxycholate and cholate hydrate. However, these bile salts failed to form co-crystals with SipD³⁹⁻³⁴³. The co-crystal structures of SipD³⁹⁻³⁴³-deoxycholate and SipD³⁹⁻³⁴³-chenodeoxycholate complexes were solved by molecular replacement and refined to a resolution of 1.9 Å. The crystallographic statistics are listed in **Table 5**. Both structures contained two molecules of SipD³⁹⁻³⁴³ in the asymmetric unit and the bile salts were bound in identical hydrophobic pockets [**Figure 4-1**]. These pockets had a surface area of ~520 Å² and were formed at the interface of three molecules of SipD³⁹⁻³⁴³. The bile salt binding pocket was formed by the C-terminus and N-terminus of molecule A, helix α 3 and the C-terminus of helix α 8 of molecule B, and a loop from the mixed α/β region joining α -helix α 5 to α 6 (loop α 5- α 6) of molecule A2, which was related to molecule A by a crystallographic (011) translation. The three molecules of SipD forming the bile salt binding pocket are shown in **Figures 4-2** and **4-3**. The bile salt binding pocket was lined by the following residues: R41, I45, K338, and F340 of molecule A, N104, S107, A108, L318, L322,

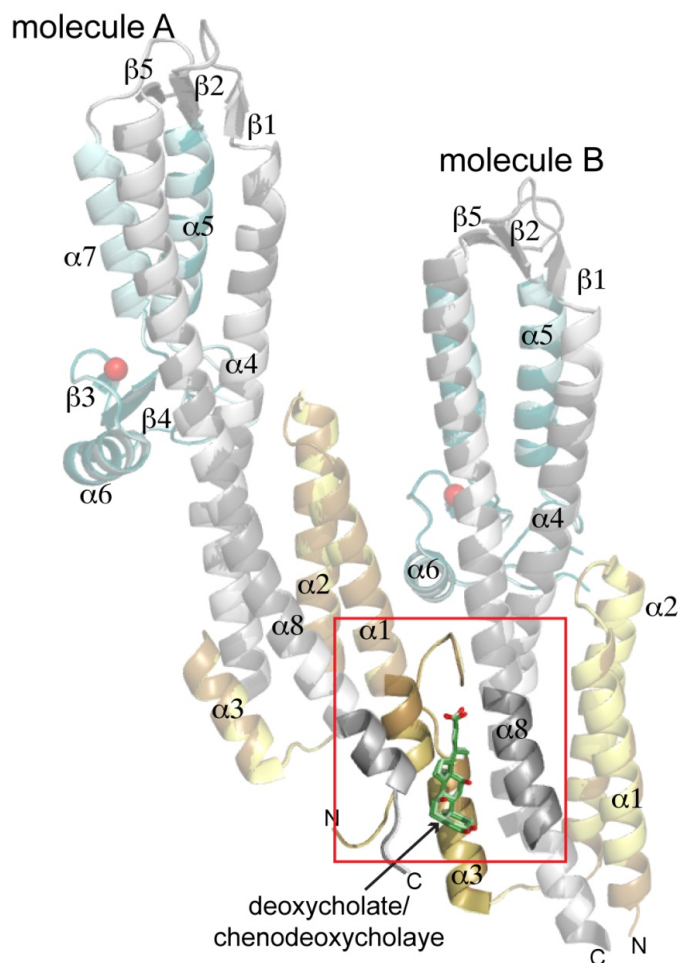


Figure 4-1: An overlay of the structures of SipD³⁹⁻³⁴³ bound to deoxycholate and chenodeoxycholate showing the bile salt binding site (red box). The bile salt binding site was formed by the N-terminus of $\alpha 1$ and the C-terminus of $\alpha 8$ from molecule A along the C-terminus of $\alpha 8$ and $\alpha 3$ from molecule B. The structure of SipD-deoxycholate complex is colored in darker shades.

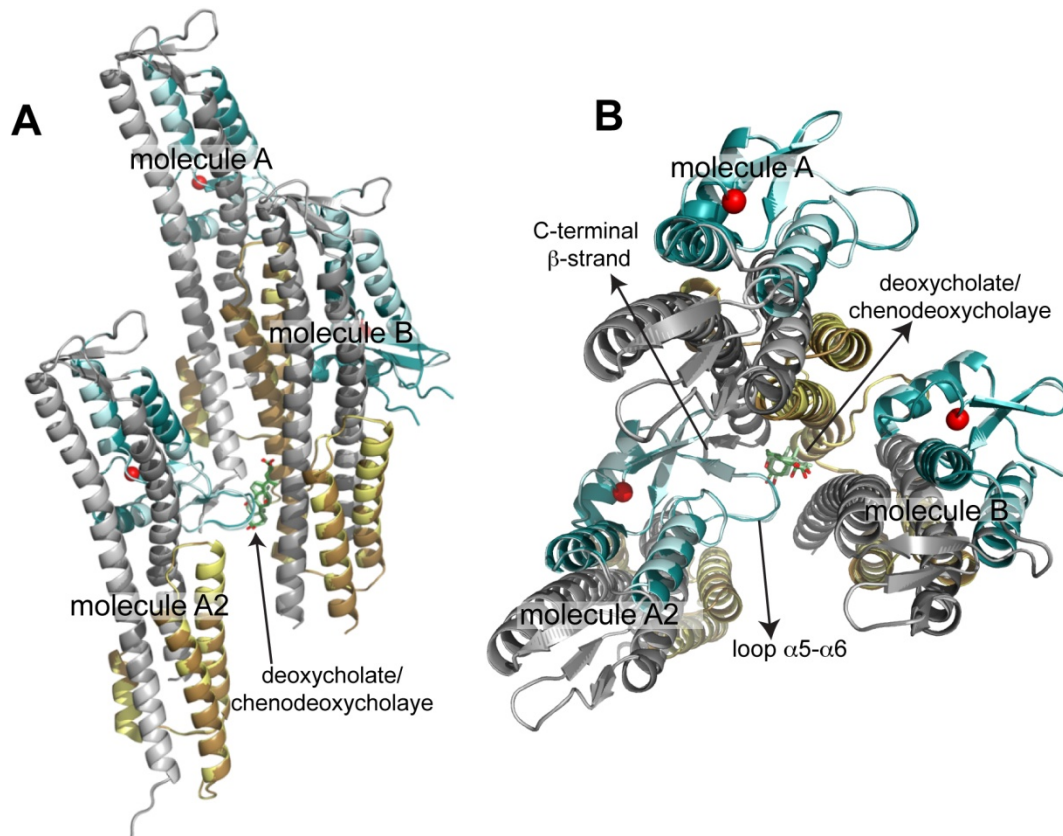


Figure 4-2: (A) Side view of the structures of SipD-deoxycholate and SipD-chenodeoxycholate complexes showing the asymmetric unit containing two molecules (A and B) of SipD. Molecule A2 was related to molecule A by a crystallographic (011) translation. A loop within the mixed α/β region of molecule A2 (loop α 5- α 6) was in contact with the bile salt. (B) Top view of the three molecules of SipD bound to one molecule of deoxycholate or chenodeoxycholate. The C-terminus of molecule A formed a parallel β -sheet with molecule A2 (*see chapter 8 section 8.1.4*). The structure of SipD-deoxycholate complex is colored in darker shades.

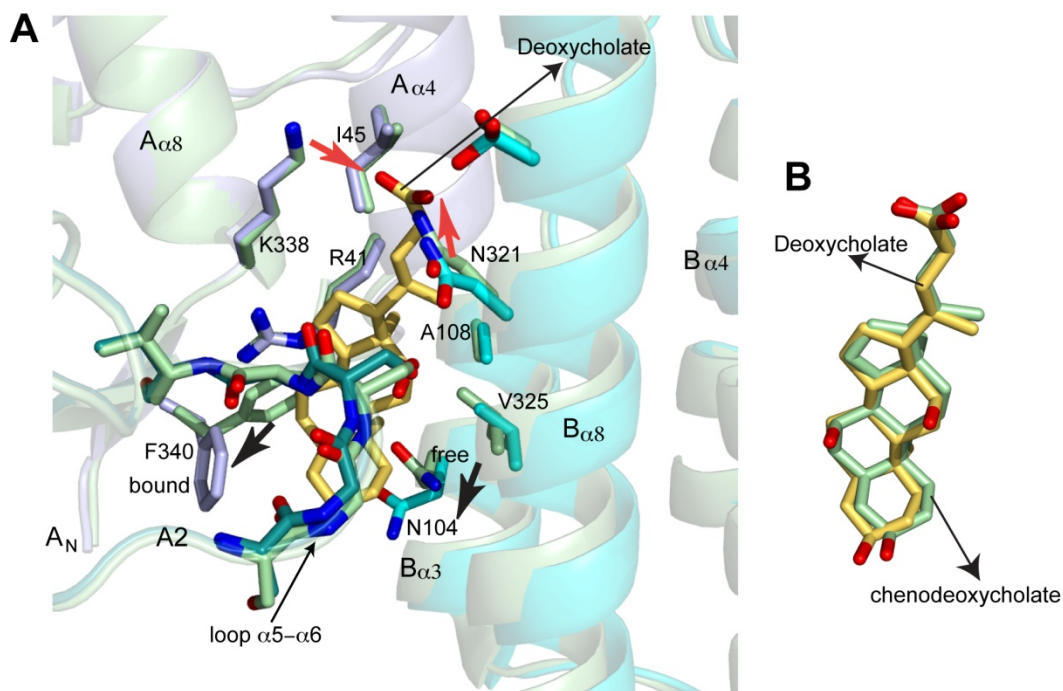


Figure 4-3: (A) Expanded view of the deoxycholate-binding pocket in SipD³⁹⁻³⁴³. The residues lining the binding pocket are shown as sticks. The structure of apo SipD³⁹⁻³⁴³ is colored green and the three molecules (A, B, and A2) of SipD³⁹⁻³⁴³-deoxycholate complex are colored in shades of blue. The conformational changes in residues F340 and N104 upon binding bile salts are marked with black arrows. The hydrogen bonding between the carboxyl group of deoxycholate and residues K338 and N104 of SipD³⁹⁻³⁴³ are marked with red arrows. The structure of chenodeoxycholate-bound SipD³⁹⁻³⁴³ showed identical conformational changes in F340 and N104. (B) Superposition of deoxycholate and chenodeoxycholate showing the relative orientation of chenodeoxycholate with respect to deoxycholate in A.

N321, V325, and T329 of molecule B, and S221 and G222 of molecule A2. The interaction between SipD³⁹⁻³⁴³ and bile salts was predominantly hydrophobic in nature but was stabilized by hydrogen bonds between the carboxyl groups of the bile salts and residues K338 (molecule A) and N321 (molecule B) of SipD³⁹⁻³⁴³. No large scale conformational changes were seen in SipD³⁹⁻³⁴³ upon binding to bile salts and each of the complex structures could be aligned with the WT SipD³⁹⁻³⁴³ structure with a backbone C_α rmsd of > 0.2 Å. However, residue N104 was shifted 83° downwards and residue F340 was shifted 102° outwards in order to accommodate the bile salts [Figure 4-3].

4.2.2. *Effect of deoxycholate on the invasiveness of Salmonella* - The ability of *Salmonella* to invade eukaryotic cells is repressed by bile (3). *Salmonella* invasion assays were done to determine if deoxycholate or chenodeoxycholate alone had similar effects on the invasiveness of *Salmonella*. Increasing concentrations (0 mM, 1 mM, 2 mM, 3 mM, and 4 mM) of deoxycholate or chenodeoxycholate were added to the growth medium of different strains of *Salmonella*, which were then allowed to invade human intestinal epithelial cells (*the protocol for the Salmonella invasion assay was described in chapter 2, section 2.8.2*). Addition of chenodeoxycholate yielded highly viscous bacterial cultures, which were unsuitable for the *Salmonella* invasion assays. A *sipD*⁻ strain complemented with the WT *sipD* gene (*sipD*⁺) showed a gradual decrease in invasiveness with increasing concentrations of deoxycholate [Figure 4-4]. However, decrease in the invasiveness of WT *S. typhimurium* strain SL1344 was less pronounced as compared to the *sipD*⁺ strain. The *sipD*⁻ strain containing a nonpolar knockout in the *sipD* gene was considered as the negative control for the *Salmonella* invasion assays.

Table 5. Crystallographic statistics for SipD³⁹⁻³⁴³-deoxycholate and SipD³⁹⁻³⁴³-chenodeoxycholate complex structures

	C244S SipD ³⁹⁻³⁴³ - deoxycholate	WT SipD ³⁹⁻³⁴³ - chenodeoxycholate
PDB ID	3O01	3O02
Data collection		
Unit-cell parameters (Å, °)	a = 201.93 b = 52.33 c = 57.31 β = 90.3	a = 202.22 b = 52.37 c = 57.32 β = 90.20
Space group	C2 (No. 5)	C2 (No. 5)
Resolution range ^a	50.0-1.9 (1.97-1.90)	50.0-1.9 (1.97-1.90)
Wavelength (Å)	1.0000	1.0000
Temperature (K)	100	100
Observed reflections	170,803	169,943
Unique reflections	46,924	46,661
Mean <I/σ(I)> ^a	20.3 (1.9)	27.9 (3.7)
Completeness	98.5 (88.1)	97.9 (83.5)
Redundancy ^a	3.6 (3.1)	3.69 (2.8)
R _{merge} (%) ^{a,b}	5.3 (38.1)	5.3 (23.0)
Refinement		
Resolution (Å)	27.98 – 1.90	24.97 – 1.90
Reflections (working/test)	45,527/2,249	43,463/2,308
R _{factor} /R _{free} (%) ^c	19.6/25.8	18.5/23.6
No. of atoms (protein A:B)/Ni ²⁺ /ligand/water)	2,184:2,053/1/28/25 2	2,177:2,032/1/28/330
Model quality		
R.m.s deviations		
Bond lengths (Å)	0.017	0.018
Bond angles (°)	1.556	1.614
Average B factor (Å ²)		
All atoms	32.0	28.2
Protein (chain A/B)	31.5 / 32.3	27.6 / 27.9
Ni ²⁺	26.6	21.8
Deoxycholate or Chenodeoxycholate	28.6	26.2
Water	34.0	33.5
Coordinate error based on maximum likelihood (Å)	0.26	0.26
Ramachandran plot		
Most favored (%)	98.9	98.9
Additionally allowed (%)	1.1	1.1

^a Values in parentheses are for highest resolution shell

^b $R_{\text{merge}} = \sum_{hkl} \sum_i |I_i(hkl) - \langle I(hkl) \rangle| / \sum_{hkl} \sum_i I_i(hkl)$, where $I_i(hkl)$ is the intensity measured for the i th reflection and $\langle I_i(hkl) \rangle$ is the average intensity of all reflections with indices hkl .

^c $R_{\text{factor}} = \sum_{hkl} ||F_{\text{obs}}(hkl)| - |F_{\text{calc}}(hkl)|| / \sum_{hkl} |F_{\text{obs}}(hkl)|$; R_{free} is calculated in an identical manner using 5% of randomly selected reflections that were not included in the refinement

4.2.3. *Effect of mutagenesis around bile salt binding site* - SipD residues surrounding the bile salt binding pocket were mutated and the mutations were introduced into the *sipD*⁻ knockout strain using the rescue plasmid pRK2. The rationale behind each of the SipD point mutations are listed in **Table 6**. The resultant *Salmonella* strains containing point mutations in SipD were used to perform *Salmonella* invasion assays and their invasiveness was compared to the *sipD*⁺ strain. Addition of deoxycholate diminished the invasiveness of the *sipD*⁺ strain. Therefore, SipD mutants unable to bind deoxycholate were expected to show percent invasion values similar to or higher than the *sipD*⁺ strain. A standard concentration of 2.5 mM deoxycholate was used for the *Salmonella* invasion assays. However, all SipD mutants showed a phenotype similar to WT and *sipD*⁺ strains, where addition of deoxycholate reduced their invasiveness. Results of the *Salmonella* invasion assays using point mutants of SipD are shown in **Figure 4-6**.

4.2.4. *Effect of deoxycholate on the secretion of SipD and SipB* - The effect of deoxycholate on the secretion of SipD and SipB was determined in order to test the hypothesis that deoxycholate represses invasion of *Salmonella* by downregulating the secretion of SipD or SipB. The proteins secreted by WT *S. typhimurium* in the presence and absence of deoxycholate was immunoblotted using anti-SipD and anti-SipB antibodies. Initially, *Salmonella* was grown with 2.5 mM deoxycholate and the secreted proteins were probed with anti-GroEL (loading control) and anti-SipD antibodies. However, 2.5 mM deoxycholate produced more intense bands for both GroEL and SipD suggesting non-specific extraction of proteins. Therefore, a concentration of 1 mM deoxycholate was used for later experiments.

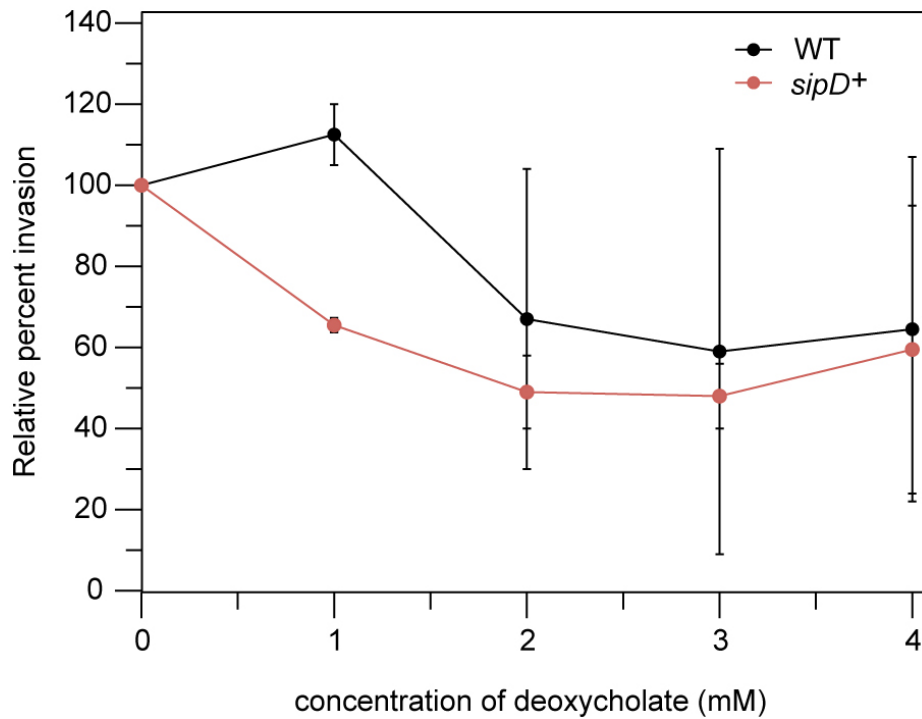


Figure 4-4: Plots showing the effect of increasing concentrations of deoxycholate on the invasiveness of WT *S. typhimrium* and the *sipD*⁻ strain expressing a plasmid-encoded WT *sipD* gene (*sipD*⁺). Percent invasiveness for each strain was calculated relative to the invasiveness in the absence of deoxycholate (0 mM). The *sipD*⁻ was used as the negative control and assayed with 0 mM deoxycholate (data point was 0% invasion and was not included).

Table 6. Rationales behind the design of point mutations around the bile salt binding site of SipD³⁹⁻³⁴³

WT residue	Mutation	Rationale
F340	F340H	Smaller five-membered imidazole ring.
	F340L	Hydrophobic residue lacking an aromatic ring.
	F340V	Short hydrophobic residue.
	F340Y	Similar aromatic ring structure.
	F340G	Higher flexibility.
	F340P	Higher rigidity.
	F340W	Larger (indole) ring.
K338	K338E	Oppositely charged.
	K338L	Shorter in length and hydrophobic in nature.
	K338M	Shorter in length and hydrophobic in nature.
N321	N321Q	Polar but longer in length.
	N321D	Similar in length but negatively charged.
	N321L	Hydrophobic in nature.
N104	N104D	Negatively charged. Cannot hydrogen bond with the carboxyl group of bile salt.
S107	S107A	Hydrophobic in nature. Cannot hydrogen bond with R41 (Figure 4-4).
	S107T	Similar in nature. Can form a hydrogen bond with R41.
S110	S110A	Hydrophobic in nature. Cannot hydrogen bond with G42.
	S110T	Similar in nature. Can hydrogen bond with G42.
S107 S110	S107A S110A	Cannot hydrogen bond with R41 and G42.
	S107G S110G	Cannot hydrogen bond with R41 and G42. Higher flexibility.
	S107T S110T	Hydrogen bonding with R41 and G42 will be retained.

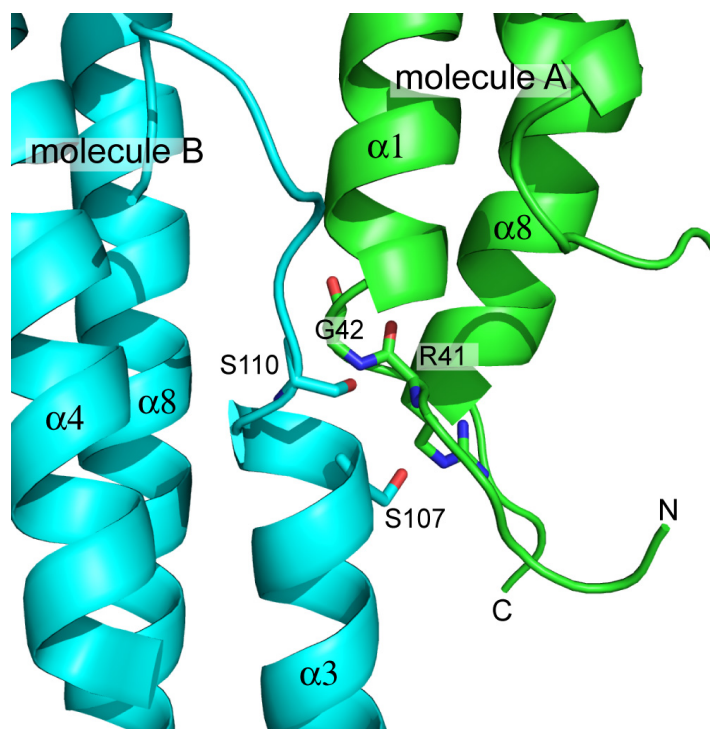


Figure 4-5: The structure of SipD³⁹⁻³⁴³ showing the interaction between the two molecules in the asymmetric unit. Residues S107 and S110 of molecule B formed hydrogen bonds with the backbone amide groups of residues R41 and G42.

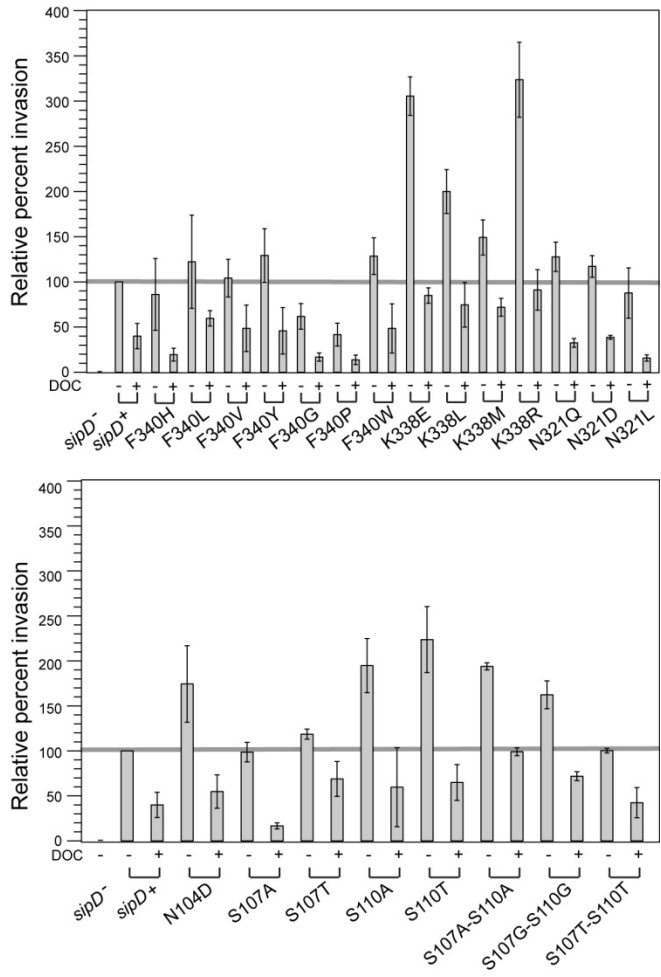


Figure 4-6: Plots showing the invasiveness of *Salmonella* strains containing mutations in SipD with (+) or without (-) 2.5 mM deoxycholate. Percent invasion was calculated relative to that of the invasiveness for the *sipD*⁺ strain in the absence of deoxycholate.

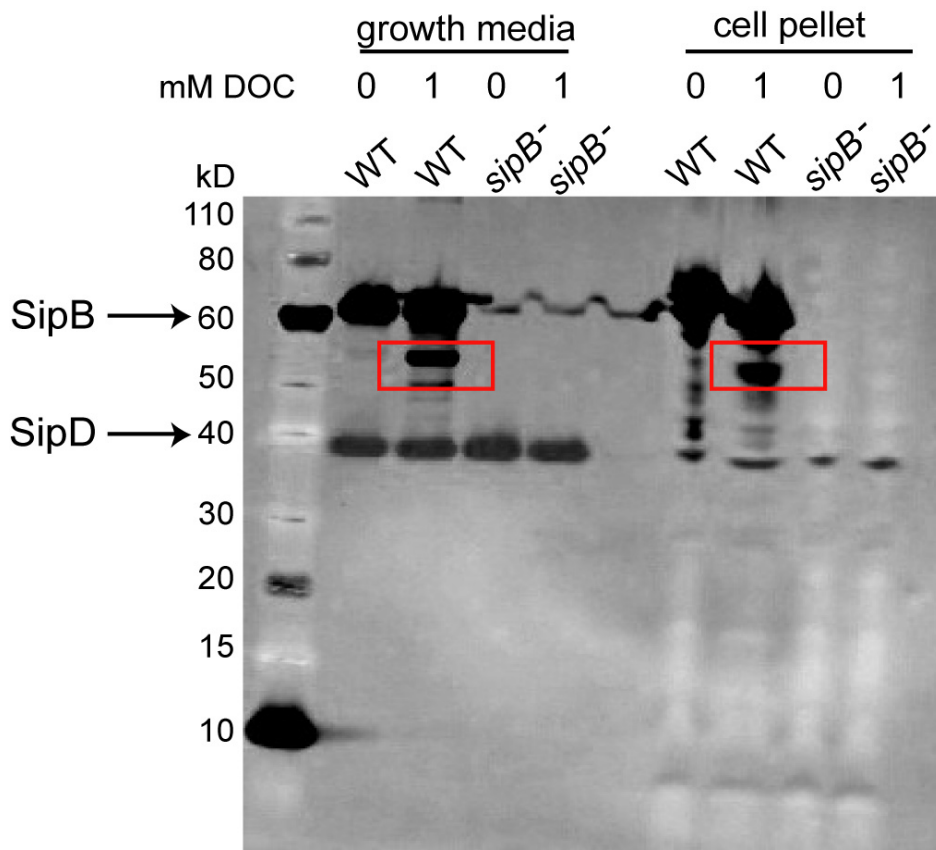


Figure 4-7: An immunoblot showing the degradation of SipB in *Salmonella* upon addition of 1 mM deoxycholate (DOC). The band corresponding to the degradation product of SipB is boxed. The *sipB⁻* strain was used as a negative control and the expression of SipD was unaffected by 1 mM DOC.

The amount of SipD and SipB secreted into the growth medium or associated with the cell pellet was unaltered in presence of deoxycholate. However, the anti-SipB antibody bound to a 55 kD band in addition to the band for full length SipB (62 kD) in the deoxycholate containing cultures of *Salmonella* [Figure 4-7]. This suggested that the bile salt was causing the degradation of SipB into a 55 kD product which still retained the epitope against the anti-SipB antibody (*details of the protocol used for immunoblotting are described in chapter 2, section 2.9.1*).

4.3. Discussion

Enteric pathogens such as *Salmonella* and *Shigella* are sensitive to bile salts present in the human intestine (1). The bile salt deoxycholate was reported to bind to the T3SS tip proteins of *Salmonella* (SipD) and *Shigella* (IpaD) (6). Interestingly, bile repressed the ability of *Salmonella* to invade cultured eukaryotic cells while stimulating the invasiveness of *Shigella* (3, 4). In order to gain insight into how bile salts interact with the tip protein of *Salmonella*, the crystal structures of SipD³⁹⁻³⁴³ bound to bile salts deoxycholate and chenodeoxycholate were solved and are reported herein. In these structures, deoxycholate and chenodeoxycholate were bound in an identical manner at a hydrophobic pocket formed at the interface of three molecules of SipD³⁹⁻³⁴³. Further, the carboxyl groups of the bile salts were within hydrogen bonding distance of the side chain amide group of N321 and the amine group of K338 of SipD³⁹⁻³⁴³. Site-directed mutagenesis aimed at disrupting the SipD-deoxycholate interaction failed to affect the invasiveness of *Salmonella*. This phenotype suggested that the substitution of one or two amino acids might be insufficient to disrupt the interaction between SipD and deoxycholate.

Growth of *Shigella* in presence of deoxycholate results in the recruitment of the *Shigella* translocon protein IpaB on the T3SS tip complex (5). This suggests that the tip complex of

Shigella might be using bile salts as a sensor to trigger the next step in the formation of the translocon and this might explain why deoxycholate upregulates the invasiveness of *Shigella*. The secretion levels of *Salmonella* SipD and the *Salmonella* translocon protein SipB in presence or absence of deoxycholate were compared to test if deoxycholate represses the invasiveness of *Salmonella* by affecting the secretion of these two proteins. Although deoxycholate did not affect the secretion of SipD, SipB underwent degradation into a ~55 kD product when *Salmonella* was grown in presence of 1 mM deoxycholate. A possibility is that the binding of bile salts to SipD at the tip complex interferes with the assembly of the translocon, and as a result SipB is destabilized and is degraded by proteases. Further studies on the interaction between SipD and SipB in the presence of bile salts will shed light on this problem.

4.3.1. Heterogeneity of the bile salt binding sites - In total, four crystal structures of tip proteins bound to bile salts have been reported. The first two structures are those of SipD³⁹⁻³⁴³-deoxycholate and SipD³⁹⁻³⁴³-chenodeoxycholate complexes reported herein. The third structure corresponds to *Shigella* IpaD¹²¹⁻³¹⁹ bound to deoxycholate (7). IpaD¹²¹⁻³¹⁹ lacked the N-terminal α -helical hairpin. The asymmetric unit of the IpaD¹²¹⁻³¹⁹-deoxycholate complex consists of two molecules of IpaD¹²¹⁻³¹⁹ (chain A and chain B) bound to two molecules of deoxycholate (DOC A and DOC B) at two slightly overlapping sites [**Figure 4-8**]. DOC A was bound to chain A on the same side as the mixed α/β region whereas DOC B was bound to chain B on the opposite side as the mixed α/β region. The binding site of DOC B is closer to the bile salt binding site in the SipD-deoxycholate complex reported herein. Nonetheless, the multiple structures of tip-bile salt complexes show that multiple regions of the tip protein can interact with deoxycholate.

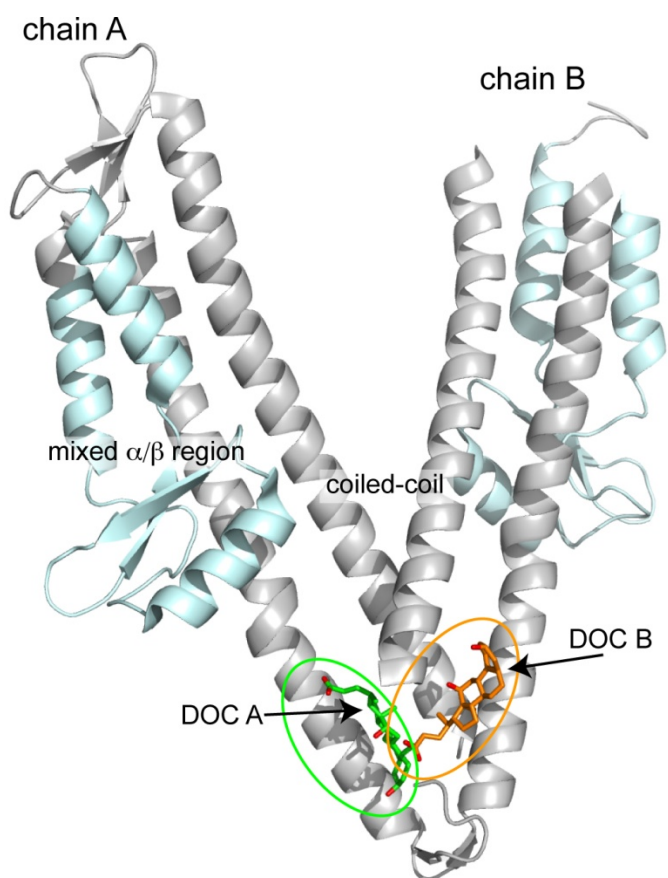


Figure 4-8: Crystal structure of IpaD¹²¹⁻³¹⁹ bound to deoxycholate (7). The two chains of IpaD¹²¹⁻³¹⁹ are labeled and the two bile salt binding sites are circled. DOC A and DOC B stand for the two molecules of deoxycholate. DOC A was bound on the same side as the mixed α/β region (colored cyan) of chain A. DOC B was on the opposite side as the mixed α/β region of chain B. This figure was prepared using PDB ID 3R9V.

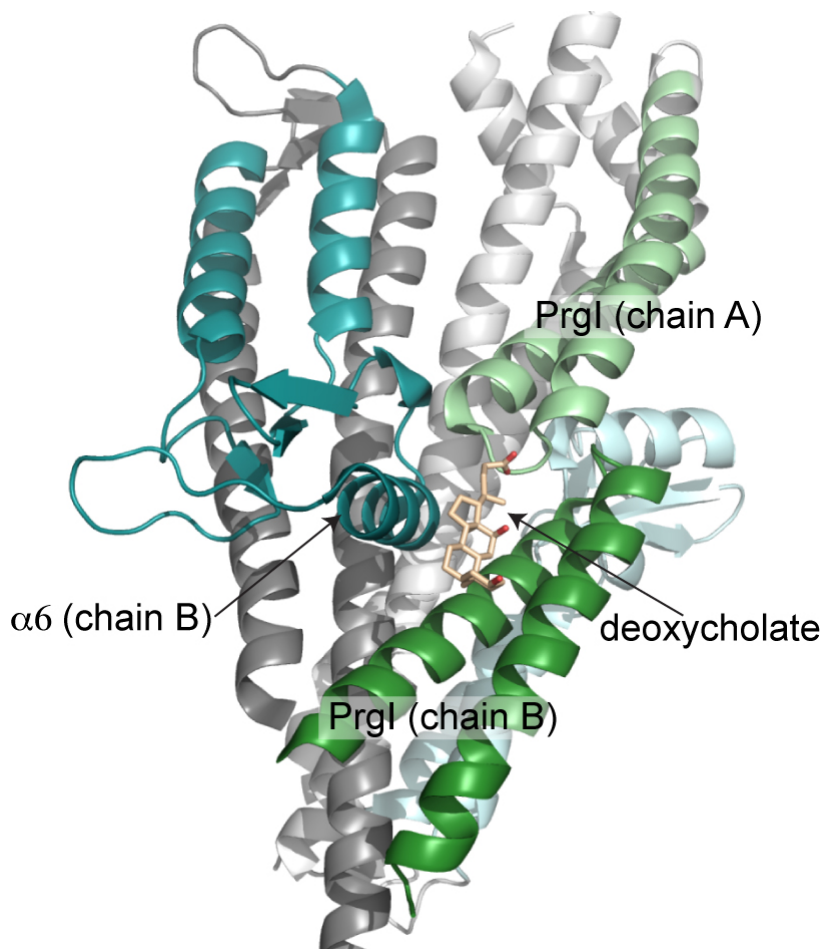


Figure 4-9: Cartoon showing the structure of a SipD¹²⁷⁻³⁴³-PrgI fusion molecule bound to deoxycholate (8). The deoxycholate molecule is shown as sticks. Deoxycholate was bound at the interface of PrgI from chain A and helix $\alpha 6$ of SipD and the central portion of PrgI of chain B. This figure was prepared using PDB ID 3ZQB.

Finally, deoxycholate was crystallized with a fusion molecule composed of the *Salmonella* needle protein PrgI connected to SipD residues 127 to 343 by means of a 5-residue Gly-Gly-Ser-Gly-Gly linker (8). **Figure 4-9** shows the structure of the SipD¹²⁷⁻³⁴³-PrgI fusion molecule bound to deoxycholate. SipD¹²⁷⁻³⁴³ lacks the N-terminal α -helical hairpin domain. The SipD¹²⁷⁻³⁴³-PrgI-deoxycholate complex contains two molecules of SipD¹²⁷⁻³⁴³ (chain A and chain B) dimerized along their coiled coils. PrgI folded against the convex side of the coiled coil, immediately below the mixed α/β region of each of the SipD¹²⁷⁻³⁴³ molecules. Deoxycholate bound at a pocket formed by the P-S-D-P turn motif of PrgI from chain A along with PrgI and helix $\alpha 6$ of SipD¹²⁷⁻³⁴³ from chain B.

The interaction between bile salts and tip proteins was also studied by NMR (9, 10) and fluorescence spectroscopy (6, 10). NMR titration of ¹⁵N-labeled SipD³⁹⁻³⁴³ (9) or ¹⁵N-labeled IpaD³⁸⁻³²¹ (10) with bile salts perturbed several residues that were globally distributed on the tip proteins. Additionally, two Förster resonance energy transfer (FRET)-based assays were used to study the interaction between full length IpaD and deoxycholate (6, 10). Using FRET between a fluorescein molecule attached to the carboxyl group of deoxycholate and a coumarin molecule attached to full length IpaD (6), deoxycholate was predicted to bind at a pocket formed by the N-terminal helices and the coiled coil of full length IpaD. A separate study determined how bile salt binding changed FRET between FIAsh tags placed at four tetracysteine (TC) pockets on different locations of IpaD (10) and concluded that deoxycholate binding induces large-scale conformational changes throughout the tip protein.

Taken together, the heterogeneity in the mode of interaction between the tip proteins SipD and IpaD and bile salts could be attributed to the use of different constructs of SipD and IpaD with or without the N-terminal α -helical hairpin domain, the use of different techniques (X-ray

crystallography, NMR, and Fluorescence), or the absence of a distinct bile salt binding pocket on the tip proteins. Nevertheless, a common feature seen in the crystal structures is that bile salts bound at the interface of two or more protein molecules. Moreover, both NMR and fluorescence-based studies concluded that bile salt binding induced global conformational changes in the tip proteins. Thus, it is possible that bile salts bind at the interface of the needle and tip proteins or two tip proteins and influence the packing of the tip complex, which in turn affects the regulation of the T3SS of *Salmonella* and *Shigella* in a contrasting manner. Such conformational changes might prevent the binding of SipB to the tip complex in *Salmonella* leading to the degradation of SipB while, in *Shigella*, they promote the attachment of IpaB on the tip complex. Bile-mediated repression might be how *Salmonella* exploits the concentration of bile to sense its local environment and prevents premature activation of the T3SS thereby conserving valuable resources.

4.4. References

1. Gunn, J. S. (2000) Mechanisms of bacterial resistance and response to bile, *Microbes. Infect.* 2, 907-913.
2. Linda, C. (2010) Physiology.
3. Prouty, A. M., and Gunn, J. S. (2000) *Salmonella enterica* serovar typhimurium invasion is repressed in the presence of bile, *Infect. Immun.* 68, 6763-6769.
4. Pope, L. M., Reed, K. E., and Payne, S. M. (1995) Increased protein secretion and adherence to HeLa cells by *Shigella* spp. following growth in the presence of bile salts, *Infect. Immun.* 63, 3642-3648.
5. Olive, A. J., Kenjale, R., Espina, M., Moore, D. S., Picking, W. L., and Picking, W. D. (2007) Bile salts stimulate recruitment of IpaB to the *Shigella flexneri* surface, where it

- colocalizes with IpaD at the tip of the type III secretion needle, *Infect. Immun.* 75, 2626-2629.
6. Stensrud, K. F., Adam, P. R., La Mar, C. D., Olive, A. J., Lushington, G. H., Sudharsan, R., Shelton, N. L., Givens, R. S., Picking, W. L., and Picking, W. D. (2008) Deoxycholate interacts with IpaD of *Shigella flexneri* in inducing the recruitment of IpaB to the type III secretion apparatus needle tip, *J. Biol. Chem.* 283, 18646-18654.
 7. Barta, M. L., Guragain, M., Adam, P., Dickenson, N. E., Patil, M., Geisbrecht, B. V., Picking, W. L., and Picking, W. D. (2012) Identification of the bile salt binding site on IpaD from *Shigella flexneri* and the influence of ligand binding on IpaD structure, *Proteins* 80, 935-945.
 8. Lunelli, M., Hurwitz, R., Lambers, J., and Kolbe, M. (2011) Crystal structure of PrgI-SipD: insight into a secretion competent state of the type three secretion system needle tip and its interaction with host ligands, *PLoS Pathog.* 7, e1002163.
 9. Wang, Y., Nordhues, B. A., Zhong, D., and De Guzman, R. N. (2010) NMR Characterization of the Interaction of the *Salmonella* Type III Secretion System Protein SipD and Bile Salts, *Biochemistry* 49, 4220-4226.
 10. Dickenson, N. E., Zhang, L., Epler, C. R., Adam, P. R., Picking, W. L., and Picking, W. D. (2010) Conformational Changes in IpaD from *Shigella flexneri* upon Binding Bile Salts Provide Insight into the Second Step of Type III Secretion, *Biochemistry*.

CHAPTER 5: Expression of the *Salmonella* translocon protein SipB for NMR studies

5.1. Introduction

The T3SS translocon sits on the tip complex and associates with the host cell membrane to form the translocation pore. The pore is ~ 30-35 Å in diameter and allows the passage of effectors directly into the host cell cytoplasm (1). The translocon is composed of the membrane proteins SipB and SipC in *Salmonella* (2). In the bacterial cytoplasm SipB and SipC are partitioned and stabilized by the chaperone SicA (3). Following contact with host cell the translocon proteins assemble on the tip complex to form the functional translocon (4).

The secondary structure prediction for SipB is shown in **Figure 5-1**. SipB contains an N-terminal hydrophilic domain, two transmembrane helices, and a C-terminal amphipathic region predicted to be α -helical (5) [**Figures 5-1 to 5-3**]. The signal for T3SS-mediated secretion was reported to be within residues 3 to 8 of SipB while residues 80 to 100 were important for binding to SicA (6). The transmembrane helices within residues 313 to 333 and 399 to 419 are connected by a hydrophilic loop (residues 333 to 399) (5) [**Figure 5-3**]. The transmembrane helices could intimately associate with model bilayers thereby positioning the loop region within the lumen of liposomes (5). The C-terminal amphipathic region although peripherally associated with membranes, was reported necessary for the insertion of SipB into bilayers (5) [**Figure 5-3**]. A peptide derived from the C-terminal region could inhibit membrane fusion of SipB and the entry of *Salmonella* into HeLa cells (7).

How the translocon assembles on the tip complex is poorly understood. Constructs corresponding to the N-terminal hydrophilic domain, the hydrophilic loop region, and the C-terminal amphipathic region of SipB were expressed in *E. coli* in order to determine their

structure and molecular interactions with other components of the needle apparatus like SipD and SipC. Structural characterization of the different regions of SipB was useful in designing an ideal construct for use in NMR studies.

5.2. Results

5.2.1. *Expression and purification of SipB* - Residues 1 to 16 and 50 to 72 in SipB were predicted (8) to form random coils [Figure 5-1]. Further, residues 51-72 of the SipB homolog IpaB was reported to bind its chaperone IpgC, which is homologous to the *Salmonella* chaperone SicA (9). Flexible regions that need to be stabilized by a chaperone could lead to a poor NMR spectrum. Therefore, 81 residues from the N-terminus were not included in the construct representing the N-terminal hydrophilic domain of SipB. The hydrophobic transmembrane helices were also not included in the expression constructs of SipB. The “DAS” Transmembrane Prediction server (10) was used to localize the two transmembrane helices in SipB within residues 313 to 333 and 399 to 419 [Figures 5-2 & 5-3]. Finally, the C-terminus of SipB, was predicted to form an α -helix with an amphipathic region within residues 526 to 593 (5) [Figure 5-3]. Accordingly, DNA segments coding for SipB residues 82 to 312 (SipB⁸²⁻³¹²), 340 to 404 (SipB³⁴⁰⁻⁴⁰⁴), 436 to 518 (SipB⁴³⁶⁻⁵⁹³), and 521 to 593 (SipB⁵²¹⁻⁴⁹³) were subcloned into pET22B, which appended a C-terminal hexahistidine tag (LEH₆) to the recombinant protein. These regions of SipB were also subcloned into pET21A, which appended an N-terminal His-GB1 tag to enhance the solubility of the recombinant proteins. The constructs of SipB were expressed in *E. coli* BL21 (DE3) DNAY cells.

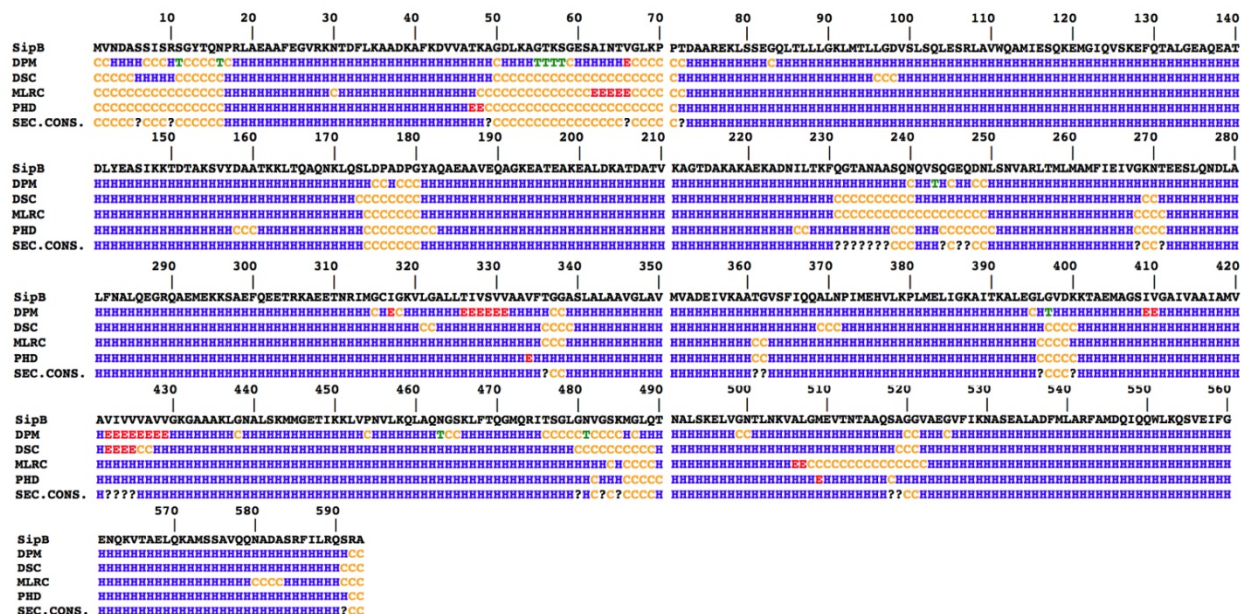


Figure 5-1: The predicted secondary structure of SipB. The secondary structure of SipB was predicted using four algorithms: DPM (11), DSC (12), MLRC (13), and PHD (14). SEC. CONS. stands for secondary consensus, which is a combined representation of the four prediction algorithms. Residues having high α -helical propensity are marked as “H” in blue, random coil regions are represented by “C” in yellow, regions likely to form extended β -strands are shown as “E” in red, and residues forming turns are labeled as “T” in green.

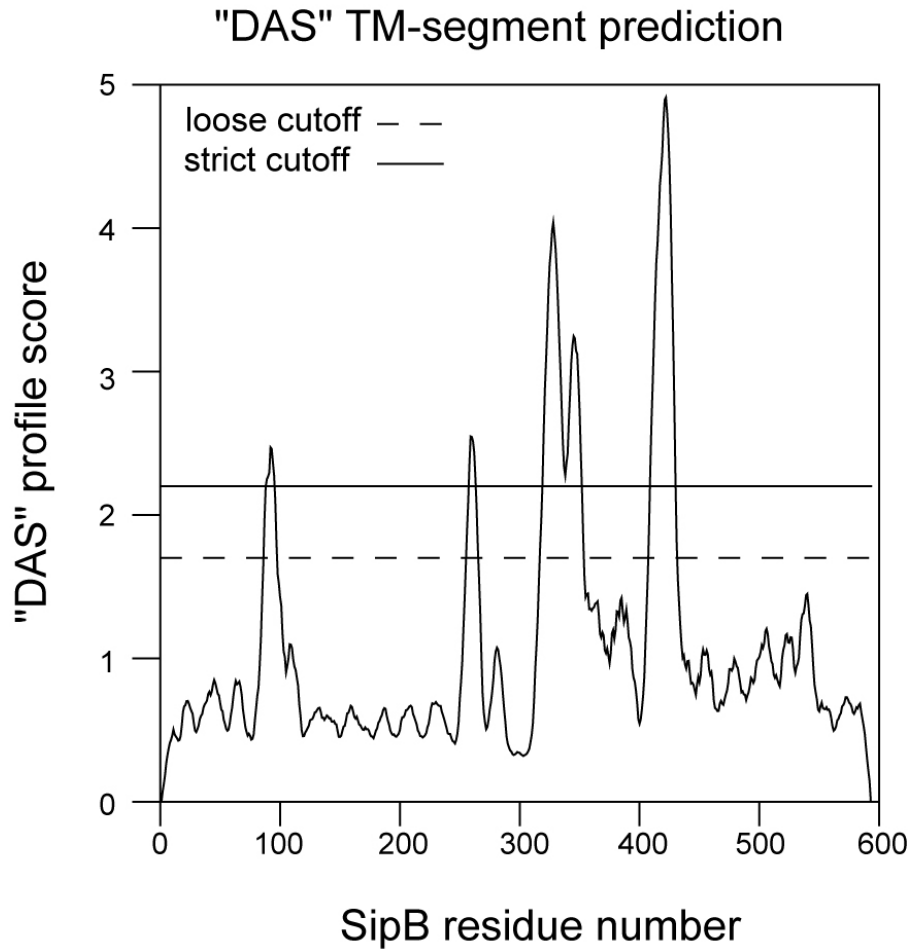


Figure 5-2: A hydropathy plot showing the location of the hydrophobic transmembrane helices in SipB. Regions within SipB residues 313-333 and 399-419 were predicted to contain transmembrane helices. The “DAS” Transmembrane Prediction server (10) was used to generate the hydropathy plot.

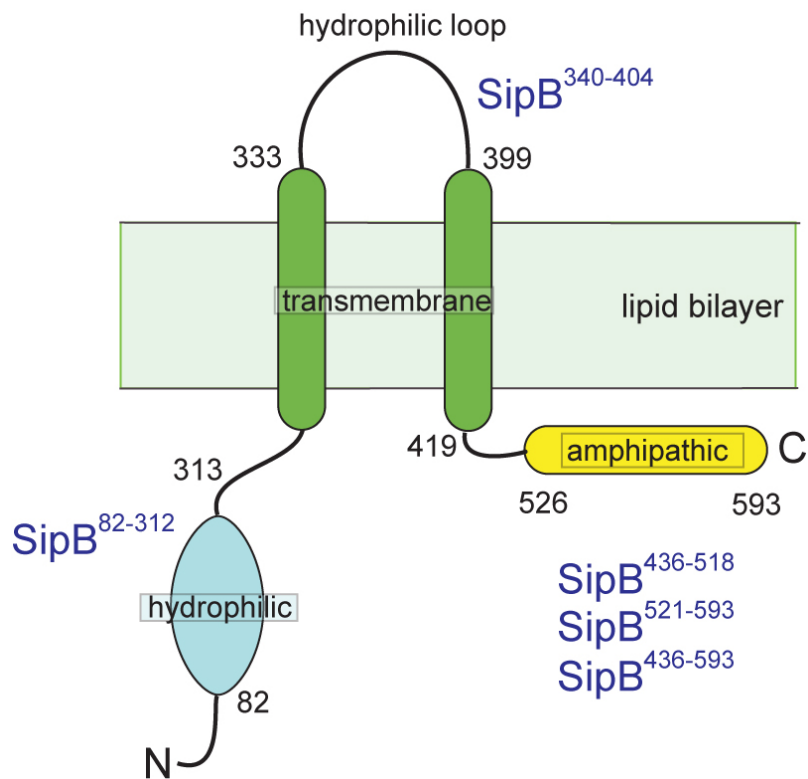


Figure 5-3: A schematic representation of the different regions of SipB based on the predicted transmembrane regions (shown in **Figure 5-2**) and membrane-binding studies with purified SipB (5). The diagram is based on the topology of SipB in phospholipid bilayers and vesicles (5). The N-terminal hydrophilic domain is colored blue, the transmembrane helices associated with a lipid membrane is colored green, and the amphipathic region is colored yellow. The expression constructs corresponding to each region within SipB are also labeled.

SipB⁸²⁻³¹² within both pET22B and pET21A afforded high levels of recombinant protein expression [Figure 5-4A]. The pET21A expression vector was used for later experiments owing to ease in purification (*protocol used for the purification of SipB⁸²⁻³¹² is described in chapter 2, section 2.1*). SipB³⁴⁰⁻⁴⁰⁴ showed very low protein expression from both the expression vectors. SipB⁴³⁶⁻⁵¹⁸ could be expressed only as a fusion protein containing the His₆-GB1 solubility tag and the recombinant protein was unstable in solution upon removal of the solubility tag [Figures 5-4B & 5-4C]. Moreover, SipB⁴³⁶⁻⁵¹⁸ retaining the His₆-GB1 tag (SipB⁴³⁶⁻⁵¹⁸_{-GB1}) produced CD and NMR spectra closely resembling that of free GB1. Thus, this construct was not used for NMR studies. Expression of SipB⁴³⁶⁻⁵⁹³ led to the death of bacterial cells suggesting that this region was toxic to *E. coli*. SipB⁸²⁻³¹² was further characterized using CD and NMR spectroscopy and used for NMR titrations with SipD (*NMR titrations of SipB and SipD are described in chapter 6, section 6.2*).

5.2.2. *CD Spectroscopy* - The secondary structure of SipB⁸²⁻³¹² was examined using CD spectroscopy. The resultant spectrum had well defined minima at 208 nm and 222 nm, indicating a highly α -helical fold [Figure 5-5A]. The thermal melting profile of SipB⁸²⁻³¹² at 222 nm showed a distinct unfolding event with a T_m of 54 °C. To further localize the boundaries of the folded regions, we generated truncations SipB⁸²⁻²⁶⁷, SipB⁸²⁻²⁴⁰, and SipB⁸²⁻²²⁶. All three truncations were α -helical, with T_m values similar to that of SipB⁸²⁻³¹². SipB⁸²⁻²⁶⁷, SipB⁸²⁻²⁴⁰, and SipB⁸²⁻²²⁶ had T_m values of 53.8 °C, 59.8 °C, and 50.2 °C respectively [Figure 5-5B]. NMR spectroscopy was employed for further characterization of the SipB truncations.

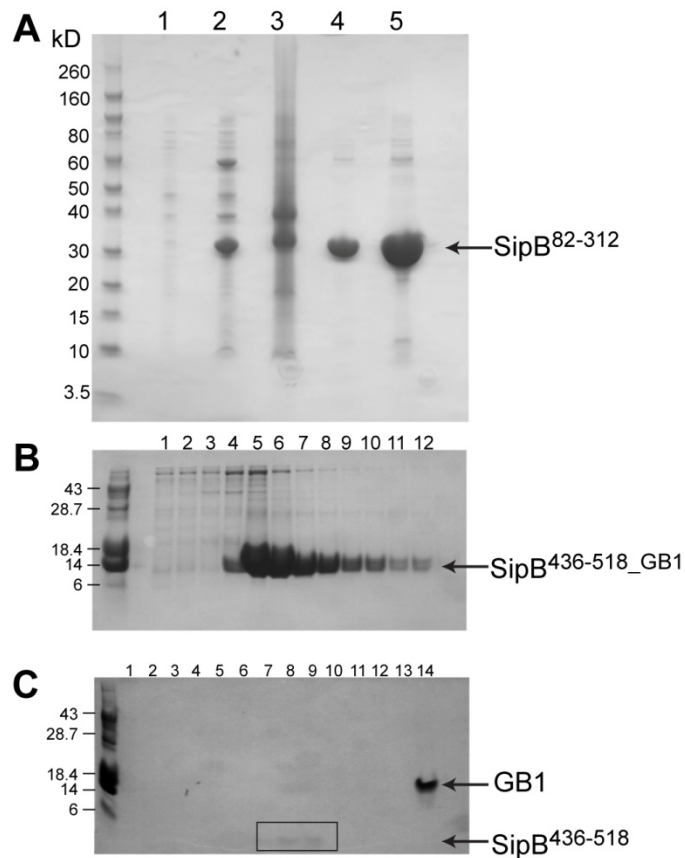


Figure 5-4: (A) SDS-PAGE showing the purification of SipB⁸²⁻³¹². Lane 1 shows the bacterial supernatant before induction of protein expression, lane 2 shows bacterial supernatant after induction of protein expression, lane 3 shows the bacterial cell pellet after induction of protein expression, lane 4 shows SipB⁸²⁻³¹² after purification using Ni⁺²-affinity chromatography, and lane 5 shows SipB⁸²⁻³¹² after dialysis into a low salt buffer and concentration (*purification of SipB⁸²⁻³¹² is described in chapter 2, section 2.1*). (B) SDS-PAGE showing the purification of SipB⁴³⁶⁻⁵¹⁸ containing the His₆-GB1 tag (SipB⁴³⁶⁻⁵¹⁸_GB1). Lanes 1 and 2 contain the flow through and wash respectively. Lanes 3 through 12 contain fractions eluted from the Ni⁺²-affinity column containing increasing amounts of SipB⁴³⁶⁻⁵¹⁸_GB1. (C) SDS-PAGE showing the separation of SipB⁴³⁶⁻⁵¹⁸ from the His-GB1 tag after digestion with Tobacco Etch Virus protease. Removal of the His-GB1 solubility tag (lane 14) destabilized SipB⁴³⁶⁻⁵¹⁸ and the recombinant protein was degraded in solution. Extremely low amounts of SipB⁴³⁶⁻⁵¹⁸ (boxed) were detected in the flow through and wash fractions (lanes 1-13)

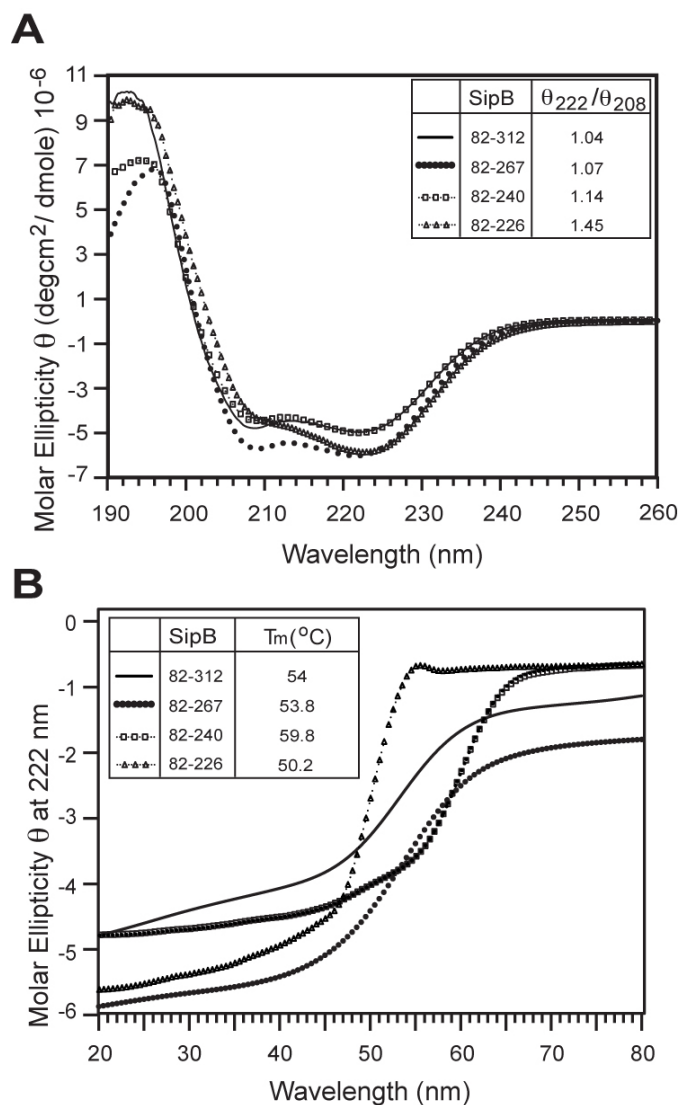


Figure 5-5: (A) CD spectra of the truncations SipB⁸²⁻³¹², SipB⁸²⁻²⁶⁷, SipB⁸²⁻²⁴⁰, and SipB⁸²⁻²²⁶ showing a highly α -helical secondary structure indicated by the negative ellipticity at 208 nm and 222 nm. (B) Thermal denaturation of SipB⁸²⁻³¹² showed a distinct unfolding event with a T_m of 54 °C suggesting the presence of a folded domain. The truncations SipB⁸²⁻²⁶⁷, SipB⁸²⁻²⁴⁰, and SipB⁸²⁻²²⁶ showed thermal denaturation profiles similar to SipB⁸²⁻³¹².

5.2.3. ^1H - ^{15}N -TROSY spectra of SipB constructs - A ^1H - ^{15}N -TROSY (15) spectrum of SipB⁸²⁻³¹² showed less than 3% of the backbone amide groups and the remaining peaks were broadened [Figure 5-6A]. Protein concentrations as low as 200 μM , high acquisition temperatures, and high salt containing buffer did not improve the NMR spectrum of SipB⁸²⁻³¹², suggesting that its poor quality was due to highly dynamic regions within the protein rather than protein oligomerization. The truncations SipB⁸²⁻²⁶⁷, SipB⁸²⁻²⁴⁰, and SipB⁸²⁻²²⁶ were designed in order to optimize the NMR construct for the N-terminal domain of SipB. Deletion of residues 312 to 266 (SipB⁸²⁻²⁶⁷) did not have any effect on the ^1H - ^{15}N -TROSY spectrum [Figure 5-6B]. However, deletion of residues 312 to 239 (SipB⁸²⁻²⁴⁰), or 312 to 225 (SipB⁸²⁻²²⁶) yielded much improved spectra showing > 80% of the backbone amide groups [Figures 5-6C & 5-6D]. The recently solved crystal structure of SipB⁸²⁻²²⁶ showed that this region forms a trimeric coiled coil (16). Further, NMR titrations of ^{15}N -SipD³⁹⁻³⁴³ with unlabeled SipB⁸²⁻²²⁶ detected an interaction between these two proteins (NMR titrations of ^{15}N -SipD³⁹⁻³⁴³ with SipB⁸²⁻²²⁶ is described in chapter 6, section 6.2). Thus, attempts were made to assign the backbone NMR resonances of ^{15}N -SipB⁸²⁻²²⁶ in order to determine which residues of SipB⁸²⁻²²⁶ are affected on titration with unlabeled SipD³⁹⁻³⁴³.

5.2.4. 3D-HNCA experiments with SipB⁸²⁻²²⁶ - Initially, a 3D-HNCA (17) dataset was collected using 1 mM of ^{15}N - ^{13}C -SipB⁸²⁻²²⁶ and the first free induction decay (FID) was analyzed to determine the optimal experiment parameters. However, the FID showed poor signal-to-noise ratio, which did not improve upon increasing the number of scans from 16 to 32 [Figures 5-7A & 5-7B]. A fresh sample was prepared using 0.4 mM ^{15}N - ^{13}C -SipB⁸²⁻²²⁶ to avoid protein oligomerization, which can lead to poor NMR signal. The first FIDs from three 3D-HNCA (17) datasets collected with

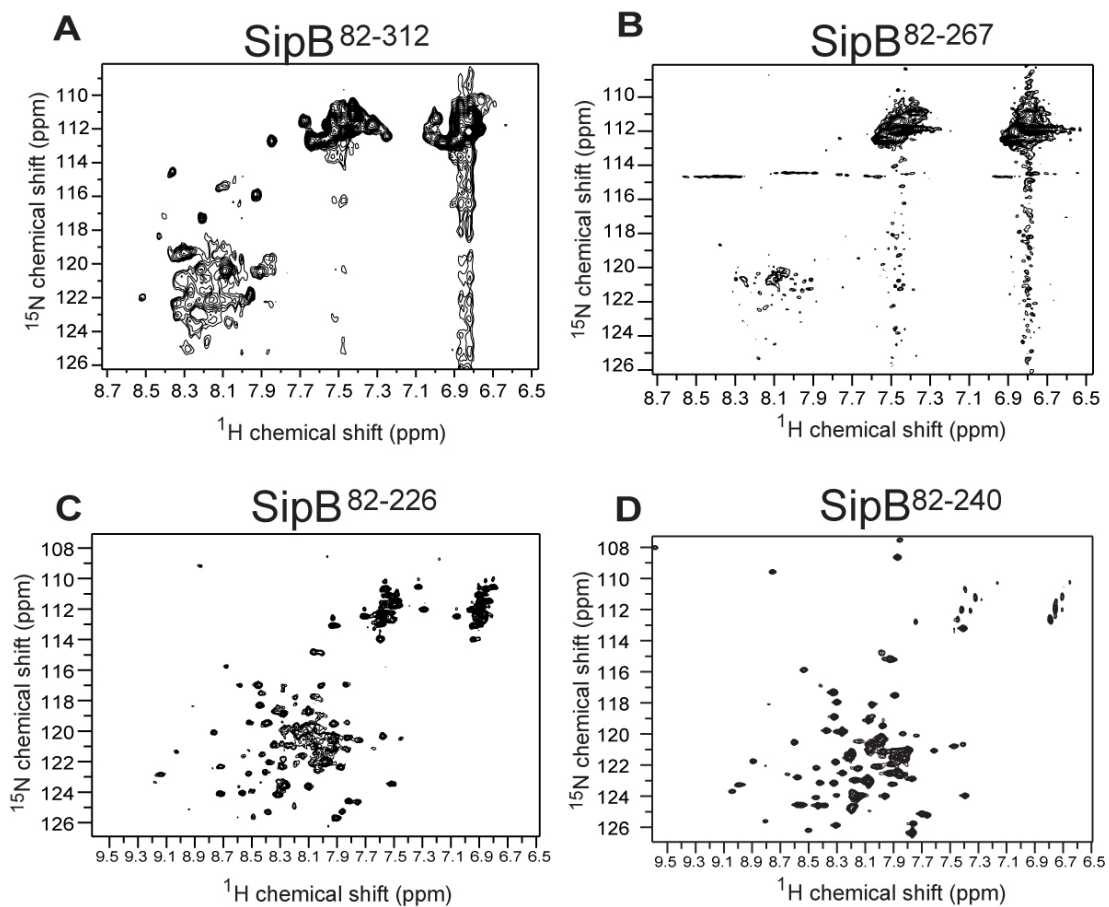


Figure 5-6: (A) & (B) ^1H - ^{15}N -TROSY spectra of SipB⁸²⁻³¹² and SipB⁸²⁻²⁶⁷ respectively showing poorly resolved peaks. (C) & (D) ^1H - ^{15}N -TROSY spectra of SipB⁸²⁻²²⁶ and SipB⁸²⁻²⁴⁰ showing well resolved backbone NMR peak resonances.

56, 64, and 84 scans showed no increase in the signal-to-noise ratio [Figures 5-7C to 5-7E] and thus the complete 3D-HNCA (17) spectra were not collected.

5.2.5. Size exclusion chromatography of SipB – Size exclusion chromatography (SEC) was used to determine the oligomeric states of SipB⁸²⁻³¹², SipB⁸²⁻²⁴⁰, and SipB⁸²⁻²²⁶. Purified SipB truncations were chromatographed through a Superdex 75 SEC column that was previously calibrated with proteins of known molecular weights. SipB⁸²⁻³¹² eluted at 107.18 ml, which is very close to the elution volume of Blue Dextran (107.51 ml) [Figure 5-8A]. Blue Dextran has a molecular weight of 200 kD and was used as a marker for the void volume of the SEC column. Monomeric SipB⁸²⁻³¹² is 26.2 kD in size and thus was estimated to form a heptameric complex to elute similar to a 200 kD protein. SipB⁸²⁻²⁴⁰ had a molecular weight of 18 kD and eluted at 106.34 ml and 135.46 ml [Figure 5-8B]. This indicated the presence of a large oligomeric population that travels through the void volume of the SEC column and a smaller trimeric population (~ 49 kD). The 17 kD SipB⁸²⁻²²⁶ also showed a biphasic elution and two elutions were seen at 104.52 ml and 141.63 ml [Figure 5-8C]. The smaller species corresponded to a dimer while, the larger population eluted in the void volume.

5.3. Discussion

In *Salmonella* the tip protein SipD assembles the T3SS tip complex and the translocon proteins SipB and SipC assemble the translocon. SipD, SipB, and SipC are critical for the attachment of *Salmonella* to cultured human intestinal epithelial cells and for the delivery of effectors directly into the cytoplasm of the host cells (4). Initial contact with the host cell membrane triggers the colocalization of SipB and SipC on SipD (4).

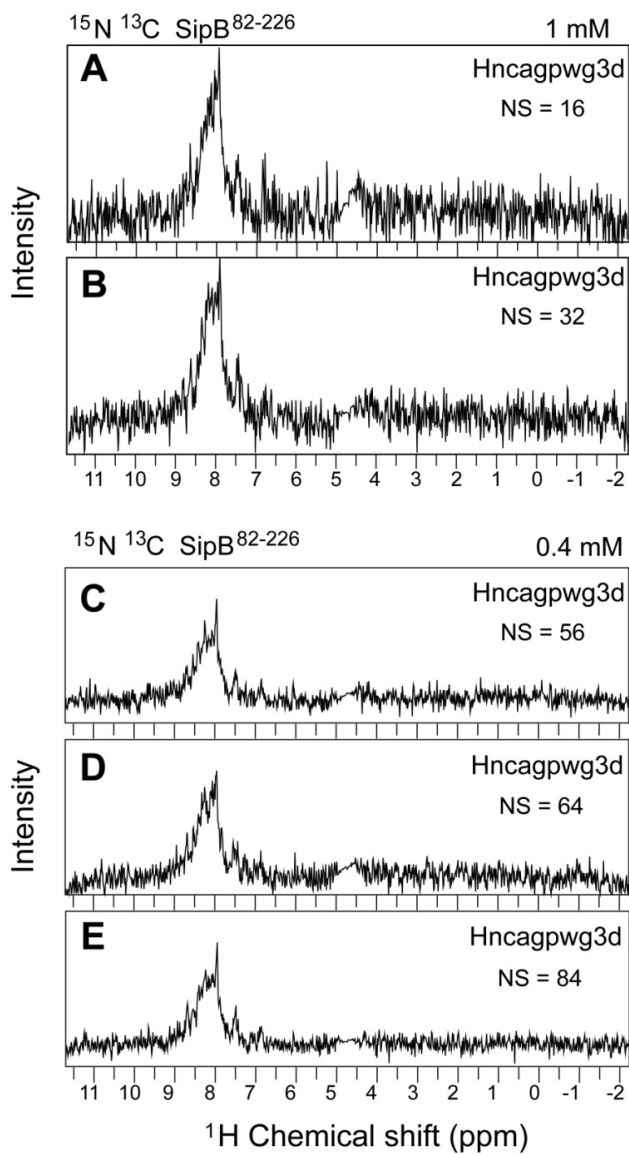


Figure 5-7: The first free induction decay (FID) from 3D-HNCA (*15*) experiments using ^{15}N - ^{13}C -SipB⁸²⁻²²⁶. Panels **A** and **B** were collected using 1 mM protein while, the panels **C**, **D**, and **E** correspond to a protein concentration of 0.4 mM. The number of scans used for the acquisition of each experiment is labeled on the respective panels.

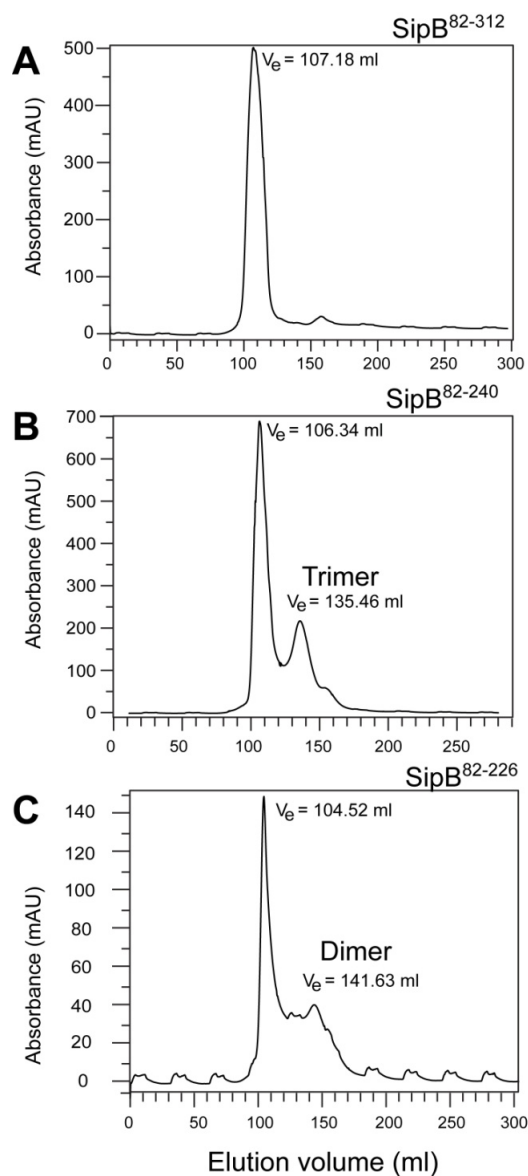


Figure 5-8: Size exclusion chromatography (SEC) of the truncations of SipB. (A) SEC of SipB⁸²⁻³¹² shows a single oligomeric population that flows through the void volume and elutes at 107.18 ml. (B) SEC of SipB⁸²⁻²⁴⁰ shows a small trimeric population ($V_e = 135.46$ ml) and a large oligomeric population ($V_e = 106.34$ ml). (C) SEC of SipB⁸²⁻²²⁶ shows a small dimeric population ($V_e = 141.63$ ml) and a large oligomeric population ($V_e = 104.52$ ml).

The delivery of effectors through the translocon is a poorly understood process and the structure of the translocon is unknown. Constructs corresponding to different regions of SipB were expressed in *E. coli* for further study.

Initial tests for expression showed that SipB³⁴⁰⁻⁴⁰⁴ corresponding to the hydrophilic loop region had extremely low levels of protein expression in *E. coli*. The C-terminus of SipB is needed for integration into lipid membranes (5). This region is predicted to form an α -helix, which can peripherally associate with the lipid membrane. SipB⁴³⁶⁻⁵¹⁸ and SipB⁵²¹⁻⁵⁹³ were designed to contain the proximal and distal portion of the C-terminal amphipathic region. SipB⁴³⁶⁻⁵¹⁸ was unstable without the GB1 solubility tag and SipB⁵²¹⁻⁵⁹³ was toxic to *E. coli* [Figures 5-4B & 5-4C]. Previously others were able to purify SipB⁴²⁸⁻⁵⁹³ (5), which is similar to the SipB⁴³⁶⁻⁵¹⁸ and SipB⁵²¹⁻⁵⁹³ constructs combined. Therefore, a SipB⁴³⁶⁻⁵⁹³ construct was also generated. However, SipB⁴³⁶⁻⁵⁹³ also had very low level of protein expression. This discrepancy could be attributed to the slightly different constructs, or use of a higher amount of IPTG (0.1 mM versus 1 mM) and a different growth medium (Tryptic soy broth versus LB broth) (5, 18). It is also noteworthy, that the reported purification protocol for SipB⁴²⁸⁻⁵⁹³ involved the extraction of the protein from cell pellets using GuHCL followed by refolding in Tris-HCL buffer (5, 18).

Only SipB⁸²⁻³¹² containing the N-terminal hydrophilic region could be over-expressed and purified to yield high quantities of recombinant protein that was stable in solution [Figure 5-4A]. CD and thermal denaturation of SipB⁸²⁻³¹² revealed a highly α -helical secondary structure containing a folded domain, which underwent a distinct unfolding event with a T_m of 54 °C [Figures 5-5A & 5-5B]. These results are in agreement with previous reports of the presence of protease-resistant domain within residues 26 to 309 of SipB (19). SipB⁸²⁻³¹² produced a narrow ¹H-¹⁵N-TROSY (15) spectrum with unresolved peaks and less than 3% of the backbone amide

groups visible. The poor quality of NMR data might be due to oligomerization or highly dynamic regions within the protein molecule. Thus low protein concentration (0.2 mM) and high acquisition temperatures (upto 42 °C) were used to rule out protein oligomerization. However, these conditions did not improve the quality of the NMR spectrum suggesting the presence of flexible regions within SipB⁸²⁻³¹².

SipB contained three regions within residues 82 to 312 that were predicted to form random coils. These regions were located within residues 173-182, 231-250, and 268-271 [**Figure 5-1**]. In order to obtain an ideal NMR spectrum corresponding to the N-terminal domain of SipB the flexible regions had to be removed. However, removal of residues 173-182 from the central portion of SipB⁸²⁻³¹² might destabilize the tertiary structure of the remaining polypeptide. Therefore, predicted random coil regions from the C-terminal end of SipB⁸²⁻³¹² were truncated to generate SipB⁸²⁻²²⁶, SipB⁸²⁻²⁴⁰, and SipB⁸²⁻²⁶⁷. Removal of the region within residues 268-271 in SipB⁸²⁻²⁶⁷ did not affect the NMR spectrum [**Figure 5-6B**]. In contrast, removal of both the predicted flexible patches within residues 231-271 in SipB⁸²⁻²⁴⁰ and SipB⁸²⁻²²⁶ produced ¹H-¹⁵N-TROSY (15) spectra showing > 80% of the backbone amide groups [**Figures 5-6C & 5-6D**]. The crystal structure of SipB⁸²⁻²²⁶ was recently determined and shown to form a three-helix bundle (16). The structure of SipB⁸²⁻²²⁶ agrees with the predicted secondary structure of SipB in **Figure 5-1**. In the secondary structure prediction residues 95-98 and 175-180 were predicted to adopt a random coil conformation. In SipB⁸²⁻²²⁶ these regions were disordered. One difference however, was that residues 124 and 125 were predicted to have α -helical character but in SipB⁸²⁻²²⁶ these residues form a helical turn and are disordered as well. NMR titrations of SipB⁸²⁻²²⁶ with unlabeled SipD³⁹⁻³⁴³ showed that this region of SipB could interact with the tip protein (see chapter 6). Hence, attempts were made to assign the backbone NMR resonances of SipB⁸²⁻²²⁶.

Despite a well-dispersed 2D-NMR spectrum, ^{15}N - ^{13}C -SipB⁸²⁻²²⁶ yielded poor signal-to-noise ratio in a 3D-HNCA spectrum [Figures 5-7A & 5-7B] and low protein concentration and increased number of scans did not make any difference to the NMR signal [Figures 5-7C to 5-7E].

Purified full length SipB was reported to form homohexamers using its N-terminal domain (19). Although SipB⁸²⁻²⁴⁰ and SipB⁸²⁻²²⁶ were designed to lack predicted flexible regions these constructs might still retain the oligomerization motif within the N-terminal domain. Size exclusion chromatography of SipB⁸²⁻²²⁶ revealed the presence of a major population of > 200 kD oligomer similar to SipB⁸²⁻³¹² [Figures 5-8A & 5-8C]. SipB⁸²⁻²²⁶ also formed a minor population roughly corresponding to a dimeric species [Figure 5-8C]. Similarly, SipB⁸²⁻²⁴⁰ yielded a large oligomeric species and a smaller trimeric species [Figure 5-8B]. Thus, SEC suggested that removal of their respective flexible regions shifted the equilibrium of SipB⁸²⁻²²⁶ and SipB⁸²⁻²⁴⁰ to a heterogenous oligomer population. Therefore, the poor signal in a 3D-HNCA (17) experiment using ^{15}N - ^{13}C -SipB⁸²⁻²²⁶ could be due to a small monomeric population at 25 °C, which was forming independent of the concentration of protein molecules. The significance of the oligomerization of SipB using its N-terminal domain is unknown.

In summary, SipB⁸²⁻³¹² could be easily expressed and maintained in solution. The presence of flexible regions in addition to a folded domain within SipB⁸²⁻³¹² resulted in a poor NMR signal. These flexible regions were located within residues 231-271 and their truncation resulted in improved 2D-NMR spectra. However, even though SipB⁸²⁻²⁴⁰ and SipB⁸²⁻²²⁶ had well dispersed 2D-NMR spectra they produced low signals in a 3D-HNCA experiment probably due to a small monomeric population. One way to counter this problem would be to design point

mutations that introduce surface charges on Sipb, thereby preventing oligomer formation while still retaining the function of the translocon protein.

5.4. References

1. Ide, T., Laarmann, S., Greune, L., Schillers, H., Oberleithner, H., and Schmidt, M. A. (2001) Characterization of translocation pores inserted into plasma membranes by type III-secreted Esp proteins of enteropathogenic *Escherichia coli*, *Cell. Microbiol.* 3, 669-679.
2. Kaniga, K., Tucker, S., Trollinger, D., and Galan, J. E. (1995) Homologs of the *Shigella* IpaB and IpaC invasins are required for *Salmonella typhimurium* entry into cultured epithelial cells, *J.Bacteriol.* 177, 3965-3971.
3. Tucker, S. C., and Galan, J. E. (2000) Complex function for SicA, a *Salmonella enterica* serovar typhimurium type III secretion-associated chaperone, *J Bacteriol* 182, 2262-2268.
4. Lara-Tejero, M., and Galan, J. E. (2009) *Salmonella enterica* serovar typhimurium pathogenicity island 1-encoded type III secretion system translocases mediate intimate attachment to nonphagocytic cells, *Infect. Immun.* 77, 2635-2642.
5. McGhie, E. J., Hume, P. J., Hayward, R. D., Torres, J., and Koronakis, V. (2002) Topology of the *Salmonella* invasion protein SipB in a model bilayer, *Mol Microbiol* 44, 1309-1321.
6. Kim, B. H., Kim, H. G., Kim, J. S., Jang, J. I., and Park, Y. K. (2007) Analysis of functional domains present in the N-terminus of the SipB protein, *Microbiology* 153, 2998-3008.

7. Hayward, R. D., Hume, P. J., McGhie, E. J., and Koronakis, V. (2002) A Salmonella SipB-derived polypeptide blocks the 'trigger' mechanism of bacterial entry into eukaryotic cells, *Mol Microbiol* 45, 1715-1727.
8. Deleage, G., Blanchet, C., and Geourjon, C. (1997) Protein structure prediction. Implications for the biologist, *Biochimie* 79, 681-686.
9. Lunelli, M., Lokareddy, R. K., Zychlinsky, A., and Kolbe, M. (2009) IpaB-IpgC interaction defines binding motif for type III secretion translocator, *Proc. Natl. Acad. Sci. U.S.A.* 106, 9661-9666.
10. Cserzo, M., Wallin, E., Simon, I., von Heijne, G., and Elofsson, A. (1997) Prediction of transmembrane alpha-helices in prokaryotic membrane proteins: the dense alignment surface method, *Protein Eng* 10, 673-676.
11. Deleage, G., and Roux, B. (1987) An algorithm for protein secondary structure prediction based on class prediction, *Protein Eng* 1, 289-294.
12. King, R. D., and Sternberg, M. J. (1996) Identification and application of the concepts important for accurate and reliable protein secondary structure prediction, *Protein Sci* 5, 2298-2310.
13. Guermeur, Y., Geourjon, C., Gallinari, P., and Deleage, G. (1999) Improved performance in protein secondary structure prediction by inhomogeneous score combination, *Bioinformatics* 15, 413-421.
14. Rost, B., and Sander, C. (1993) Prediction of protein secondary structure at better than 70% accuracy, *J Mol Biol* 232, 584-599.
15. Czisch, M., and Boelens, R. (1998) Sensitivity enhancement in the TROSY experiment, *J. Magn. Reson.* 134, 158-160.

16. Barta, M. L., Dickenson, N. E., Patil, M., Keightley, A., Wyckoff, G. J., Picking, W. D., Picking, W. L., and Geisbrecht, B. V. (2012) The structures of coiled coil domains from type III secretion system translocators reveal homology to pore-forming toxins, *J Mol Biol* 417, 395-405.
17. Grzesiek, S., Dobeli, H., Gentz, R., Garotta, G., Labhardt, A. M., and Bax, A. (1992) ¹H, ¹³C, and ¹⁵N NMR backbone assignments and secondary structure of human interferon-gamma, *Biochemistry* 31, 8180-8190.
18. Hayward, R. D., and Koronakis, V. (1999) Direct nucleation and bundling of actin by the SipC protein of invasive Salmonella, *EMBO J* 18, 4926-4934.
19. Hayward, R. D., McGhie, E. J., and Koronakis, V. (2000) Membrane fusion activity of purified SipB, a Salmonella surface protein essential for mammalian cell invasion, *Mol Microbiol* 37, 727-739.

Chapter 6: The interaction between the *Salmonella* tip protein SipD and the N-terminal hydrophilic domain of the translocon protein SipB

6.1. Introduction

The *Salmonella* translocon protein SipB was required for bacterial entry into cultured human intestinal epithelial cells (1). SipB along with SipC assemble on the tip complex to form the T3SS translocon, which allows *Salmonella* to attach to the host cell membrane and to deliver effectors through the translocation pore (1-3). The molecular interactions responsible for the attachment of the translocon to the tip complex are unknown. Purified SipB could associate with liposomes using two centrally located hydrophobic regions predicted to form transmembrane α -helices (4). SipB also contained a C-terminal amphipathic region and an N-terminal hydrophilic region. The C-terminal amphipathic region helped in the binding of SipB to lipid membranes (4). However, the role of the N-terminal domain of SipB in the assembly of the translocon is the least understood.

The N-terminal region of SipB formed a protease-resistant domain that was responsible for the homo-oligomerization of SipB into hexamers (5). The tip complex is assembled from the hydrophilic tip protein SipD. Hence, the N-terminal hydrophilic domain of SipB could be responsible for the attachment of the translocon to the tip complex. SipB residues 82 to 312 were purified from *E. coli* and NMR spectroscopy was used to detect a weak interaction between this region of SipB and the tip protein SipD. Paramagnetic relaxation enhancement (PRE) was used to determine the surfaces involved in the interaction between SipB⁸²⁻³¹² and SipD. The interaction between SipB⁸²⁻³¹² and SipD was helpful to understand how the translocon might be anchored to the tip complex.

6.2. Results

6.2.1. *NMR titrations of SipD³⁹⁻³⁴³ with the N-terminal hydrophilic region of SipB* - ¹⁵N-SipD³⁹⁻³⁴³ was titrated with increasing concentrations of unlabeled SipB⁸²⁻³¹². The backbone assignments for SipD³⁹⁻³⁴³ published previously (6) were used to identify the residues affected on interaction with SipB⁸²⁻³¹². Progressive decrease in the intensity of several peaks denoted an interaction in the intermediate-exchange NMR timescale [Figure 6-1]. Intermediate exchange implies that chemical exchange between the free and bound states occurs on an intermediate timescale. In other words, the peaks are broadened due to interference from chemical exchange during the detection period of the NMR experiment (7). The peak intensities of 182 residues in the 1:1 dataset over that of the 1:0 dataset were plotted to find the residues of SipD³⁹⁻³⁴³ most affected on interaction with SipB⁸²⁻³¹² [Figure 6-2A]. Residues showing the strongest decrease in peak intensity upon interaction with SipB⁸²⁻³¹² were distributed over a wide region of SipD³⁹⁻³⁴³, and are shown in Figures 6-2B & 6-2C. The affected peaks represent residues that are located at the binding interface as well as those that undergo conformational change due to binding. Hence, the wide distribution of the affected peaks might suggest that SipD³⁹⁻³⁴³ undergoes global conformational changes upon binding to SipB⁸²⁻³¹².

SipB⁸²⁻³¹² produced a poor ¹H-¹⁵N-TROSY spectrum (*2D-NMR spectra of ¹⁵N-SipB⁸²⁻³¹² is shown in chapter 5, section 5.2.3*), thus preventing complementary NMR titrations using ¹⁵N-labeled SipB⁸²⁻³¹². Recently, the crystal structure of a shorter fragment containing SipB residues 82 to 226 was reported (8). This construct (SipB⁸²⁻²²⁶) produced a higher quality ¹H-¹⁵N-TROSY spectrum with over 80% of the backbone amide groups well dispersed. ¹³C-ILV-labeled SipB⁸²⁻²²⁶ was titrated with unlabeled SipD³⁹⁻³⁴³ in order to determine if SipB⁸²⁻²²⁶ retains binding with SipD³⁹⁻³⁴³.

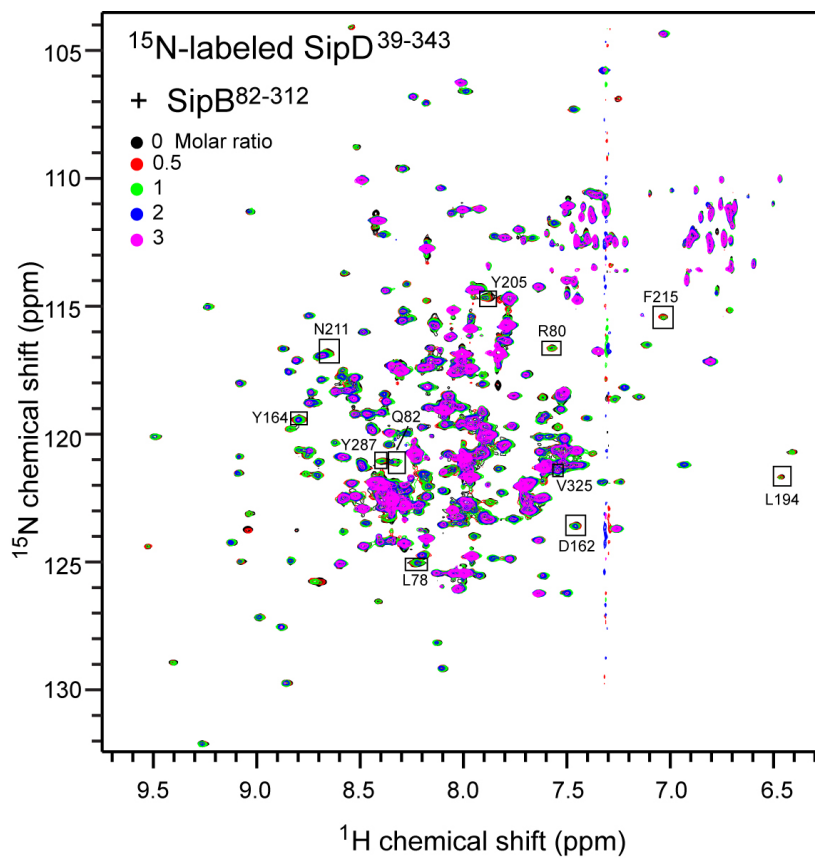


Figure 6-1: NMR titration of ^{15}N -SipD³⁹⁻³⁴³ with unlabeled SipB⁸²⁻³¹² at different molar ratios. SipB⁸²⁻³¹² interacted with SipD³⁹⁻³⁴³ in the intermediate exchange NMR timescale. The SipD³⁹⁻³⁴³ residues showing the strongest decrease in peak intensities are boxed and labeled.

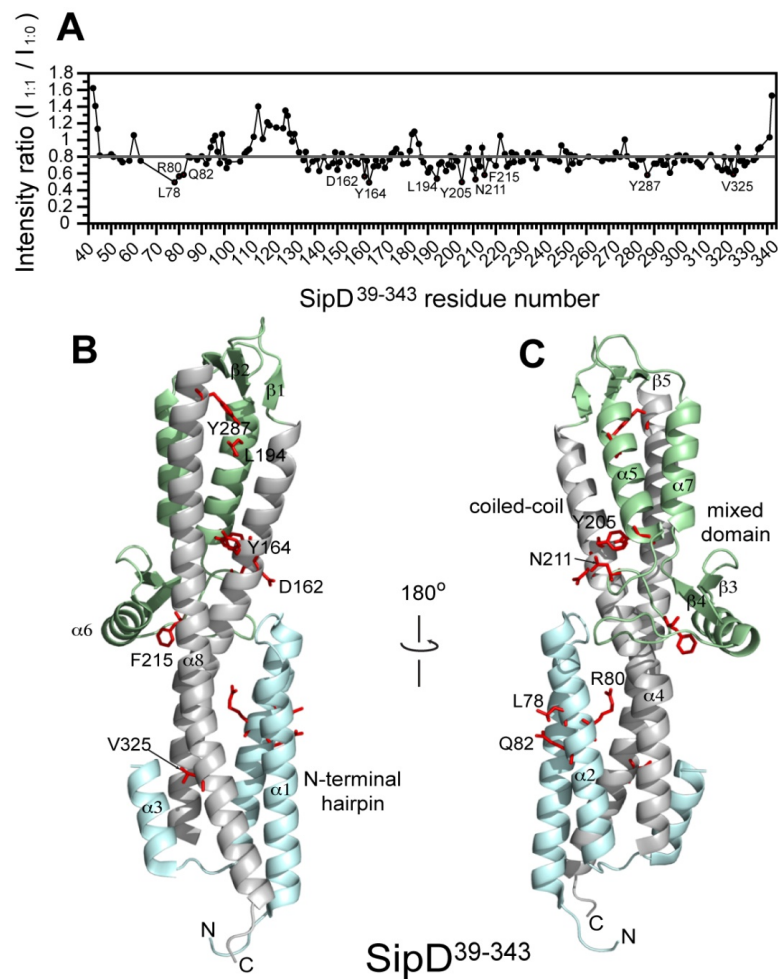


Figure 6-2: (A) Plot showing the ratio of peak intensities of ^{15}N -SipD³⁹⁻³⁴³ residues mixed with an equimolar amount of unlabeled SipB⁸²⁻³¹² (1:1) to that with no SipB⁸²⁻³¹² (1:0). (B) & (C) Two views of the structure of SipD showing the residues (red sticks) that were most affected upon titration with SipB.

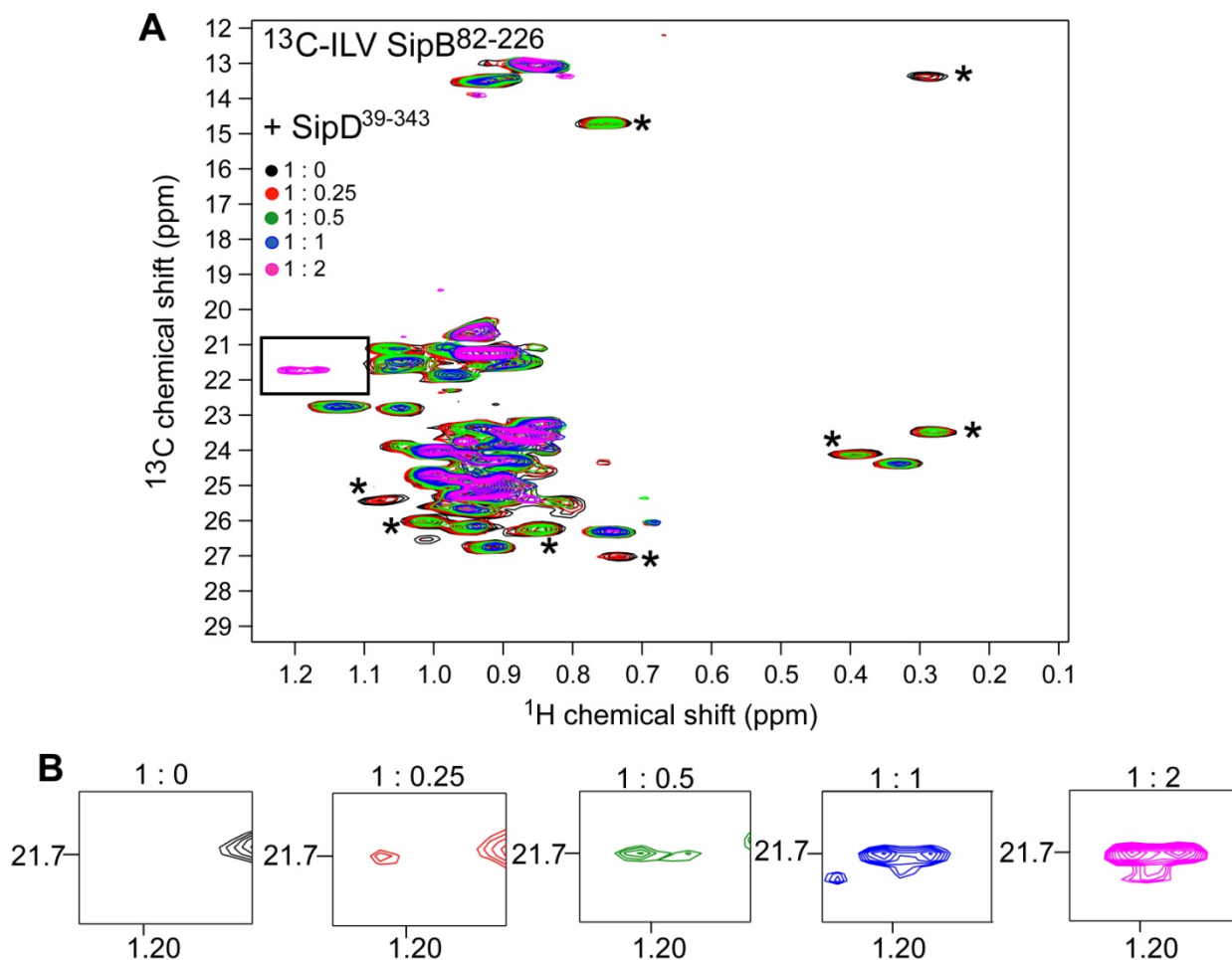


Figure 6-3: (A) ^1H - ^{13}C -HSQC spectra of ^{13}C -ILV-SipB⁸²⁻²²⁶ titrated with unlabeled SipD³⁹⁻³⁴³ at different molar ratios. The four peaks with ^{13}C chemical shift within 12-16 ppm represent the methyl groups of the four Ile residues in SipB⁸²⁻²²⁶. The methyl groups of Leu and Val residues are represented by two peaks per residue and have a ^{13}C chemical shift within 19-28 ppm. The asterisks mark the SipB⁸²⁻²²⁶ peaks that showed the strongest decrease in intensity upon addition of SipD³⁹⁻³⁴³. (B) Panels showing the appearance of two new peaks corresponding to Leu or Valine methyl groups of SipB⁸²⁻²²⁶ upon progressive addition of SipD³⁹⁻³⁴³.

SipB⁸²⁻²²⁶ also showed an interaction in the intermediate exchange regime with SipD³⁹⁻³⁴³ with the reduction in the intensities of several peaks representing the side chain methyl groups of Ile, Leu, and Val residues of SipB⁸²⁻²²⁶ [Figure 6-3].

6.2.2. *Paramagnetic Relaxation Enhancement (PRE)* - Single time point PRE (9) was used to determine which region of SipB⁸²⁻³¹² interacts with SipD³⁹⁻³⁴³. MTSL was used as the spin label and attached to specific sites on SipB⁸²⁻³¹² using cysteine point mutants (Ala-109, Lys-127, Asp-207, Lys-211, Asn-283, and Glu-303) [Figure 6-4]. CD was used to ensure that SipB⁸²⁻³¹² with cysteine substitutions and spin labeled SipB⁸²⁻³¹² were folded natively [Figure 6-5]. Further, SipD was ¹⁵N-amino acid specifically labeled in order to reduce the complexity of the NMR datasets (*¹⁵N-amino acid specific labeling of SipD³⁹⁻³⁴³ is described in Chapter 2, section 2.1.1*). A molar ratio of SipD to SipB⁸²⁻³¹² of 1:0.5 was chosen for the PRE experiments. A higher ratio yielded lower data quality due to excessive peak broadening. Residues in SipD within ~ 20 Å of the spin label on SipB⁸²⁻³¹² would experience a high PRE effect, and show reduced peak intensities in the paramagnetic spectrum compared to the diamagnetic spectrum. Therefore, no PRE effect on SipD residues would be observed if the spin label on SipB⁸²⁻³¹² is farther away from the surface of interaction. Representative 2D-NMR spectra used for PRE experiments are shown in **Figures 6-6 & 6-7**.

Spin labels on SipB⁸²⁻³¹² at positions Ala-109, Lys-127, and Glu-303 produced weak or moderate PRE effect on SipD and all peaks had an I_{para}/I_{dia} ratio above 0.6 [Figures 6-6 to 6-9]. On the other hand, spin labels at positions Asp-207, Lys-211, and Asn-283 induced the strongest PRE effect on certain SipD residues. In the crystal structure of SipB⁸²⁻²²⁶, Asp-207 and Lys-211 are close to each other, while the position of Asn-283 is unknown, but can be expected to lie on helix α 4 modeled over the crystal structure of SipB⁸²⁻²²⁶ [Figures 6-4].

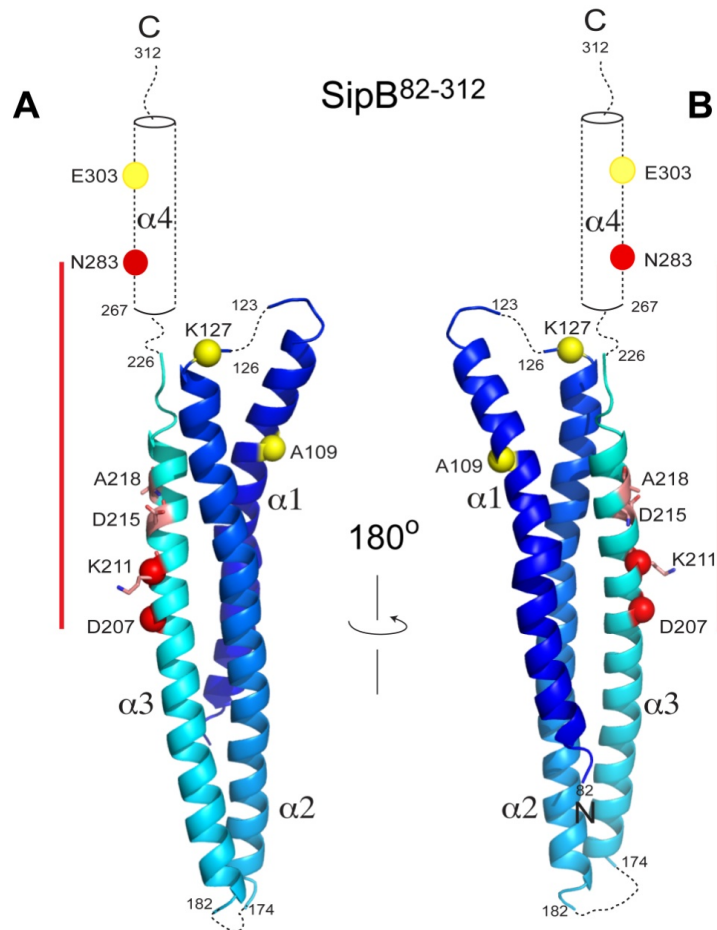


Figure 6-4: Two views of the model of SipB⁸²⁻³¹² showing the structure of SipB⁸²⁻²²⁶ with the addition of residues that were missing in the crystal structure. The region within residues 227 to 312 is represented as helix $\alpha 4$ based on their predicted α -helical propensities. The spheres represent the positions of the spin labels that were attached on SipB⁸²⁻³¹² in order to determine their PRE effect on SipD³⁹⁻³⁴³. Yellow spheres represent spin labels, which did not produce a high PRE effect on SipD³⁹⁻³⁴³. Red spheres represent spin labels that produced a high PRE effect on the residues of SipD³⁹⁻³⁴³. The residues shown as pink sticks denote the position of the mutations in SipB that yielded non-invasive strains of *Salmonella*.

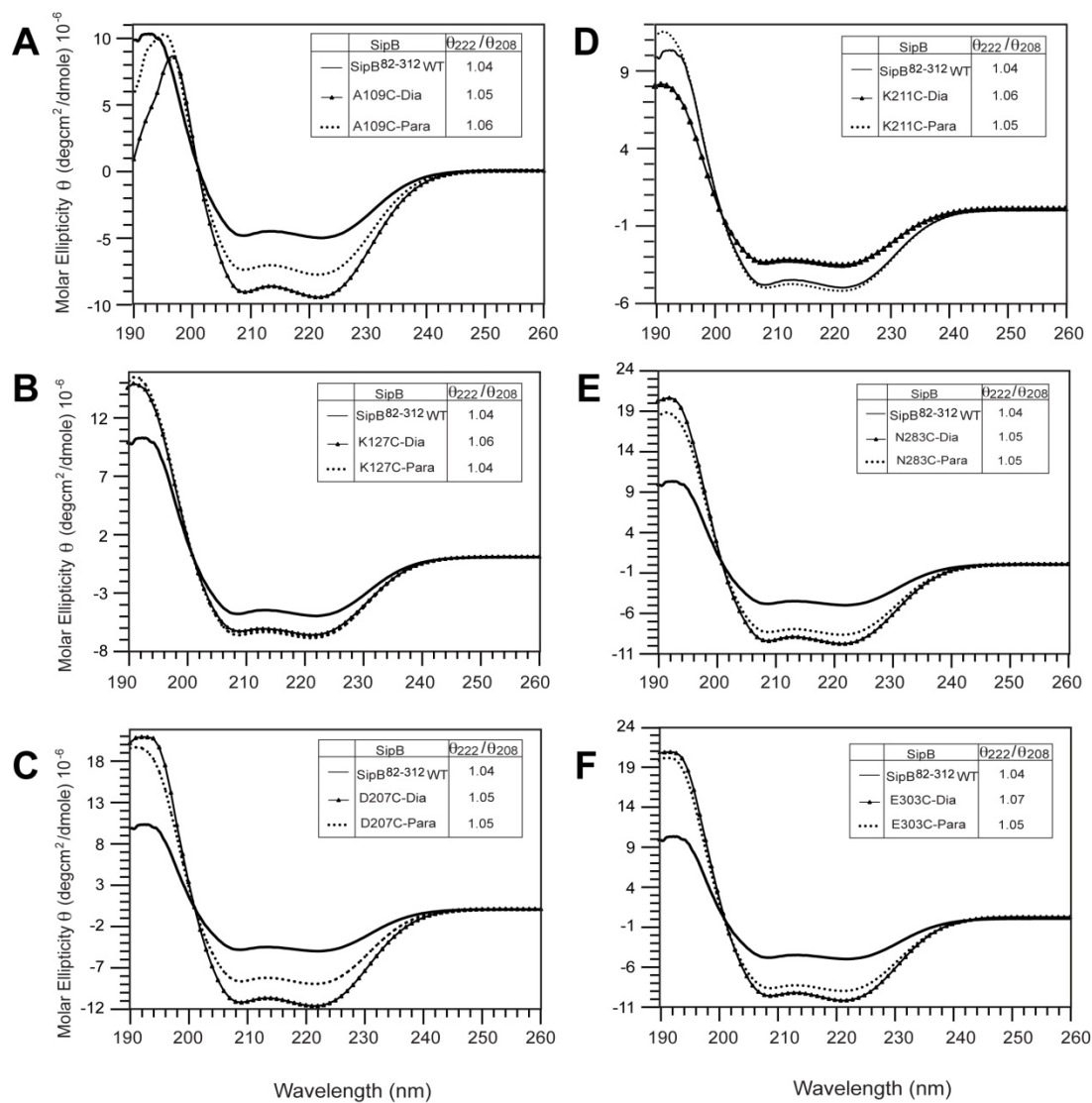


Figure 6-5: CD spectra of WT SipB⁸²⁻³¹² compared to the cysteine mutants before (Dia) and after attachment of the spin label (Para). (A) through (F) shows CD spectra of SipB⁸²⁻³¹² containing cysteine mutants A109C, K127C, D207C, K211C, N283C, and E303C respectively. The $\theta_{222}/\theta_{208}$ ratio denoting interhelical contacts within each form of SipB⁸²⁻³¹² are mentioned.

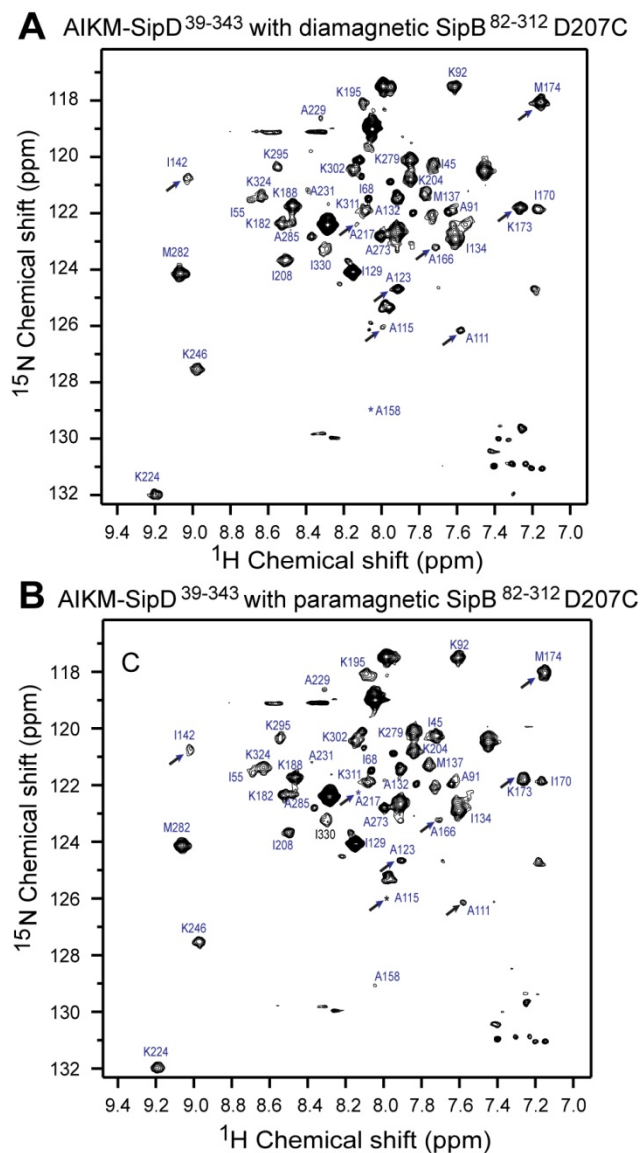


Figure 6-6: (A) ^1H - ^{15}N -HSQC spectra of SipD³⁹⁻³⁴³ ^{15}N -amino acid specifically labeled at Ala, Lys, Ile, and Met (AIKM) mixed with diamagnetic (without spin label) D207C SipB⁸²⁻³¹². (B) ^1H - ^{15}N -HSQC spectra of ^{15}N -AIKM-SipD³⁹⁻³⁴³ mixed with paramagnetic (with spin label MTSL) D207C SipB⁸²⁻³¹². Arrows represent the SipD³⁹⁻³⁴³ residues that showed decreased peak intensity in presence of the spin label at D207C of SipB⁸²⁻³¹².

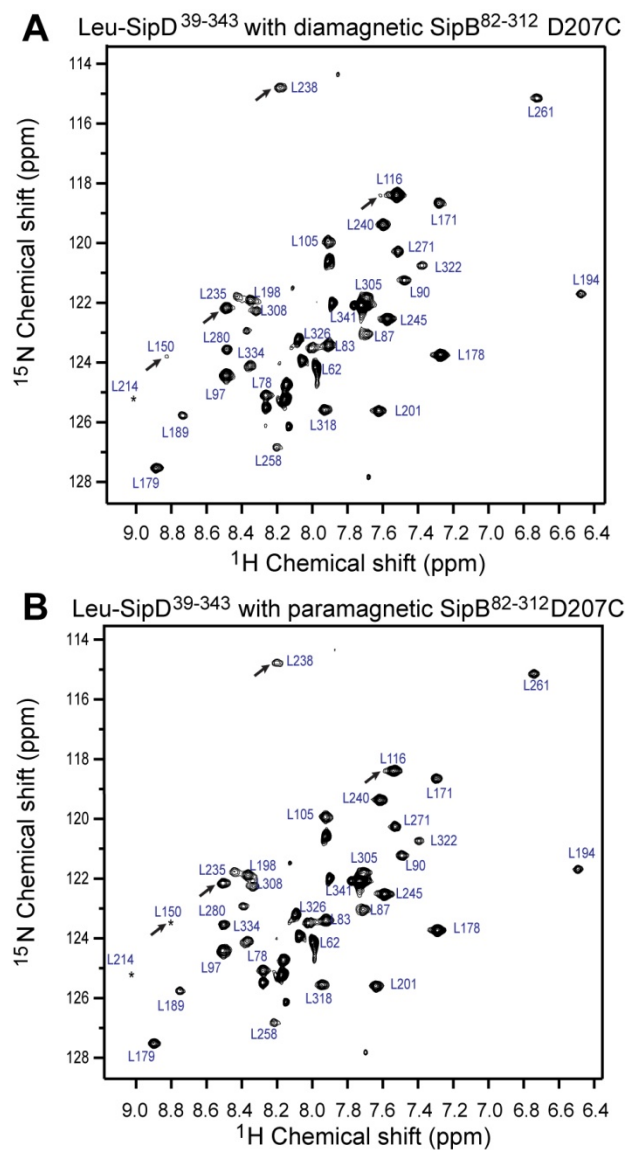


Figure 6-7: (A) ^1H - ^{15}N -TROSY spectra of SipD³⁹⁻³⁴³ ^{15}N -amino acid specifically labeled at Leu residues (Leu) mixed with diamagnetic (without spin label) D207C SipB⁸²⁻³¹². (B) ^1H - ^{15}N -TROSY spectra of ^{15}N -Leu-SipD³⁹⁻³⁴³ mixed with paramagnetic (with spin label MTSL) D207C SipB⁸²⁻³¹². Arrows represent the SipD³⁹⁻³⁴³ residues that showed decreased peak intensity in presence of the spin label at D207C of SipB⁸²⁻³¹².

Residues on SipD experiencing the strongest PRE effect were Ala-115, Leu-116, Ala-123, Leu-214, Ala-217, and Leu-280 [Figures 6-6 to 6-10]. These residues had an $I_{\text{para}}/I_{\text{dia}}$ ratio below 0.6, and mapped around the mixed α/β region of SipD³⁹⁻³⁴³. The results of PRE studies, summarized in Figure 6-10, show that the mixed α/β domain of SipD interacts with a surface along helix $\alpha 3$ and $\alpha 4$ of SipB⁸²⁻³¹².

6.2.3. *HADDOCK modeling of the SipD³⁹⁻³⁴³-SipB⁸²⁻²²⁶ complex* - Results of NMR titrations and PRE experiments were used to generate a structural model of the SipD-SipB⁸²⁻²²⁶ complex using HADDOCK (10). The active residues on SipD³⁹⁻³⁴³ and SipB⁸²⁻²²⁶ used for the docking are listed in Table 7. Figure 6-11 shows the highest scoring model out of the 200 structures generated by a HADDOCK run using default parameters. HADDOCK scores the models based on a weighted sum of four energy terms. These include electrostatic, van der Waals, desolvation, and restraints violation energies. The model with the smallest weighted sum is ranked first (10). In the model depicted in Figure 6-11, SipB⁸²⁻²²⁶ binds close to the mixed α/β region of SipD³⁹⁻³⁴³ along helix $\alpha 4$ and the complex is stabilized predominantly by electrostatic interactions between polar and charged residues, which are conserved among *Salmonella* species. HADDOCK predicted a total buried surface area of $\sim 2024.4 \text{ \AA}^2$. Such a large buried surface area might indicate tight interaction. Direct binding studies are required to estimate the affinity between SipD³⁹⁻³⁴³ and SipB⁸²⁻²²⁶.

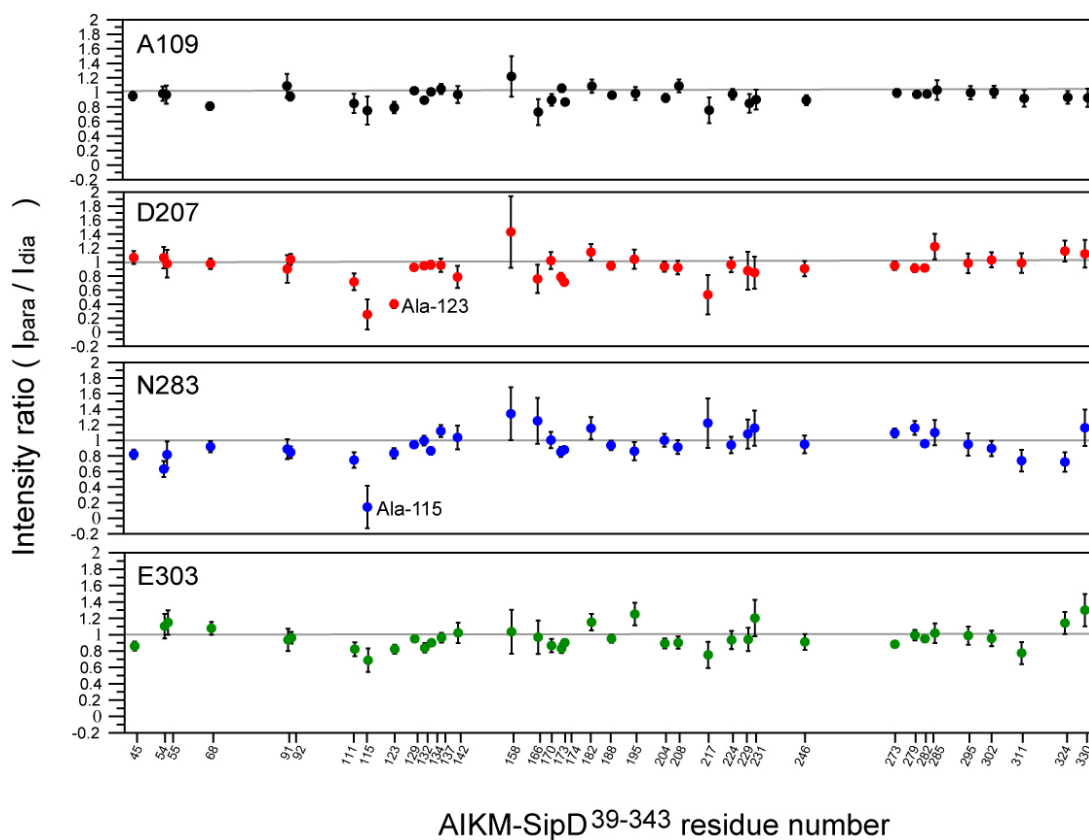


Figure 6-8: Results of PRE experiments with AIKM-SipD³⁹⁻³⁴³ and four spin label positions on SipB⁸²⁻³¹². Each panel represents the I_{para}/I_{dia} ratio of SipD peaks for one spin label position, which is labeled on the top left. The SipD³⁹⁻³⁴³ residues are labeled at the x-axis. The gray line represents a peak intensity ratio of 1, which suggests no PRE effect.

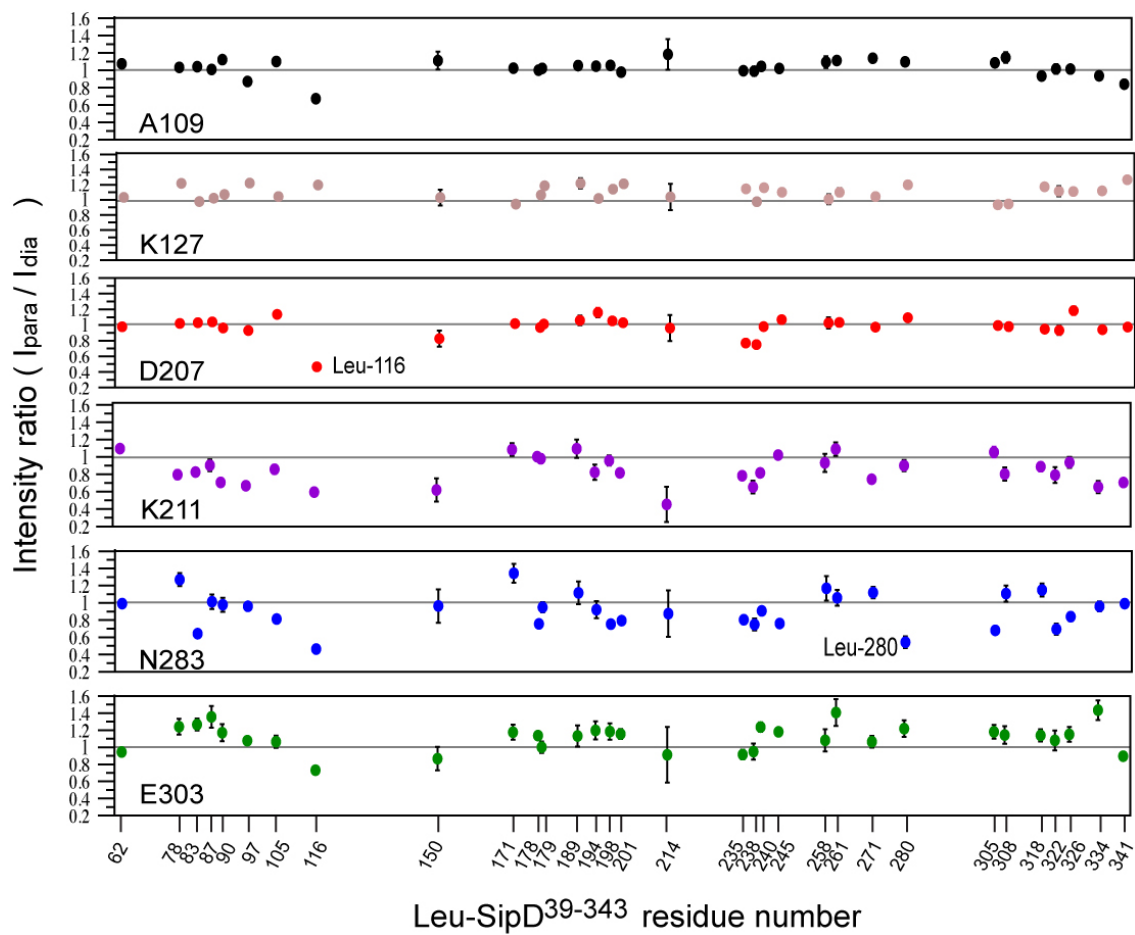


Figure 6-9: Results of PRE experiments with Leu-SipD³⁹⁻³⁴³ and six spin label positions on SipB⁸²⁻³¹². Each panel represents the I_{para}/I_{dia} ratio of SipD peaks for one spin label position, which is labeled on the bottom left. The SipD³⁹⁻³⁴³ residues are labeled at the x-axis. The gray line represents a peak intensity ratio of 1, which suggests no PRE effect.

SipD ³⁹⁻³⁴³ residues showing PRE effect					
Position of spin label on SipB ⁸²⁻³¹²	A109	D207	K211	N283	E303
Weak PRE effect $I_{para} / I_{dia} = 0.80 - 0.70$	A115, A123, A166, A217	A111, I142, A166, K173, M174, L235, L238	L78, L90, L235, L271, L308, L322, L341	A111, K311, L178, L198, L201, L235, L238, L245	A217, K311, L116
Moderate PRE effect $I_{para} / I_{dia} = 0.70 - 0.60$	L116	-	L97, L150, L238, L334	K54, L83, L305, L322	A115
Strong PRE effect $I_{para} / I_{dia} < 0.60$	-	A115, A123, A217, L116	L116, L214	A115, L116, L280	-
<p>SipB⁸²⁻³¹² schematic showing spin labels E303, N283, K127, A109, K211, D207. Helices are labeled α1, α2, α3, α4. Residues 174, 182, 226, 267, 312 are also indicated.</p>	<p>SipD structure with spin labels A166, A217, L116, A123.</p>	<p>SipD structure with spin labels M174, K173, L238, L235, I142, A115.</p>	<p>SipD structure with spin labels L271, L78, L90, L308, L322, L341, L214, L305, L150, L97, L334, L238, L235, L245, L201, L198, L178.</p>	<p>SipD structure with spin labels L280, L178, L198, L201, L245, L305, L83, K54, L116, A115, L280.</p>	<p>SipD structure with spin labels K311, L116.</p>

Figure 6-10: Summary of the results of PRE experiments. The SipD³⁹⁻³⁴³ residues showing weak (yellow), moderate (orange), or strong (red) PRE effect are listed and mapped onto the crystal structure of SipD³⁹⁻³⁴³. In order to show the position of Ala-123, a loop region from residue Ser-118 to Ala-132 missing in the crystal structure of SipD³⁹⁻³⁴³, was added using Molscript (11). Each column corresponds to one spin label on SipB⁸²⁻³¹². The spin label at K127 did not produce a PRE effect and all the residues of Leu-SipD³⁹⁻³⁴³ had I_{para}/I_{dia} ratios higher than 0.8. Thus, the column for K127 was omitted.

6.2.4. *Salmonella* invasion assay and Immunoblotting - Several single point mutations were made along helix α 3 and α 4 of SipB. These mutations were tested for their effect on the ability of *Salmonella* to enter human intestinal epithelial cells in a *Salmonella* invasion assay. However, most of the substitutions did not have any significant effect on the invasiveness of *Salmonella* [Figure 6-12]. In contrast *Salmonella* strains expressing SipB K211A, SipB D215A, and SipB A218D were completely non-invasive. These three residues lie on consecutive turns of α 3 in SipB⁸²⁻²²⁶ [Figure 6-4]. To further investigate the cause of non-invasiveness the expression of SipB in the non-invasive strains of *Salmonella* was tested. The LB growth medium, cell pellet and cytoplasm of *Salmonella* expressing SipB K211A, SipB D215A, and SipB A218D were probed with anti-SipB⁸²⁻³¹² and anti-SipD antibodies. Bands corresponding to smaller fragments of SipB, around 30kD in size, were seen in the non-invasive strains [Figure 6-13]. In contrast, the *sipB*⁺ strain of *Salmonella* contained a full length SipB around 60kD in size. This suggests that the point mutations K211A, D215A and A218D were causing SipB to be degraded in *Salmonella*. The expression profile of SipD was used as an internal control, and showed a 40kD band corresponding to full length SipD.

6.3. Discussion

The *Salmonella* translocators SipB and SipC are homologous to IpaB, IpaC (*Shigella* sp), BipB, BipC (*Burkholderia* sp), YopB, YopD (*Yersinia* sp), and PopB, PopD (*Pseudomonas*) among others (12). Although structural information exists for only the N-terminal domain of SipB and IpaB, membrane binding and pore formation by the translocators, have been studied extensively (13-18). Purified translocon proteins can integrate into lipid membranes, but they need to assemble on the needle tip for delivery of effectors and T3SS-mediated bacterial entry into host cells (1, 3, 5, 19). Therefore, the assembly of the translocon on the tip plays an

important role in the function of the T3SS. Currently, the mechanism of this assembly process is unknown. The N-terminal hydrophilic domain of SipB was proposed to bind to the tip protein and thereby attach the translocon to the tip complex.

Initial CD spectroscopy and thermal scanning experiments showed the presence of a folded domain within residues 82 to 312 of SipB (*CD spectra of SipB constructs are shown in chapter 5, section 5.2.2*). Others have also reported a protease-resistant domain at the N-terminus of SipB (5). This was confirmed by the recent crystal structure showing that the N-terminal domain was made up of three antiparallel α -helices. Interestingly, this region is also responsible for forming oligomers of SipB (5). Hence, it was hypothesized that the N-terminal domain of SipB binds to SipD and helps in the assembly of the translocon using its oligomerization motif. Although the latter remains to be tested, evidence of interaction between SipB⁸²⁻³¹² and SipD³⁹⁻³⁴³ is reported here.

SipB⁸²⁻³¹² did not produce an ideal NMR spectrum, whereas the backbone resonances of SipD³⁹⁻³⁴³ were already assigned (6). Owing to these reasons, ¹⁵N-SipD³⁹⁻³⁴³ was used to perform NMR titrations with unlabeled SipB⁸²⁻³¹². Several peaks showed a decrease in intensity representing an interaction in the intermediate exchange NMR timescale, which is consistent with a weak interaction between SipD³⁹⁻³⁴³ and SipB⁸²⁻³¹². The affected residues were globally distributed on SipD³⁹⁻³⁴³. Such a weak interaction may be needed to provide SipB with sufficient conformational flexibility, to sense the host environment and recruit SipC, or switch the translocon to an “actively secreting” state. Owing to the absence of chemical shifts, the single time-point PRE method (9) was used to identify the residues in SipD³⁹⁻³⁴³ that are interacting with SipB⁸²⁻³¹².

Table 7: List of residues defined as “active” for HADDOCK modeling of the SipD³⁹⁻³⁴³-SipB⁸²⁻²²⁶ complex using HADDOCK. Active residues are those that might be directly involved in interaction.

SipD³⁹⁻³⁴³	SipB⁸²⁻²²⁶
L78	Q183
Q82	E185
S85	A186
K92	Q190
S98	K193
E100	T196
S107	E197
A144	K199
S148	E200
N196	D203
N203	K204
S210	D207
N211	V210
S236	K211
D269	T214
G270	K217
N284	A218
Q310	E221
K324	K222

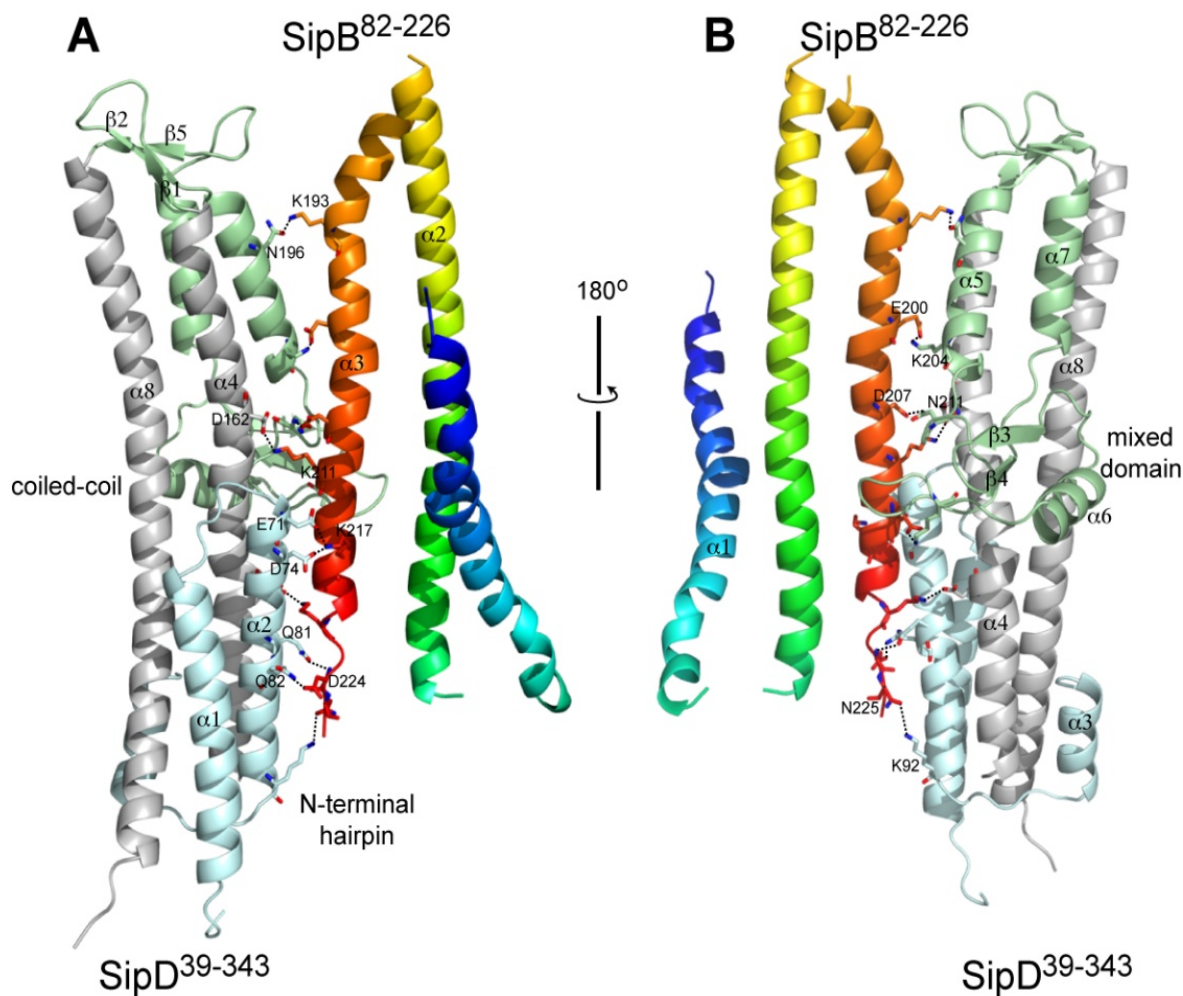


Figure 6-11: (A) & (B) Two views of the highest scoring model of the complex of SipD³⁹⁻³⁴³ and SipB⁸²⁻²²⁶ obtained by haddock modeling, using results of NMR titrations and PRE. SipB⁸²⁻²²⁶, colored in rainbow spectrum, binds near the mixed α/β region of SipD³⁹⁻³⁴³ (in green). Residues of SipD³⁹⁻³⁴³ and SipB⁸²⁻²²⁶ participating in electrostatic interactions (dotted lines) are represented as sticks and labeled.

Nuclear dipoles within ~ 20 Å from a paramagnetic spin label will undergo increased relaxation. In the single time point method (9), this phenomenon can be observed as a reduction in the peak intensity of the affected nuclei in the presence of the spin label. Spin labels were attached to six positions on SipB⁸²⁻³¹², and SipD³⁹⁻³⁴³ was labeled with specific ¹⁵N-amino acids. Results of PRE experiments showed that a region on SipB⁸²⁻³¹² from residues Asp207 to Asn283 binds to the mixed α/β region of SipD³⁹⁻³⁴³.

In support of our results, deletion of the mixed α/β region (residues 192 to 267) of IpaD, the homolog of SipD, prevented the localization of IpaB on the *Shigella* needle tip (20). Furthermore, the *Salmonella* needle protein PrgI was shown to bind at the lower portion of the coiled coil in SipD (21). Together with a cryo-EM model of the needle (22), this finding suggests that in the assembled tip complex the mixed α/β region of SipD faces outside. Additionally, Epler *et al.* reported similar observations on the assembled tip complex of *Shigella* (23). These results complement our findings, because if the mixed α/β region is exposed on the needle tip, it will be free to bind to SipB. Incorporating these results, a model was proposed where the N-terminal domain of SipB provides the anchor, which attaches the translocon to the needle tip [Figure 6-14].

Single amino acid substitutions were made, along helix $\alpha 3$ and $\alpha 4$ of SipB, to disrupt its interaction with SipD. However, these mutations did not have any negative impact on the invasiveness of *Salmonella*. This can be explained by the nature of the residues lining the binding interface between SipD and SipB. The surface of SipB⁸²⁻²²⁶ interacting with SipD³⁹⁻³⁴³ is rich in charged residues like Lys, Arg, Asp, and Glu. Likewise, the surface of the mixed α/β region of SipD³⁹⁻³⁴³ is composed of polar and charged residues.

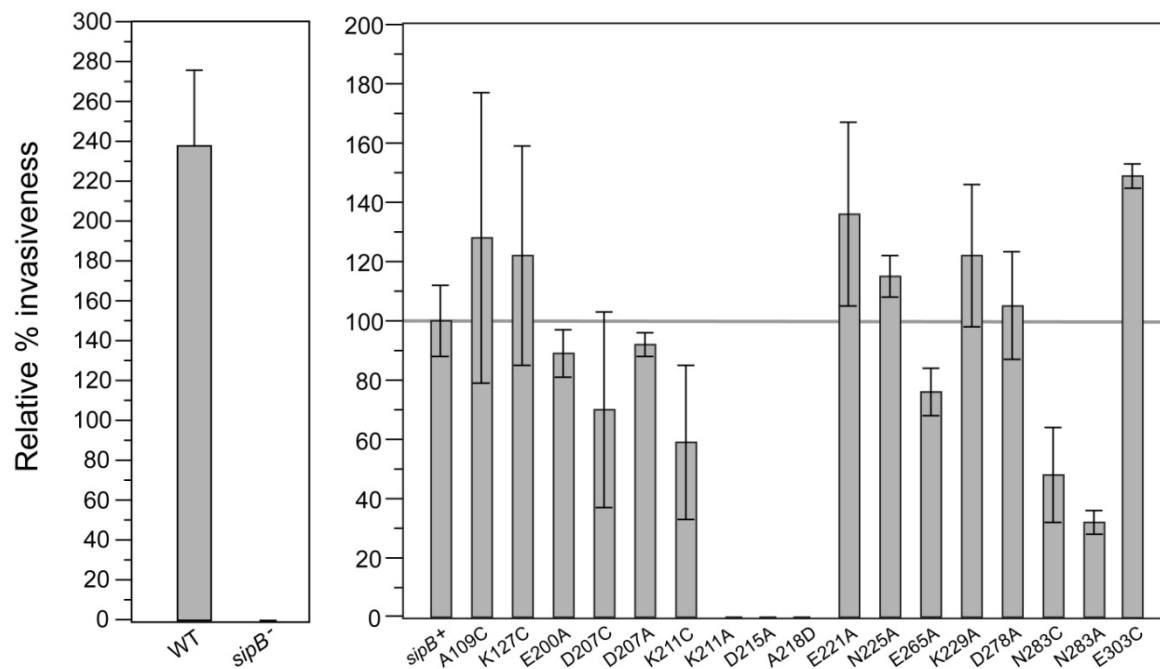


Figure 6-12: Results of *Salmonella* invasion assay done with strains of *Salmonella* expressing SipB with single point mutations. Most substitutions did not affect the invasiveness of *Salmonella*. However, strains *sipB* K211A, *sipB* D215A, and *sipB* A218D were non-invasive.

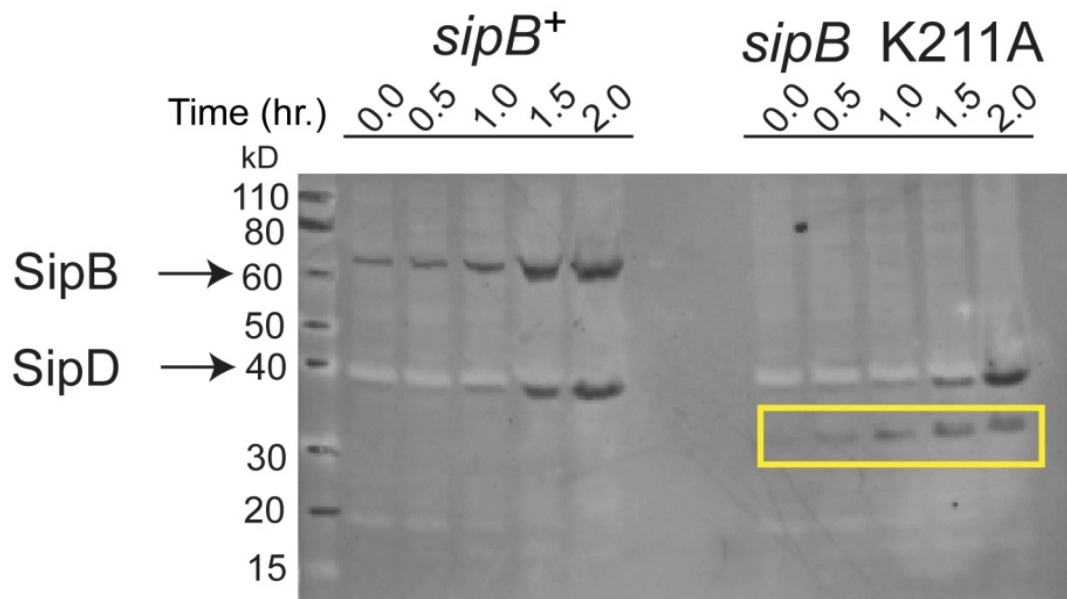


Figure 6-13: An immunoblot showing the secretion profile of the non-invasive mutant *sipB* K211A compared to *sipB*⁺ strain of *Salmonella* at increasing time points (0-2 hours). The numbers indicate hours at which cultures were harvested after adding IPTG. SipD was seen as a gradually intensifying band at 40 kD. In the *sipB*⁺ strain a band at 62 kD denotes full length SipB. In the *sipB* K211A mutant strain the 62 kD band was absent but a 30 kD band (yellow box) corresponding to a degradation product of SipB was observed.

Therefore, the interaction between SipD³⁹⁻³⁴³ and SipB⁸²⁻³¹² is most probably mediated by a multitude of electrostatic interactions and a single point mutation might not be sufficient to disrupt this binding in *Salmonella*. A sensitive patch was found within SipB residues Lys-211, Asp-215, and Ala-218, which upon mutagenesis, lead to the degradation of SipB in *Salmonella*. Why single point mutations on the surface of SipB would cause such an extreme response is unclear and several speculations can be put forward to explain this observation. SipB has one known chaperone SicA, which binds to both SipB and SipC within the bacterial cytoplasm and partitions them to prevent their aggregation and degradation (24). SicA is thought to bind to residues 80-160 of SipB (25). Studies with *S. flexneri* IpgC have further narrowed the chaperone-binding site to residues 15 to 73 of IpaB (26). This region is absent in the crystal structure of SipB⁸²⁻²²⁶ or IpaB⁷⁴⁻²²⁴, however, it is not unlikely that the sensitive patch on SipB packs against the chaperone-binding site and mutations which affect the local tertiary structure also affect chaperone binding and lead to reduced stability of SipB. Alternatively, the mutations could affect the interaction of SipB with other proteins necessary to maintain it within the bacterial cytoplasm. In this context, SipB is known to form complexes with proteins like InvE, a secretion regulator for the translocators (27), and the OrgABC sorting platform (28), which controls the secretion of various T3SS substrates in a spatiotemporal manner. Further analysis of complex formation of T3SS proteins needs to be undertaken to answer these questions with certainty.

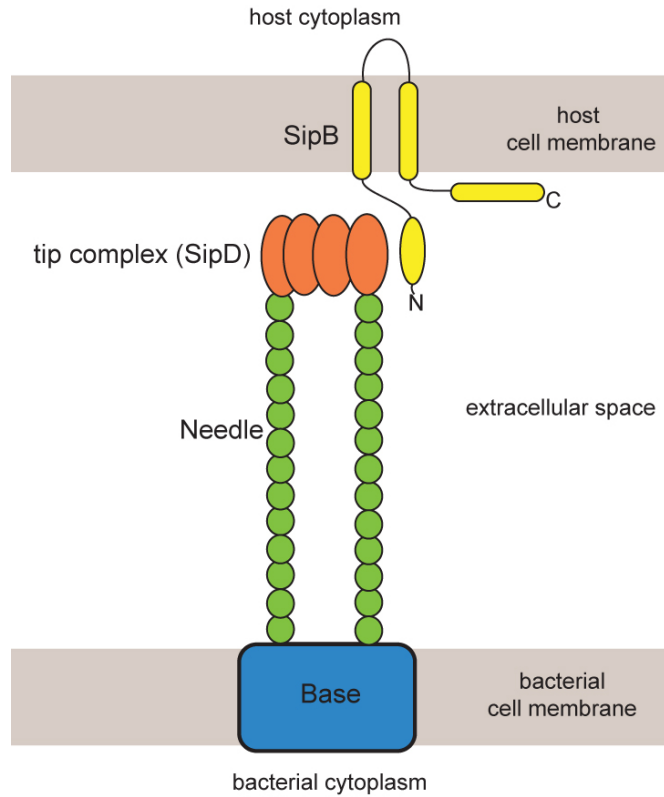


Figure 6-14: A model explaining how the interaction between SipD and SipB could facilitate the attachment of the translocon on the tip complex.

In summary, the N-terminal hydrophilic domain of SipB interacts with the tip protein SipD. The surfaces involved in this interaction were located to the mixed α/β region of SipD³⁹⁻³⁴³ and along helix $\alpha 3$ and $\alpha 4$ of SipB⁸²⁻³¹². These findings suggest a possible mechanism for the assembly of the translocon where the N-terminal domain of one molecule of SipB binds to the mixed α/β region of one molecule of SipD [Figure 6-14]. This interaction might help to anchor the translocon on the tip complex and correctly insert the transmembrane domains of SipB into the host cell membrane. Further studies are required to fully understand how the translocon protein SipC binds to SipB and SipD in order to assemble the translocon in *Salmonella*.

6.4. References

1. Lara-Tejero, M., and Galan, J. E. (2009) *Salmonella enterica* serovar typhimurium pathogenicity island 1-encoded type III secretion system translocases mediate intimate attachment to nonphagocytic cells, *Infect. Immun.* 77, 2635-2642.
2. Kaniga, K., Tucker, S., Trollinger, D., and Galan, J. E. (1995) Homologs of the Shigella IpaB and IpaC invasins are required for *Salmonella typhimurium* entry into cultured epithelial cells, *J.Bacteriol.* 177, 3965-3971.
3. Collazo, C. M., and Galan, J. E. (1997) The invasion-associated type III system of *Salmonella typhimurium* directs the translocation of Sip proteins into the host cell, *Mol Microbiol* 24, 747-756.
4. McGhie, E. J., Hume, P. J., Hayward, R. D., Torres, J., and Koronakis, V. (2002) Topology of the *Salmonella* invasion protein SipB in a model bilayer, *Mol Microbiol* 44, 1309-1321.

5. Hayward, R. D., McGhie, E. J., and Koronakis, V. (2000) Membrane fusion activity of purified SipB, a *Salmonella* surface protein essential for mammalian cell invasion, *Mol Microbiol* 37, 727-739.
6. Wang, Y., Nordhues, B. A., Zhong, D., and De Guzman, R. N. (2010) NMR Characterization of the Interaction of the *Salmonella* Type III Secretion System Protein SipD and Bile Salts, *Biochemistry* 49, 4220-4226.
7. Kleckner, I. R., and Foster, M. P. (2011) An introduction to NMR-based approaches for measuring protein dynamics, *Biochim Biophys Acta* 1814, 942-968.
8. Barta, M. L., Dickenson, N. E., Patil, M., Keightley, A., Wyckoff, G. J., Picking, W. D., Picking, W. L., and Geisbrecht, B. V. (2012) The structures of coiled coil domains from type III secretion system translocators reveal homology to pore-forming toxins, *J Mol Biol* 417, 395-405.
9. Gillespie, J. R., and Shortle, D. (1997) Characterization of long-range structure in the denatured state of staphylococcal nuclease. I. Paramagnetic relaxation enhancement by nitroxide spin labels, *J. Mol. Biol.* 268, 158-169.
10. de Vries, S. J., van Dijk, M., and Bonvin, A. M. (2010) The HADDOCK web server for data-driven biomolecular docking, *Nat Protoc* 5, 883-897.
11. J., K. P. (1991) MOLSCRIPT: a program to produce both detailed and schematic plots of protein structures, *J. Appl. Cryst.* 24, 946-950.
12. Mueller, C. A., Broz, P., and Cornelis, G. R. (2008) The type III secretion system tip complex and translocon, *Mol. Microbiol.* 68, 1085-1095.

13. Neyt, C., and Cornelis, G. R. (1999) Insertion of a Yop translocation pore into the macrophage plasma membrane by *Yersinia enterocolitica*: requirement for translocators YopB and YopD, but not LcrG, *Mol Microbiol* 33, 971-981.
14. Montagner, C., Arquint, C., and Cornelis, G. R. (2011) Translocators YopB and YopD from *Yersinia enterocolitica* form a multimeric integral membrane complex in eukaryotic cell membranes, *J Bacteriol* 193, 6923-6928.
15. Hume, P. J., McGhie, E. J., Hayward, R. D., and Koronakis, V. (2003) The purified *Shigella* IpaB and *Salmonella* SipB translocators share biochemical properties and membrane topology, *Mol. Microbiol.* 49, 425-439.
16. Miki, T., Okada, N., Shimada, Y., and Danbara, H. (2004) Characterization of *Salmonella* pathogenicity island 1 type III secretion-dependent hemolytic activity in *Salmonella enterica* serovar Typhimurium, *Microb. Pathog.* 37, 65-72.
17. Menard, R., Prevost, M. C., Gounon, P., Sansonetti, P., and Dehio, C. (1996) The secreted Ipa complex of *Shigella flexneri* promotes entry into mammalian cells, *Proc Natl Acad Sci U S A* 93, 1254-1258.
18. Terajima, J., Moriishi, E., Kurata, T., and Watanabe, H. (1999) Preincubation of recombinant Ipa proteins of *Shigella sonnei* promotes entry of non-invasive *Escherichia coli* into HeLa cells, *Microb Pathog* 27, 223-230.
19. De Geyter, C., Vogt, B., Benjelloun-Touimi, Z., Sansonetti, P. J., Ruyschaert, J. M., Parsot, C., and Cabaux, V. (1997) Purification of IpaC, a protein involved in entry of *Shigella flexneri* into epithelial cells and characterization of its interaction with lipid membranes, *FEBS Lett* 400, 149-154.

20. Johnson, S., Roversi, P., Espina, M., Olive, A., Deane, J. E., Birket, S., Field, T., Picking, W. D., Blocker, A. J., Galyov, E. E., Picking, W. L., and Lea, S. M. (2007) Self-chaperoning of the type III secretion system needle tip proteins IpaD and BipD, *J. Biol. Chem.* 282, 4035-4044.
21. Rathinavelan, T., Tang, C., and De Guzman, R. N. (2011) Characterization of the Interaction between the *Salmonella* Type III Secretion System Tip Protein SipD and the Needle Protein PrgI by Paramagnetic Relaxation Enhancement, *J. Biol. Chem.* 286, 4922-4930.
22. Galkin, V. E., Schmied, W. H., Schraidt, O., Marlovits, T. C., and Egelman, E. H. (2010) The structure of the *Salmonella typhimurium* type III secretion system needle shows divergence from the flagellar system, *J. Mol. Biol.* 396, 1392-1397.
23. Epler, C. R., Dickenson, N. E., Bullitt, E., and Picking, W. L. (2012) Ultrastructural Analysis of IpaD at the Tip of the Nascent MxiH Type III Secretion Apparatus of *Shigella flexneri*, *J. Mol. Biol.* 420, 29-39.
24. Tucker, S. C., and Galan, J. E. (2000) Complex function for SicA, a *Salmonella enterica* serovar typhimurium type III secretion-associated chaperone, *J Bacteriol* 182, 2262-2268.
25. Kim, B. H., Kim, H. G., Kim, J. S., Jang, J. I., and Park, Y. K. (2007) Analysis of functional domains present in the N-terminus of the SipB protein, *Microbiology* 153, 2998-3008.
26. Lunelli, M., Lokareddy, R. K., Zychlinsky, A., and Kolbe, M. (2009) IpaB-IpgC interaction defines binding motif for type III secretion translocator, *Proc. Natl. Acad. Sci. U.S.A.* 106, 9661-9666.

27. Kubori, T., and Galan, J. E. (2002) Salmonella type III secretion-associated protein InvE controls translocation of effector proteins into host cells, *J Bacteriol* *184*, 4699-4708.
28. Lara-Tejero, M., Kato, J., Wagner, S., Liu, X., and Galan, J. E. (2011) A sorting platform determines the order of protein secretion in bacterial type III systems, *Science* *331*, 1188-1191.

Chapter 7: The interaction between the *Shigella* needle protein MxiH and the tip protein IpaD

7.1. Introduction

The tip complex of the *Shigella* T3SS is assembled from five copies of the tip protein IpaD. The IpaD monomers bind to the needle protein MxiH to form the tip complex (1). The atomic structure of the tip complex of *Shigella* was recently determined using Cryo-EM (1). However, the low resolution (20 Å) of the structure limited detailed analysis of the molecular interactions between the IpaD and MxiH. The interaction between the tip proteins *Salmonella* SipD and *Shigella* IpaD with their respective needle proteins *Salmonella* PrgI and *Shigella* MxiH was reported to be in the intermediate exchange NMR timescale suggestive of a weak binding affinity (2, 3). Further, PRE was used to locate the binding site of *Salmonella* PrgI on the coiled coil of *Salmonella* SipD (2).

The structure of SipD and PrgI from *Salmonella* closely resembles the structures of IpaD and MxiH from *Shigella* (4-7). Despite the structural and functional homology between the components of T3SS of *Salmonella* and *Shigella*, these two pathogens were reported to form needles with different structures (8, 9). Particularly, upon polymerization into the needle, the *Shigella* MxiH was shown to develop a β -hairpin conformation at the C-terminus (8). Differences in the structures of the needles could lead to differences in how the tip protein interacts with the needle proteins in *Salmonella* and *Shigella*. In order to answer this question, PRE was used to locate the binding site of *Shigella* MxiH on the tip protein IpaD. The interaction between the needle protein and the tip protein in *Shigella* highlights the significance of the coiled coil of the tip protein in the assembly of the tip complex.

7.2. Results

7.2.1. *Backbone assignment of a full length, functional double mutant of MxiH* - Full length WT MxiH polymerizes in solution and hence is unsuitable for biochemical assays. MxiH^{CΔ5} was used previously for NMR titration with IpaD. However, MxiH^{CΔ5} also prevents the formation of the needle in *Shigella* and is therefore non-functional in a *Shigella* invasion assay. Substitution of MxiH residues Val68 and Val70 with Alanine was reported to prevent *in vitro* polymerization of full length MxiH (10). Further, the MxiH^{V68AV70A} variant was functional in a *Shigella* invasion assay (10). A ¹H-¹⁵N-HSQC spectrum of MxiH^{V68AV70A} has several peak shifts and new peaks in comparison to ¹⁵N MxiH^{CΔ5} [Figure 7-1]. Backbone amides of MxiH^{V68AV70A} were assigned using 3D-HNCA and 3D-CBCA(CO)NH datasets. A portion of the 3D-HNCA dataset for ¹³C-¹⁵N-MxiH^{V68AV70A} is shown in Figure 7-3. The 83-residue MxiH^{V68AV70A} yields 80 peaks in the ¹H-¹⁵N-HSQC spectrum [Figure 7-2]. The remaining 3 were proline residues, which lack a backbone amide group. Assignments could be made for 78 out of the 80 peaks, which amounts to 98% of the backbone amide groups in MxiH^{V68AV70A}. The backbone amide peaks assignments of MxiH^{V68AV70A} are shown in Figure 7-2. Residues Trp10, Glu17, Leu26, Ala38, and Asn66 were overlapped with residues Glu29, Asp20, Leu15, Asp21, and Asp8 respectively. Residues Leu37 and Leu 47 could not be assigned possibly because of peak broadening or peak overlap.

7.2.2. *NMR titration of ¹⁵N-MxiH^{V68AV70A} with unlabeled IpaD³⁸⁻³³² and IpaD¹³⁰⁻³³²* - ¹⁵N-MxiH^{V68AV70A} was titrated with IpaD³⁸⁻³³² at five molar ratios (1:0, 1:0.25, 1:0.5, 1:1, and 1:2). Several backbone amide peaks of MxiH^{V68AV70A} showed a progressive decrease in peak intensity upon addition of IpaD³⁸⁻³³² indicating an interaction in the intermediate exchange NMR timescale [Figure 7-4A].

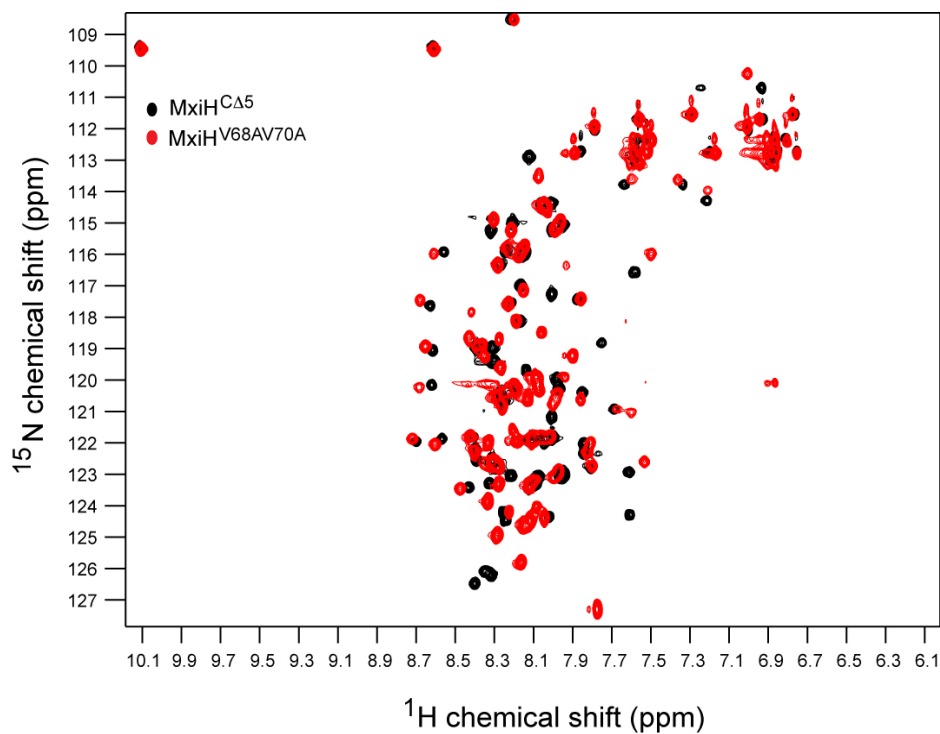


Figure 7-1: An overlay of the ^1H - ^{15}N -HSQC spectra of MxiH $^{\text{C}\Delta 5}$ (black) and MxiH $^{\text{V68AV70A}}$ (red). Several backbone amide peaks were shifted and new peaks were observed in the ^1H - ^{15}N -HSQC spectrum of MxiH $^{\text{V68AV70A}}$.

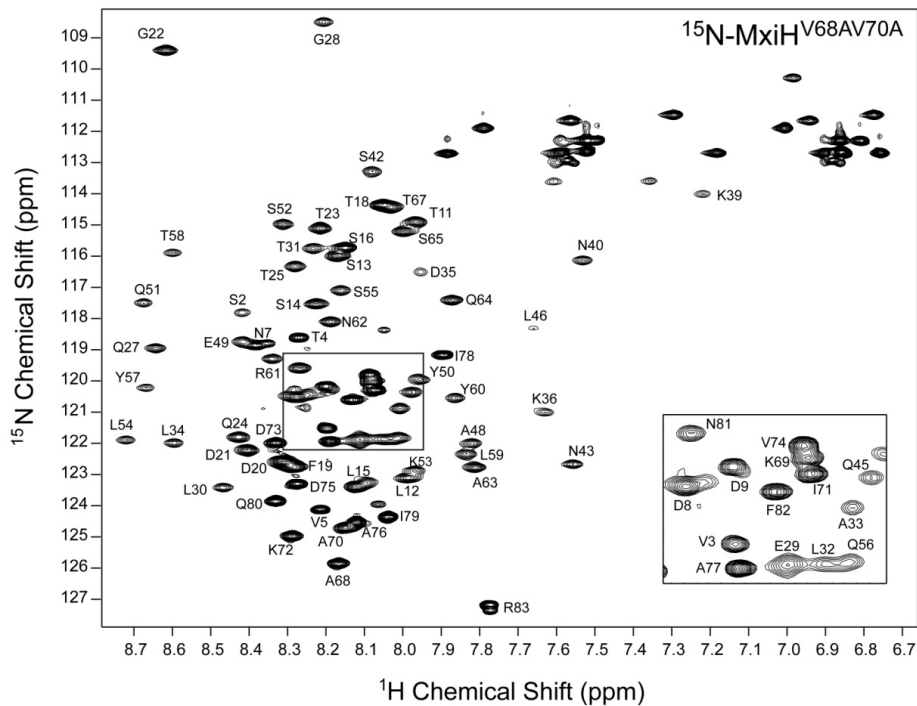


Figure 7-2: The assigned ^1H - ^{15}N -HSQC spectrum of $\text{MxiH}^{\text{V68AV70A}}$. Residues Trp10, Glu17, Leu26, Ala38, and Asn66 were hidden under the peaks for residues Glu29, Asp20, Leu15, Asp21, and Asp8 respectively. These assignments were used for NMR titration of $\text{MxiH}^{\text{V68AV70A}}$ with IpaD^{38-332} and $\text{IpaD}^{130-332}$.

Calculation of the peak intensity ratios of the 1:1 dataset over 1:0 dataset ($I_{1:1}/I_{1:0}$) showed that residues 21 to 64 were the most affected and the $I_{1:1}/I_{1:0}$ ratio was below the average intensity ratio of 0.5 [Figure 7-4B]. $^{15}\text{N-MxiH}^{\text{V68AV70A}}$ was also titrated with $\text{IpaD}^{130-332}$, which lacked the N-terminal α -helical hairpin. $\text{IpaD}^{130-332}$ induced decrease in the intensity of the same backbone peaks of $^{15}\text{N-MxiH}^{\text{V68AV70A}}$ as IpaD^{38-332} [Figure 7-5] suggesting that the N-terminal α -helical hairpin is dispensable for the interaction between MxiH with IpaD.

7.2.3. PRE experiments with $^{15}\text{N-MxiH}^{\text{V68AV70A}}$ and IpaD^{38-332} - Initially, PRE experiments (11) were performed using $^{15}\text{N-MxiH}^{\text{V68AV70A}}$ and IpaD^{38-332} . Cysteine substitutions were made on IpaD^{38-332} in order to attach a spin label and MTSL was used as the spin label. Unlabeled (diamagnetic) or spin labeled (paramagnetic) IpaD was mixed with $^{15}\text{N-MxiH}^{\text{V68AV70A}}$ and each sample was used to collect a $^1\text{H-}^{15}\text{N}$ -HSQC spectra. Intensities of the backbone amide peaks of $\text{MxiH}^{\text{V68AV70A}}$ from the paramagnetic (I_{para}) and diamagnetic (I_{dia}) were compared to obtain the $I_{\text{para}}/I_{\text{dia}}$ ratios. However, a comparable PRE effect was observed irrespective of the position of the spin label on IpaD^{38-332} [Figure 7-6]. This suggested a non-specific effect of the spin label probably due to the oligomerization of $\text{MxiH}^{\text{V68AV70A}}$ or the $\text{MxiH}^{\text{V68AV70A}}$ - IpaD^{38-332} complex. Therefore, the MxiH^{CA5} construct was used for later PRE experiments.

7.2.4. PRE experiments using $^{15}\text{N-MxiH}^{\text{CA5}}$ and IpaD^{38-332} - In total 10 spin label positions on IpaD^{38-332} were tested for the PRE effect they induced on $^{15}\text{N-MxiH}^{\text{CA5}}$ [Figure 7-7]. These spin labels were along the coiled coil of IpaD^{38-332} on helices $\alpha 4$ and $\alpha 8$. An increased PRE effect on $^{15}\text{N-MxiH}^{\text{CA5}}$ was observed when the spin label on IpaD^{38-332} was moved to the “bottom” of the coiled coil. The results of the PRE experiments are shown in Figure 7-8. The highest PRE effect on $^{15}\text{N-MxiH}^{\text{CA5}}$ was induced by the spin labels at R132C and C322, denoting that MxiH^{CA5} were closest to these spin label positions.

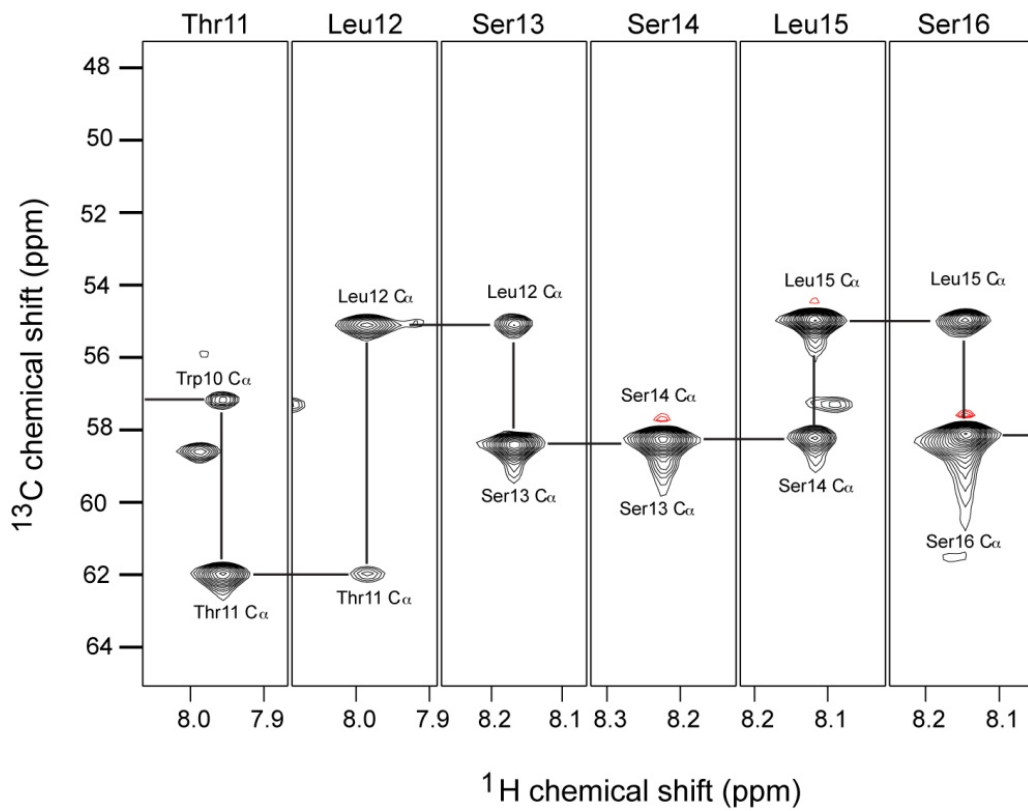


Figure 7-3: A portion of the 3D-HNCA strips of ^{13}C - ^{15}N -MxiH^{V68AV70A} showing the C_α and the ^1H - ^{15}N resonances of the current and preceding residues. The connectivity between the strips is shown as lines. The ^{15}N chemical shift is on the z-axis

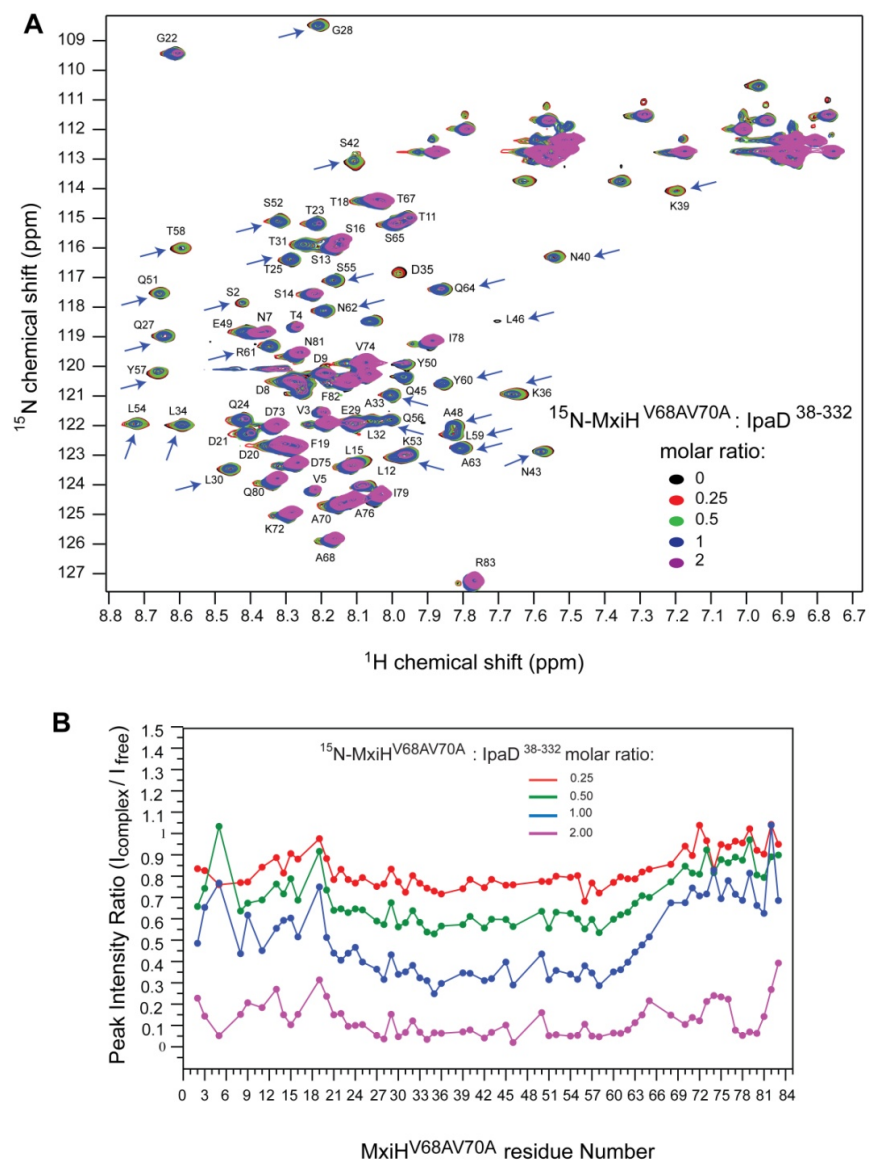


Figure 7-4: (A) NMR titration of ^{15}N -MxiH^{V68AV70A} with IpaD³⁸⁻³³² at five molar ratios. The peaks marked with arrows showed a decrease in intensity upon addition of IpaD³⁸⁻³³². (B) Quantification of the NMR titration of MxiH^{V68AV70A} and IpaD³⁸⁻³³². The ratio of peak intensities for each of the complex (1:0.25, 1:0.5, 1:1, 1:2) datasets over the free (1:0) dataset is plotted against the residues of MxiH^{V68AV70A}. Residues 21 to 64 in MxiH^{V68AV70A} were the most affected by IpaD³⁸⁻³³².

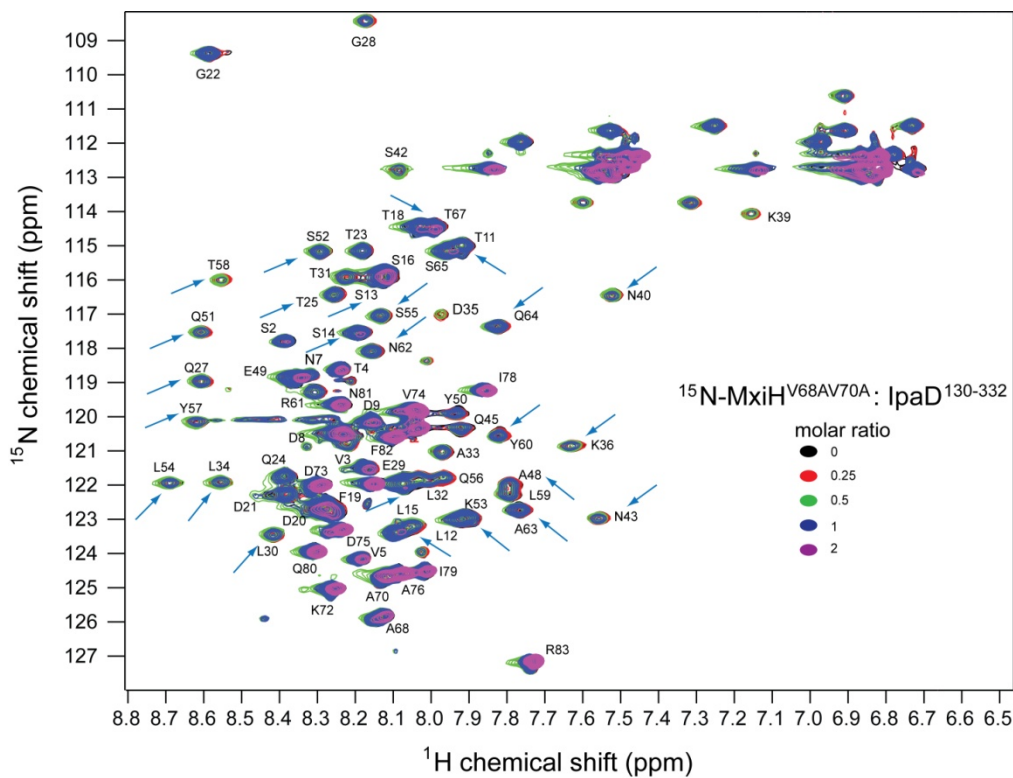


Figure 7-5: NMR titration of ^{15}N -MxiH^{V68AV70A} with IpaD¹³⁰⁻³³² that lacked the N-terminal α -helical hairpin. IpaD¹³⁰⁻³³² affected the same residues (marked by arrows) of MxiH^{V68AV70A} as IpaD³⁸⁻³³². This suggests that the N-terminal α -helical hairpin is not required for the interaction between MxiH and IpaD.

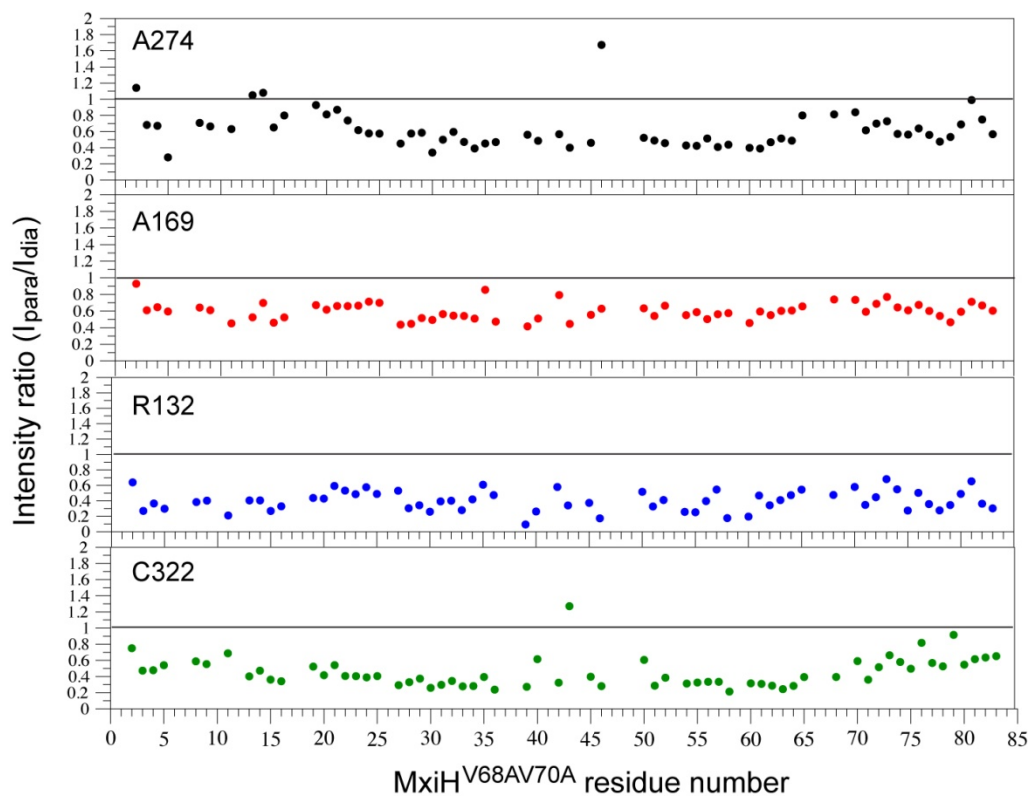


Figure 7-6: Results of PRE experiments using ^{15}N -MxiH^{V68AV70A} and IpaD³⁸⁻³³², which was spin labeled at four positions. Refer to figure 7-7 for the location of the spin labels on IpaD³⁸⁻³³². A PRE effect was observed on MxiH^{V68AV70A} irrespective of the position of the spin label suggesting a non-specific interaction possibly due to aggregation of the protein molecules in solution. ^{15}N -MxiH^{CΔ5} was used instead of ^{15}N -MxiH^{V68AV70A} for later experiments.

The residues in MxiH^{CΔ5} that showed the highest PRE effect when the spin label was placed at R132C of IpaD³⁸⁻³³² are shown in **Figure 7-9**. These residues mapped to the helix-turn-helix head domain of MxiH^{CΔ5}.

7.3. Discussion

The atomic structures of T3SS needle and tip proteins from *Salmonella* and *Shigella* have been determined (4-7, 10). The needle proteins form an α -helical hairpin with flexible N- and C-termini (6, 7). The tip proteins are highly α -helical and adopt a roughly oblong shape with a long central coiled coil (4, 5, 12). The coiled coil is positioned in between an N-terminal and a C-terminal domain (4, 5, 12). The tip proteins assemble at the needle tip to form the tip complex, which blocks premature secretion of effectors and acts as a platform for the assembly of the translocon (13). It is not known where the *Shigella* needle protein MxiH binds on the tip protein IpaD. In order to answer this question we analyzed the molecular interaction between MxiH and IpaD using NMR spectroscopy and PRE (11).

Purified full length versions of the needle proteins *Salmonella* PrgI and *Shigella* MxiH undergo spontaneous polymerization (7). In order to counter this problem truncated needle proteins lacking the last five residues (PrgI^{CΔ5} and MxiH^{CΔ5}) have been used for *in vitro* studies (7, 14). However Poyraz *et al.* (10) reported that the MxiH^{V68AV70A} double mutant is both functional and soluble. Hence, this variant was initially used to conduct NMR titrations with IpaD³⁸⁻³³². The interaction between ¹⁵N-MxiH^{V68AV70A} and IpaD³⁸⁻³³² was found to be in the intermediate exchange NMR timescale and several backbone amide peaks of MxiH^{V68AV70A} showed a decrease in peak intensity. ¹⁵N-MxiH^{CΔ5} was titrated with unlabeled IpaD³⁸⁻³³² previously and both fast exchange and intermediate exchange interactions were observed (3).

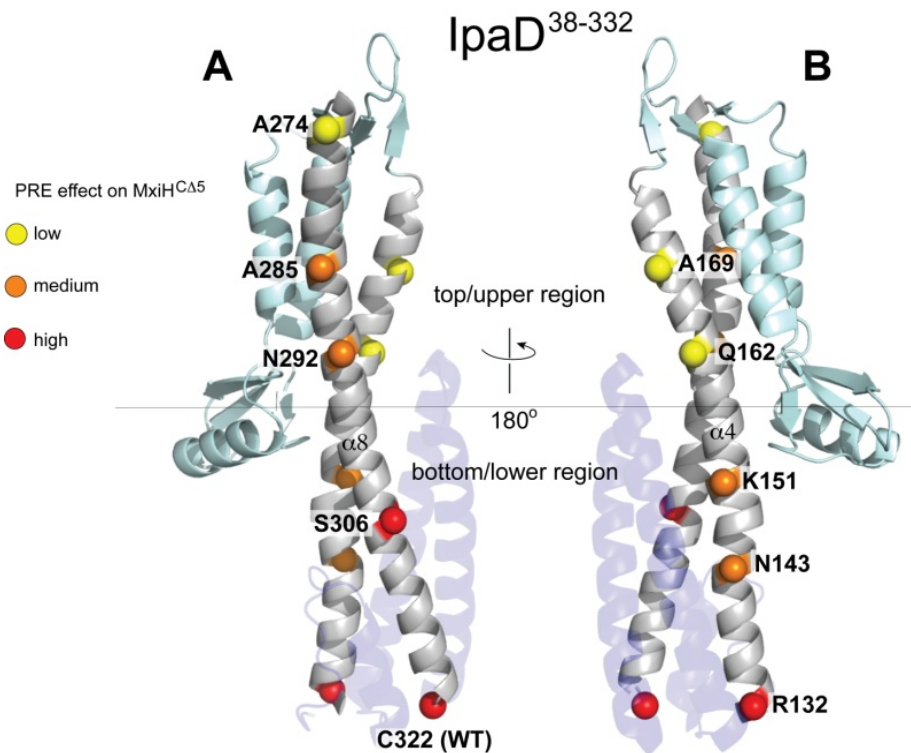


Figure 7-7: (A) & (B) Two views of the structure of IpaD³⁸⁻³³² showing the positions of the spin labels used for PRE experiments with ¹⁵N-MxiH^{CA5}. The N-terminal α -helical hairpin is shown in the background. The spin labels are colored according to the PRE effect they induced in MxiH^{CA5}. Spin labels on the “bottom” of the coiled coil of IpaD³⁸⁻³³² induced high PRE effect on MxiH^{CA5} residues.

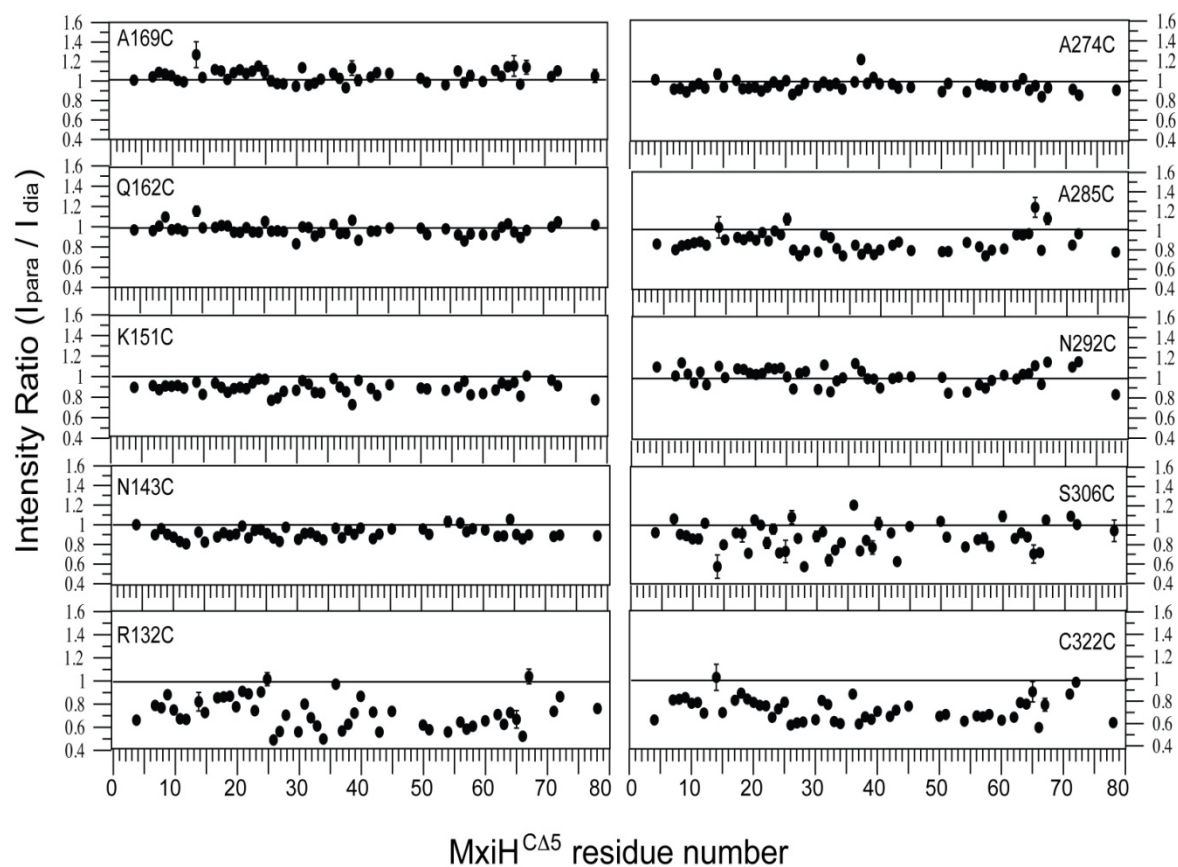


Figure 7-8: Results of the PRE experiments using ^{15}N -MxiH $^{\text{C}\Delta 5}$ and spin labeled IpaD $^{38-332}$. Each panel represents one spin label position on IpaD $^{38-332}$. The positions of the spin labels on the structure of IpaD $^{38-332}$ are shown in figure 7-7. The data points in each panel represent the $I_{\text{para}}/I_{\text{dia}}$ ratio of that residue of MxiH $^{\text{C}\Delta 5}$. Spin labels at R132 on helix $\alpha 4$ and C322 and S306 on helix $\alpha 8$ produced the strongest PRE effect on MxiH $^{\text{C}\Delta 5}$.

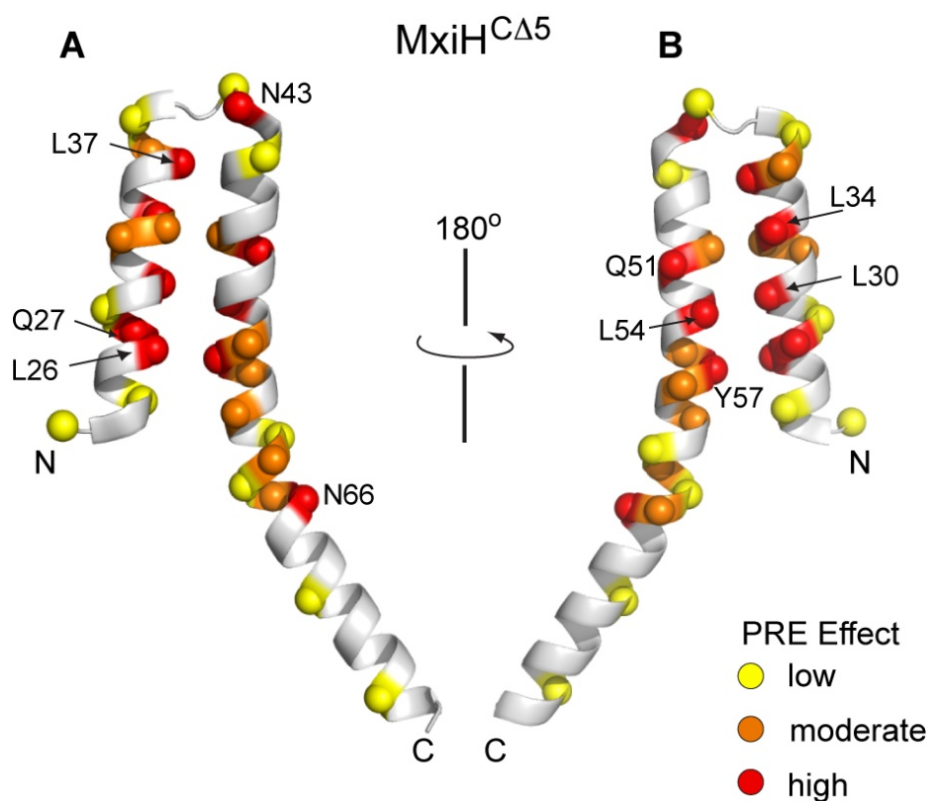


Figure 7-9: (A) & (B) Two views of MxiH^{CΔ5} showing the residues that were most affected by a spin label at residue R132 of IpaD³⁸⁻³³². The MxiH^{CΔ5} residues are colored according to their I_{para}/I_{dia} ratio. Yellow represents low PRE effect and an I_{para}/I_{dia} ratio of 0.80-0.70, orange represents moderate PRE effect and an I_{para}/I_{dia} ratio of 0.70-0.60, and red represents high PRE effect and an I_{para}/I_{dia} ratio < 0.60 .

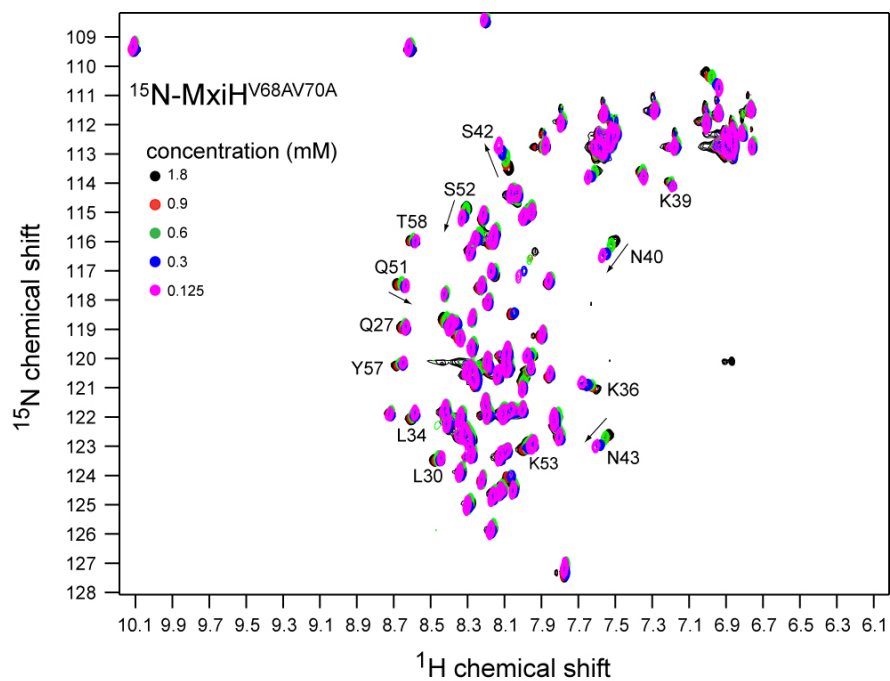


Figure 7-10: Concentration-dependent chemical shifts in ^{15}N -MxiH $^{\text{V68AV70A}}$. ^1H - ^{15}N -HSQC spectra from samples of ^{15}N -MxiH $^{\text{V68AV70A}}$ having five different concentrations are overlaid. The backbone amide peaks that are labeled showed peak shifts in the fast exchange NMR timescale. These shifts represent MxiH-MxiH interaction.

However, we did not observe any fast exchange peaks upon titration of MxiH^{V68AV70A} with IpaD³⁸⁻³³². ¹⁵N-MxiH^{V68AV70A} undergoes concentration-dependent peak shifts in the fast exchange NMR timescale [Figure 7-10]. These shifts represent interaction between two molecules of MxiH.

In *Shigella* IpaD, *Salmonella* SipD, and *Burkholderia* BipD the N-terminal domain is composed of an α -helical hairpin (4, 5). The N-terminal domain is thought to prevent premature polymerization of the tip proteins because its removal in IpaD and BipD led to the self-oligomerization of the tip proteins (4). Further evidence of a self-chaperoning function of the N-terminal α -helical hairpin domain comes from the observation that IpaD lacking this domain can still facilitate the invasion of eukaryotic cells by *Shigella* (13). Recently it was shown that the N-terminal α -helical hairpin domain of SipD might actually hinder its interaction with the needle protein PrgI because its removal increased the affinity between the two proteins (15). However, no studies had analyzed the direct interaction between MxiH and IpaD in the presence and absence of the N-terminal domain. Therefore, ¹⁵N-MxiH^{V68AV70A} was titrated with IpaD¹³⁰⁻³³² that lacked the N-terminal α -helical hairpin and it was found that this domain was dispensable for the interaction between IpaD and MxiH. This observation supports the hypothesis that the N-terminal α -helical hairpin as a self-chaperone for IpaD and prevents premature oligomerization but is not necessary for interaction with the needle protein.

PRE is a useful technique to locate binding interfaces involved in weak protein-protein interactions due to the ability of the paramagnetic spin label to affect NMR active nuclei within a large radius (~ 20 Å) (11). Hence, to locate the binding site of MxiH^{V68AV70A} on IpaD³⁸⁻³³², spin labels were attached to the latter. PRE had been previously used to show that PrgI, the *Salmonella* homolog of MxiH binds along the coiled coil of SipD, the *Salmonella* homolog of

IpaD (2). Following this observation, the spin labels on IpaD³⁸⁻³³² were attached along the coiled coil. However, after the collection of a few datasets, it was found that the spin labels were producing a non-specific PRE effect on MxiH^{V68AV70A} irrespective of their position on the coiled coil of IpaD³⁸⁻³³². This indicated that either MxiH^{V68AV70A} or the MxiH^{V68AV70A}-IpaD³⁸⁻³³² complex was aggregating in solution. In order to rule out these experimental artifacts, much lower concentrations of both the proteins were used without any change in the pattern of the PRE effect on MxiH^{V68AV70A}. Finally, ¹⁵N-MxiH^{V68AV70A} was substituted with ¹⁵N-MxiH^{CΔ5}.

After several trials a concentration of 0.1 mM ¹⁵N-MxiH^{CΔ5} and 0.05 mM IpaD³⁸⁻³³² was chosen for the PRE experiments to avoid aggregation of the proteins in solution. Spin labels on the coiled coil of IpaD³⁸⁻³³² that were closer to the antiparallel β-sheet (top) did not produce any PRE effect on MxiH^{CΔ5}. In contrast, when spin labels were attached on helices α4 and α8 towards the “bottom” of the coiled coil, a high PRE effect was observed in MxiH^{CΔ5} residues [Figure 7-7 & 7-8]. This suggested that MxiH binds to the bottom of the coiled coil of IpaD similar to the *Salmonella* PrgI interaction (2). The needle proteins *Salmonella* PrgI and *Shigella* MxiH are oriented in opposite directions in the polymerized needles (8, 9). The N-terminus of PrgI is on the surface of the *Salmonella* needle but the C-terminus of MxiH is on the surface of the *Shigella* needle. Further, a β-hairpin forms at the C-terminus of MxiH upon polymerization of the needle (8). These differences would lead to the assumption that the interaction between the needle and tip would be different between *Salmonella* and *Shigella*. However, despite having completely opposite orientations in the *Salmonella* and *Shigella* needles, the needle proteins bind to the tip proteins at a similar location, which is the bottom of the coiled coil of the tip protein. The coiled coil is a common feature in the tip proteins *Yersinia* LcrV (12) and *Burkholderia* BipD (16), in addition to *Salmonella* SipD (5) and *Shigella* IpaD (4). Our results highlight the

functional significance of the coiled coil because in both *Salmonella* and *Shigella* a common mode of interaction was used by the tip and the needle proteins. It is thus tempting to speculate that the assembly of the tip complex of the T3SS might follow a common principle where the coiled coil of the tip protein binds to the needle proteins.

7.4. References

1. Epler, C. R., Dickenson, N. E., Bullitt, E., and Picking, W. L. (2012) Ultrastructural Analysis of IpaD at the Tip of the Nascent MxiH Type III Secretion Apparatus of *Shigella flexneri*, *J. Mol. Biol.* 420, 29-39.
2. Rathinavelan, T., Tang, C., and De Guzman, R. N. (2011) Characterization of the Interaction between the *Salmonella* Type III Secretion System Tip Protein SipD and the Needle Protein PrgI by Paramagnetic Relaxation Enhancement, *J. Biol. Chem.* 286, 4922-4930.
3. Zhang, L., Wang, Y., Olive, A. J., Smith, N. D., Picking, W. D., De Guzman, R. N., and Picking, W. L. (2007) Identification of the MxiH needle protein residues responsible for anchoring invasion plasmid antigen D to the type III secretion needle tip, *J. Biol. Chem.* 282, 32144-32151.
4. Johnson, S., Roversi, P., Espina, M., Olive, A., Deane, J. E., Birket, S., Field, T., Picking, W. D., Blocker, A. J., Galyov, E. E., Picking, W. L., and Lea, S. M. (2007) Self-chaperoning of the type III secretion system needle tip proteins IpaD and BipD, *J. Biol. Chem.* 282, 4035-4044.
5. Chatterjee, S., Zhong, D., Nordhues, B. A., Battaile, K. P., Lovell, S. W., and De Guzman, R. N. (2011) The Crystal Structure of the *Salmonella* Type III Secretion System

- Tip Protein SipD in Complex with Deoxycholate and Chenodeoxycholate, *Protein Sci.* *20*, 75-86.
6. Deane, J. E., Roversi, P., Cordes, F. S., Johnson, S., Kenjale, R., Daniell, S., Booy, F., Picking, W. D., Picking, W. L., Blocker, A. J., and Lea, S. M. (2006) Molecular model of a type III secretion system needle: Implications for host-cell sensing, *Proc. Natl. Acad. Sci. U.S.A.* *103*, 12529-12533.
 7. Wang, Y., Ouellette, A. N., Egan, C. E., Rathinavelan, T., Im, W., and De Guzman, R. N. (2007) Differences in the electrostatic surfaces of the type III secretion needle proteins PrgI, BsaL, and MxiH, *J. Mol. Biol.* *371*, 1304-1314.
 8. Fujii, T., Cheung, M., Blanco, A., Kato, T., Blocker, A. J., and Namba, K. (2012) Structure of a type III secretion needle at 7-A resolution provides insights into its assembly and signaling mechanisms, *Proc. Natl. Acad. Sci. U.S.A.* *109*, 4461-4466.
 9. Loquet, A., Sgourakis, N. G., Gupta, R., Giller, K., Riedel, D., Goosmann, C., Griesinger, C., Kolbe, M., Baker, D., Becker, S., and Lange, A. (2012) Atomic model of the type III secretion system needle, *Nature* *486*, 276-279.
 10. Poyraz, O., Schmidt, H., Seidel, K., Delissen, F., Ader, C., Tenenboim, H., Goosmann, C., Laube, B., Thunemann, A. F., Zychlinsky, A., Baldus, M., Lange, A., Griesinger, C., and Kolbe, M. (2010) Protein refolding is required for assembly of the type three secretion needle, *Nat. Struct. Mol. Biol.* *17*, 788-792.
 11. Gillespie, J. R., and Shortle, D. (1997) Characterization of long-range structure in the denatured state of staphylococcal nuclease. I. Paramagnetic relaxation enhancement by nitroxide spin labels, *J. Mol. Biol.* *268*, 158-169.

12. Mueller, C. A., Broz, P., Muller, S. A., Ringler, P., Erne-Brand, F., Sorg, I., Kuhn, M., Engel, A., and Cornelis, G. R. (2005) The V-antigen of *Yersinia* forms a distinct structure at the tip of injectosome needles, *Science* 310, 674-676.
13. Picking, W. L., Nishioka, H., Hearn, P. D., Baxter, M. A., Harrington, A. T., Blocker, A., and Picking, W. D. (2005) IpaD of *Shigella flexneri* is independently required for regulation of Ipa protein secretion and efficient insertion of IpaB and IpaC into host membranes, *Infect. Immun.* 73, 1432-1440.
14. Deane, J. E., Cordes, F. S., Roversi, P., Johnson, S., Kenjale, R., Picking, W. D., Picking, W. L., Lea, S. M., and Blocker, A. (2006) Expression, purification, crystallization and preliminary crystallographic analysis of MxiH, a subunit of the *Shigella flexneri* type III secretion system needle, *Acta Crystallograph. Sect.F. Struct. Biol. Cryst. Commun.* 62, 302-305.
15. Lunelli, M., Hurwitz, R., Lambers, J., and Kolbe, M. (2011) Crystal structure of PrgI-SipD: insight into a secretion competent state of the type three secretion system needle tip and its interaction with host ligands, *PLoS Pathog.* 7, e1002163.
16. Erskine, P. T., Knight, M. J., Ruaux, A., Mikolajek, H., Wong Fat Sang, N., Withers, J., Gill, R., Wood, S. P., Wood, M., Fox, G. C., and Cooper, J. B. (2006) High Resolution Structure of BipD: An Invasion Protein Associated with the Type III Secretion System of *Burkholderia pseudomallei*, *J. Mol. Biol.* 363, 125-136.

Chapter 8: Summary and future directions

Several Gram-negative bacteria that are pathogenic to humans are completely dependent on the function of the T3SS in order to invade host cells (1). The bacterial species harboring the T3SS are responsible for several widespread illnesses that continue to have a negative impact on human health worldwide (1). More than a decade of extensive research has been performed to understand the architecture, function, and regulation of the T3SS. The needle apparatus of the T3SS is capped by a hydrophilic tip complex and a membrane bound translocon (2). The structure and function of the tip complex and the translocon are poorly understood. Work described in this dissertation was directed towards addressing some of the gaps in the current understanding of the tip complex and the translocon of the T3SS.

8.1. The structure of SipD

8.1.1. *Comparison of SipD and IpaD* - The tip complex is required for the insertion of the translocon into the plasma membrane of the target eukaryotic cell thereby enabling the translocation of effectors into the eukaryotic cell cytoplasm (3, 4). The tip complex also regulates secretion through the needle by blocking premature secretion of effectors until contact with the target cell is established (5, 6). Thus the tip complex is both an assembly platform and a sensor and its structure holds clues to how it fulfills these roles. Intact tip complexes of *Shigella* (7) and *Yersinia* (8) have been visualized. However, the structure of the tip complex of *Salmonella* is not known. Several copies of a hydrophilic tip protein SipD assemble the tip complex in *Salmonella* (9, 10). The atomic structure of SipD was necessary to understand the structure of the intact tip complex of *Salmonella*. Therefore, SipD³⁹⁻³⁴³ was crystallized using sparse-matrix vapor diffusion screening. Crystallization data was collected at the Advanced

Photon Source and the structure of SipD was solved at 1.9 Å resolution using molecular replacement with the SipD homolog from *Chromobacterium* as the search model. The structure of SipD was compared to the tip proteins IpaD (11) from *Shigella*, BipD (12) from *Burkholderia*, and LcrV (13) from *Yersinia*. IpaD and SipD showed almost identical domain architecture and aligned with a C_{α} rmsd of 1.4 Å (for 186 C_{α} atoms). A long central coiled coil was the most distinct feature of both SipD and IpaD. There was an α -helical hairpin followed by a short α -helix on the N-terminal side, a mixed α/β region on the C-terminal side, and a three-stranded antiparallel β -sheet on one end of the coiled coil. The mixed α/β region was made up of three α -helices and two β -strands. The first major difference between SipD and IpaD was that the loop connecting α -helices α_3 to α_4 (loop α_3 - α_4) was disordered in SipD but not in IpaD. The second difference was that the longitudinal axes of α -helices α_1 - α_3 were tilted at different angles in SipD and IpaD. These differences might correspond to different modes of function of the tip complexes of *Salmonella* and *Shigella*. For instance, the higher flexibility of loop α_3 - α_4 of SipD might form a more dynamic surface on the tip complex of SipD. Subtle changes in the dynamic states of the tip complex could potentially allow *Shigella* and *Salmonella* to fine-tune their physiological responses to specific environmental cues. Likewise, changes in the helical axes of SipD and IpaD might lead to the formation of tip complexes with different structures or with different surface properties. As a matter of fact, SipD is unable to compliment a non invasive strain of *Shigella* that lacks IpaD (14). This indicates that even though SipD and IpaD share close structural resemblance these two tip proteins function in a different manner. High-resolution structures are required for a thorough analysis of the physical and chemical properties of the intact tip complexes of *Salmonella* and *Shigella* in order to understand how they function.

8.1.2. *Implications of the crystal structure of SipD¹³¹⁻³⁴³* - The central coiled coil was a common feature of SipD, IpaD, BipD, as well as LcrV (15). The N-terminal α -helical hairpin however, was absent in LcrV (13). It was hypothesized that the N-terminal hairpin acts as a self-chaperone for the tip proteins SipD, IpaD, and BipD (11). A chaperone can assist in the folding of a protein or, in case of the T3SS, could prevent premature interactions with other proteins. The crystal structure of SipD¹³¹⁻³⁴³ lacking the N-terminal α -helical hairpin was determined to answer this question. SipD¹³¹⁻³⁴³ could maintain the folding of the coiled coil and the mixed α/β region in the absence of the N-terminal hairpin. This concluded that the N-terminal hairpin is not required for folding of SipD and suggested a possible role in how SipD interacts with other proteins. In fact, isothermal titration calorimetry using PrgI and SipD with or without the N-terminal hairpin indicated that the affinity between these two proteins increases in absence of the N-terminal hairpin of SipD (16). Removal of this domain in *Shigella* IpaD induces self-oligomerization of the tip protein (11). Therefore, it is likely that the N-terminal hairpin folds against the coiled coil and masks the interfaces required for the formation of the tip complex within the bacterial cytoplasm. Another interesting observation is that the N-terminal hairpin folds independent of the rest of SipD. A completely folded form of the 37kD tip protein is too large to pass through the 25 Å channel of the needle. Therefore, the tip protein must be transported through the needle in a partially folded or completely unfolded state. Thus, it is possible that the N-terminal hairpin unfolds during the transport of SipD through the needle and once SipD reaches the needle tip this region moves away to expose the surfaces required for the assembly of the tip complex [Figures 8-1 & 8-2].

8.1.3. *Potential applications of the crystal structures of SipD* - The tip complexes of *Shigella* (7) and *Yersinia* (8) were determined using electron microscopy. The atomic structures of the tip

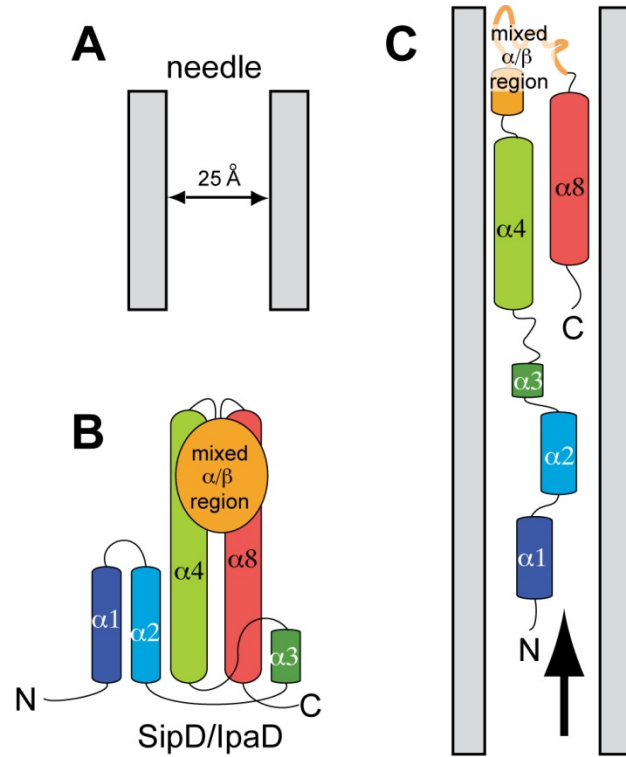


Figure 8-1: Proposed state of SipD before and during transport through the needle. (A) Estimated diameter of the inner channel of the needle (17, 18). (B) Schematic diagram of the folded state of SipD before transport through the needle. (C) Proposed partially unfolded state of SipD during transport through the needle.

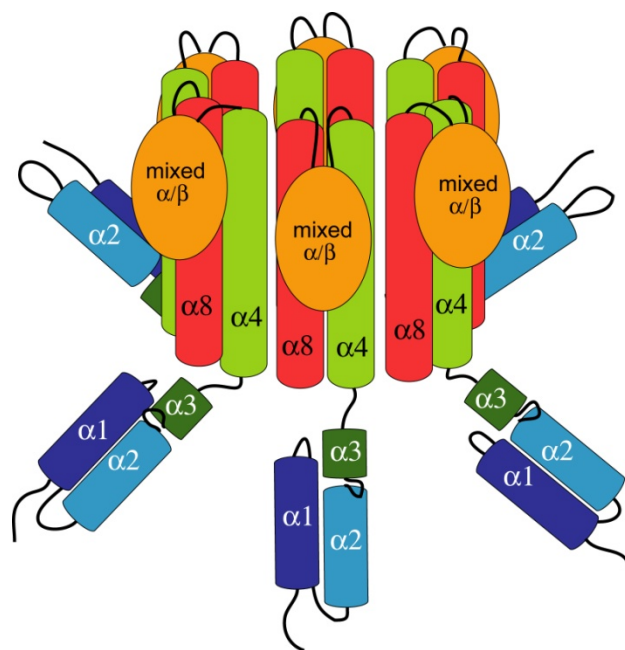


Figure 8-2: Proposed state of SipD at the needle tip in the assembled tip complex. The tip proteins assemble along their coiled coils. The N-terminal α -helical hairpin of SipD is splayed away to expose the surfaces required for the assembly of the tip complex. Six SipD molecules are shown at the tip complex based on the three-dimensional model of the *Salmonella* needle (19) and experimental restraints derived using PRE (20).

proteins *Shigella* IpaD (11) and *Yersinia* LcrV (13, 21) were then modeled into the three-dimensional reconstructions of their tip complexes. Although the low resolution of the resultant models prevented analysis of the molecular interfaces it was found that five molecules of IpaD and LcrV polymerize to form the needle complexes of *Shigella* and *Yersinia* respectively. There is however, a lack of consensus regarding the stoichiometry of the *Salmonella* tip complex. Galkin et al.(19) determined the structure of the *Salmonella* needle using cryo-EM and reported 6.3 molecules of the needle protein PrgI per turn of the needle. This information was combined with experimental restraints derived using paramagnetic relaxation enhancement (PRE) to model six molecules of SipD at the tip complex (20). In contrast, Loquet et al.(22) used solid state NMR (ssNMR) to report that the *Salmonella* needle contained 5.7 subunits of PrgI per turn of the needle. This suggests that *Salmonella* needles might assemble with heterogeneous helical parameters and could potentially assemble tip complexes with varying stoichiometry. The crystal structures of SipD reported herein in combination with other techniques like electron microscopy and computational modeling could be used to generate models of the *Salmonella* tip complex and thereby solve this puzzle. The lack of high resolution structures of the intact tip complex might be due to several impediments. First, the tip complex is probably loosely attached to the needle and is thus lost during purification. Second, the tip complex might adopt heterogeneous conformations on each of the needles. This property can reduce the quality of three-dimensional reconstructions of the tip complexes. One way to circumvent these hurdles is to model the structure of the intact tip complexes from experimentally derived restraints. The crystal structure reported herein might prove to be useful for such approaches for modeling of the tip complex. In fact, PRE was used to characterize the interaction between SipD and PrgI

and obtain restraints for structure calculation of *Salmonella* tip complexes (20) using the crystal structure of SipD reported in this dissertation.

8.1.4. Mutagenesis of SipD - The tip complex blocks premature secretion of effectors, senses the presence of host cell, and also works as an assembly platform for the translocon (2). This raises the question whether the different functional roles are played by the tip proteins as a whole or are assigned to the different domains. Indeed, mutagenesis of the *Shigella* IpaD shows that each domain of the tip protein might play a different role (14). Short deletions were made in SipD in order to test the function of its domains. Deletion of only five residues (residues 338-343) from the C-terminus of SipD yielded a non-invasive phenotype in *Salmonella* even though the folding of SipD was unaltered. Interestingly, deletion of five residues from the C-terminus of the needle proteins *Salmonella* PrgI (23) and *Shigella* MxiH (24) prevents the polymerization of the needle. Further, in *Shigella* IpaD a similar deletion prevents the localization of IpaD on the bacterial surface (9). These results strongly suggest that the extreme C-terminus is required for the formation of the tip complex. Thus, the needle and the tip proteins seem to follow a common mode of function where the C-terminus is required for the polymerization of the needle and the tip complex respectively. It is possible that the C-terminus of each of the tip proteins are positioned close in space in the tip complex and takes part in extensive protein-protein interactions to stabilize the tip complex [Figure 8-3A]. The amino acid sequence of the deleted portion is Lys-Ser-Phe-Leu-Gln. The Lys residue might form salt-bridges, Ser and Gln could be involved in H-bonds, while Phe from multiple copies of the tip proteins could form base-stacking interactions, and Gln and Leu might participate in van der Waals interactions. Alternatively, it is possible that the C-terminus of the tip proteins binds to the needle proteins and thereby attaches

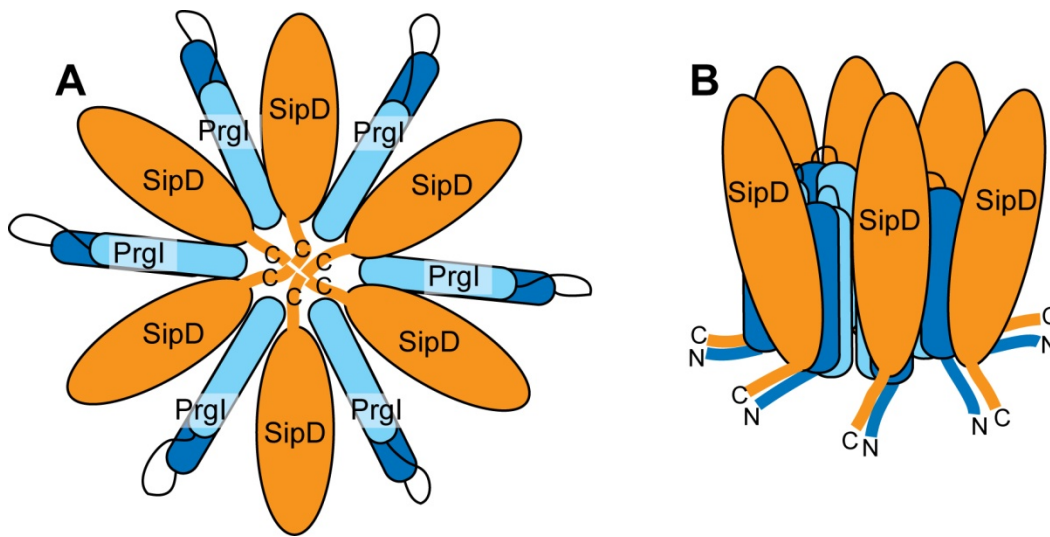


Figure 8-3: Two proposed models showing the possible interactions mediated through the extreme C-terminus of SipD. SipD is colored orange and the two α -helices of PrgI are colored light blue (C-terminal helix) and dark blue (N-terminal helix). **(A)** Top-view of the tip complex where the C-termini of several SipD molecules could interact with each other to assemble the tip complex. **(B)** An alternative model showing the side-view of the tip complex where the C-terminus of SipD contacts the N-terminus of the needle proteins. Both the C-terminus of SipD (*chapter 4 figure 4-2*) and N-terminus of PrgI (22) can adopt an extended β -strand conformation.

the tip complex on the needle. In support of this model, residues Ser339, Phe340, and Leu341 adopt a β -strand conformation and form a two-stranded parallel β -sheet along with residues Val223, Lys224, and Val225 within the mixed α/β region of another molecule of SipD (*chapter 4 section 4.2.1*). Incidentally, the N-terminal tails of PrgI molecules within the polymerized needle also adopts an extended conformation. Thus it is tempting to speculate that in the assembled tip complex the C-terminus of SipD might form a β -sheet along with the N-terminus of PrgI [**Figure 8-3B**].

Residues 116 to 124 were deleted from the 25-residue loop $\alpha 3$ - $\alpha 4$ of SipD. Like the deletion of residues 338-343, this nine-residue deletion did not affect the structure of SipD. However, more surprisingly, this deletion had no effect on the invasiveness of *Salmonella*. Previous studies indicate that loop $\alpha 3$ - $\alpha 4$ is most probably oriented on the outer surface of the tip complex (20). If that case this region should be involved in formation of the translocon. On the contrary, if loop $\alpha 3$ - $\alpha 4$ is oriented towards the internal surface of the tip complex, it would probably make contacts with other tip proteins or needle proteins or might regulate the diameter of the needle channel. In each of these cases, deletion of this loop should be expected to affect the function of SipD. However, it is also possible that this flexible loop region is required for intermolecular motions, perhaps for adjusting the position of the N-terminal hairpin with respect to the core of SipD [**Figure 8-4**]. In that case deletion of just nine residues might not be sufficient to produce an easily identifiable phenotype using a *Salmonella* invasion assay.

The tip proteins SipD, IpaD, BipD, and LcrV contain an antiparallel β -sheet on one end of the coiled coil. This end was arbitrarily denoted as the “top” of the tip protein while, the opposite end was referred to as the “bottom” of the tip protein.

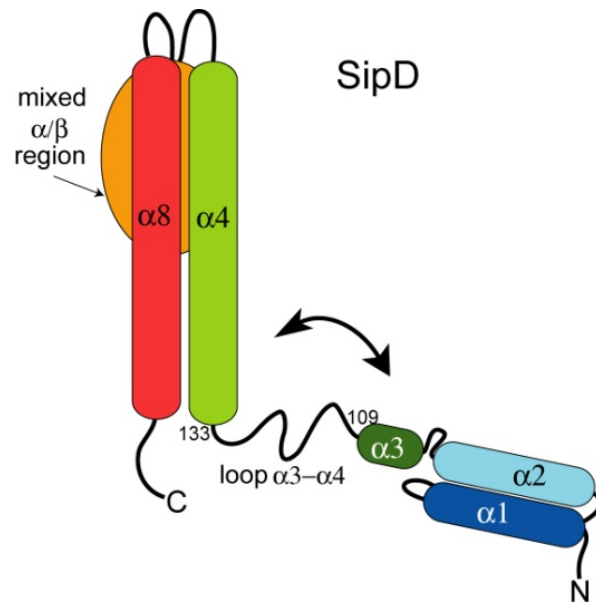


Figure 8-4: Schematic diagram of SipD showing a possible role of loop $\alpha 3$ - $\alpha 4$ in controlling the orientation of the N-terminal α -helical hairpin with respect to the coiled coil of SipD.

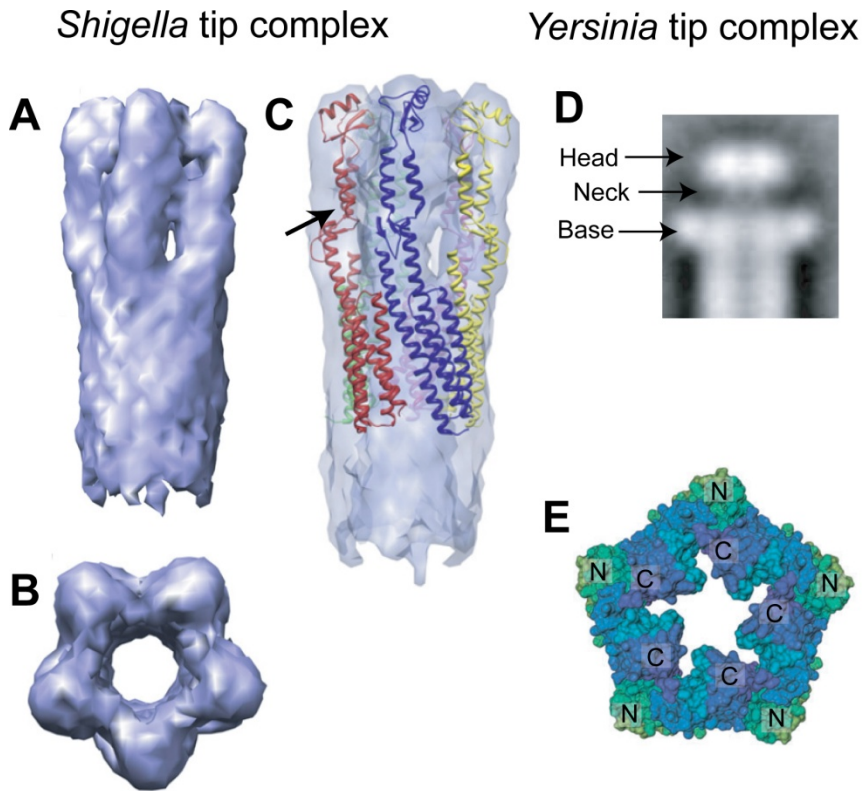


Figure 8-5: Structures of the tip complex of *Shigella* (7) and *Yersinia* (8, 21). (A) Side-view of the three-dimensional reconstruction of tip complex formed by IpaD showing an elongated structure at the needle tip of *Shigella* (7). (B) Top-view of the *Shigella* tip complex showing pentameric symmetry. Five IpaD molecules were fitted into the *Shigella* tip complex. (C) The Side-view of the *Shigella* tip complex with five IpaD molecules. The mixed α/β region (marked by arrow) of IpaD was rotated by an angle of 160° in order to fit the electron density map of the *Shigella* tip complex. (A), (B), and (C) from Epler CR, Dickenson NE, Bullitt E, Picking WL., Ultrastructural analysis of IpaD at the tip of the nascent MxiH type III secretion apparatus of *Shigella flexneri*, *J Mol Biol.* 2012; 420:29-39. Published with permission © 2012 Elsevier Ltd. All rights reserved. (D) Electron micrograph showing the tip complex of *Yersinia* (8). Distinct head, neck, and base substructures were visible at the tips of the *Yersinia* needles. From Mueller CA, Broz P, Müller SA, Ringler P, Erne-Brand F, Sorg I, Kuhn M, Engel A, Cornelis GR, The V-antigen of *Yersinia* forms a distinct structure at the tip of injectisome needles, *Science.* 2005; 310:674-6. Reprinted with permission from AAAS. (E) Five molecules of the *Yersinia* tip protein LcrV were fitted into the EM reconstruction of the *Yersinia* tip complex (21). The N-terminus of LcrV formed the base

substructure and the C-terminus formed the head. From Broz P, Mueller CA, Müller SA, Philippsen A, Sorg I, Engel A, Cornelis GR., Function and molecular architecture of the *Yersinia* injectisome tip complex, Mol Microbiol. 2007; 65:1311-20. Reproduced with permission © Blackwell Publishing Limited.

This antiparallel β -sheet is another conserved structural element in the tip proteins and might play an important role in the function of the T3SS. Therefore, two or four residues were removed from β -strand $\beta 2$, which is part of the three-stranded antiparallel β -sheet at the top of SipD. These deletions rendered *Salmonella* unable to invade intestinal epithelial cells.

However, this phenotype could be attributed to structural changes near the top of SipD.

Nevertheless, these results implied that the antiparallel β -sheet is important to maintain the native folding of SipD. Interestingly, this region was suggested to act like a hinge, which allows a 165° rotation of the mixed α/β region of IpaD to form the *Shigella* tip complex (7) [Figure 8-5].

However, such a drastic rotation would require complete reorganization of the intramolecular interactions between the mixed α/β region and the coiled coil of IpaD. The thermodynamic parameters driving such a large-scale conformational change are unclear. Moreover, no such drastic rotation in LcrV was reported to occur during the formation of the *Yersinia* tip complex (21) [Figure 8-5]. However, it is not improbable for the same structural motif to play divergent roles in the assembly of the tip complexes in different bacterial species. Therefore, the antiparallel β -sheet can potentially be crucial for the correct assembly of the tip complex.

8.2. Implications of the interaction between SipD and bile salts

The tip complex is exposed on the bacterial surface and can potentially interact with small molecules present within the host environment (10). *Salmonella* and *Shigella* travel through the digestive system of humans in order to invade the epithelial cells of the small and large intestines respectively. Therefore, it is not surprising that the tip proteins SipD and IpaD can bind to bile salts (25). It is however, intriguing that *Salmonella* (26) and *Shigella* (27) react differently to bile salts. The bile salt deoxycholate enhances invasion of host cells in *Shigella* possibly by triggering the recruitment of the translocon protein IpaB to the needle tip (27, 28). The invasiveness of *Salmonella*, on the other hand, is repressed in presence of deoxycholate. The crystal structures of SipD bound to bile salts deoxycholate and chenodeoxycholate showed that bile salts bind at a hydrophobic pocket at the interface of three molecules of SipD. The effect of deoxycholate on the secretion of SipB was also tested and it was found that SipB was degraded into a smaller fragment when *Salmonella* was grown with deoxycholate. Thus, it is possible that binding of SipD to deoxycholate affects its interaction with the translocon protein.

Although bile affects T3SS function, the interaction between the *Shigella* IpaD (28) and deoxycholate is not a necessary for the invasiveness of *Shigella* (29, 30). Likewise, in *Salmonella* deoxycholate does not completely abolish the invasiveness of *Salmonella*. What then is the physiological significance of interaction between bile salts and tip proteins? One possible theory is that *Salmonella* and *Shigella* use bile salts as a spatiotemporal probe. In other words, the tip complex of these pathogens might be sensitive to the concentration of bile, which will be highest in the upper gastrointestinal tract and gradually decrease in the small and large intestines. In case of *Salmonella* for example, it has been proposed that high concentration of bile salts prevent premature activation of effector secretion in the upper gut, perhaps by

interfering with the formation of the translocon, but when *Salmonella* reaches the small intestines and the amount of bile salts is lower this negative effect on translocon formation is relieved and the T3SS is fully activated (26). However, this model cannot completely explain the effect of deoxycholate on the T3SS of *Shigella*. The contrasting response to bile salts in *Salmonella* and *Shigella* could perhaps be attributed to the fact that *Salmonella* colonizes the small intestinal epithelium while, *Shigella* colonizes the large intestinal epithelium. Another possibility is that the interaction between bile salts and isolated tip proteins is distinct from the interaction between bile salts and the assembled tip complex. One approach to test this hypothesis could be to analyze the interaction between bile salts and tip proteins that have been chemically cross-linked to mimic the assembled tip complex.

8.3. The needle-tip interaction in *Shigella*

How the tip complex is attached on the needle is not clearly understood. NMR spectroscopy and PRE were used to show that the *Shigella* needle protein MxiH binds at the bottom of the coiled coil of the tip protein IpaD. Similar results were reported for *Salmonella* where the needle protein PrgI also bound to the bottom of the coiled coil of the tip protein SipD (20). However, the needles from *Salmonella* (22) and *Shigella* (31) reportedly had drastic differences. In *Salmonella* needles, the N-terminus of PrgI was displayed on the outer surface of the needle whereas in the *Shigella* needles, the N-terminus of MxiH was reported to face the inner channel of the needle. This discrepancy contradicts the conserved mode of interaction between the needle and tip proteins. The structural models of the *Shigella* needles were generated by fitting the crystal structure of MxiH (32) into three-dimensional EM reconstructions of *Shigella* needles (31, 32). The structure of the *Salmonella* needle on the other hand was determined by a combination of ssNMR, electron microscopy, and computational modeling. Recently, ssNMR

was used to generate a homology model of the *Shigella* needles (33). In complete contrast to the earlier models, this model showed that the conserved C-terminus of MxiH is oriented to the internal surface and the variable N-terminus of MxiH is oriented towards the exterior of the *Shigella* needle [Figure 8-6]. Further, the ssNMR-derived models of *Salmonella* (22) and *Shigella* (33) reported that the needle proteins within the polymerized needles adopt similar secondary structural features. The N-terminus of both *Salmonella* PrgI and *Shigella* MxiH adopts an extended conformation followed by a proximal α -helix, a loop, and a distal C-terminal α -helix [Figure 8-6]. The ssNMR-based models are in agreement with the results of PRE experiments, which show that both *Salmonella* PrgI and *Shigella* MxiH bind to the bottom of the coiled coil of their respective tip proteins SipD and IpaD. Given that the coiled coil is a common feature in all tip proteins it can be speculated that this region plays an evolutionarily conserved role in the assembly of the tip complex. As a matter of fact, coiled coils are a common structural motif observed among the components of the needle apparatus (32, 34). It is likely that the coiled coil is used a building block in the architecture of the needle apparatus. Characterization of the interaction within the tip proteins will further explain how they travel through the needle and assemble the tip complex.

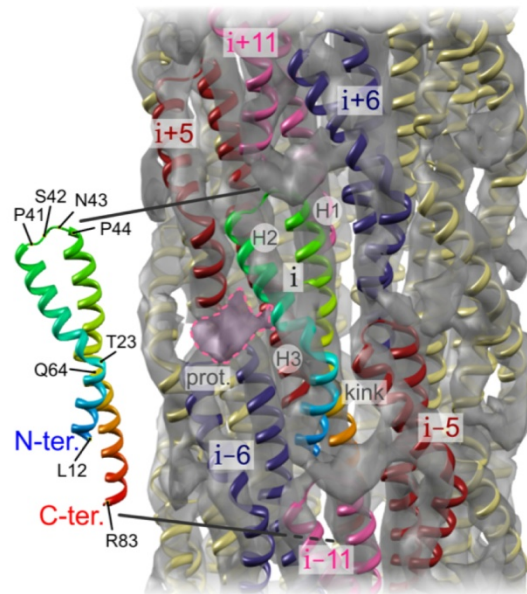


Figure 8-6: A homology model of the *Shigella* needle determined using solid state NMR (33). This model shows that the N-terminus of MxiH is displayed on the surface of the needle and the C-terminus lines the inner channel of the needle. The agreement of the model with the cryo-EM map (31) reported earlier is shown. An extended density labeled prot. was reported to fit a β -hairpin in the C-terminus of MxiH. In the above model this density was hypothesized to fit a rigidly extended N-terminal tail of MxiH. Figure reproduced from PLoS Pathog. 2013; 9(3): e1003245. PLOS copyright policies allow anyone to download, reuse, reprint, modify, distribute, and/or copy articles in PLOS journals with proper citations. No permission is required from the authors or the publishers.

8.4. Interaction between SipD and SipB: implications for the assembly of the translocon

The tip complex is followed by the translocon that connects the needle apparatus with the respective tip proteins SipD and IpaD. Given that the coiled coil is a common feature in all tip proteins it host cell membrane and provides a passage for the effectors in form of a translocation pore. Deletion of SipB affects the function of the translocon more drastically than deletion of SipC (4). SipB is also larger in size and contains two transmembrane helices while SipC contains only one. Thus, SipB is considered as the major translocon protein in *Salmonella* (34). SipB contains a hydrophilic protease-resistant domain at the N-terminus (35). This N-terminal domain was hypothesized to bind to the hydrophilic tip protein SipD to anchor the translocon on the tip complex. A combination of NMR spectroscopy and PRE was used to provide evidence of interaction between SipD and SipB and locate their binding interfaces. It was found that a region of SipB within residues Asp207 to Asn283 binds to the mixed α/β region of SipD.

The major translocon protein *Salmonella* SipB and its homolog IpaB from *Shigella* contain similar predicted secondary structural elements. Further, SipB can complement for IpaB to restore invasion of HeLa cells and lysis of macrophages by *Shigella* (36). SipB and IpaB are not only important for the formation of translocon but are also translocated into the target host cell (37, 38). They can activate caspase-1 leading to the apoptosis of macrophages (39, 40). The multiple roles of SipB and IpaB are segregated within distinct functional domains (35, 41). Previous studies have tested the importance of the N-terminal regions of SipB and IpaB (41-43). Like other T3SS substrates, their extreme N-termini were required for their secretion through the needle apparatus. Up to residues 120 -160 were required for binding to the chaperone SicA in case of SipB and IpgC in case of IpaB. Several deletions of ~ 10 amino acids were generated in IpaB (42). It was found that deletions within residues 207 to 247 did not have any effect on the

function of IpaB. However, deletion of residues 247-286 caused changes in the structure of IpaB (42). These residues lie within the SipD-binding surface of SipB reported herein. It is not clear why the IpaB mutations failed to produce a distinct phenotype in *Shigella*. It is however, noteworthy that point mutations K211A, D215A, and A218D in SipB yielded non-invasive strains of *Salmonella* but deletion of residues 207-217 in IpaB did not affect the function of the T3SS of *Shigella*. These results suggest that IpaB and SipB might have differences in how they function. In fact, complete deletion of IpaB in *Shigella* (6) causes an increase in the secretion of late effectors but deletion of SipB in *Salmonella* does not have any appreciable effect on effector secretion (5). In contrast to the mutagenesis of IpaB discussed above, Shen et al. (41) reported that deletions within residues 227-266 in IpaB produced a defect in regulation of effector secretion. Given that the localization of IpaB at the needle tip is required to prevent premature secretion of effectors in *Shigella*, this result suggests that residues 227-266 of IpaB might be required for the interaction between IpaB and IpaD. This observation therefore, agrees with our results that residues 207-283 within SipB bind to SipD. The regions downstream of the N-terminus of the major translocon proteins form two transmembrane helices which are required for their binding to the host cell membrane (34). The extreme C-terminus is also required for the membrane-insertion of SipB into the lipid membrane (35). The C-terminus of IpaB was also found to bind to IpaC (44). Incidentally, the C-terminus of SipC was found to mediate its interaction with SipB (45).

The observations discussed above can be combined to propose a model for the assembly of the translocon in *Salmonella*. In the bacterial cytoplasm SipB remains bound to the chaperone SicA. SipB most probably exits the needle in a partially folded form probably still retaining some helical character. At the needle tip, the hydrophilic N-terminal domain of SipB binds to the mixed α/β region of SipD displayed at the exterior surface of the tip complex. This interaction could be important for correctly embedding the transmembrane helices of SipB into the host cell membrane. When SipC is subsequently secreted, the C-termini of SipB and SipC might interact to form an active translocon. However, it is also possible that other regions of SipB besides the N-terminal domain are involved in the interaction with SipD or perhaps there are regions of SipB, which bind both SipD and SipC at the same time. Further, the molecular interactions responsible for polymerization of multiple copies of SipB at the translocon remain to be elucidated. The N-terminus of SipB is also responsible for oligomerization of SipB *in vitro* (35). Thus, it is plausible that the N-terminal domain of one molecule of SipB binds to one molecule of SipD and simultaneously contacts the N-terminal domain of an adjacent SipB molecule. This proposed model is depicted in **Figure 8-7**. Further studies need to be directed towards answering how full length SipB binds to itself and to SipD and SipC.

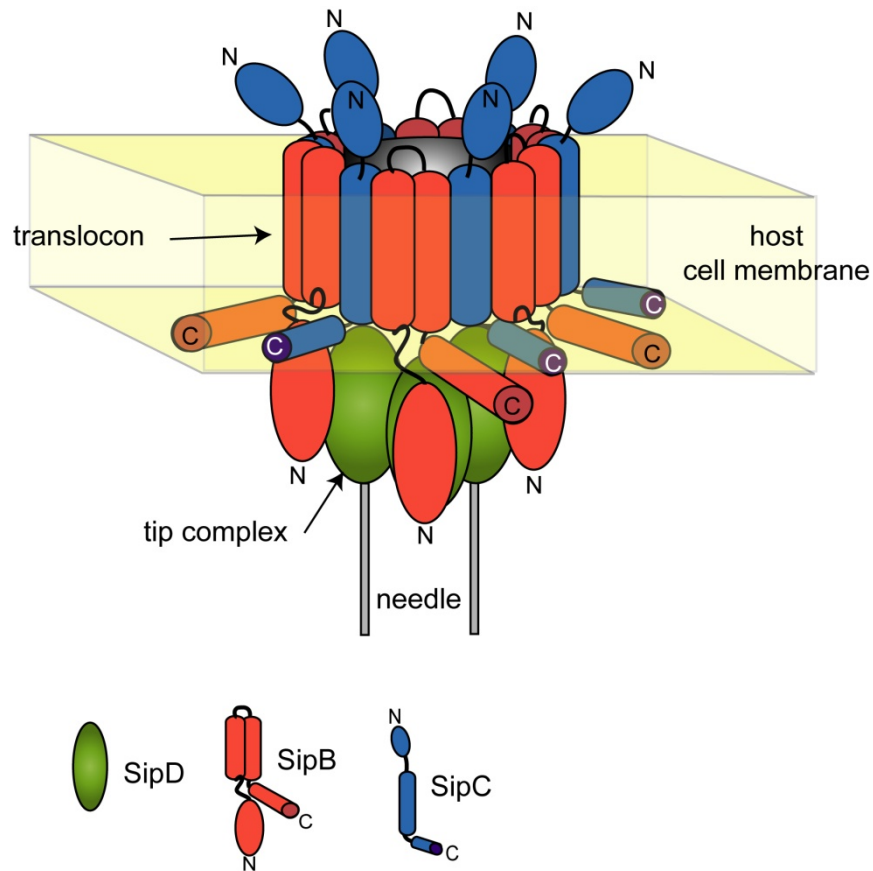


Figure 8-7: Proposed model of the assembled translocon of *Salmonella* built using six-fold symmetry based on previous reports (19, 20). SipD is represented as green ellipses. The N-terminal domain of one SipB binds to the mixed α/β region (not shown) of one SipD. Two transmembrane helices of SipB are embedded within the host cell membrane and the C-terminal amphipathic helix is peripherally associated with the host cell membrane. One SipC (blue) is bound to one molecule of SipB.

8.5. Conclusions

The T3SS is a macromolecular protein complex presenting multiple interfaces that can be targeted to disrupt its assembly. However, detailed molecular characterization of the interfaces is required to understand the underlying mechanism of assembly and to develop strategies to disrupt such interactions. Weak protein-protein interactions and structural heterogeneity are typical of large macromolecular complexes and they also pose challenges to obtain atomic resolution structures of such assemblies (46, 47). NMR is well suited to study such weak interactions in solution and PRE has an advantage over other biochemical and biophysical tools because it is sensitive to long range interactions (46, 48). Probing how protein components of the needle apparatus interact *in vitro* will generate useful data that can then be applied to understand the overall assembly of the T3SS. The results of the experimental work described in this dissertation advance our understanding of the needle, tip, and translocon proteins and also forward mechanistic models of how these proteins interact with each other to form the different components of the needle apparatus. This knowledge will ultimately lead to a better appreciation of the workings of the T3SS.

8.6. References

1. Cornelis, G. R. (2006) The type III secretion injectisome, *Nat. Rev. Microbiol.* 4, 811-825.
2. Mueller, C. A., Broz, P., and Cornelis, G. R. (2008) The type III secretion system tip complex and translocon, *Mol. Microbiol.* 68, 1085-1095.

3. Blocker, A., Gounon, P., Larquet, E., Niebuhr, K., Cabiliaux, V., Parsot, C., and Sansonetti, P. (1999) The tripartite type III secretion of *Shigella flexneri* inserts IpaB and IpaC into host membranes, *J. Cell Biol.* 147, 683-693.
4. Miki, T., Okada, N., Shimada, Y., and Danbara, H. (2004) Characterization of *Salmonella* pathogenicity island 1 type III secretion-dependent hemolytic activity in *Salmonella enterica* serovar Typhimurium, *Microb. Pathog.* 37, 65-72.
5. Kaniga, K., Tucker, S., Trollinger, D., and Galan, J. E. (1995) Homologs of the *Shigella* IpaB and IpaC invasins are required for *Salmonella typhimurium* entry into cultured epithelial cells, *J. Bacteriol.* 177, 3965-3971.
6. Menard, R., Sansonetti, P. J., and Parsot, C. (1993) Nonpolar mutagenesis of the ipa genes defines IpaB, IpaC, and IpaD as effectors of *Shigella flexneri* entry into epithelial cells, *J. Bacteriol.* 175, 5899-5906.
7. Epler, C. R., Dickenson, N. E., Bullitt, E., and Picking, W. L. (2012) Ultrastructural Analysis of IpaD at the Tip of the Nascent MxiH Type III Secretion Apparatus of *Shigella flexneri*, *J. Mol. Biol.* 420, 29-39.
8. Mueller, C. A., Broz, P., Muller, S. A., Ringler, P., Erne-Brand, F., Sorg, I., Kuhn, M., Engel, A., and Cornelis, G. R. (2005) The V-antigen of *Yersinia* forms a distinct structure at the tip of injectisome needles, *Science* 310, 674-676.
9. Sani, M., Botteaux, A., Parsot, C., Sansonetti, P., Boekema, E. J., and Allaoui, A. (2007) IpaD is localized at the tip of the *Shigella flexneri* type III secretion apparatus, *Biochim. Biophys. Acta* 1770, 307-311.

10. Lara-Tejero, M., and Galan, J. E. (2009) *Salmonella enterica* serovar typhimurium pathogenicity island 1-encoded type III secretion system translocases mediate intimate attachment to nonphagocytic cells, *Infect. Immun.* 77, 2635-2642.
11. Johnson, S., Roversi, P., Espina, M., Olive, A., Deane, J. E., Birket, S., Field, T., Picking, W. D., Blocker, A. J., Galyov, E. E., Picking, W. L., and Lea, S. M. (2007) Self-chaperoning of the type III secretion system needle tip proteins IpaD and BipD, *J. Biol. Chem.* 282, 4035-4044.
12. Erskine, P. T., Knight, M. J., Ruaux, A., Mikolajek, H., Wong Fat Sang, N., Withers, J., Gill, R., Wood, S. P., Wood, M., Fox, G. C., and Cooper, J. B. (2006) High Resolution Structure of BipD: An Invasion Protein Associated with the Type III Secretion System of *Burkholderia pseudomallei*, *J. Mol. Biol.* 363, 125-136.
13. Derewenda, U., Mateja, A., Devedjiev, Y., Routzahn, K. M., Evdokimov, A. G., Derewenda, Z. S., and Waugh, D. S. (2004) The structure of *Yersinia pestis* V-antigen, an essential virulence factor and mediator of immunity against plague, *Structure* 12, 301-306.
14. Picking, W. L., Nishioka, H., Hearn, P. D., Baxter, M. A., Harrington, A. T., Blocker, A., and Picking, W. D. (2005) IpaD of *Shigella flexneri* is independently required for regulation of Ipa protein secretion and efficient insertion of IpaB and IpaC into host membranes, *Infect. Immun.* 73, 1432-1440.
15. Chatterjee, S., Zhong, D., Nordhues, B. A., Battaile, K. P., Lovell, S. W., and De Guzman, R. N. (2011) The Crystal Structure of the Salmonella Type III Secretion System Tip Protein SipD in Complex with Deoxycholate and Chenodeoxycholate, *Protein Sci.* 20, 75-86.

16. Lunelli, M., Hurwitz, R., Lambers, J., and Kolbe, M. (2011) Crystal structure of PrgI-SipD: insight into a secretion competent state of the type three secretion system needle tip and its interaction with host ligands, *PLoS Pathog.* 7, e1002163.
17. Schraidt, O., and Marlovits, T. C. (2011) Three-dimensional model of Salmonella's needle complex at subnanometer resolution, *Science* 331, 1192-1195.
18. Hodgkinson, J. L., Horsley, A., Stabat, D., Simon, M., Johnson, S., da Fonseca, P. C., Morris, E. P., Wall, J. S., Lea, S. M., and Blocker, A. J. (2009) Three-dimensional reconstruction of the Shigella T3SS transmembrane regions reveals 12-fold symmetry and novel features throughout, *Nat Struct Mol Biol* 16, 477-485.
19. Galkin, V. E., Schmied, W. H., Schraidt, O., Marlovits, T. C., and Egelman, E. H. (2010) The structure of the Salmonella typhimurium type III secretion system needle shows divergence from the flagellar system, *J. Mol. Biol.* 396, 1392-1397.
20. Rathinavelan, T., Tang, C., and De Guzman, R. N. (2011) Characterization of the Interaction between the *Salmonella* Type III Secretion System Tip Protein SipD and the Needle Protein PrgI by Paramagnetic Relaxation Enhancement, *J. Biol. Chem.* 286, 4922-4930.
21. Broz, P., Mueller, C. A., Muller, S. A., Philippsen, A., Sorg, I., Engel, A., and Cornelis, G. R. (2007) Function and molecular architecture of the Yersinia injectisome tip complex, *Mol. Microbiol.* 65, 1311-1320.
22. Loquet, A., Sgourakis, N. G., Gupta, R., Giller, K., Riedel, D., Goosmann, C., Griesinger, C., Kolbe, M., Baker, D., Becker, S., and Lange, A. (2012) Atomic model of the type III secretion system needle, *Nature* 486, 276-279.

23. Wang, Y., Ouellette, A. N., Egan, C. E., Rathinavelan, T., Im, W., and De Guzman, R. N. (2007) Differences in the electrostatic surfaces of the type III secretion needle proteins PrgI, BsaL, and MxiH, *J. Mol. Biol.* 371, 1304-1314.
24. Kenjale, R., Wilson, J., Zenk, S. F., Saurya, S., Picking, W. L., Picking, W. D., and Blocker, A. (2005) The needle component of the type III secretion apparatus of *Shigella* regulates the activity of the secretion apparatus, *J. Biol. Chem.* 280, 42929-42937.
25. Stensrud, K. F., Adam, P. R., La Mar, C. D., Olive, A. J., Lushington, G. H., Sudharsan, R., Shelton, N. L., Givens, R. S., Picking, W. L., and Picking, W. D. (2008) Deoxycholate interacts with IpaD of *Shigella flexneri* in inducing the recruitment of IpaB to the type III secretion apparatus needle tip, *J. Biol. Chem.* 283, 18646-18654.
26. Prouty, A. M., and Gunn, J. S. (2000) *Salmonella enterica* serovar typhimurium invasion is repressed in the presence of bile, *Infect. Immun.* 68, 6763-6769.
27. Pope, L. M., Reed, K. E., and Payne, S. M. (1995) Increased protein secretion and adherence to HeLa cells by *Shigella* spp. following growth in the presence of bile salts, *Infect. Immun.* 63, 3642-3648.
28. Olive, A. J., Kenjale, R., Espina, M., Moore, D. S., Picking, W. L., and Picking, W. D. (2007) Bile salts stimulate recruitment of IpaB to the *Shigella flexneri* surface, where it colocalizes with IpaD at the tip of the type III secretion needle, *Infect. Immun.* 75, 2626-2629.
29. Veenendaal, A. K., Hodgkinson, J. L., Schwarzer, L., Stabat, D., Zenk, S. F., and Blocker, A. J. (2007) The type III secretion system needle tip complex mediates host cell sensing and translocon insertion, *Mol Microbiol* 63, 1719-1730.

30. Schiavolin, L., Meghraoui, A., Cherradi, Y., Biskri, L., Botteaux, A., and Allaoui, A. (2013) Functional insights into the Shigella type III needle tip IpaD in secretion control and cell contact, *Mol Microbiol* 88, 268-282.
31. Fujii, T., Cheung, M., Blanco, A., Kato, T., Blocker, A. J., and Namba, K. (2012) Structure of a type III secretion needle at 7-A resolution provides insights into its assembly and signaling mechanisms, *Proc. Natl. Acad. Sci. U.S.A.* 109, 4461-4466.
32. Deane, J. E., Roversi, P., Cordes, F. S., Johnson, S., Kenjale, R., Daniell, S., Booy, F., Picking, W. D., Picking, W. L., Blocker, A. J., and Lea, S. M. (2006) Molecular model of a type III secretion system needle: Implications for host-cell sensing, *Proc. Natl. Acad. Sci. U.S.A.* 103, 12529-12533.
33. Demers, J. P., Sgourakis, N. G., Gupta, R., Loquet, A., Giller, K., Riedel, D., Laube, B., Kolbe, M., Baker, D., Becker, S., and Lange, A. (2013) The common structural architecture of Shigella flexneri and Salmonella typhimurium type three secretion needles, *PLoS Pathog* 9, e1003245.
34. Barta, M. L., Dickenson, N. E., Patil, M., Keightley, A., Wyckoff, G. J., Picking, W. D., Picking, W. L., and Geisbrecht, B. V. (2012) The structures of coiled coil domains from type III secretion system translocators reveal homology to pore-forming toxins, *J Mol Biol* 417, 395-405.
35. McGhie, E. J., Hume, P. J., Hayward, R. D., Torres, J., and Koronakis, V. (2002) Topology of the Salmonella invasion protein SipB in a model bilayer, *Mol Microbiol* 44, 1309-1321.

36. Hermant, D., Menard, R., Arricau, N., Parsot, C., and Popoff, M. Y. (1995) Functional conservation of the Salmonella and Shigella effectors of entry into epithelial cells, *Mol Microbiol* 17, 781-789.
37. Collazo, C. M., and Galan, J. E. (1997) The invasion-associated type III system of Salmonella typhimurium directs the translocation of Sip proteins into the host cell, *Mol Microbiol* 24, 747-756.
38. Thirumalai, K., Kim, K. S., and Zychlinsky, A. (1997) IpaB, a *Shigella flexneri* invasin, colocalizes with interleukin-1 beta-converting enzyme in the cytoplasm of macrophages, *Infect Immun* 65, 787-793.
39. Hilbi, H., Moss, J. E., Hersh, D., Chen, Y., Arondel, J., Banerjee, S., Flavell, R. A., Yuan, J., Sansonetti, P. J., and Zychlinsky, A. (1998) Shigella-induced apoptosis is dependent on caspase-1 which binds to IpaB, *J Biol Chem* 273, 32895-32900.
40. Hersh, D., Monack, D. M., Smith, M. R., Ghori, N., Falkow, S., and Zychlinsky, A. (1999) The Salmonella invasin SipB induces macrophage apoptosis by binding to caspase-1, *Proc Natl Acad Sci U S A* 96, 2396-2401.
41. Shen, D. K., Saurya, S., Wagner, C., Nishioka, H., and Blocker, A. J. (2010) Domains of the Shigella flexneri type III secretion system IpaB protein involved in secretion regulation, *Infect Immun* 78, 4999-5010.
42. Guichon, A., Hersh, D., Smith, M. R., and Zychlinsky, A. (2001) Structure-function analysis of the Shigella virulence factor IpaB, *J Bacteriol* 183, 1269-1276.
43. Kim, B. H., Kim, H. G., Kim, J. S., Jang, J. I., and Park, Y. K. (2007) Analysis of functional domains present in the N-terminus of the SipB protein, *Microbiology* 153, 2998-3008.

44. Page, A. L., Fromont-Racine, M., Sansonetti, P., Legrain, P., and Parsot, C. (2001) Characterization of the interaction partners of secreted proteins and chaperones of *Shigella flexneri*, *Mol Microbiol* 42, 1133-1145.
45. Myeni, S. K., Wang, L., and Zhou, D. (2013) SipB-SipC complex is essential for translocon formation, *PLoS One* 8, e60499.
46. Vaynberg, J., and Qin, J. (2006) Weak protein-protein interactions as probed by NMR spectroscopy, *Trends Biotechnol* 24, 22-27.
47. Madl, T., Guttler, T., Gorlich, D., and Sattler, M. (2011) Structural analysis of large protein complexes using solvent paramagnetic relaxation enhancements, *Angewandte Chemie* 50, 3993-3997.
48. Clore, G. M., Tang, C., and Iwahara, J. (2007) Elucidating transient macromolecular interactions using paramagnetic relaxation enhancement, *Curr Opin Struct Biol* 17, 603-616.